

MASTER'S THESIS

Analysis of Submarine Groundwater Discharge to Manila Bay

3D Density Dependant Hydrogeological Modeling of the South-eastern
coastal zone of Bataan, Philippines

by

AILEEN SORIAO MIRASOL-ROBERT

PRESTIGE MASTERS IN SYSTEM EARTH MODELING

Faculty of Geosciences, Utrecht University

September 2010





MASTER'S THESIS

Analysis of Submarine Groundwater Discharge to Manila Bay

3D Density Dependent Hydrogeological Modeling of
the South-eastern coastal zone of Bataan,
Philippines

By

AILEEN SORIAO MIRASOL-ROBERT

PRESTIGE MASTERS IN SYSTEM EARTH MODELING

Faculty of Geosciences, Utrecht University

September 2010

This paper is a master's thesis submitted as partial fulfillment of the requirements for the degree of PRESTIGE MASTERS IN SYSTEM EARTH MODELING at Utrecht University, The Netherlands, 31 August 2010.

Thesis Advisers:

Dr. Hans Dürr

Department of Physical Geography
Faculty of Geosciences, Utrecht University

Dr. Gualbert Oude Essink

Subsurface and Groundwater Systems
Deltares, the Netherlands

*For Brice
For my Family
For the Philippines*

Table of Contents

List of Tables	9
List of Figures	10
List of Appendices	15
Summary	17
Chapter 1	
Introduction	21
1.1 Background.....	22
1.2 Definition of Submarine Groundwater Discharge	23
1.3 Driving mechanism of SGD	26
1.4 Interests and Issues Related to SGD.....	27
1.5 Quantify and Qualify SGD	29
1.5.1 Historical Overview	29
1.5.2 SGD Measuring Techniques	36
1.5.3 SGD Studies Worldwide	44
1.6 Philippines: an SGD key site	46
1.7 Thesis Outline	51
References	52
Chapter 2	
3D Density Dependent Modeling of Submarine Groundwater Discharge	63
2.1 Abstract	64
2.2 Introduction.....	65
2.3 Regional setting and features of Manila Bay	66
2.4 Study area and Physiography	67
2.5 Geology and Hydrogeology	75
2.6 Numerical Model.....	85

2.6.1	Governing Equations.....	85
2.6.2	PMWIN and MOCDENS3D.....	89
2.7	Model Set-up.....	90
2.7.1	Hydrogeologic Parameters.....	92
2.7.2	Boundary Conditions.....	92
2.7.3	Modeling Approach.....	95
2.8	Model Scenarios.....	96
2.8.1	Base Case.....	96
2.8.2	Sensitivity Analysis.....	106
2.9	Conclusions.....	116
	References.....	118

Chapter 3

Simulation of Climate and Anthropogenic Effects on SGD 121

3.1	Abstract.....	122
3.2	Introduction.....	123
3.2.1	Background.....	123
3.3	Model Set-Up.....	132
3.4	Model Scenarios.....	133
3.4.1	Translation of scenarios to model input.....	134
3.4.2	Results and Discussions.....	138
3.5	Conclusions.....	148
	References.....	149

Acknowledgements 151

Appendix 155

List of Tables

Title	Page
Chapter 1	
Table 1.1 List of various methods used to locate and quantify SGD.....	31
Table 1.2 Summary of SGD occurrence and rates throughout the world. Some locations have multiple SGD estimates depending on the method/technique used and some on the timing of measurement.....	38
Table 1.3 Global scale relative contribution of submarine groundwater discharge to freshwater outflow	45
Chapter 2	
Table 2.1 Geologic description of each hydrogeologic group	82
Table 2.2 Model Specifications.....	91
Table 2.3 Hydrologic parameters used in the simulation of the reference case	93
Table 2.4 Summary of inputs for each section/part of the reference case scenario (Scenario 1)	100
Table 2.5 Various scenarios created for the sensitivity analysis.	106
Chapter 3	
Table 3.1 Various scenarios used for the simulation of climate and anthropogenic effects on SGD.....	134

List of Figures

Title	Page
Chapter 1	
Figure 1.1 Simplified hydrologic cycle showing the different components of the hydrologic system and the 2 types of SGD based on source.....	24
Figure 1.2 Diagram of the zone between the coastal aquifer and the ocean illustrating the three pathways of groundwater transport to the continental shelf.	25
Figure 1.3 Schematic depiction (no scale) of processes associated with SGD. Arrows indicate the direction of fluid movement.....	25
Figure 1.4 Map of the world showing the distribution of published studies of SGD. Details can be found in Table 1.2.....	37
Figure 1.5 Major characteristics of the Philippines which make it a key study site for SGD related research. (A) Geological map of the Philippines (B) Population Density, 2000 (C) Slope map of the Philippines	48
Figure 1.6 Embayment in the Philippines with harmful algal bloom occurrences.....	49
Figure 1.7 Photo showing the incident of a milkfish mass mortality in Bolinao, Pangasinan due to harmful algal blooms (HABs) on 02 Feb 2002.....	50
Chapter 2	
Figure 2.1 Regional Setting of Manila Bay. The model area is shown in rectangular orange box, Details in Figure 2.2	68
Figure 2.2 Digital Terrain Model of the model area. Also shown are the different geographical features, including water bodies.....	69

Figure 2.3	Mean monthly rainfall in Limay and Balanga stations. Blue line represents the monthly variation in temperature. Also indicated are the years when the measurements were taken.	70
Figure 2.4	3D surface of the study area with land-use overlay.	71
Figure 2.5	Graph showing the rainfall, calculated average run-off, ET and effective recharge in the study area.	74
Figure 2.6	Extraction wells in the area and corresponding extraction rates in m^3d^{-1}	74
Figure 2.7	(A) Geological Map of Bataan. (B) DEM showing locations of available borehole data, corresponding to the grey dots in Figure 2.7A.	76
Figure 2.8	Interpreted cross-section logs from borehole data.	77
Figure 2.9	Index map showing the swath of seismic track lines of and the area covered by the isopach maps. Numbers indicate the sampling sites used by the authors.	79
Figure 2.10	Seismic reflection profiles across the bay mouth.	80
Figure 2.11	(A) Isopach map of muddy sediments (B) Variations in sand composition (%) of the bay sediments in the study area.	81
Figure 2.12	Representative hydrogeologic profile for the study area. Also shown are the cross section logs used for the interpretation.	83
Figure 2.13	Created 3D (hydro) Geology Model of the study area. (A) Combined cross sections (B) Block model – sea is blanked for a better view of the underlying confining units.	84
Figure 2.14	3D view of the model area showing the model extent in km.	91
Figure 2.15	Mean sea level difference (m). 0 is equivalent to present day msl.	94
Figure 2.16	(Animation) Time series development of the freshwater wedge in the spin-up run (S1-R1) . (A) shows the block model time series concentration development and (B) the representative profile sections for a detailed observation. Time is in years.. Applied translucency = 30%.	97

Figure 2.17	Change in TDS concentration in some observation wells. Conc (i, j, k) is the concentration at observation well location layer, row, column respectively.....	98
Figure 2.18	(A) Initial concentration distribution of Total Dissolved Solids (TDS) (B) The sea is blanked for a better view of the concentrations.....	99
Figure 2.19	Scenario 1 model results – monthly total integrated SGD shoreline flux (in 2005) compared with rainfall and calculated effective recharge. Shaded region corresponds to the time Taniguchi <i>et al.</i> (2008) did the SGD measurements and used as comparison for the subsequent model results analysis.....	101
Figure 2.20	Scenario 1 model results - total integrated shoreline flux year 2005 average compared with Taniguchi <i>et al.</i> (2008) measured SGD flux	102
Figure 2.21	(A) Latitudinal variation of model SGD fluxes compared with radon measurements. (B) Plot of model SGD fluxes vs. distance from the coastline. Location of these transects are the red dots in Figure 2.21A. (model results both extracted from Jan-2005).....	103
Figure 2.22	Distribution of Rn-222 (dpm L ⁻¹) in surface waters along the coast of the Bataan Peninsula and along a shore normal transit out into Manila Bay	104
Figure 2.23	Graph of the resulting 2005 year average total SGD shoreline flux from the different scenarios. Also shown in red is the percentage difference of each sensitivity run result to the reference case. All values are converted to m ³ /day per m shoreline width.....	110
Figure 2.24	Comparison of the different 3D Geology created for the different scenarios and their subsequent influence on the developed freshwater wedge. All 3D concentration plots are extracted from Jan 2005 result. Translucency of 30% is applied to see the form of the wedge.....	112
Figure 2.25	Zoomed concentration screenshots at Y=-3500 at the freshwater-saltwater interface of the different geology scenarios. This location is directly in front of Lucanin River Catchment. On the right side is the same screenshots with the confining units overlain, and sea blanked for better view of concentrations. Arrows indicate direction of water flow.....	113

Chapter 3

Figure 3.1	Global average temperature and CO ₂ concentration since 1880.....	124
Figure 3.2	Trends in sea level rise from 1880 to present derived from tide gauge observations and satellite.....	127
Figure 3.3	Global sea level rise projections. Yellow zone and lines represent the minimum and maximum estimate of sea level rise by the IPCC group in 2007, the red zone and line represents the higher sea level rise projections from other studies	128
Figure 3.4	Locations of available rain gauges in Manila Bay.	135
Figure 3.5	Mean monthly rainfall values at different rain gauge sites. Location of rain gauge stations shown in Figure 3.4	135
Figure 3.6	Procedure to create daily rainfall input for ENSO case. Available mean monthly rainfall data from the study area (Limay rainfall) is combined with the ratio of daily rainfall/mean monthly rainfall from Port Area to obtain a rainfall data for Limay which includes the daily rainfall “signal”.	136
Figure 3.7	Monthly values of the Oceanic Niño Index from 1950 through present.	138
Figure 3.8	(A) Strong El Niño periods (B) Comparison of Scenario 1 and Scenario 6 model SGD flux results (C) Corresponding scenario rainfall input values used for each stress period.....	139
Figure 3.9	(A) Strong La Niña periods (B) Comparison of Scenario 1 and Scenario 6 model SGD flux results (C) Corresponding scenario rainfall input values used for each stress period.....	141
Figure 3.10	(A) Weak and strong La Niña periods (cold episodes) (B) Comparison of Scenario 1 and Scenario 6 model SGD flux results and the corresponding scenario rainfall input values used for each stress period.	142
Figure 3.11	Graph of the resulting 2055 year average total SGD shoreline flux from the different sea level rise scenarios. Also shown in red is the percentage difference of each scenario result to the reference case. All values are converted to m ³ /day per m shoreline width.....	144

Figure 3.12 Graph of the resulting 2055 year average total SGD shoreline flux from the different ant anthropogenic induced scenarios. Also shown in red is the percentage difference of each scenario result to the reference case and in blue to Scenario 7-0 (no sea level rise scenario). All values are converted to m³/day per m shoreline width. 145

Figure 3.13 Comparison of calculated average monthly effective recharge with changing land-use conditions. 145

Figure 3.14 Graph of the resulting 2055 year average total SGD shoreline flux from the different ant combined anthropogenic induced and max sea level rise scenarios. Also shown in red is the percentage difference of each scenario result to the reference case. All values are converted to m³/day per m shoreline width..... 146

List of Appendices

Title	Page
Appendix I: Abbreviations	155
Appendix II: Preparation of MOCDENS3D (MODFLOW and MOC3D) Packages	157
Appendix III: Created Hydrogeologic Profiles.....	199
Appendix IV: Time series development of the freshwater wedge	205

Summary

Submarine groundwater discharge (SGD) has been recognized as a potential direct pathway for water and dissolved nutrients from land to sea. Nutrients of anthropogenic origin, e.g. from septic tanks, agricultural fertilizers or factory wastes, heavy metals, radionuclides and organic compounds find their way to the ocean via SGD. SGD is a widespread phenomenon and might be of ecological significance, since it can play an important role in the marine geochemical cycles of elements and can lead to environmental deterioration of coastal zones especially in areas where its magnitude rivals surface runoff.

Almost all coastal zones are subject to flow of groundwater either as submarine springs or disseminated seepage and with the deteriorating quality of groundwater due to anthropogenic stresses – coastal areas are likely to experience environmental degradation. Occurrences can result in coastal eutrophication, bacterial development, viruses, hypoxia, increase of algal blooms and harmful algal blooms (red tide), marine biota, fish/shellfish mortality and even human casualties. The effects associated with nutrients via SGD are biological, economical and social, thus SGD is a phenomenon which cannot be taken for granted. Understanding the mechanism behind its occurrence and the factors influencing it are all important especially to coastal management.

This thesis examined the different hydrogeologic processes and factors which influence the magnitude of SGD flux, also the effects of changing climate conditions, sea level rise and how anthropogenic induced factors influence the SGD.

The selected study area is located on the Southeastern coast of the Bataan Peninsula in the Philippines. It is situated on the SE slopes of Mt. Mariveles, a potentially active stratovolcano. The area stretches on 12 km of coastline where preliminary SGD flux measurements were made earlier.

A regional scale modular variable-density groundwater flow model (MOCDENS3D) has been used to estimate the magnitude of submarine groundwater discharge to Manila Bay (**Chapter 2**). Key features of the groundwater system include high relief in the upper slopes and narrow low relief coastal plain. The model domain incorporates both the terrestrial recharge and re-circulated water in the coastal sediments. Different scenarios were run to evaluate the sensitivity of SGD to different hydrogeologic parameters, e.g. changes in geology, topography, also the changes in water sources and sinks such as rainfall, rivers, and groundwater extraction wells.

Model results are consistent with previously measured SGD rates using seepage meters and geochemical tracers by [Taniguchi *et al.* \(2008\)](#). Simulations results show that significant SGD from terrestrial origin discharges to Manila Bay from the southeastern flank of Mt. Mariveles as a consequence of the steep topography, geology and high rainfall conditions. There's also a marine component (sea-water recirculation) in the SGD flux result but its contribution is difficult to quantify.

Model SGD rates peak during the rainy season and there's a month delay to the peak rainfall, this shows the major influence of rainfall (recharge) on the SGD flux. Sensitivity

analysis results allow the quantification of the major influence of geology especially the presence of confining units, topography and other hydrogeological parameters on SGD fluxes. The presence of confining layers greatly affects the offshore extent of SGD, and therefore its potential impact on the regional environment.

The modeling is extended to incorporate the effects of changing climate conditions (ENSO), sea level rise, and anthropogenic induced changes, such as changes in land-use and groundwater extraction to the magnitude of SGD flux in **Chapter 3**. El Niño–Southern Oscillation (ENSO) alters rates of precipitation evapotranspiration, and soil moisture patterns; sea level rise influences the freshwater heads, and groundwater concentrations; excessive pumping of ground water lowers the level of the water table and removes water from storage in the aquifer; and land-use modifications, changes the amount of groundwater recharge by altering the infiltration rates. To determine how these factors affect the magnitude of SGD, several scenarios were developed. These simulations are a continuation of those presented in **Chapter 2**, thus the same physical and hydrological parameters, and boundary conditions as in the reference case (**Scenario 1**) are implemented in the model, otherwise indicated to be different.

ENSO affects SGD fluxes in two different ways. During El Niño, the SGD fluxes are significantly reduced at an average of 7% change. La Niña does not change or influence the SGD flux greatly. High amounts of rain poured during La Nina are just flushed out of the system through the drains. The geology determines the capacity of water that can be handled by the aquifer and thus as long as there is no change in the geology, there is a limit to the amount of

water that the system can handle. Sea level rise have a minor effect on the SGD fluxes, lowering of SGD fluxes by 2-3% depending on the height of sea level rise. Excessive groundwater extraction and land-use changes can greatly influence the magnitude of SGD flux especially when combined with sea level rise resulting to 8-10% change in the SGD fluxes by year 2055.

This study enabled the first 3D approach and representation of SGD systems, resulting in a more realistic model, and therefore in a better understanding of the underlying mechanisms. Data from field campaigns ideally should be coupled to hydrogeological modeling in order to establish key control factors of SGD rates and to ultimately allow coupling water fluxes to nutrient fluxes.

Chapter 1

Introduction



Image: Mt. Mariveles Volcano viewed from the sea (Source: Dr. Fernando Siringan)

1.1 Background

Submarine groundwater discharge (SGD) has been recognized as a potential direct pathway for water and dissolved nutrients from land to sea (Johannes, 1980; Charette, 2001; Slomp and van Cappellen, 2004; Dürr *et al.*, 2008; Spiteri *et al.*, 2008). Nutrients of anthropogenic origin, e.g. from septic tanks, agricultural fertilizers or factory wastes, heavy metals, radionuclides and organic compounds find their way to the ocean via SGD. SGD is a widespread phenomenon and might be of ecological significance, since it can play an important role in the marine geochemical cycles of elements and can lead to environmental deterioration of coastal zones especially in areas where its magnitude rivals surface runoff. Although of great importance, assessing groundwater fluxes and their impacts on the near-shore marine environment is still much more difficult compared to river fluxes, as there is no simple means to directly measure these fluxes to the sea. Major rivers however can be gauged and well analyzed, thus allowing relatively precise estimates of freshwater and contaminant inputs to the ocean. Another issue is the cultural and disciplinary differences between hydrogeologists and coastal oceanographers which have inhibited interactions.

Almost all coastal zones are subject to flow of groundwater either as submarine springs or disseminated seepage and with the deteriorating quality of groundwater due to anthropogenic stresses – coastal areas are likely to experience environmental degradation (Burnett *et al.*, 2006). Occurrences can result in coastal eutrophication, bacterial development, viruses, hypoxia, increase of algal blooms and harmful algal blooms (commonly known as “red

tide”), marine biota, fish/shellfish mortality and even human casualties. The effects associated with nutrients via SGD are biological, economical and social, thus SGD is a phenomenon which cannot be taken for granted. Understanding the mechanism behind its occurrence and the factors influencing it are all important especially to coastal management.

1.2 Definition of Submarine Groundwater Discharge

SGD’s definition is rather vague and has been used in different ways. [Zekster *et al.*, \(1983\)](#) defined it as the net groundwater discharge which is essentially the groundwater coming from recharge. On the other hand, [Church \(1996\)](#) defined it as the direct groundwater outflow from land to sea which includes the re-circulated SGD component (RSGD). Because of this confusion, several misunderstandings arise as noted by [Taniguchi and Iwakawa \(2004\)](#) when comparing SGD to freshwater discharges, SGD hydrological model results and oceanographic mass balances.

In this research, SGD will follow the definition of [Li *et al.* \(1999\)](#), [Church \(1996\)](#) and [Taniguchi *et al.* \(2002\)](#) which represents the total groundwater discharge i.e. all direct discharge of subsurface fluids from land to the sea. The total SGD includes 2 major components based on source: (1) freshwater SGD and (2) re-circulated SGD ([Figure 1.1](#)). The freshwater component SGD comes directly from the effective recharge on land, while the re-circulated component is derived from several mechanisms such as wave set up, tidally driven oscillation, and convection (either density or thermal) ([Taniguchi *et al.*, 2002](#)). The separation of the re-

circulated and freshwater components of SGD is essential, since only the freshwater component represents a net input to the marine environment (Dürr *et al.*, 2008) and is the only source of calculated SGD fluxes in most hydrological models.

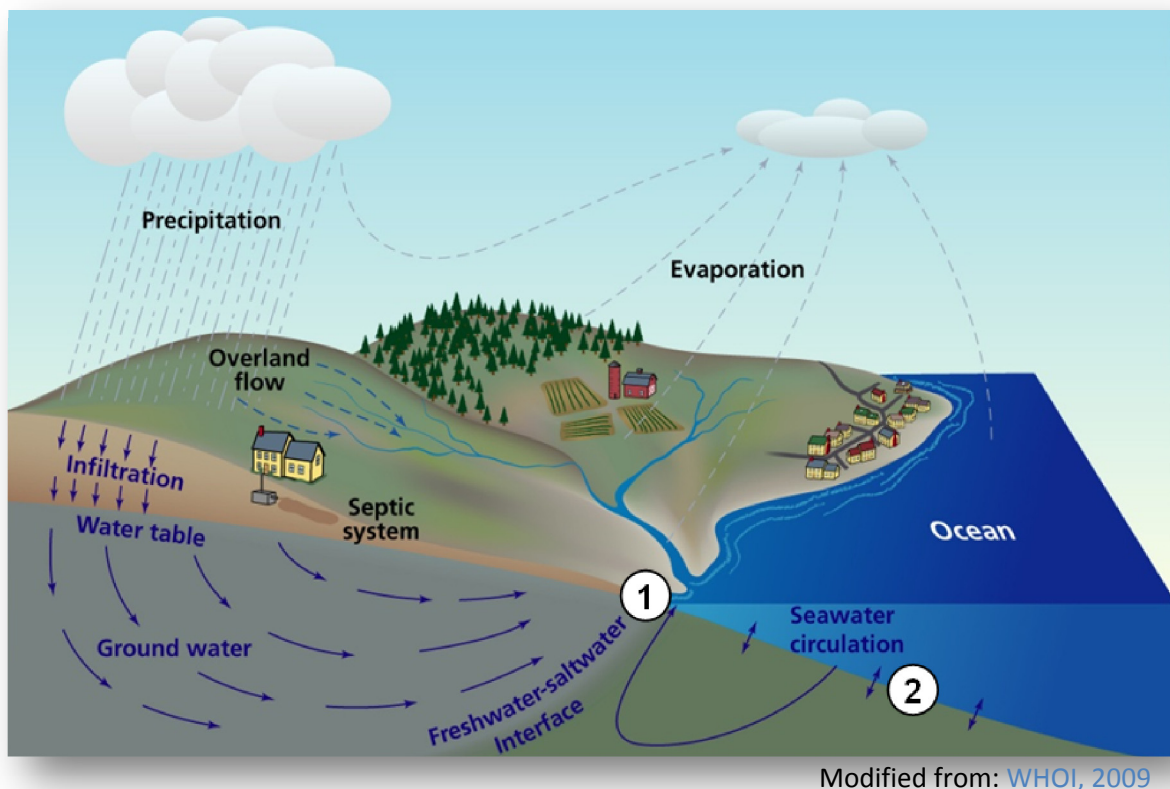
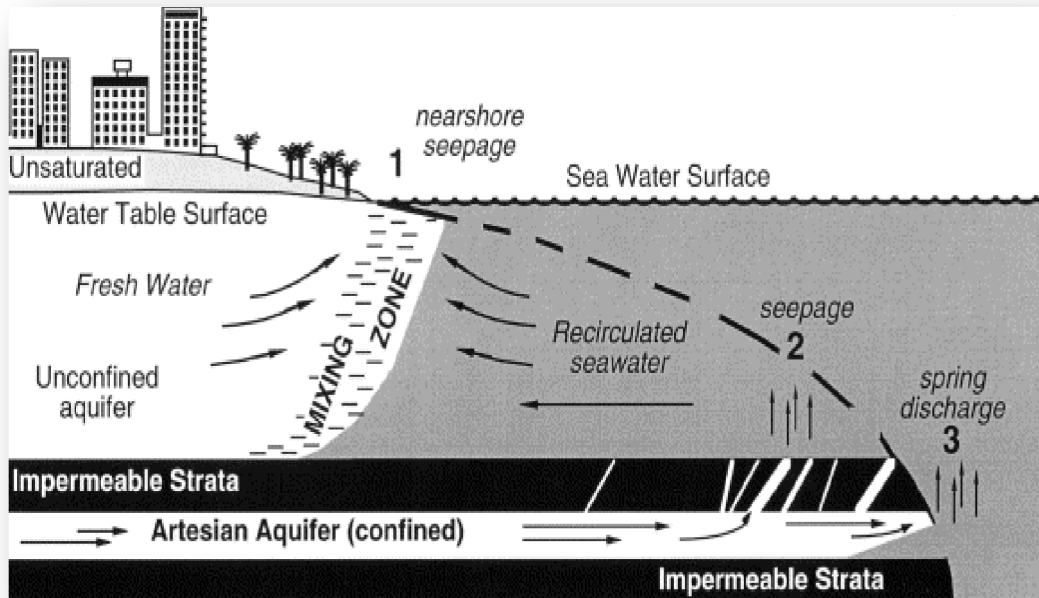


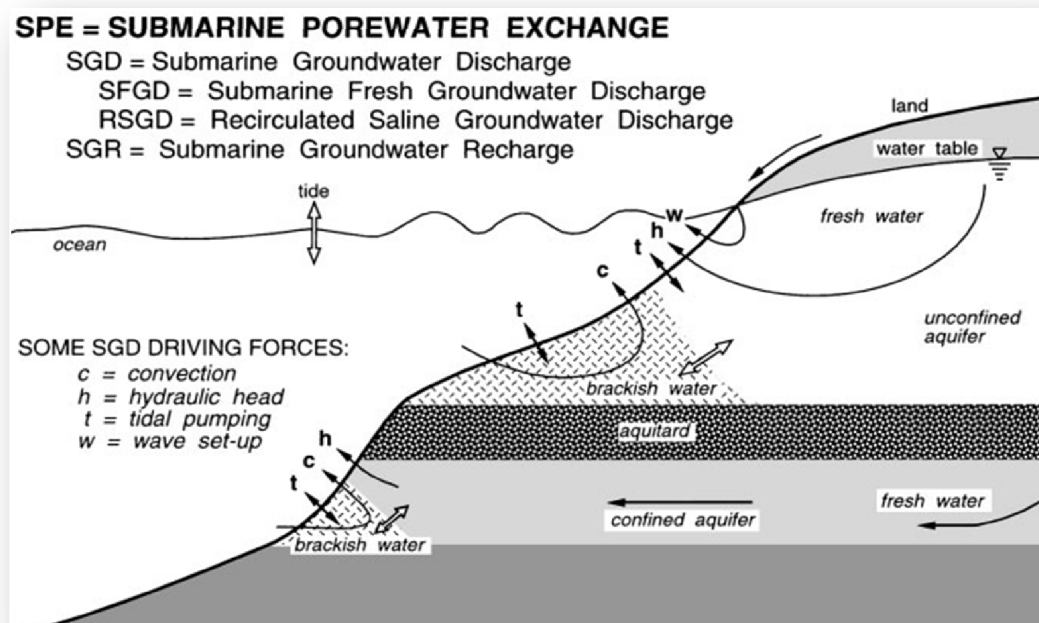
Figure 1.1 Simplified hydrologic cycle showing the different components of the hydrologic system and the 2 types of SGD based on source.

There are 3 pathways for SGD (Figure 1.2): (1) near shore seepage, (2) seepage through a break in the confining bed of an underlying aquifer, and (3) submarine spring discharge (Burnett *et al.*, 2001).



Source: Burnett *et al.*, 2001

Figure 1.2 Diagram of the zone between the coastal aquifer and the ocean illustrating the three pathways of groundwater transport to the continental shelf.



Source: Taniguchi *et al.*, 2002

Figure 1.3 Schematic depiction (no scale) of processes associated with SGD. Arrows indicate the direction of fluid movement.

1.3 Driving mechanism of SGD

The driving mechanisms of SGD can be subdivided in two groups: terrestrial and marine (Figure 1.3). The terrestrial components are: (1) the hydraulic gradient, also called the Darcy slope, used to determine the discharge (Darcy flux), which is a result of the difference in pressure head. This difference determines in which direction the water should flow. The relationship is shown by the equation:

$$i = \frac{dh}{dl} = \frac{h_1 - h_2}{length}$$

where i is the hydraulic gradient (dimensionless), dh is the difference between two hydraulic heads (length, usually in m or ft), and dl is the flow path length between the two piezometers (length, usually in m or ft); (2) Water level differences across a permeable barrier which is known to induce subterranean flow – Examples are the narrow reefs of the Florida Keys (Reich *et al.*, 2002; Chanton *et al.*, 2003) and barrier islands of Fire Island, New York (Bokuniewicz and Pavlik, 1990); and (3) Geothermal heating.

The marine components include (1) Tidal pumping (Riedl *et al.*, 1972; Nielsen, 1990); (2) Wave action which induce pressure gradients at the shore (Li *et al.*, 1999); (3) Large storms (Moore and Wilson, 2005); (4) Current induced pressure gradients which happens over topographic expressions such as sand ripples (Huettel and Gust, 1992; Huettel *et al.*, 1996); and (5) Convection (salt-fingering) (Webster *et al.*, 1996).

1.4 Interests and Issues Related to SGD

SGD is a subterranean non-point pathway of material transport, (Moore, 1999; Charette and Sholkovitz, 2002) diffuse, temporally variable, and may involve multiple aquifers, thus reliable methods to measure these fluxes need to be refined and the relative importance of the processes driving the flow needs clarification and quantification (Burnett *et al.*, 2006). The different methods used to measure SGD will be summarized in **Section 1.5**.

“It is clear that submarine groundwater discharge is widespread and, in some areas, of greater ecological significance than surface run off” (Johannes, 1980). There are different ecological significance and impacts related to SGD. SGD has initially been studied as a freshwater resource and is still now being considered for this potential in some coastal areas (Zekster, 1996). In the recent years however, the ecological studies related to SGD have been concentrated on its nutrient and material content due to several environmental concerns.

Some areas such as the Florida Keys and Hawaii, low nutrient freshwater SGD is a requirement for marine organisms e.g. corals, hydrophytes and mangroves growth (Oki *et al.*, 1999; Porter *et al.*, 2002; Grossman *et al.*, 2008). SGD is a primary factor for coral reef health and growth in the Florida Keys (Porter *et al.*, 2002) and along the arid Kona coast in the island of Hawaii (Grossman *et al.*, 2008). Anchialine ponds and other wetland biota can also be dependent on nutrients supplied by SGD (Presto *et al.*, 2007). Along the coast of Kaloko-Honokōhau (KAHO) Hawaii, urban development since 1978 lead to increased groundwater withdrawals for city fresh water supply, resulting in decreased groundwater (SGD) flux to the

coast by 50%, threatening the SGD-dependant coastal communities in the area ([Oki et al., 1999](#)). These key sites show the importance of SGD to marine biota and make them vulnerable to any change that can happen to it, both in terms of quantity and quality.

Nitrogen inputs via SGD are important to the overall nutrient budget of salt marshes ([Valiela et al., 2002](#)). In the Eastern Florida Bay, it was estimated that the SGD nutrient inputs are almost equal to the surface run-off ([Corbette et al., 1999](#); [Charette et al., 2006](#)). The estimated SGD nutrient flux to the salt marshes in South Carolina exceeds those that can be derived from all the South Carolina Rivers altogether ([Krest et al., 2000](#)). In the Great South Bay, New York, SGD accounts for >20% of freshwater input ([Bokuniewicz, 1980](#); [Bokuniewicz and Pavlik, 1990](#)) and contributes to approximately 50% of the nitrate input into the bay ([Capone and Bautista, 1985](#); [Capone and Slater, 1990](#)). Significant inputs of nitrogen and dissolved organic phosphorus from groundwater have been observed by [Lapointe et al. \(1990\)](#) in the Florida Keys. In many of the cases cited above, the high nitrogen concentrations can be because of contamination from household septic systems and fertilizers from agricultural lands.

High nutrient SGD to coastal waters can strongly influence productivity and can result in coastal eutrophication, hypoxia and may trigger algae blooms, including harmful algal blooms, having negative impacts on the economy of coastal zones ([LaRoche et al., 1997](#); [Paerl, 1997](#); [Hussain et al., 1999](#); [Gobler and Sanudo-Wilhelmy, 2001](#); [Kim et al., 2003](#); [Hwang et al., 2005](#); [Hu et al., 2006](#); [Lee and Kim, 2006](#)). Specific examples include the coastal eutrophication in the coral reef lagoons in Mauritius ([Paytan et al., 2004](#)); HABs in Florida, USA ([Hu et al., 2006](#)),

Southern Sea, South Korea (Lee and Kim, 2006), and Manila Bay, Philippines (Taniguchi *et al.*, 2008)

SGD supplied nutrients have also been related to increase bacterial concentrations in coastal waters resulting to massive mortalities of benthic and marine organisms, indirectly affecting the organisms depending on them e.g. birds (Boehm *et al.*, 2004; Boehm *et al.*, 2006); Pathogenic bacteria and viruses which causes acute gastrointestinal illness in humans have been also related to SGD (Paytan *et al.*, 2004).

1.5 Quantify and Qualify SGD

1.5.1 Historical Overview

Although fairly recent in terms of popularity, the knowledge of SGD has been around for decades. According to Kohout (1966), Strabo, who lived from 63 BC to 21 AD, mentioned the submarine springs 2.5 miles off-shore from Latakia, Syria in the Mediterranean. Another historical account tells of water vendors in Bahrain collecting potable water from off-shore submarine springs for shipboard and land use (Williams, 1946). Etruscan citizens using coastal springs for “hot baths” (Pausanius, ca. 2nd century AD), and submarine “springs bubbling freshwater as if from pipes” along the Black Sea (Pliny the Elder, ca. 1st century AD) (*in* Burnett *et al.*, 2006).

Some physical concepts which lead to the awareness of SGD include the findings of Newell *et al.* (1953) where from an ecological perspective found that seawater can and does

cycle in advective way through sediments due to the fresh groundwater hydraulic head; the idea of mixing zone or zone of dispersion conceptualized by [Cooper \(1959\)](#); quantitative corroboration of Cooper's hypothesis and the use of the advection-diffusion equation to account for hydrodynamic dispersion by [Henry \(1959, 1964\)](#); and the idea and quantification of continuous cycling of seawater as a result of hydrodynamic dispersion by [Kohout \(1960, 1964\)](#). Follow up studies by [Kohout \(1965, 1967, 1977\)](#) postulated thermal convection as a possible mechanism for seawater circulation in the Floridian plateau.

[Manheim \(1967\)](#) identified a localized SGD in the Southeastern Atlantic Coast. Subsequent developments later on focus on the identification and quantification of the different driving mechanism for SGD such as: the significance of surf action on movement of seawater through marine sediments in intertidal and sub tidal zone of a sandy beach ([Riedl, 1971](#); [Reidl and Machan, 1972](#)); sub tidal pumping resulting to seawater circulation ([Riedl, 1972](#)); saline fluid convection as a mechanism of seawater cycling, reflux and cycling along mixing zones ([Simms, 1984](#)); and the advective cycling of seawater through sediments due to fresh groundwater head ([Reilly and Goodman, 1985](#)).

Table 1.1 List of various methods used to locate and quantify SGD. (Modified from: Spiteri, 2006)

Method	Description	Additional comments	References
Remote Sensing			
Aerial Thermal Imagery	Exploits seasonal temperature differences between groundwater, with a relatively constant temperature throughout the year and surface water with a seasonally-variable temperature.	Advantage: -Used as a proxy to locate hot spots of SGD prior to field measurements	Portnoy <i>et al.</i> , 1998; Miller and Ullman 2004; Mulligan and Charette, 2006
Tracer Studies			
Salinity/conductivity	Tracing of low-salinity freshwater into more saline receiving coastal waters	Most obvious tracers for locating SGD	Breier <i>et al.</i> , 2005; Stieglitz, 2005
Temperature	Analysis of temperature-depth sediment profiles		Taniguchi <i>et al.</i> , 2003; 2006
Radium isotopes (^{223}Ra , ^{224}Ra , ^{226}Ra and ^{228}Ra)	Ra absorbed onto charged surfaces of mineral grains but is liberated upon exposure to seawater, leading to higher Ra concentrations in SGD than in the receiving coastal waters.	Natural isotopes generated in the uranium-thorium decay series, widely used to identify SGD at the local to regional scale. Often include the re-circulated seawater component as well. Advantage: -Ra isotopes (as well as tracers in general) provide an integrated	e.g., Charette <i>et al.</i> , 2001; Abraham <i>et al.</i> , 2003; Crotwell and Moore, 2003; Breier <i>et al.</i> , 2005; Boehm <i>et al.</i> , 2006; Moore, 2006; Paytan <i>et al.</i> , 2006; Shellenbarger <i>et al.</i> , 2006; Windom <i>et al.</i> , 2006

		estimate of SGD over a large area, smoothing out small-scale temporal and spatial variability.	
Radon-222	The Rn formed by the decay of dissolved and particle-bound Ra is transported as a dissolved gas within the groundwater, resulting in a progressive enrichment of Rn in groundwater prior to discharge. Being a noble gas, Rn is highly unreactive and conservative.	Disadvantage: -Subject to losses at the air-sea interface which may limit its use in shallow water environments (Burnett et al., 2003b)	Stieglitz, 2005 ; Burnett and Dulaiova, 2006 ; Povinec et al., 2006
Others: (1) barium (2) uraniumthorium-series nuclides (3) fluorescein (4) sulfur		hexafluoride (SF6) SF6 often used in systems with high groundwater velocities and discharge rates.	(1) Shaw et al., 1998 (2) Porcelli and Swarzenski, 2003 (3) Corbett et al., 2000 (4) Dillon et al., 1999
Seepage Meters			
Manual seepage meters	Measurement of the volume of water entering the plastic collection bag over a known time and area and calculation of the average flow rate of fluid across the sediment-water boundary.	Advantage: -Inexpensive, point measurement of SGD.	Giblin and Gaines, 1990 ; Portnoy et al., 1998 ; Michael et al., 2005
Automated seepage meters: (1) dye-dilution (2) thermal (3) ultrasonic		Advantage: -Less labor-intensive than conventional seepage meters.	(1) Sholkovitz et al., 2003 (2) Taniguchi and Iwakawa, 2001 (3) Paulsen et al., 2001

Hydrological Methods			
Darcy's Law	$Q = -KA \frac{dh}{dl}$ <p>where Q - groundwater discharge (L^3T^{-1}) K - hydraulic conductivity (LT^{-1}) A - cross-sectional (L^2) $\frac{dh}{dl}$ - hydraulic gradient (-) derived from the hydraulic head, h (L), measured in at least two piezometers separated by a distance, l (L).</p>	<p>Disadvantages:</p> <p>-The hydraulic conductivity often varies by orders of magnitude within an aquifer and thus averaged values might not always be representative.</p> <p>-Since piezometers, (as well as seepage meters), provide a very local estimate, many meters are usually needed to resolve the temporal and spatial variability of the discharge measurements. In fact, piezometer nests are often used in conjunction with seepage meters to get hydraulic conductivity estimates from the observed seepage rates and hydraulic gradient.</p>	e.g. Giblin and Gaines, 1990
Water balance method	Estimation of the freshwater SGD as the difference between all long-term averaged input and outputs of water flow through a groundwater shed, represented mathematically as:	Mostly used for global-scale estimates of SGD.	Oberdorfer et al., 1990 ; Taniguchi et al., 2005

	$FSGD = P - E_T - D_S - dS$ <p>where P - precipitation E_T - evapotranspiration D_S - surface discharge dS - change in the water storage assumed to ~ 0 over long time scales.</p>		
Hydrograph separation	<p>Estimation of the freshwater SGD based on the assumption that discharges along the shoreline is the same as the base flow of a stream or river.</p> <p>Commonly used by Russian scientists to quantify continental and global SGD.</p>	<p>Disadvantage: -Although relatively simple, it (as well as the water balance method) is typically inaccurate, since the uncertainties associated to the specified components are often on the same order of magnitude as the freshwater discharge itself</p>	<p>Zektser et al., 1973; Zektser and Dzhamalov, 1981</p>
Numerical Modeling			
Variable-density flow models	<p>Since there are no analytical solutions for non-trivial density driven flow problems, solutions can only be obtained with numerical methods (Holzbecher, 1998).</p>	<p>Originally developed to predict saltwater intrusion (Reilly and Goodman, 1985; Oude Essink, 1998; Bobba, 1993).</p> <p>Advantage: -Small-scale temporal complexities, such as tidal pumping and spatial heterogeneities in aquifers can</p>	<p>Oude Essink, 1998; Uchiyama et al., 2000; Kaleris et al., 2002; Langevin, 2003; Destouni and Prieto, 2003; Smith, 2004; Michael, 2004; Robinson et al., 2007</p>

		<p>also be incorporated.</p> <p>Disadvantages:</p> <ul style="list-style-type: none">-The required small time stepping, fine grid spacing and coupled iterative simulations increase the computational demands drastically. A compromise between the degree of spatial and temporal detail and computation capabilities must be found based on the scope of the investigation.-Accurate quantification of SGD is often hampered by insufficient field data (Loaiciga and Zektser, 2003).	
--	--	---	--

1.5.2 SGD Measuring Techniques

More recent studies made on SGD are primarily devoted to developing and adapting new tracer techniques and methods for the identification and quantification of SGD. [Table 1.1](#) shows the different techniques used to locate and quantify SGD. It is difficult to quantify SGD because until now there are no methods available to directly measure the SGD flux, all of the methods summarized in [Table 1.1](#) are indirect requiring several assumptions and having large uncertainties. To increase the confidence in the SGD value determined, multiple methods should be used. Measured fluxes coupled with hydrogeologic modeling can be the best approach.

Choosing the type of method to quantify SGD is largely dependent on the type of data, time, resources available, and most importantly the purpose of the investigation. Different methods have different requirements, scale, advantages, disadvantages and measure different SGD components.

Different techniques will measure fresh SGD or re-circulated SGD or both, therefore it is important to determine what component of SGD is being measured ([Oberdofer, 2003](#)). [Garrison et al. \(2003\)](#) distinguish the fresh and re-circulated seawater components. Most hydrogeologic modeling techniques and CTD profiling have been only applied to the freshwater SGD component and thus results from this 2 methods can be compared ([Oberdofer, 2003](#)). Seepage meter measurements can result from either fresh or re-circulated SGD component and therefore care has to be taken when comparing it to hydrogeologic models. Scale is also

another important factor to be taken into account. Modeling, CTD profiles, and radium determinations are applied on regional scale whereas seepage meter and radon measurements tend to be more localized to a given portion of shoreline, and so the results from these techniques can be less or exceed those that result from regional models.

The ultimate factor in determining the type of technique to be used in the SGD quantification is the purpose of the investigation. If the purpose of the investigation is to determine the terrestrial input of SGD to the coastal zone, then techniques that can distinguish freshwater inputs should be used. If the purpose is to determine the nutrient budget, then techniques which give the total input of SGD should be used. However, it is important still to separate the freshwater and re-circulated component of SGD even for this purpose since the freshwater SGD gives the net input of nutrients to the marine environment.

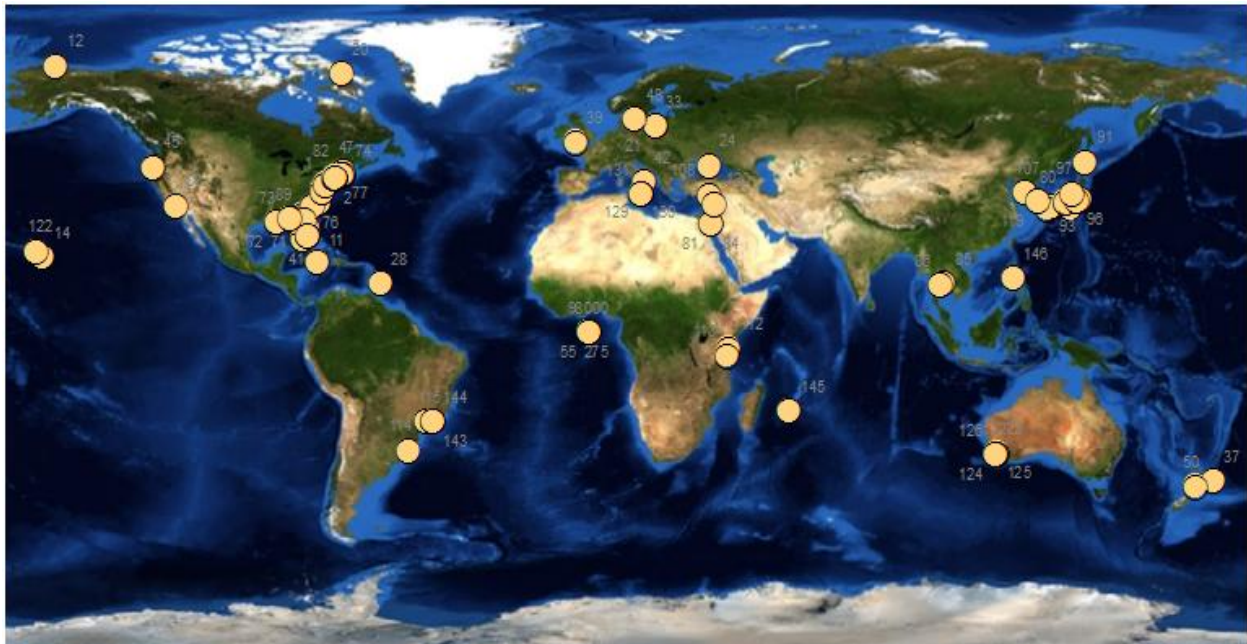


Figure 1.4 Map of the world showing the distribution of published studies of SGD. Details can be found in [Table 1.2](#).

Table 1.2 Summary of SGD occurrence and rates throughout the world. Some locations have multiple SGD estimates depending on the method/technique used and some on the timing of measurement.

Location	SGD flux	Method	Reference
Crescent, FL	42 m ³ s ⁻¹ (1500 ft ³ s ⁻¹)	Salinity	Brooks (1961)
Hawaii Island	10-100 million gallons day ⁻¹	Thermal image analysis	Fischer <i>et al.</i> (1964)
Italy	Unknown	Salinity, water quality	Burdon (1964)
Florida coast, USA	No data	Boreholes, sampling	Kohout (1966)
Mediterranean	Unknown	Salinity	Kohout (1966)
East coast, FL Peninsula	Unknown	Seafloor coring, salinity	Manheim (1967)
Hawke Bay, New Zealand	Unknown	Sea temperature, salinity	Ridgway and Stanton (1969)
Golden Bay, New Zealand	Unknown	Water quality	Williams (1977)
Great South Bay, NY	40 liters day ⁻¹ m ⁻²	Seepage meter	Bokuniewicz (1980)
Perth, Australia	Unknown	Nitrate	Johannes (1980)
Discovery Bay, Jamaica	Unknown	Nitrate	D'Elia <i>et al.</i> (1981)
Off the coast, GA	Unknown	Seafloor coring, salinity	Manheim and Paull (1981)
West FL	25 liters s ⁻¹	Flow meter on the drum placed over the vent	Fanning <i>et al.</i> (1981)
Black Sea, Crimea	Unknown	Salinity, ²²² Rn	Kir'yakov <i>et al.</i> (1983)
Baffin Island, Canada	0.34 m ³ s ⁻¹	Remote acoustic imaging of the plume	Hay (1984)
Off the coast, NJ	Unknown	Side-scan sonar image	Robb (1984)
Off the west coast, FL Peninsula	Unknown	Temperature, water quality, biological community	Paull <i>et al.</i> (1984)
East coast of FL (Indian River Lagoon)	(0.77-1.03) x 10e ⁻⁶ m s ⁻¹	Seepage meter	Zimmermann <i>et al.</i> (1985)
Great South Bay, NY	3.6–18.3 m ³ m ⁻² yr ⁻¹	Sediment chemistry	Capone and Bautista (1985)
Perth, Australia	4.8 x 10e ⁴ m ³ day ⁻¹	Salinity	Johannes and Hearn (1985)
Plymouth, UK	Unknown	Thermal image analysis	Roxburgh (1985)

Barbados, West Indies	$(8.5-14.4) \times 10e^{-4} \text{ cm s}^{-1}$	Seepage meter, Piezometer	Lewis (1987)
Salt marsh estuaries, SC	$0.15-0.75 \text{ liters m}^{-2} \text{ h}^{-1}$	Seepage meter	Whiting and Childers (1989)
Nankai wedge, Japan	0.27 m day^{-1}	Temperature	Henry <i>et al.</i> (1989); Lallemand <i>et al.</i> (1992)
Cape Cod, MA	$(4.3 - 5.5) \times 10e^4 \text{ m}^3 \text{ day}^{-1}$	Seepage meter	Giblin and Gaines (1990)
Cape Cod, MA	$(0.94 - 1.2) \times 10e^4 \text{ m}^3 \text{ day}^{-1}$	Water balance	Giblin and Gaines (1990)
Cape Cod, MA	$(4.4 - 8.9) \times 10e^4 \text{ m}^3 \text{ day}^{-1}$	Salinity budget	Giblin and Gaines (1990)
Cape Cod, MA	$0.79 \times 10e^4 \text{ m}^3 \text{ day}^{-1}$	Hydraulic dynamics	Giblin and Gaines (1990)
Coastal bays of New England	$2 - 4 \text{ liters m}^{-2} \text{ h}^{-1}$	Salinity, seepage meter	Valiela <i>et al.</i> (1990)
Buttermilk Bay, MA	19 cm d^{-1}	Darcy's law/water balance	Weiskel and Howes (1991)
Laholm Bay, Sweden	75 m year^{-1}	Seepage meter	Vanek and Lee (1991)
Chesapeake Bay, VA	$0.02 - 3.69 \text{ l m}^{-2} \text{ h}^{-1}$	Seepage meter	Reay <i>et al.</i> (1992)
North Slope of AK	0.07 m year^{-1}	Heat flow	Deming <i>et al.</i> (1992)
Off the coast, FL Keys	$5.4 - 8.9 \text{ liters m}^{-2} \text{ day}^{-1}$	Seepage meter	Simmons (1992)
Off the coast, Wilmington (NC)	$6 - 20 \text{ liters m}^{-2} \text{ day}^{-1}$	Seepage meter	Simmons (1992)
Onslow Bay	$0.6 - 2.0 \text{ cm d}^{-1}$	Seepage meter	Simmons (1992)
Off the coast, OR	Unknown	Side-scan sonar image, biological community	Tobin <i>et al.</i> (1993)
Puck Bay, Baltic Sea	Unknown	Temperature, Conductivity	Jankowska <i>et al.</i> (1994)
Beppu, Japan	Unknown	Temperature, water quality	Kohno and Tagawa (1996)
Capo Palinuro, Italy	Unknown	Geochemistry	Stuben <i>et al.</i> (1996)
Chesapeake Bay, MD	Unknown	Thermal image analysis	Banks <i>et al.</i> (1996)
Chesapeake Bay, USA	$2.7 \times 10^7 \text{ m}^3 \text{ day}^{-1}$	^{222}Rn	Hussain <i>et al.</i> (1999)
Chesapeake Bay, VA	$0.63 \text{ liters m}^{-2} \text{ h}^{-1}$ (including 65% re-circulated water)	Seepage meter	Gallagher <i>et al.</i> (1996)
Mississippi Delta	1.0 cm d^{-1}	$^{226}, ^{228}\text{Ra}$	Krest <i>et al.</i> (1999)
NE coast Gulf of Mexico, USA	$2.5 \times 10^4 - 9.9 \times 10^4 \text{ m}^3 \text{ day}^{-1} \text{ km}^{-2}$	^{222}Rn , CH_4	Cable <i>et al.</i> (1996)
Northeast Gulf of Mexico	$1.4 - 11.5 \text{ cm d}^{-1}$	CH_4	Bugna <i>et al.</i> (1996)
Northeast Gulf of Mexico	$2 - 10 \text{ cm d}^{-1}$	Radon	Cable <i>et al.</i> (1996a)

Northeast Gulf of Mexico	1.4 – 11.5 cm d ⁻¹	Radon and CH ₄	Cable <i>et al.</i> (1996b)
Northeast Gulf of Mexico, FL	10 - 80 ml m ⁻² min ⁻¹	Seepage meter	Bugna <i>et al.</i> (1996)
Northeast Gulf of Mexico, FL	10 - 80 ml m ⁻² min ⁻¹	Seepage meter	Cable <i>et al.</i> (1996a)
Northeast Gulf of Mexico, FL	180 - 710 m ³ s ⁻¹ / 500 m ³ s ⁻¹	Rn, Ra	Cable <i>et al.</i> (1996b)
Off the coast, SC	350 m ³ s ⁻¹	Ra	Moore (1996)
Oita Prefecture, Japan	No data	Temperature, electrical conductivity, video	Kohno and Tagawa (1996)
Puck Bay, Baltic Sea	4.7 liters s ⁻¹ km ⁻²	Nutrient, isotope	Piekarek-Jankowska (1996)
Sagami Bay, Japan	310-500 m ³ day ⁻¹ (area: 2 km ²)	Heat flow, chemical composition	Tsunogai <i>et al.</i> (1996)
Sagami Bay, Japan	310–500 m ³ day ⁻¹	Geochemistry, heat flow	Tsunogai <i>et al.</i> (1996)
South Atlantic Bight	350 m ³ s ⁻¹	²²⁶ Ra	Moore (1996)
Northeast Gulf of Mexico	2 – 24 L m ⁻¹ min ⁻¹	Seepage meter	Cable <i>et al.</i> (1997)
Northeast Gulf of Mexico, FL	0.23 - 4.4 m ³ s ⁻¹	Seepage meter	Cable <i>et al.</i> (1997a)
Northeast Gulf of Mexico, FL	17.7 ml m ⁻² min ⁻¹	Seepage meter	Cable <i>et al.</i> (1997b)
Crescent Beach, FL, USA	2.6×10 ⁴ – 7.3×10 ⁵ m ³ day ⁻¹	Boreholes, sampling	FGS (1998)
Nauset Marsh, MA	72 cm d ⁻¹	seepage chambers/aerial thermal imagery	Portnoy <i>et al.</i> (1998)
NE coastal Gulf of Mexico, FL	1 - 10 liters m ⁻² day ⁻¹	Seepage meters, numerical modeling	Rasmussen (1998)
NE coastal Gulf of Mexico, FL	4.5 - 7.3 liters m ⁻² day ⁻¹	Seepage meters, numerical modeling	Rasmussen (1998)
Northeast Gulf of Mexico	0.1 – 1.0 cm d ⁻¹	Seepage meter	Rasmussen (1998)
Suruga Bay, Japan	No data	Carbon isotopes	Tsunogai <i>et al.</i> (1998)
Tokyo Bay, Japan	0.03 - 0.42 m year ⁻¹	Groundwater temperature depth profiles	Taniguchi <i>et al.</i> (1998)
Tokyo Bay, Japan	8.2×10 ⁻⁵ – 1.1×10 ⁻³ m day ⁻¹	Temperature	Taniguchi <i>et al.</i> (1998)
Biscayne Bay/Florida Bay	1 – 3 cm d ⁻¹	Seepage meter	Corbett <i>et al.</i> (1999)
Eastern Florida Bay, FL	1.93 cm d ⁻¹	seepage meters/radon	Corbett <i>et al.</i> (1999)

Keys and Florida Bay, FL	7.2 - 21.2 ml m ⁻² min ⁻¹	Seepage meter	Corbett <i>et al.</i> (1999)
Biscayne Bay/Florida Bay	1.7 ± 0.3 cm d ⁻¹	CH ₄ , Radon	Corbett <i>et al.</i> (2000a)
North Inlet SC	3.15 cm d ⁻¹	radium isotopes	Krest <i>et al.</i> (2000)
South of Osaka Bay, Japan	(1.4 - 4.3) x 10e ⁻⁴ cm s ⁻¹	Seepage meter	Taniguchi (2000)
Biscayne Bay/Florida Bay	6.8 - 10.5 cm d ⁻¹	H/He	Top <i>et al.</i> (2001)
Biscayne Bay/Florida Bay	1.2 - 1.7 cm d ⁻¹	Radon	Top <i>et al.</i> (2001)
Biscayne Bay/Florida Bay	1.2 - 1.7 cm d ⁻¹	Radon	Top <i>et al.</i> (2001)
Waquoit Bay, MA	0.9 cm d ⁻¹	radium isotopes	Charette <i>et al.</i> (2001)
Baltic Sea	4.6x10 ³ - 6x10 ³ m ³ day ⁻¹ km ⁻¹	Modeling	Kaleris <i>et al.</i> (2002)
Kenya, southern coast	6.1 - 17.9 m ² day ⁻¹	Modeling	Kamermans <i>et al.</i> (2002)
Pettaquamcutt, RI	0.15 - 2.2 cm d ⁻¹	radium isotopes	Kelly and Moran (2002)
Zanzibar island	0.4 - 10.2 m ² day ⁻¹	Modeling	Kamermans <i>et al.</i> (2002)
Biscayne Bay, FL, USA	3.4x10 ⁴ - 3.7x10 ⁵ m ³ day ⁻¹	Modeling	Langevin (2003)
Delaware estuary, USA	1.21x10 ⁶ - 2.51x10 ⁶ m ³ day ⁻¹	²²² Rn	Schwartz (2003)
Kahana Bay, HI	8.4 ± 2.1 (inner bay) 2.3 ± 1.0 (middle bay)	different tracers	Garrison <i>et al.</i> (2003)
Kurobe fan, Japan	No data	Temperature, conductivity, geochemistry	Tokunaga <i>et al.</i> (2003)
Northeast Gulf of Mexico	5 - 50 cm d ⁻¹	Radon	Lambert and Burnett (2003)
Northeast Gulf of Mexico	1.5 m ³ min ⁻¹	²²³ , ²²⁴ , ²²⁶ , ²²⁸ Ra	Moore (2003)
Northeast Gulf of Mexico	0.06 m ³ min ⁻¹	Numerical model	Smith and Zawadzki (2003)
Northeast Gulf of Mexico	2 m ³ min ⁻¹	Seepage meter	Taniguchi <i>et al.</i> (2003)
Ovacif-Silifke, Turkey	6.4x10 ⁴ m ³ day ⁻¹	Hydro chemical tests, dye tracers	Elhatip (2003)
Patos Lagoon, Brazil	6.25x10 ⁷ m ³ day ⁻¹	Hydrochemistry	Windom and Niencheski (2003)
Rishiri Island, Japan	No data	Electrical conductivity	Marui (2003)
Sao Paulo, Brazil	0.021 - 0.048 m day ⁻¹	²²⁶ Ra, ²²² Rn	Oliveira <i>et al.</i> (2003)

Western Australia	$9 \times 10^{-3} - 3.6 \times 10^{-3} \text{ m day}^{-1}$	Temperature	Taniguchi <i>et al.</i> (2003b)
Chesapeake Bay, VA	$1.7 - 3.2 \text{ m d}^{-1}$	radium isotopes	Charette and Buesseler (2004)
Kashima coast, Japan	$283-640 \text{ m}^3 \text{ day}^{-1} \text{ km}^{-1}$	Modeling	Uchiyama <i>et al.</i> (2000)
Mississippi Delta	2.5 cm d^{-1}	$^{223}, ^{224}\text{Ra}$	Moore and Krest (2004)
Osaka Bay, Japan	2000: $1 \times 10^{-2} - 3.3 \times 10^{-2} \text{ m d}^{-1}$	Seepage meters	Taniguchi and Iwakawa (2004)
Osaka Bay, Japan	2001: $4.9 \times 10^{-3} - 8.2 \times 10^{-2} \text{ m d}^{-1}$	Seepage meters	Taniguchi and Iwakawa (2004)
Lebanon coast	$9.3 \times 10^5 \text{ m}^3 \text{ d}^{-1}$	Temperature, remote sensing	Shaban <i>et al.</i> (2005)
Onslow Bay	$0-0.2 \text{ cm d}^{-1}$	Numerical model	Wilson (2005)
Suruga Bay, Japan	$0.04-1.56 \text{ m d}^{-1}$	Remote sensing, seepage meters	Taniguchi <i>et al.</i> (2005)
Yellow Sea	$1.8 \times 10^9 \text{ m}^3 \text{ d}^{-1}$	$^{226}\text{Ra}, ^{228}\text{Ra}$	Kim <i>et al.</i> (2005)
Yeoja Bay, Korea	24 cm d^{-1}	Radium isotopes	Hwang <i>et al.</i> (2005)
Yeoja Bay, Korea	$2.6 \times 10^7 \text{ m}^3 \text{ d}^{-1}$	Nutrients, Ra isotopes	Hwang <i>et al.</i> (2005)
Cockburn Sound, W Australia	$2.5-3.7 \text{ m}^3 \text{ m}^{-1} \text{ d}^{-1}$	Seepage meter	Burnett <i>et al.</i> (2006)
Cockburn Sound, W Australia	$3.2 \text{ m}^3 \text{ m}^{-1} \text{ d}^{-1}$	Radium isotopes	Burnett <i>et al.</i> (2006)
Cockburn Sound, W Australia	$2-2.7 \text{ m}^3 \text{ m}^{-1} \text{ d}^{-1}$	Radon	Burnett <i>et al.</i> (2006)
Cockburn Sound, W Australia	$2.5-4.8 \text{ m}^3 \text{ m}^{-1} \text{ d}^{-1}$	Modeling	Burnett <i>et al.</i> (2006)
Donnalucata, Sicily	$1.2 \times 10^3 - 7.4 \times 10^3 \text{ m}^3 \text{ day}^{-1}$	^{222}Rn	Burnett and Dulaiova (2006)
Donnalucata, Sicily boat basin	$300-800 \text{ m}^3 \text{ d}^{-1}$	Seepage meter	Burnett <i>et al.</i> (2006)
Donnalucata, Sicily boat basin	$1200-7400 \text{ m}^3 \text{ d}^{-1}$	Radon	Burnett <i>et al.</i> (2006)
Donnalucata, Sicily shoreline flux	$10-30 \text{ m}^3 \text{ m}^2 \text{ d}^{-1}$	Seepage meter	Burnett <i>et al.</i> (2006)
Donnalucata, Sicily shoreline flux	$1000 \text{ m}^3 \text{ m}^2 \text{ d}^{-1}$	Radium isotopes	Burnett <i>et al.</i> (2006)
Donnalucata, Sicily shoreline flux	$30-200 \text{ m}^3 \text{ m}^2 \text{ d}^{-1}$	Radon	Burnett <i>et al.</i> (2006)
Gulf of Aqaba, Israel	388.8 cm d^{-1}	Radium isotopes	Shellenbarger <i>et al.</i> (2006)
Gulf of Thailand - Sri Racha (dry)	1.9 cm d^{-1}	Manual and automated	Burnett <i>et al.</i> (2006a)

Gulf of Thailand - Hua Hin (wet)	10.2 cm d ⁻¹	seepage meters	
Huntington Beach, California	101 cm d ⁻¹	Radium isotopes	Boehm et al.(2006)
Mauritius - (Klondyke Hotel)	radon: 5.6-9.6 m ³ m ⁻¹ d ⁻¹ seepage meter: 2-11 m ³ m ⁻¹ d ⁻¹	Radon, seepage meter	Burnett et al.(2006)
Mauritius - (South Beach)	radon: 5.2-9.2 m ³ m ⁻¹ d ⁻¹ seepage meter: 1 m ³ m ⁻¹ d ⁻¹ - 8.8 m ³ m ⁻¹ d ⁻¹	radon, seepage meter	Burnett et al. (2006)
Mauritius - (Spring)	radon: 26-56 m ³ m ⁻¹ d ⁻¹ seepage meter: 0.4 m ³ m ⁻¹ d ⁻¹ - 120 m ³ m ⁻¹ d ⁻¹	Radon, seepage meter	Burnett et al. (2006)
Shelter Island, Long Island NY	0.4-17.5 m ³ m ⁻¹ d ⁻¹	Seepage meter	Burnett et al. (2006)
Shelter Island, Long Island NY	16-26 m ³ m ⁻¹ d ⁻¹	Radium isotopes	Burnett et al. (2006)
Shelter Island, Long Island NY	8-16 m ³ m ⁻¹ d ⁻¹	Radon	Burnett et al. (2006)
Shelter Island, Long Island NY	18-20 m ³ m ⁻¹ d ⁻¹	Radon	Burnett et al. (2006)
Shelter Island, Long Island NY	0.23-1.4 m ³ m ⁻¹ d ⁻¹	Modeling	Burnett et al. (2006)
Shelter Island, Long Island NY	0.5 m ³ m ⁻¹ d ⁻¹	Modeling	Burnett et al. (2006)
Shelter Island, Long Island NY	10 m ³ m ⁻¹ d ⁻¹	Modeling	Burnett et al. (2006)
south-eastern Sicily	58 m ³ s ⁻¹ per km of coast	Radon	Povinec et al. (2006)
Ubatuba, Brazil	5-270 cm d ⁻¹	manual meters	Burnett et al. (2006)
Ubatuba, Brazil	0-360 cm d ⁻¹	continuous heat	Burnett et al. (2006)
Ubatuba, Brazil	2-109 cm d ⁻¹	dye dilution	Burnett et al. (2006)
Ubatuba, Brazil	1-29 cm d ⁻¹	continuous radon	Burnett et al. (2006)
Ubatuba, Brazil	28-184 cm d ⁻¹	MLS SF6	Burnett et al. (2006)
Mississippi Delta	0.1 cm d ⁻¹	H/He, Rn	McCoy et al. (2007b)
Mississippi Delta	0.0-0.04 cm d ⁻¹	Numerical model	Thompson et al., (2007)
Onslow Bay	0-4.4 cm d ⁻¹	Radon	McCoy et al. (2007a)
Bataan, Philippines	12.4 m ³ d ⁻¹ m ⁻¹ shoreline	radon, seepage meter	Taniguchi et al. (2008)
Isola La Cura, Northern Venice Lagoon (Italy)		radium	Garcia-Solsona et al. (2008)

1.5.3 SGD Studies Worldwide

Figure 1.4 shows the locations of published studies that have reported SGD estimates based on different methods. Details of these SGD estimates are summarized in Table 1.2.

Taniguchi *et al.* (2002) was the first to provide a comprehensive review of the worldwide occurrence or magnitude of SGD; however this compilation was limited to literature citations of discharge estimates using seepage meters, piezometers, and/or geochemical / geophysical tracers. Gallardo and Marui (2006) did the same few years later which included SGD estimates other than those techniques mentioned in Taniguchi *et al.* (2002). Burnett *et al.* (2006) did an extensive inter-comparison study of 5 sites using multiple methods. In the recent years, SGD studies were extended to Korea (Kim *et al.*, 2003), Hawaii (Garrison *et al.*, 2003), North-East Australia (Stieglitz, 2005), the West coast of the United States (Boehm *et al.*, 2006), Brazil (Windom *et al.*, 2006), Thailand (Burnett *et al.*, 2006a), Israel (Shellenbarger *et al.*, 2006) and Philippines (Taniguchi *et al.*, 2008).

The locations of the available published studies are mostly concentrated on the east coast of the United States, Europe, Japan and Oceania, whereas regions such as South America, Africa, India, China, and especially Asia have not yet been extensively investigated.

Global estimates of SGD rates are mostly obtained using hydrological methods (Table 1.3). Values from these estimates are generally lower than those obtained using water balance approach, possibly because of the underestimation of the coastal aquifer thickness (Burnett *et al.*, 2003). At the local scale, the variation in SGD is quite significant. According to Taniguchi *et*

al. (2002), SGD rates may vary from 3 % (Valiela *et al.*, 1978) to 87 % (Valiela and Costa, 1988) of total freshwater fluxes. In some areas, such as in enclosed bays, karstic and fractured systems (e.g., Hawaii; Garrison *et al.*, 2003), or at locations where rivers are small or non-existent (e.g., Yucatan peninsula; Hanshaw and Back, 1980), SGD is a prominent discharge pathway.

Table 1.3 Global scale relative contribution of submarine groundwater discharge to freshwater outflow. (Modified from: Taniguchi *et al.*, 2002 and Gallardo and Marui, 2006)

Reference	Role of SGD	Method
Nance (1970)	1% of surface runoff	Hydrogeologic assumptions
Garrels and McKenzie (1971)	10% of surface runoff	Water balance
Zekster <i>et al.</i> (1973)	10% of surface runoff	Water balance
Lvovich (1974)	31% of the total water flux	Water balance
Berner and Berner (1987)	6% of the total water flux	Literature review
COSODII (1987)	0.3% of surface runoff	Hydrological assumptions
Zekster and Loaiciga (1993)	6% of total water flux	Hydrograph separation
	2% of global precipitation	Water balance
Church (1996)	0.01-10% of surface runoff	Literature review
Burnett <i>et al.</i> (2003a)	0.3-16% of global river flow	Literature review
SCOR/LOICZ Report (2004)	6% of surface runoff	Literature review
Slomp and van Cappellen (2004)	5% of total global water flux	Literature review?

1.6 Philippines: an SGD key site

The Philippines' coastal zones (Total land area=300,000km²; Total Coastline=36,289 km) that represent nearly half of the country surface area are characterized by high rainfall, karstic and volcanic terrains (Figure 1.5a), and high relief (Figure1.5c) (Bokuniewicz *et al.*, 2003; Taniguchi *et al.*, 2008), features commonly associated to the presence of SGD in coastal areas. 75% of the population live in coastal areas and the population growth is the highest of SE-Asia (National Statistics Office - Manila) (Figure 1.5b), which means that anthropogenic activities have a huge impact on groundwater resources in terms of quantity, and quality and thus on freshwater SGD and related nutrients. The economy of this country is largely dependent on coastal resources (e.g. fish, corals, sea grass, etc.), and its marine habitat is one of the most diverse in the world (Carpenter and Springer, 2005). The major source of potable water in this country is groundwater, since there is an economical and cultural difficulty for tapping on surface water source.

On both economic and environmental aspect, SGD have very significant influence. Therefore it is critical to fully understand the mechanism, variability and impact of SGD in this region, as well as the controlling factors. In addition to this, the global SGD database has very few information of SGD on Asian countries so any additional knowledge would be very significant.

All around the country algal blooms have been occurring over the past decades: Figure 1.6 shows the different embayment affected by harmful algal blooms (HABs) and the years of

observed occurrences. Effects of HABs include massive fish kills (Figure 1.7) and even human casualties. There are more than 2000 cases of paralytic shellfish poisoning (period: 1983-2002) and more than 100 human deaths (Relox and Bajarías, 2003).

Manila Bay is one of the areas heavily affected by HABs in the Philippines (Taniguchi *et al.*, 2008) and it was previously thought that the cause of these blooms is eutrophication. Results of the study made by Taniguchi *et al.* (2008) however confirmed the occurrence of SGD in this area with elevated nutrient levels. SGD flux from the shallow aquifers was estimated to be about $12 \text{ m}^3 \text{ m}^{-1} \text{ day}^{-1}$ ($8.3 \times 10^8 \text{ m}^3 \text{ y}^{-1}$) with potential magnitude of DIN input at 42% to 96% of river input (Taniguchi *et al.*, 2008). Therefore, SGD instead of the river supplied nutrients may be triggering the observed HAB outbreaks. There is a *possibility* that the same scenario is occurring to other sites affected by HABs displayed in Figure 1.6.

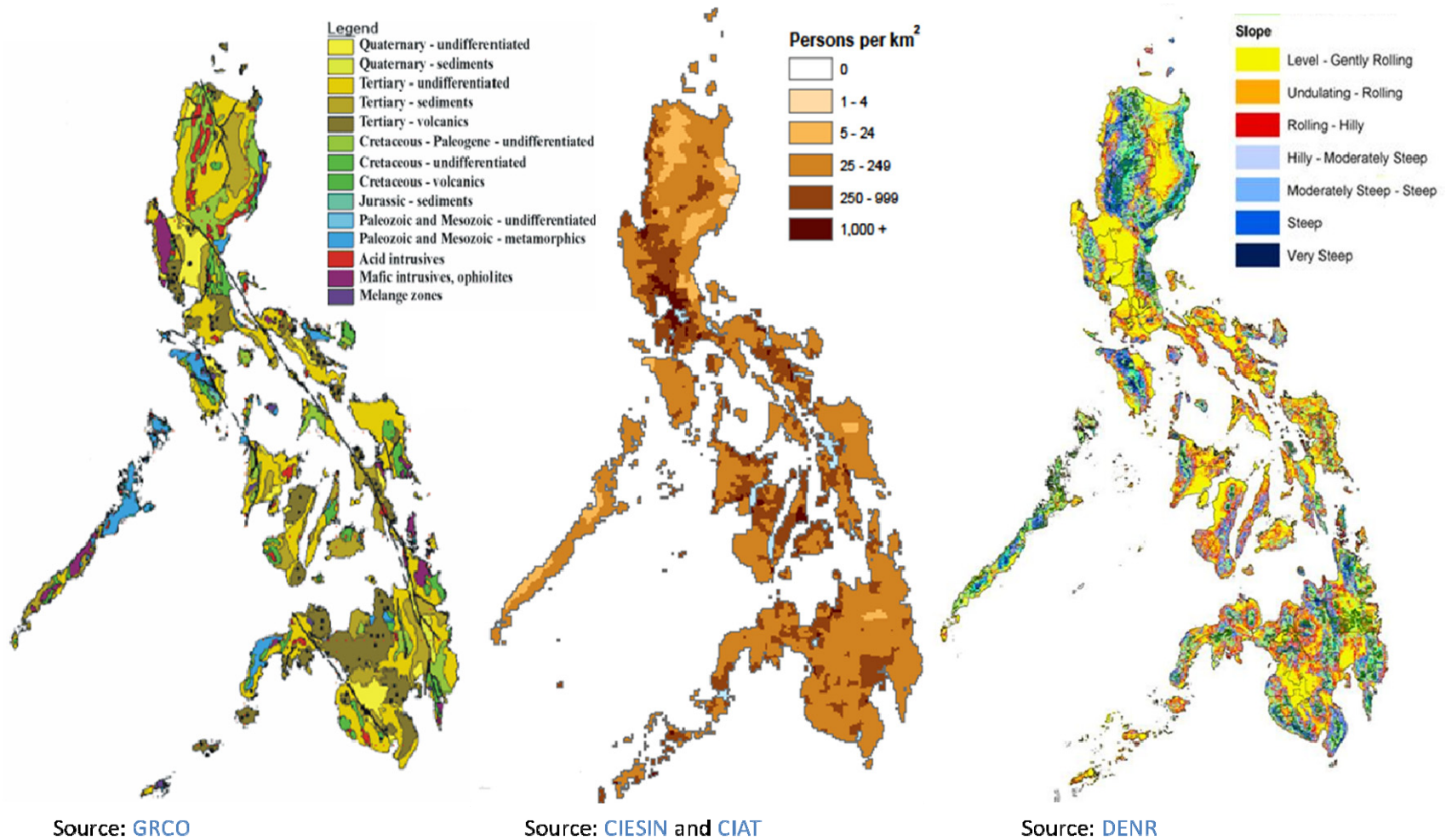


Figure 1.5 Major characteristics of the Philippines which make it a key study site for SGD related research. **(A)** Geological map of the Philippines **(B)** Population Density, 2000 **(C)** Slope map of the Philippines

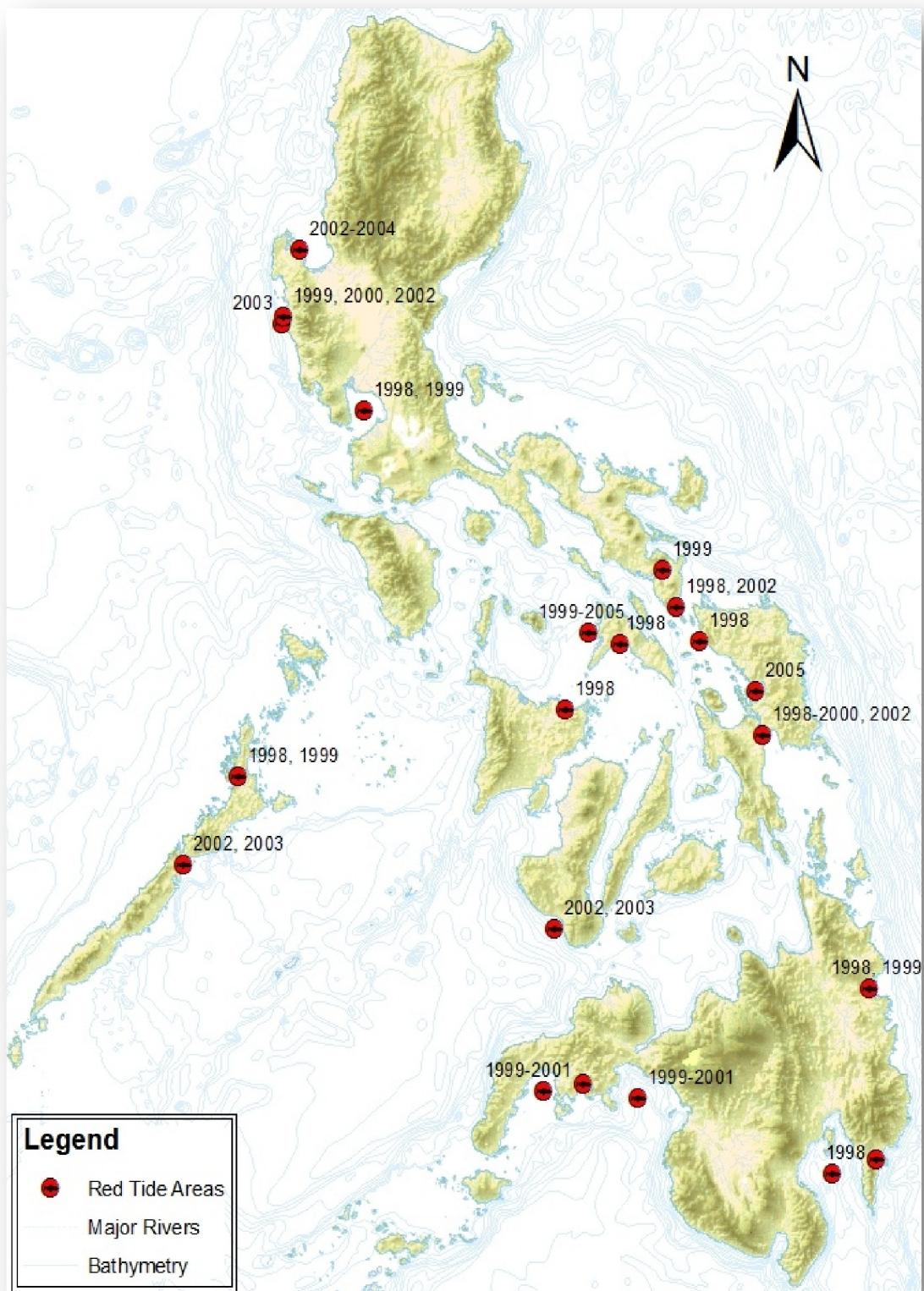


Figure 1.6 Embayment in the Philippines with harmful algal bloom occurrences.



Source: [Relox and Bajarias., 2003](#)

Figure 1.7 Photo showing the incident of a milkfish mass mortality in Bolinao, Pangasinan due to harmful algal blooms (HABs) on 02 Feb 2002.

1.7 Thesis Outline

The major goals of this study are to:

- (1) Understand and determine the hydrogeologic factors that influence the magnitude of SGD flux, and find out which of these factors are more important in driving SGD through hydrogeological modeling and comprehensive sensitivity analysis.
- (2) Analyze the effect of changing climate conditions and sea level rise to the magnitude of SGD flux by means of multiple simulations. Also how anthropogenic induced factors influence the SGD flux.

In **Chapter 2**, a regional scale modular variable-density groundwater flow model (MOCDENS3D) has been used to estimate the magnitude of submarine groundwater discharge to Manila Bay focusing on an area situated at the south-eastern flank of Mt. Mariveles volcano in Bataan Peninsula, Philippines, a potentially active stratovolcano. The model domain incorporates both the terrestrial recharge and also the re-circulated water in the coastal sediments. Different scenarios were run to evaluate the sensitivity of SGD to different hydrogeologic parameters, e.g. changes in geology, topography, also the changes in water sources and sinks such as rainfall, rivers, and groundwater extraction wells.

In **Chapter 3**, the modeling is extended to incorporate the effects of changing climate conditions and also sea level rise to the magnitude of SGD flux. Also examined are the anthropogenic induced changes, such as changes in land-use and groundwater extraction.

References

- Abraham DM, MA Charette, MC Allen, A Rago and KD Kroeger (2003). Radiochemical estimates of submarine groundwater discharge to Waquoit Bay, Massachusetts. *Biological Bulletin*; pp 205, 246-7.
- Banks W, R Paylor and W Hughes (1996). Using thermal infrared imagery to delineate groundwater discharge. *Groundwater*; 34: 434-44.
- Berner EK, and RA Berner (1987). *The Global Water Cycle*, Prentice-Hall, Englewood Cliffs, NJ, pp12-24.
- Bobba AG (1993). Mathematical models for salt-water intrusion in coastal aquifers. In: *Water Resources Management*, Kluwer, 7, 3-37.
- Boehm AB, A Paytan, GG Shellenbarger and KA Davis (2006). Composition and flux of groundwater from a California beach aquifer: Implications for nutrient supply to the surf zone, *Continental Shelf Research*, 26, 269-282.
- Boehm AB, GG Shellenbarger and A Paytan (2004). Groundwater discharge: potential association with fecal indicator bacteria in the surf zone, *Environ. Sci. Technol.* 38 (13) (2004). pp. 3558-3566.
- Bokuniewicz, H (1980). Groundwater seepage into Great South Bay, New York. *Estuar Coast Mar Sci*; 10:437-44.
- Bokuniewicz H and V Pavlik (1990). Groundwater seepage along a barrier island. *Biogeochemistry*; 10:257-76.
- Bokuniewicz H, R Buddemeier, B Maxwell and C Smith (2003). The typological approach to submarine groundwater discharge (SGD). *Biogeochemistry*, 66(1). 145-158.
- Breier JA, CF Breier and HN Edmonds (2005). Detecting submarine groundwater discharge with synoptic surveys of sediment resistivity, radium, and salinity. *Geophysical Research Letters*, 32, doi: 10.1029/2005GL 024639.
- Brooks HK (1961). The submarine spring off Crescent Beach, Florida. *Quarterly Journal of the Florida Academy of Sciences* 24: 122-134.
- Bugna GC, JP Chanton, JE Young, WC Burnett and PH Cable (1996). The importance of groundwater discharge to the methane budget of nearshore and continental shelf waters of the NE Gulf of Mexico. *Geochim Cosmochim Acta*; 60:4735-46.
- Burdon DJ (1964). *Karst groundwater investigations, Greece*. Food and Agric. Org. United Nations, FAO/SF:2/Gre.
- Burnett WC and H Dulaiova (2003). Estimating the dynamics of groundwater input into the coastal zone via continuous radon-222 measurements. *J Environ Radioact* ;69:21-35.
- Burnett WC and H Dulaiova (2006). Radon as a tracer of submarine groundwater discharge into a boat basin in Donnalucata, Sicily. *Cont Shelf Res* ;26:862-73
- Burnett WC, M Taniguchi and J Oberdorfer (2001). Measurement and significance of the direct discharge of groundwater into the coastal zone. *J Sea Res* ;46/2:109-16

- Burnett WC, H Bokuniewicz, M Huettel, WS Moore and M Taniguchi (2003a). Groundwater and porewater inputs to the coastal zone, *Biogeochemistry*, 66, 3-33
- Burnett WC, JE Cable and DR Corbett (2003b). Radon tracing of submarine groundwater discharge in coastal environments. In: *Land and Marine Hydrogeology* (eds., M. Taniguchi, K. Wang, and T. Gamo). Elsevier Publications, 25-43.
- Burnett WC, PK Aggarwal, A Aureli, H Bokuniewicz, JE Cable, MA Charette, E Kontar, S Krupa, KM Kulkarni, A Loveless, WS Moore, JA Oberdorfer, J Oliveira, N Ozyurt, P Povinec, AMG Privitera, R Rajar, RT Ramessur, J Scholten, T Stieglitz, M Taniguchi and JV Turner (2006). Quantifying submarine groundwater discharge in the coastal zone via multiple methods, *Science of the total environment*, Volume: 367, Issue: 2-3 (August 31, 2006). pp: 498-543
- Cable J, G Bugna, W Burnett and J Chanton (1996a). Application of ^{222}Rn and CH_4 for assessment of groundwater discharge to the coastal ocean. *Limnol Oceanogr*; 41:1347–53.
- Cable JE, Burnett WC, Chanton JP (1997b). Magnitudes and variations of groundwater seepage into shallow waters of the Gulf of Mexico. *Biogeochemistry*; 38:189–205.
- Cable JE, Burnett WC, Chanton JP, Corbett DR, Cable PH (1997a). Field evaluation of seepage meters in the coastal marine environment. *Estuar Coast Shelf Sci*; 45:367–75
- Cable JE, Burnett WC, Chanton JP, Weatherly GL. (1996b). Estimating groundwater discharge into the northeastern Gulf of Mexico using radon-222. *Earth Planet Sci Lett*; 144:591–604
- Capone DG, Bautista MF (1985). A groundwater source of nitrate in nearshore marine sediments. *Nature*; 313:214–6.
- Capone DG, and JM Slater (1990). Interannual patterns of water table height and groundwater derived nitrate in nearshore sediments. *Biogeochemistry*; 10:277–88.
- Carpenter KE and VG Springer (2005). The center of the center of marine shore fish biodiversity: the Philippine Islands. *Environmental Biology of Fishes*; 72: 467-480.
- Chanton JP (2003). Seepage rate variability derived by Atlantic tidal height. *Biogeochemistry*; 66:187–202.
- Charette MA, KO Buesseler and JE Andrews (2001). Utility of radium isotopes for evaluating the input and transport of groundwater-derived nitrogen to a Cape Cod estuary. *Limnol Oceanogr*; 46:465–70
- Charette MA and ER Sholkovitz (2002). Oxidative precipitation of groundwater derived ferrous iron in the subterranean estuary of a coastal bay. *Geophys Res Lett*; 29:1444
- Charette MA and MC Allen (2006). Precision groundwater sampling in coastal aquifers using a direct push shielded-screen well-point system. *Groundwater Monitoring & Remediation*; 26(2): 87-93.
- Charette MA and KO Buesseler (2004). Submarine groundwater discharge of nutrients and copper to an urban subestuary of Chesapeake Bay (Elizabeth River). *Limnology and Oceanography*; 49:376-385.
- Church TM (1996). An underground route for the water cycle. *Nature*; 380:579–80.
- Corbett DR, J Chanton, W Burnett, K Dillon, C Rutkowski, and J Fourqurean (1999). Patterns of groundwater discharge into Florida Bay. *Limnol Oceanogr*; 44:1045–55.

- Corbett DR, L Kump, K Dillon, W Burnett, and J Chanton (2000). Fate of wastewater-borne nutrients under low discharge conditions in the subsurface of the Florida Keys, USA. *Marine Chemistry*; 69(1-2): 99-115.
- COSOD II (1987). Fluid circulation in the crust and the global geochemical budget. Report of the Second Conference on Scientific Ocean Drilling, Strasbourg, France, 6-8 July.
- Crotwell AM and WS Moore (2003). Nutrient and radium fluxes from submarine groundwater discharge to Port Royal Sound, South Carolina. *Aquat Geochem*; 9:191–208
- D'Elia CF, DKL Webb, and JW Porter (1981). Nitrate-rich groundwater inputs to Discovery Bay, Jamaica: a significant source of N to local coral reefs? *Bull Mar Sci*; 31:903–10.
- Deming D, JH Sass, AH Lachenruch and RF De Rito (1992). Heat flow and subsurface temperatures evidence for basin-scale groundwater flow, north slope of Alaska. *Geological Society of America Bulletin*; 104: 528–542.
- Destouni G and C Prieto (2003). On the possibility for generic modeling of submarine groundwater discharge. *Biogeochemistry*; 66: 171-186.
- Dillon KS, DR Corbett, JP Chanton, WC Burnett and DJ Furbish (1999). The use of sulfur hexafluoride (SF₆) as a tracer of septic tank effluent in the Florida Keys. *Journal of Hydrology*; 220:129-140.
- Dürr HH, LPH van Beek, CP Slomp, H Middelkoop and M Bierkens (2008). Global land-ocean linkage: direct inputs of water and associated nutrients to coastal zones via Submarine Groundwater Discharge (SGD). *Proceedings 20th Salt Water Intrusion Meeting (June 23-27, 2008; Naples, Florida, USA)*. 72-75.
- Elhatip H (2003). The use of hydrochemical techniques to estimate the discharge of Ovacık submarine springs in the Mediterranean coast of Turkey. *Environ Geol*; 43:714–719
- Fanning, KA, RH Byrne, JA Breland, PR Betzer, WS Moore, RJ Elsinger and TE Pyle (1981). Geothermal springs of the West Florida continental shelf: Evidence for dolomitization and radionuclide enrichment. *Earth and planetary science letters*; 52-2:345-354
- FGS (1998) Springs of Florida (revised). Florida Geological Survey, Geol Bull 31
- Fischer WA, RM Moxham, F Polcyn and GH Landies (1964). Infrared surveys of Hawaiian volcanoes. *Science*; 146: 733–742.
- Gallagher DL, AM Dietrich, WG Reay, MC Hayes, GM Simmons Jr. (1996). Ground water discharge of agricultural pesticides and nutrients to estuarine surface water. *Ground Water Monitoring and Remediation (Winter)*: 118–129.
- Gallardo AH and A Marui (2006). Submarine groundwater discharge: an outlook and recent advances and current knowledge. *Geo-Mar Lett*; 26: 102-113
- Garcia-Solsona E, P Masqué, J Garcia-Orellana, J Rapaglia, AJ Beck, JK Cochran, HJ Bokuniewicz, L Zaggia, and F Collavini (2008). Estimating submarine groundwater discharge around Isola La Cura, northern Venice Lagoon (Italy) by using the radium quartet. *Marine Chemistry*, - In Press, Corrected Proof(-): -.
- Garrels RM and FT MacKenzie (1971). *Evolution of Sedimentary Rocks*, Norton & Co., New York.
- Garrison GH, CR Glenn and GM McMurtry (2003). Measurement of submarine groundwater discharge in Kahana Bay, Oahu, Hawaii. *Limnol Oceanogr*; 48:920–8

- Giblin AE and AG Gaines (1990). Nitrogen inputs to a marine embayment: The importance of groundwater. *Biogeochemistry*; 10:309-328.
- Gobler CJ and SA Sañudo-Wilhelmy (2001). Temporal variability of groundwater seepage and Brown Tide bloom in a Long Island embayment. *Marine Ecology Progress Series*; 217: 299-309
- Hanshaw BB and W Back (1980). Chemical mass-wasting of the northern Yucatan Peninsula by groundwater dissolution. *Geology*; 8:222-224.
- Hay AE (1984). Remote acoustic imaging of the plume from a submarine spring in an arctic fjord. *Science*; 225: 1154–1156.
- Henry P, SJ Lallemand, X Le Pichon and SE Lallemand (1989) Fluid venting along Japanese trenches, tectonic context and thermal modeling. *Tectonophysics*; 160:277–292
- Henry HR (1964). Interface between salt water and fresh water in a coastal aquifer. In: HH Cooper Jr., FA Kohout, HR Henry and RE Glover, Editors, U.S. Geological Survey Water Supply Paper 1613-C (1964). pp C35–C70.
- Holzbecher E (1998). *Modeling Density-Driven Flow in Porous Media: Principles, Numerics, Software*, Springer Publications, Heidelberg / New York, 286 pp.
- Hu C, FE Muller-Karger and PW Swarzenski (2006). Hurricanes, submarine groundwater discharge, and Florida's red tides, *Geophys. Res. Lett.*; 33:L11601.
- Huettel M and G Gust (1992). Solute release mechanisms from confined sediment cores in stirred benthic chambers and flume flows. *Mar Ecol, Prog Ser*; 82:187–97.
- Huettel M, W Ziebis and S Forster (1996). Flow-induced uptake of particulate matter in permeable sediments. *Limnol. Oceanogr*; 41(2):309–322.
- Hussain N, TM Church and G Kim (1999). Use of ^{222}Rn and ^{226}Ra to trace submarine groundwater discharge into the Chesapeake Bay. *Mar Chem*; 65:127–34.
- Hwang DW, G Kim, Y-W Lee and H-S Yang (2005). Estimating submarine inputs of groundwater and nutrients to a coastal bay using radium isotopes. *Mar Chem*; 96:61–71.
- Jankowska H, M Matciak and J Nowacki (1994). Salinity variations as an effect of groundwater seepage. *Oceanologia*; 36:33–46.
- Johannes RE and CJ Hearn (1985). The effect of subsurface groundwater discharge on nutrient and salinity regimes in a coastal lagoon off Perth, West Australia. *Estuarine, Coastal and Shelf Science*; 21:789–800
- Johannes RE (1980). The ecological significance of the submarine discharge of groundwater. *Marine Ecology – Progress Series*; 3:365-373.
- Kaleris V, G Lagas, S Marciznek and JA Piotrowski (2002). Modelling submarine ground-water discharge: an example from the western Baltic Sea. *Journal of Hydrology*; 265:76-99.
- Kamermans P, MA Hemminga, JF Tack, MA Mateo, N Marbàn, M Mtolera, J Stapel, A Verheyden and T Van Daele (2002). Groundwater effects on diversity and abundance of lagoonal seagrasses in Kenya and on Zanzibar Island (East Africa). *Mar Ecol Prog Ser*; 231: 75–83

- Kim G, JW Ryu, HS Yang and ST Yun (2005). Submarine groundwater discharge (SGD) into the Yellow Sea revealed by ^{228}Ra and ^{226}Ra isotopes: implications for global silicate fluxes. *Earth Planet Sci Lett*; 237:156–166
- Kir'yakov PA, GV Lisichenko, VA Emel'yanov and Yu Mitropol'skii (1983). Radon Survey Detection of Submarine Groundwater Discharge Zones. [Translated from *Vodnye Resursy* (5): 153–157, September–October, 1982]. Plenum: 557–561.
- Kohno T and T Tagawa (1996). Submarine springs and groundwater study of Hiji-town in Oita prefecture. *Bull Nippon Univ*; 24:103–109
- Kohout FA (1966). Submarine springs: a neglected phenomenon of coastal hydrology. *Hydrology*; 26:391–413
- Kohout FA, MC Kolipinski (1967). Biological zonation related to groundwater discharge along the shore of Biscayne Bay, Miami Florida. In: Lauff. G. H. (ed.) *Estuaries*. Am. Assoc. Adv. Sci. 83: 488-499
- Krest JM, WS Moore and LR Gardner (2000). Marsh nutrient export supplied by groundwater discharge: evidence from radium measurements. *Glob Biogeochem Cycles*; 14:167–76.
- Krest JM, WS Moore and Rama (1999). ^{226}Ra and ^{228}Ra in the mixing zone of the Mississippi and Atchafalaya Rivers: indicators of groundwater input. *Mar. Chem.*; 64: 129–152.
- Lallemant SE, G Glaçon, A Lauriat-Rage, A Fiala-Medioni, JP Cadet, C Beck, M Sibuet, JT Iiyama, H Sakai and A Taira (1992). Seafloor manifestations of fluid seepage at the top of a 2000-metre-deep ridge in the eastern Nankai accretionary wedge: long-lived venting and tectonic implications. *Earth Planet Sci Lett*; 109: 333–346
- Lambert MJ and WC Burnett (2003). Submarine groundwater discharge estimates at a Florida coastal site based on continuous radon measurements. *Biogeochemistry*; 66: 55–73.
- Langevin CD (2003). Simulation of submarine ground water discharge to a marine estuary: Biscayne Bay, Florida. *Groundwater*; 41(6):758–771.
- Lewis JB (1987). Measurements of groundwater seepage flux onto a coral reef; spatial and temporal variations. *Limnol. Oceanogr.*; 32(5): 1165-1169.
- Li L, DA Barry, F Stagnitti and JY Parlange (1999). Submarine groundwater discharge and associated chemical input to a coastal sea. *Water Resour. Res.*; 35 (11): 3253–3259.
- Loaiciga HA and IS Zektser (2003). Estimation of Submarine Groundwater Discharge. *Water Resources*; 30: 473-479.
- Lvovich MI (1974). *World Water Resources and their Future*. Mysl. Publisher, Moscow (in Russian).
- Manheim FT (1967). Evidence for submarine discharge of water on the Atlantic Continental slope of the southern United States, and suggestions for future research. *Trans New York Acad Sci II*; 29: 839–853
- Manheim FT and CK Paull (1981). Patterns of groundwater salinity changes in a deep continental–oceanic transect off the southeastern Atlantic coast of the USA. *Journal of Hydrology*; 54: 95–105.
- McCoy CA, DR Corbett, JE Cable and RK Spruill (2007). Hydrogeological characterization and quantification of submarine groundwater discharge in the southeast Coastal Plain of North Carolina. *J. Hydrol.*; 339: 159–171.

- Michael HA, AE Mulligan and CF Harvey (2005). Seasonal oscillations in water exchange between aquifers and the coastal ocean. *Nature*; 436: 1145–1148.
- Miller DC and WJ Ullman (2004). Ecological consequences of estuarine groundwater discharge at Cape Henlopen, Delaware Bay, USA. *Ground Water Journal*; 42: 959-970.
- Moore WS and J Krest (2004). Distribution of ²²³Ra and ²²⁴Ra in the plumes of the Mississippi and Atchafalaya Rivers and the Gulf of Mexico, *Marine Chemistry*; 86: 105-119.
- Moore WS (1999). The subterranean estuary: a reaction zone of ground water and sea water. *Marine Chemistry*; 65: 111–25.
- Moore WS (2006). Radium isotopes as tracers of submarine groundwater discharge in Sicily. *Cont Shelf Res*; 26: 852–61.
- Moore WS and AM Wilson (2005). Advective flow through the upper continental shelf driven by storms, buoyancy, and submarine groundwater discharge. *Earth Planet Sci Lett*; 235: 564–76.
- Moore WS (1996). Large groundwater inputs to coastal waters revealed by ²²⁶Ra enrichments. *Nature*; 380: 612-614
- Moore WS (2003). Sources and fluxes of submarine groundwater discharge delineated by radium isotopes. *Biogeochemistry*; 66: 75–93.
- Mulligan AE and MA Charette (2006). Intercomparison of submarine groundwater discharge estimates from a sandy unconfined aquifer. *Journal of Hydrology*; 327: 411-425.
- Nace RL (1970). World hydrology: status and prospects. In: *Symposium on World Water Balance, Vol. I. IAHS Publication No. 92. IAHS/UNESCO: Louvain*; 1–10.
- Nielsen P (1990). Tidal dynamics in the water table in a beach. *Water Resour Res*; 26: 2127–34.
- Oberdorfer JA (2003). Hydrogeologic modeling of submarine groundwater discharge: comparison to other quantitative methods. *Biogeochemistry*; 66: 159-169.
- Oberdorfer JA, MA Valentino and SV Smith (1990). Groundwater contribution to the nutrient budget of Tomales Bay, California. *Biogeochemistry*; 10: 199-216.
- Oki DS, WR Souza, EL Bolke and GR Bauer (1998). Numerical analysis of the hydrogeologic controls in a layered coastal aquifer system, Oahu Hawaii USA, *Hydrogeology Journal* 6: 243-263
- Oude Essink GHP (1998). MOC3D adapted to simulate 3D density-dependent groundwater flow. *Proc. MODFLOW'98 Conference, Golden, Colorado, USA*: 291-303.
- Paerl H (1997). Coastal eutrophication and harmful algal blooms: importance of atmospheric deposition and groundwater as “new” nitrogen and other nutrient sources, *Limnol. Oceanogr.*; 42: 1154–1167.
- Paull CK, B Hecker, R Commeau, RP Freeman-Lynde, C Neumann, WP Corso, S Glubic, JE Hook, E Sikes and J Curray (1984). Biological communities at Florida Escarpment resemble hydrothermal vent taxa. *Science*; 226: 965–967.
- Paulsen RJ, CF Smith, D O'Rourke and TF Wong (2001). Development and evaluation of an ultrasonic ground water seepage meter. *Ground Water*; 39: 904-911.

- Paytan A, GG Shellenbarger, JH Street, ME Gonnee, K Davis, MB Young and WS Moore (2006). Submarine groundwater discharge: An important source of inorganic nitrogen to coral reef ecosystems. *Limnology and Oceanography*; 51: 343-348.
- Piekarek-Jankowska H (1996). Hydrochemical effects of submarine groundwater discharge to the Puck Bay (Southern Baltic Sea, Poland). *Geographia Polonica*; 67: 103–119.
- Porcelli D and PW Swarzenski (2003). The behaviour of U- and Th series nuclides in groundwater and the tracing of groundwater. *Reviews in Mineralogy and Geochemistry*; 52: 317-361.
- Porter JW and KG Porter (2002). *The Everglades, Florida Bay, and coral reefs of the Florida Keys: an ecosystem sourcebook*, CRC Press, 2002 pp: 712, 694
- Portnoy JW, BL Nowicki, CT Roman and DW Urish (1998). The discharge of nitrate-contaminated groundwater from developed shoreline to marsh-fringed estuary. *Water Resources Research*; 34: 3095-
- Povinec PP, PK Aggarwal, A Aureli, WC Burnett, EA Kontar, KM Kulkarni, WS Moore, R Rajar, M Taniguchi, JF Comanducci, G Cusimano, H Dulaiova, L Gatto, M Groening, S Hauser, I Levy-Palomo, B Oregioni, YR Ozorovich, AM Privitera and MA Schiavo (2006). Characterisation of submarine groundwater discharge offshore south-eastern Sicily. *Journal of Environmental Radioactivity*; 89: 81-101.
- Presto MK, CD Storlazzi, JB Logan, and EE Grossman (2007). Submarine groundwater discharge and seasonal trends along the coast of Kaloko-Honokohau National Historic Park, Hawaii, part I; time-series measurements of currents, waves and water properties; November 2005-July 2006: U.S. Geological Survey Open-File Report 2007-1310, 39 p.
- Rasmussen LL (1998). *Groundwater Flow, Tidal Mixing, and Haline Convection in Coastal Sediments*. Master's thesis, Florida State University, Tallahassee, Florida.
- Reay WG, DL Gallagher and GM Simmons Jr. (1992). Groundwater discharge and its impact on surface water quality in a Chesapeake Bay inlet. *Water Resources Bulletin*; 28: 1121–1134.
- Reich CD, EA Shinn, TD Hickey and AB Tihansky (2002). Tidal and meteorological influences on shallow marine groundwater flow in the upper Florida Keys. In: Porter JW, Porter KG, editors. *The Everglades, Florida Bay, and coral reefs of the Florida Keys*. Boca Raton: CRC Press; p. 659–76.
- Reilly TE and AS Goodman (1985). Quantitative analysis of saltwater-freshwater relationships in groundwater systems - A historical perspective. *Journal of Hydrology*; 80: 125-160.
- Relox Jr. JR, and FFA Bajarias (2003). Harmful algal blooms (HABs) in the Philippines. In: Furuya, K. Fukuyo, Y. (Eds.), *Extended abstracts of Workshop on Red Tide Monitoring in Asian Coastal Waters*. March 10-12, 2003, the University of Tokyo, Tokyo, pp. 65-68.
- Ridgway NM and BR Stanton (1969). Some hydrological features of Hawke Bay and nearby shelf waters. *New Zealand Journal of Marine and Freshwater Research*; 3: 545–559.
- Riedl R, N Huang and R Machan (1972). The subtidal pump: a mechanism of interstitial water exchange by wave action. *Marine Biology*; 13: 210–21.
- Robb JM (1984). Spring sapping on the lower continental slope, offshore New Jersey. *Geology*; 12: 278–282.

- Robinson C, L Li and DA Barry (2007). Effect of tidal forcing on a subterranean estuary. *Advances in Water Resources*; 30: 851-865.
- Roxburgh IS (1985). Thermal infrared detection of submarine spring associated with the Plymouth Limestone. *Hydrol Sci J*; 30: 185–96.
- Schwartz MC (2003). Significant groundwater input to a coastal plain estuary: assessment from excess radon. *Estuarine Coastal Shelf Sci*; 56: 31–42.
- SCOR-LOICZ (2004). Submarine groundwater discharge management implications, measurements and effects. IHP-VI Series on Groundwater 5. IOC Manuals and Guides 44. United Nations Educational, Scientific and Cultural Organization, Paris
- Shaban M, C Khawlie, G Abdallah and G Faour (2005). Geologic controls of submarine groundwater discharge: application of remote sensing to north Lebanon. *Environ Geol*; 47: 512–522.
- Sholkovitz E, C Herbold and M Charette (2003). An automated dye-dilution based seepage meter for timeseries measurement of submarine groundwater discharge. *Limnology and Oceanography: Methods* 1; 16-28.
- Simmons Jr. GM (1992). Importance of submarine groundwater discharge (SGWD) and seawater cycling to material flux across sediment/water interfaces in marine environments. *Mar. Ecol. Prog. Ser.*; 84: 173–184.
- Slomp CP and P Van Cappellen (2004). Nutrient inputs to the coastal ocean through submarine groundwater discharge: controls and potential impact. *Journal of Hydrology*; 295: 64-86.
- Smith L and W Zawadzki (2003). A hydrogeologic model of submarine groundwater discharge: Florida intercomparison experiment. *Biogeochemistry*; 66: 95–110.
- Smith AJ (2004). Mixed convection and density-dependent seawater circulation in coastal aquifers. *Water Resources Research*; 40:-
- Spiteri C, CP Slomp, K Tuncay and C Meile (2008). Modelling biogeochemical processes in subterranean estuaries: The effect of flow dynamics and redox conditions on submarine groundwater discharge of nutrients. *Water Resources Research*; 44:-
- Stieglitz T (2005). Submarine groundwater discharge into the near-shore zone of the Great Barrier Reef, Australia. *Mar Pollut Bull*; 51: 51–9.
- Stuben D, P Sedwick and P Colantoni (1996). Geochemistry of submarine warm springs in the limestone cavern of Grotta Azurra, Capo Palinuro, Italy: evidence for mixing-zone dolomitisation. *Chemical Geology*; 131: 113–125.
- Taniguchi M, WC Burnett, JE Cable and JV Turner (2002). Investigation of submarine groundwater discharge. *Hydrol Processes*; 16: 2115–2129.
- Taniguchi M, WC Burnett, JE Cable and JV Turner (2003a). Assessment methodologies for submarine groundwater discharge. In: Taniguchi M, Wang K, Gamo T (eds) *Land and marine hydrogeology*. Elsevier, Amsterdam, pp 1–23
- Taniguchi M, T Ishitobi and K Saeki (2005). Evaluation of time–space distributions of submarine groundwater discharge. *Ground Water*; 43(3): 336–342.
- Taniguchi M and H Iwakawa (2004). Submarine groundwater discharge in Osaka Bay, Japan. *Jpn Soc Limnol*; 5: 25–32.

- Taniguchi M, Y Sakura and T Ishii (1998). Estimations of saltwater–fresh water interfaces and groundwater discharge rates in coastal zones from borehole temperature data. In: Proc Japanese Association of Groundwater Hydrology Meet, October 1998, Tokyo, pp 86–89.
- Taniguchi M, JV Turner and AJ Smith (2003b). Evaluations of groundwater discharge rates from subsurface temperature in Cockburn Sound, Western Australia. *Biogeochemistry*; 66: 111–124.
- Taniguchi M (2000). Evaluation of the saltwater–groundwater interface from borehole temperature in a coastal region. *Geophys Res Lett*; 27: 713–6.
- Taniguchi M and H Iwakawa (2001). Measurements of submarine groundwater discharge rates by a continuous heat-type automated seepage meter in Osaka Bay, Japan, *Journal of Groundwater Hydrology*; 43: 271-278.
- Taniguchi M, WC Burnett, H Dulaiova, F Siringan, J Foronda, G Wattayakorn, S Rungsupa, EA Kontar and T Ishitobi (2008). Groundwater Discharge as an Important Land-Sea Pathway into Manila Bay, Philippines. *Journal of Coastal Research*; 24(1): 15-24.
- Tobin HJ, JC Moore, ME MacKay, DL Orange and LD Kulm (1993). Fluid flow along a strike-slip fault at the toe of the Oregon accretionary prism: implications for the geometry of frontal accretion. *Geological Society of America Bulletin*; 105: 569–582.
- Tokunaga T, T Nakata, K Mogi, M Watanabe, J Shimada, J Zhang, T Gamo, M Taniguchi, K Asai and H Saegusa (2003). Detection of submarine fresh groundwater discharge and its relation to onshore groundwater flow system: an example from offshore Kurobe alluvial fan (in Japanese). *J Jpn Assoc Groundwater Hydrol*; 45(2): 133–144.
- Top Z, L Brand, DR Corbett, WC Burnett and J Chanton (2001). Helium as a tracer of groundwater input into Florida Bay. *J. Coast. Res.*; 17(4): 859–868.
- Tsunogai U, J Ishibashi, H Wakita and T Gamo (1998). Methane-rich plumes in the Suruga Trough (Japan) and their carbon isotopic characterization. *Earth Planet Sci Lett*; 160: 97–105.
- Tsunogai U, J Ishibashi, H Wakita, T Gamo, T Masuzawa, T Nakatsuka, Y Nojiri and T Nakamura (1996). Fresh water seepage and pore water recycling on the seafloor: Sagami Trough subduction zone, Japan. *Earth Planet Sci Lett*; 138: 157–168.
- Uchiyama Y, K Nadaoka, P Rölke, K Adachi and H Yagi (2000). Submarine groundwater discharge into the sea and associated nutrient transport in a sandy beach. *Water Resources Res*; 36(6): 1467–1479.
- Valiela I, JL Bowen and KD Kroeger (2002). Assessment of models for estimation of land-derived nitrogen loads to shallow estuaries. *Appl Geochem*; 17: 935–53.
- Valiela I and JE Costa (1988). Eutrophication of Buttermilk Bay, a Cape Cod coastal embayment: concentrations of nutrients and watershed nutrient budgets. *Environmental Management*; 12: 539–553.
- Valiela I and C D’Elia (1990). Groundwater inputs to coastal waters. *Biogeochemistry*; Special Issue 10: 328
- Valiela I, JM Teal, S Volkman, D Shafer and EJ Carpenter (1978). Nutrient and particulate fluxes in a salt marsh ecosystem: tidal exchanges and inputs by precipitation and groundwater. *Limnology and Oceanography*; 23: 798–812.

- Vanek V and DR Lee (1991). Mapping submarine groundwater area—an example from Laholm Bay, southwest Sweden. *Limnology and Oceanography*; 36: 1250–1262.
- Webster IT, SJ Norquay, FC Ross and RA Wooding (1996). Solute exchange by convection within estuarine sediments. *Estuar Coast Shelf Sci*; 42: 171–83.
- Weiskel PK and BL Howes (1991). Dissolved nitrogen flux through a small coastal watershed. *Water Resources Research*; 27: 2929-2939.
- Whiting GJ and DL Childers (1989). Subtidal advective water flux as a potentially important nutrient input to southeastern USA saltmarsh estuaries. *Estuarine, Coastal and Shelf Science*; 28: 417–431.
- Williams PW (1977). Hydrology of the Waikoropupu Springs: a major tidal karst resurgence in northwest Nelson (New Zealand). *Journal of Hydrology*; 35: 73–92.
- Williams MO (1946). Bahrain: port of pearls and petroleum. *Natl Geogr*; 89: 194–210.
- Wilson AM (2005). Fresh and saline groundwater discharge to the ocean: a regional perspective, *Water Resour. Res.*; 41:-
- Windom H and F Niencheski (2003). Biogeochemical processes in a freshwater–seawater mixing zone in permeable sediments along the coast of Southern Brazil. *Mar Chem*; 83: 121–130.
- Windom HL, WS Moore, LFH Niencheski and RA Jahnke (2006). Submarine groundwater discharge: A large, previously unrecognized source of dissolved iron to the South Atlantic Ocean. *Marine Chemistry*; 102: 252–266.
- Woods Hole Oceanographic Institution (WHOI) (2009). Image: Subterranean Estuary Geochemistry Retrieved 20:39, November 27, 2009 from http://www.whoi.edu/cms/images/GroundWater_81403.jpg
- Zektser IS, RG Dzhamalov and TI Safronova (1983). Role of submarine groundwater discharge in the water balance of Australia. IAHS-AISHPublication, No. 142 “Groundwater in Resources Planning” 209–219.
- Zektser IS and HA Loaiciga (1993). Groundwater fluxes in the global hydrologic cycle: past, present and future. *J Hydrol*; 144: 405–427.
- Zektser IS (1996). Groundwater discharge into the seas and oceans: state of the art. In: Buddemeier RW, editor. *Groundwater discharge in the coastal zone* (pp. 122–123). LOICZ IGBP, LOICZ, Texel, Netherlands, Russian Academy of Sciences, Moscow, 179 pp.
- Zektser IS and RG Dzhamalov (1981). Groundwater discharge to the Pacific Ocean, *Hydrological Sciences Bulletin*; 26: 271-279.
- Zektser IS, VA Ivanov and AV Meskheteli (1973). The problem of direct groundwater discharge to the seas. *Journal of Hydrology*; 20: 1-36.
- Zimmermann CF, JR Montgomery and PR Carlson (1985). Variability of dissolved reactive phosphate flux rates in nearshore estuarine sediments: effects of groundwater. *Estuaries*; 8: 228–236.

Chapter 2

3D Density Dependent Modeling of Submarine Groundwater Discharge

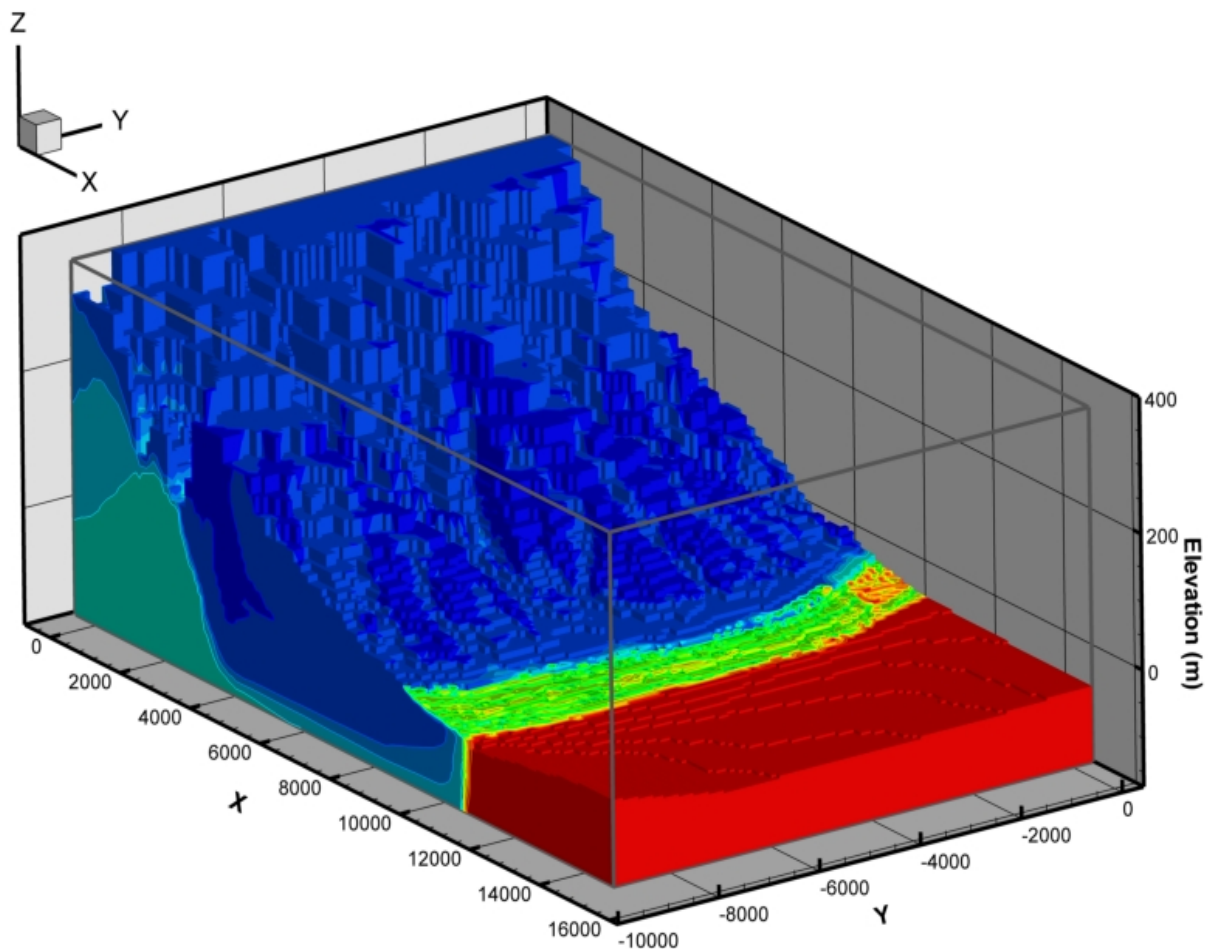


Image: Concentration distribution of base case model result, snapshot Jan 2005.

2.1 Abstract

A regional scale modular variable-density groundwater flow model (MOCDENS3D) has been used to estimate the magnitude of submarine groundwater discharge to Manila Bay. The model area is located at the south-eastern flank of Mt. Mariveles volcano in Bataan Peninsula, Philippines, a potentially active stratovolcano. The area stretches on 12 km of coastline where preliminary SGD flux measurements were made earlier. The hydrogeologic properties of these sediments are estimated using information from pumping tests, borehole data, seismic sections and geological maps. Key features of the groundwater system include high relief in the upper slopes and narrow low relief coastal plain. The model domain incorporates both the terrestrial recharge and also the re-circulated water in the coastal sediments. Different scenarios were run to evaluate the sensitivity of SGD to changes in different input parameters. SGD rates peak during the rainy season and there's a month delay to the peak rainfall. SGD shows major influence of rainfall (recharge), geology and topography. Model calculations suggest that there is substantial contribution of freshwater from terrestrial origin which discharges to the bay. The presence of confining layers greatly affects the offshore extent of SGD, and therefore its potential impact on the regional environment. Model results are consistent with previously measured SGD rates using seepage meters and geochemical tracers by [Taniguchi *et al.* \(2008\)](#).

2.2 Introduction

This chapter examines the hydrogeologic factors which influence the magnitude of submarine groundwater discharge (SGD) to Manila Bay, focusing mainly on the factors associated with volcanic systems using a 3D variable density dependent hydrogeological model (MOCSENS3D). Results of the study made by [Taniguchi *et al.* \(2008\)](#) confirmed the occurrence of SGD in this area with estimated SGD flux from the surficial aquifer to be about $12.4 \text{ m}^3 \text{ m}^{-1} \text{ day}^{-1}$ ($8.3 \times 10^8 \text{ m}^3 \text{ y}^{-1}$). This study is a part of the master research project designed to investigate and analyze the magnitude and quality of SGD to Manila Bay with accompanied field measurements via computer modelling.

SGD is defined as the total water (terrestrial freshwater and re-circulated seawater) regardless of its source and concentration flowing out of the seabed into the coastal water through the underlying sediments. A detailed discussion of SGD source and driving mechanism can be found in **Chapter 1**.

Direct measurements of SGD mostly have focused in the near shore environment where the SGD fluxes are expected to be the highest (see [Table 1.1](#) and [Table 1.2](#)). It is expected that these fluxes decrease with distance from the coast, however in cases where the confining layer extends further offshore, leakage across this layer may promote SGD kilometers beyond the shoreline in the form of submarine springs.

A fewer number of studies have attempted to quantify SGD using geochemical tracers, water balance method and hydrological modeling (see [Table 1.1](#), [Table1.2](#) and [Table 1.3](#)). Results from hydrological models are oftentimes lower than the other methods primarily due to the underestimation of some hydrologic parameters. The results presented here show the potential role of each hydrologic parameter in the magnitude of SGD using multiple sensitivity analysis.

2.3 Regional setting and features of Manila Bay

Manila Bay, a semi-enclosed estuary facing the South China Sea, is one of the best natural harbors in the world. The bay is located on the southwestern part of Luzon Island between 14°15' - 14°50' N and 120°30' - 121°00' E ([Figure 2.1](#)). It has a surface area of 1800 km² with a coastline of approximately 190 km. It is a gently sloping basin with a depth increasing at a rate of 1 meter per kilometer from the interior to the opening of the bay. It has an average depth of 25 m and is approximately 52 km long, with widths varying from 19 km at its mouth to 56 km inside the bay. Corregidor and Caballo Islands divides the entrance to the Bay into a North Channel, <4km wide and has maximum depth of 71 m and South channel which is <6 km wide and <47 m deep. The deepest parts of both channels are adjacent to the intervening islands. It is bordered by major coastal cities and municipalities.

The bay receives drainage from approximately 17000 km² of watershed consisting of 26 catchment areas. The catchment is bounded by the Sierra Madre mountain range to the east,

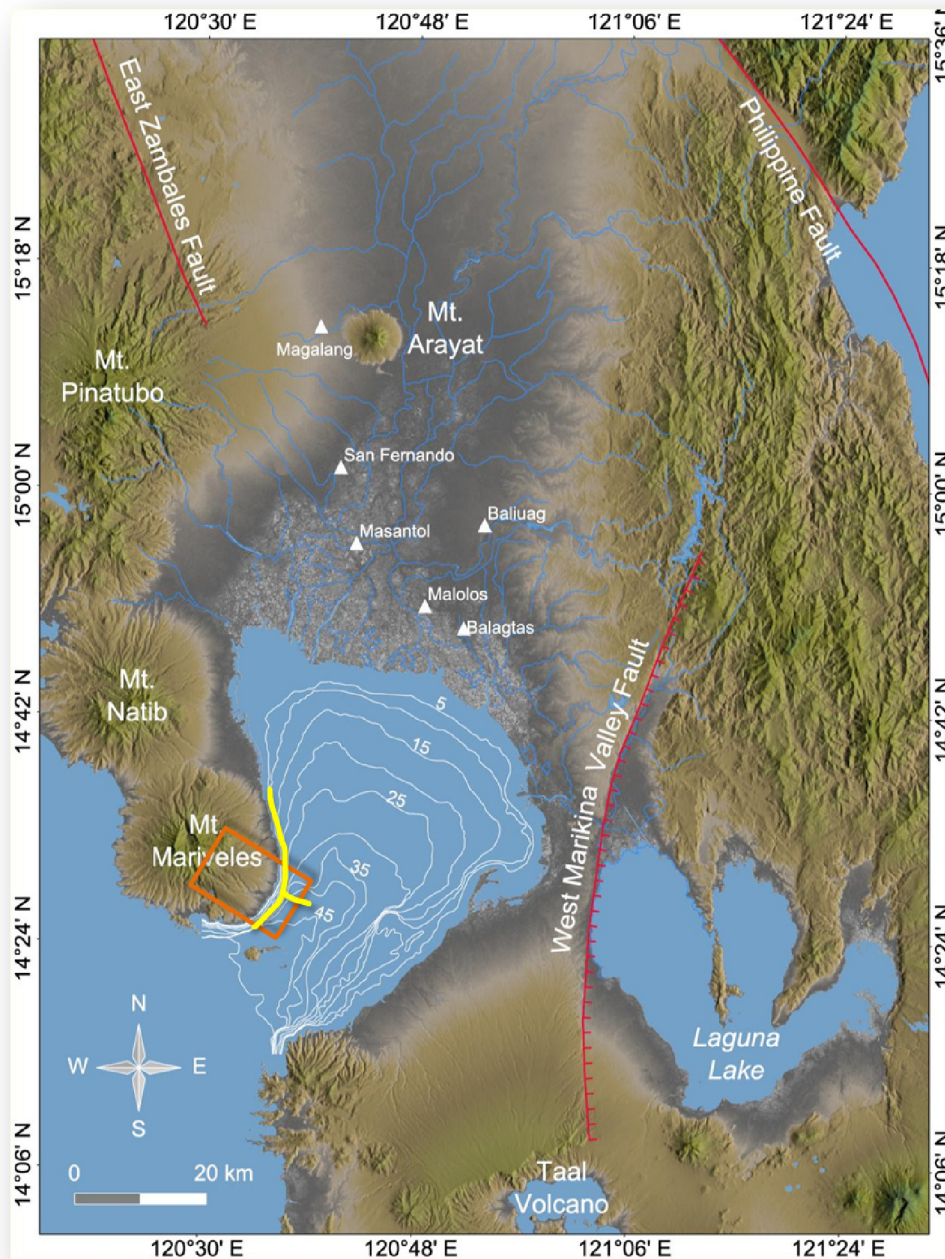
the Caraballo mountain range to the north, the Zambales Mountains to the northwest and the Bataan mountains which includes Mt. Mariveles to the west. The tide is predominantly diurnal and within the micro tidal range, average of 1.2m during spring tide and 0.4m during neap tide.

2.4 Study area and Physiography

The selected study area is located on the SE coast of the Bataan peninsula. It is situated on the SE slopes of Mt. Mariveles, a potentially active stratovolcano (Figure 2.2). It contains several structurally controlled rivers, namely from N to S: Lamao, Lucanin, Cayangcam, Pangolisanin, Babuyan, San Jose, Digunin and Doracan. All these drainage basins are elongate and east-southeast flowing except the Lamao River, owing its pattern to the structurally controlled terrain. Several ephemeral streams and springs which drain to the main rivers are also found. The area is characterized by rolling topography and steep slopes mostly 4-6% but some as much as 20%, with a relatively very narrow and flat coastal area. The ground surface reaches an elevation of approximately 850 m at the northwestern extent of the study region.

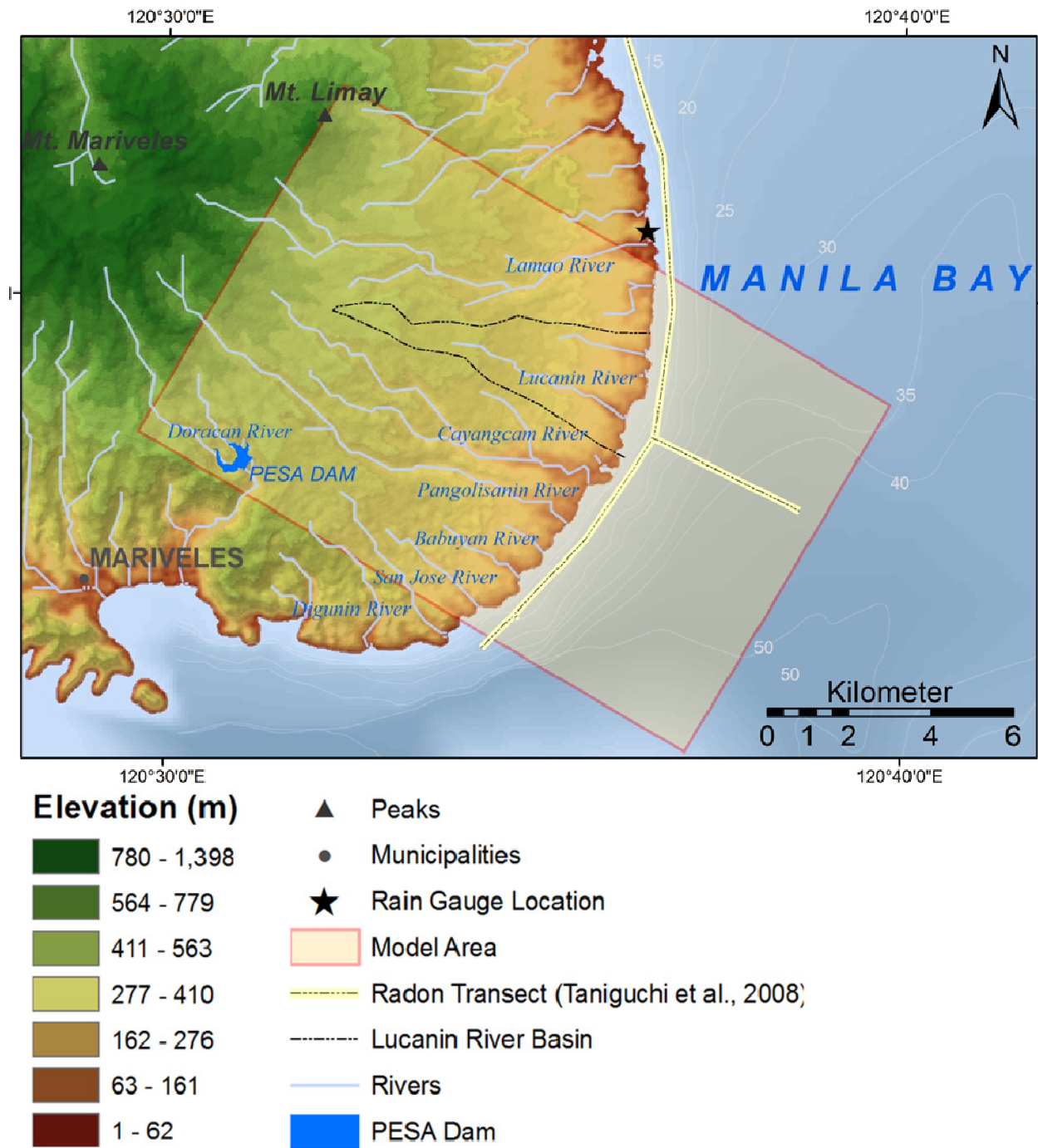
Climate affecting the area is tropical with pronounced dry (November to April) and wet (May to October) season. The average annual rainfall in the area obtained from the rain gauge station in Limay (indicated by the black star in Figure 2.2) is 3001 m yr^{-1} , using measurements taken between 1922-1930 and 1932-1939. Least rainfall is during January and February while August is the max. In Balanga, north of the study area, mean monthly temperatures are from $25.5 \text{ }^{\circ}\text{C}$ to $29 \text{ }^{\circ}\text{C}$, the lowest occur in January and February, and the warmest months are April

and May with means of 29 °C and an average annual temperature of 27.1 °C. Mean annual maximum is about 32 °C although cooler weather is experienced in the highlands.



Modified from: [Soria, 2009](#); Data Sources: SRTM from [USGS \(2004\)](#), bathymetry from [USDMA \(1982\)](#), faults from [Maletierre \(1989\)](#) and [Rimando and Knuepfer \(2006\)](#) and radon transect from [Tanguchi et al., 2008](#).

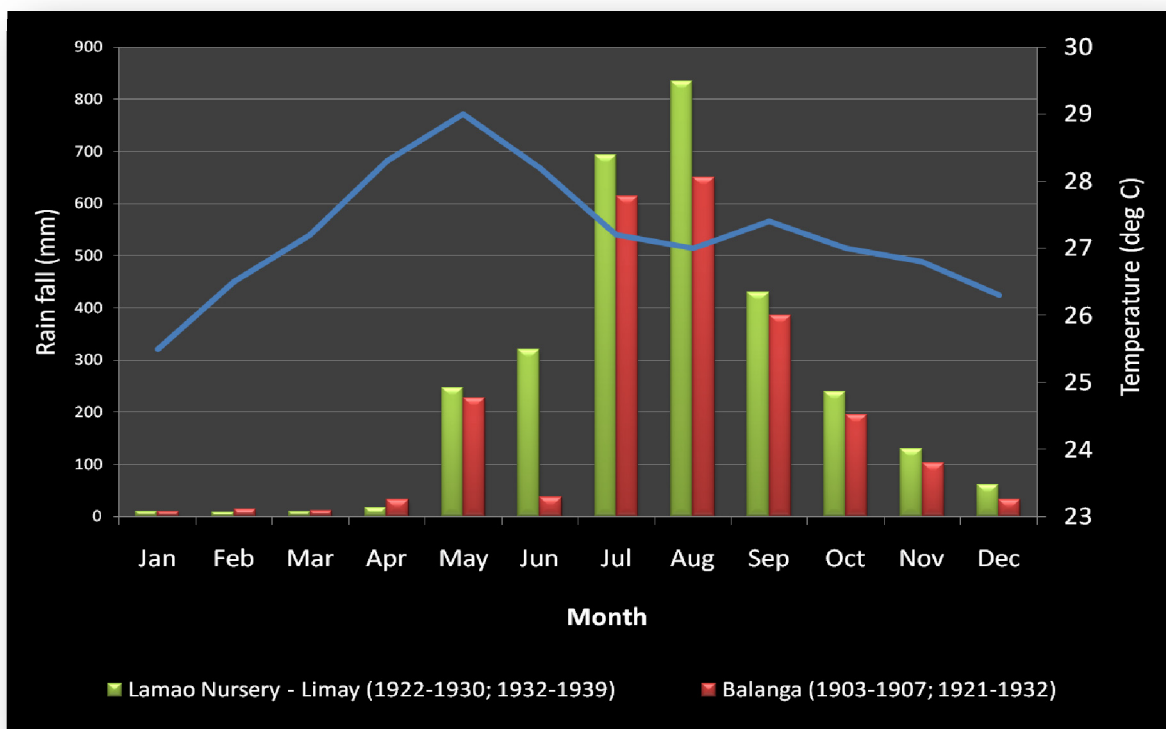
Figure 2.1 Regional Setting of Manila Bay. The model area is shown in rectangular orange box, Details in [Figure 2.2](#).



Data Sources: Aster GDEM from [ERSDAC, 2009](#), bathymetry from [USDMA, 1982](#), radon transect from [Tanguchi et. al., 2008](#), rivers from [MGB](#)

Figure 2.2 Digital Terrain Model of the model area. Also shown are the different geographical features, including water bodies.

Relative humidity averages about 85% during the rainy months and 70 percent during the dry. No normal wind spreads are reported. Wind velocity could be similar to Manila or Mindoro which range from about 5 to 20 km per hour. The southeast monsoons are dominant from June to November while the northeast monsoons and east-west winds prevail during the other months.

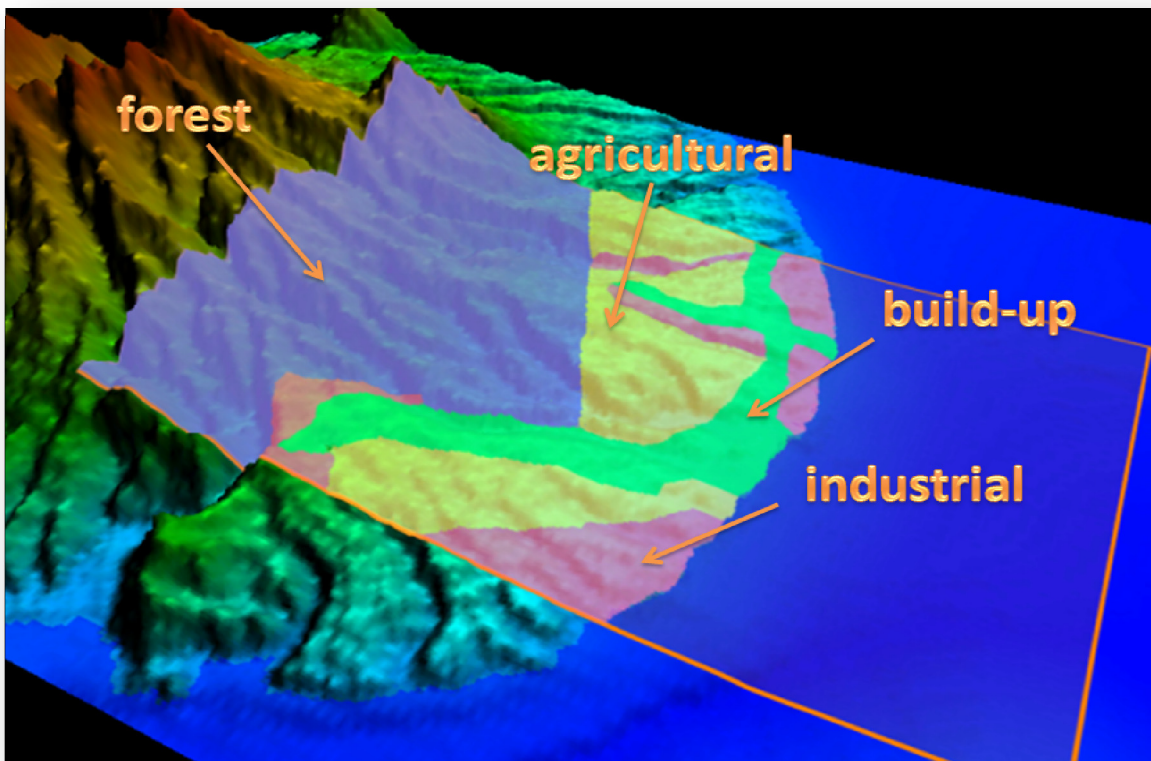


Data Sources: Rainfall and temperature data from [PAGASA](#) obtained from [Geological Oceans Laboratory, MSI](#) and [MGB](#)

Figure 2.3 Mean monthly rainfall in Limay and Balanga stations. Blue line represents the monthly variation in temperature. Also indicated are the years when the measurements were taken.

No open pan evaporation measurements are available for Bataan. Measurements in surrounding areas e.g. Manila and Angat waterbed, averaged 1050 mm and 1020 mm,

respectively. The International Rice Research Institute (IRRI) at Los Banos, Laguna reported a 1:1 relationship between rice evapotranspiration and open pan evapotranspiration in 1965. Due to lack of information, the actual evapotranspiration (aET) in the study area is estimated using the FAO Penman-Monteith Method (FAO, 1998), where the reference evapotranspiration (ET_{ref}) is multiplied by a crop factor (K_c) which represents the type of vegetation in the area. K_c is approximated using the information from the land-use map obtained from the Mariveles Municipal Planning and Development Office. ET_{ref} and K_c values used in the calculation can be found in **Appendix II**.



Data Sources: Land-use map from [Mariveles Municipal Planning and Development Office](#), DEM from [ERSDAC \(2009\)](#).

Figure 2.4 3D surface of the study area with the land-use type map overlay.

Approx 10% of the study region is composed of built-up areas. The agricultural area accounts for about 25%. Mixed fruit tree, coconut and irrigated rice paddy are the major agricultural crops in the area. A large portion of the industrial area in northeastern Mariveles is occupied by the industrial park of the Philippine National Oil Co. (PNOC) Petrochemical Development Corp. in the major development in the area is the Batangas Dos where petrochemical processing (polypropylene, polyethylene and polyvinyl chloride) plants occupy a 280 ha area (Taniguchi *et al.*, 2004). The upper parts of the drainage basins in Mariveles and Limay are covered with forest which accounts for almost 50%.

The direct run-off is estimated using the *Thorntwaite water balance approach* (Ferguson, 1996). Given by the equation:

$$Qr = 0 \quad \text{if } \frac{-0.095 + 0.208 P}{S^{0.66}} < 0$$
$$Qr = \frac{-0.095 + 0.208 P}{S^{0.66}} \quad \text{if } \frac{-0.095 + 0.208 P}{S^{0.66}} \geq 0$$

where Qr is the average monthly direct runoff, S is related to the soil and cover characteristics of the soil, which is represented through its relationship to the value of the runoff curve number (CN) given by:

$$S = \frac{100}{CN} - 10 \quad (\text{inches})$$

CN is the curve number, estimated based on land-use and P is the average monthly precipitation. The CN values used and further explanation can be found in **Appendix II**.

The method by Ferguson (1996) is chosen because the available data for rainfall is only monthly. Conventional curve number methods for estimation of direct run-off cannot be used since it calculates the run-off using short period (hourly, daily) rain events.

The effective recharge in the area is represented by:

$$R = P - aET - Ro + \Delta S$$

where, R is the effective recharge, P is precipitation, aET is the actual evapotranspiration, Ro is the run-off and ΔS is the change in soil water storage. Assuming that ΔS is negligible or close to 0, the effective recharge in the area using the mean average rainfall is represented in Figure 2.5. Here we can clearly see that precipitation exceeds aET throughout most of the year, providing abundant water to the system.

There are several extraction wells in the area. Figure 2.6 shows the location of the extraction wells and the corresponding extraction rates. Wells with very high extraction rates belong to industries such as Petron or to the Mariveles Water District (MARIWAD) which supplies the potable water in the area. Several private wells and open dug wells are still present. Near the coast, several “free flowing” wells are found.

Limited numbers of wells have information on the water quality. If available, continuous monitoring was never made. Water quality samples from the wells have very low total dissolved solids concentration (150-200 ppm or mg l^{-1} TDS) even at great depths (200m below surface). Because of this the freshwater-saltwater interface is difficult to determine. Nevertheless, there are no reported cases of salt water intrusion in the area.

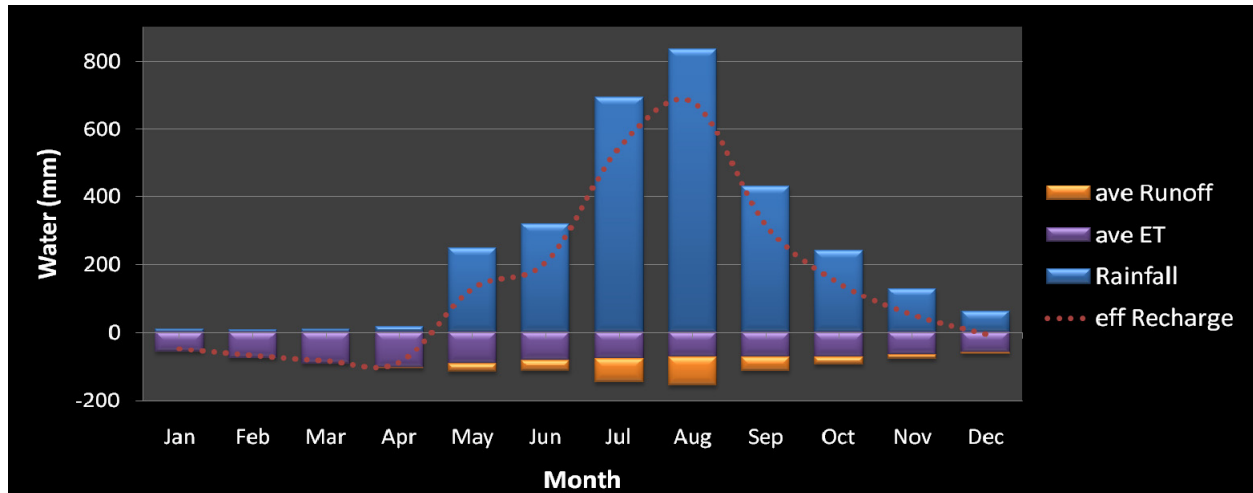
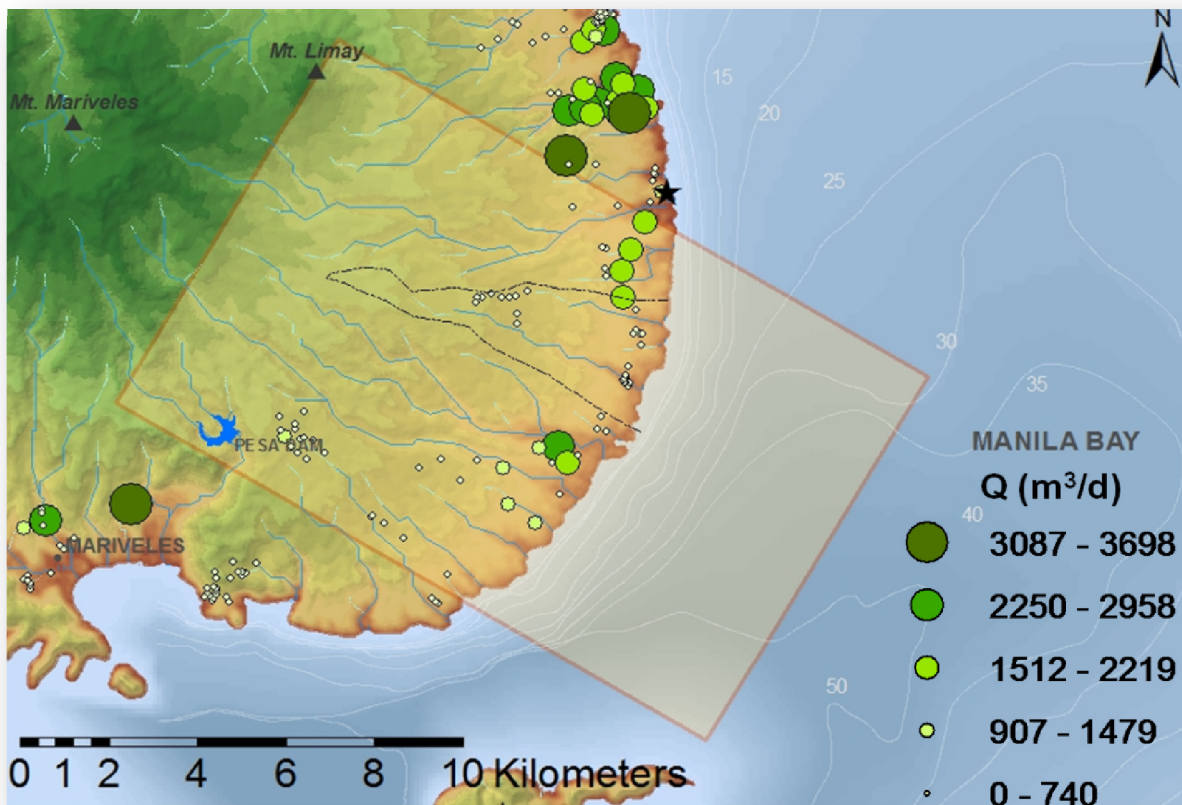


Figure 2.5 Graph showing the rainfall, calculated average run-off, ET and effective recharge in the study area.



Data Sources: Well locations and extraction rates from LWUA and fieldwork.

Figure 2.6 Extraction wells in the area and corresponding extraction rates in m^3d^{-1} .

2.5 Geology and Hydrogeology

The main rock sequence of the area includes lava flows, agglomerates, fine tuff, uncemented pyroclastic deposits, worked finer pyroclastic, intrusive andesite bodies and quaternary alluvium (Figure 2.7). This geological map is created using partly the data from Almero, 1989 in Payot *et al.*, 2005.

The lava flow occurs near the central cone and subsiding vents. It is largely of hornblende and pyroxene andesite, characterized by closely-spaced, low dipping joints, suggestive of sheeting planes. The agglomerates are mostly sub-angular to sub-rounded fragments of andesite, with greater proportion of cementing ash and/or mud. They are well lithified and widely layered. This rock occupies the slopes and topographic lows. The more recent volcanics occur as volcanic plug with late Pleistocene to Pleistocene andesite flow. They are generally andesite and/or dacitic in composition these rocks occupy the center portion of the Bataan volcanic cones.

More than 80% of Bataan is underlain by various intercalated pyroclastic rock occurring as densely cemented breccias, agglomerates, tuff, mudflows, volcanic conglomerates, re-worked tuff and cemented to poorly cemented volcanoclastic deposits. The pyroclastic sequence is normal to irregular to lenticular.

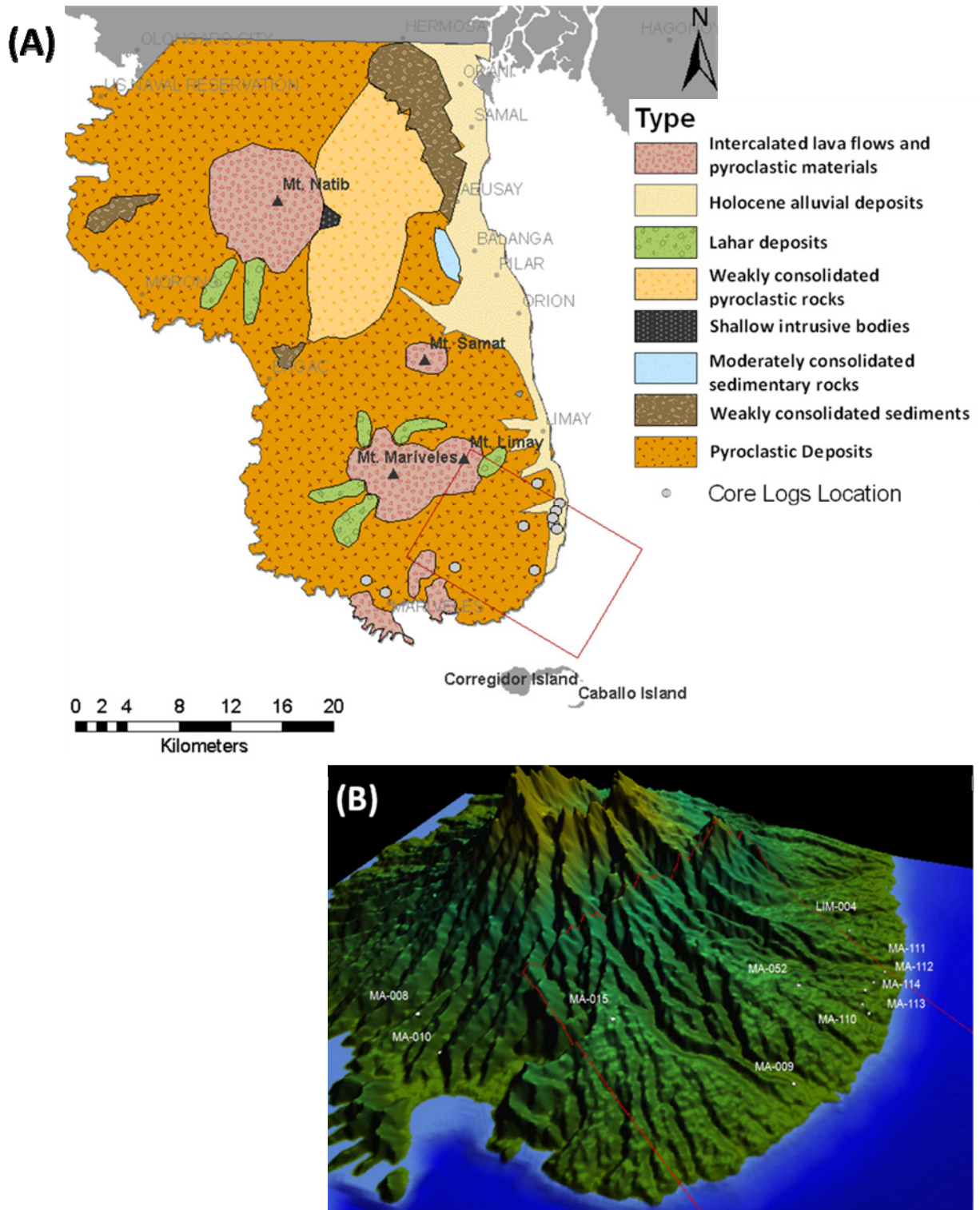


Figure 2.7 (A) Geological Map of Bataan. **(B)** DEM showing locations of available borehole data, corresponding to the grey dots in **Figure 2.7A**.

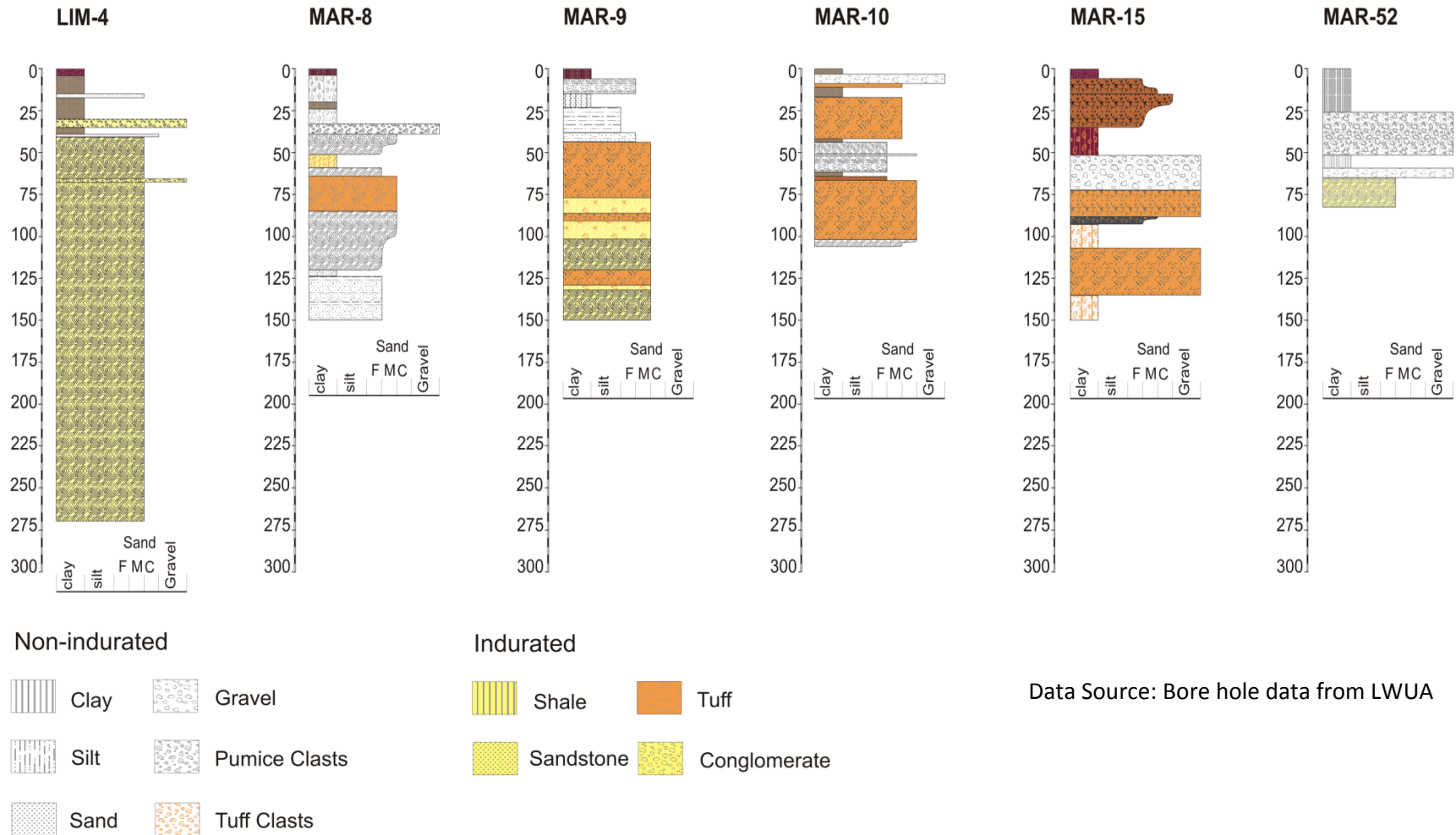
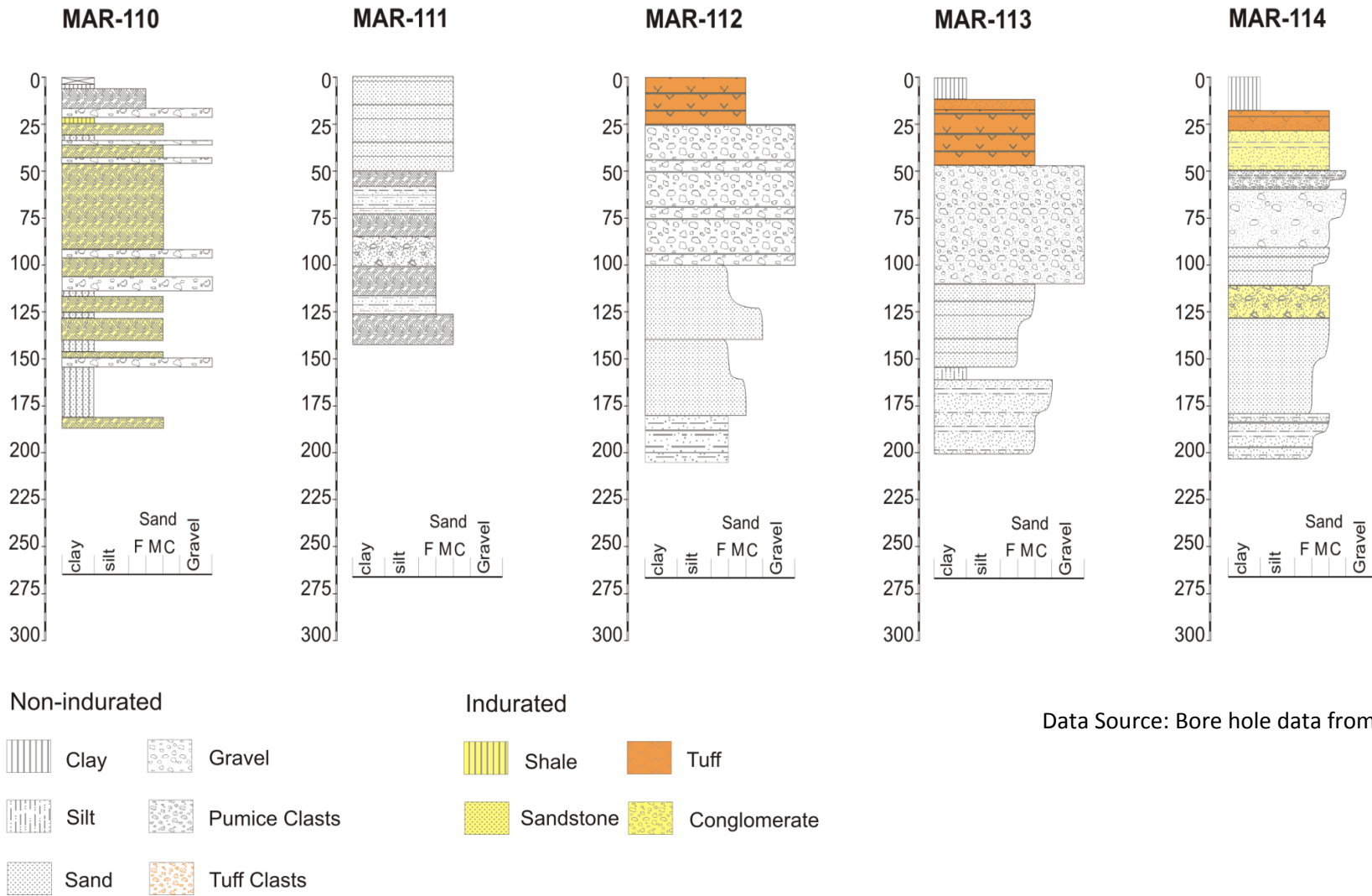


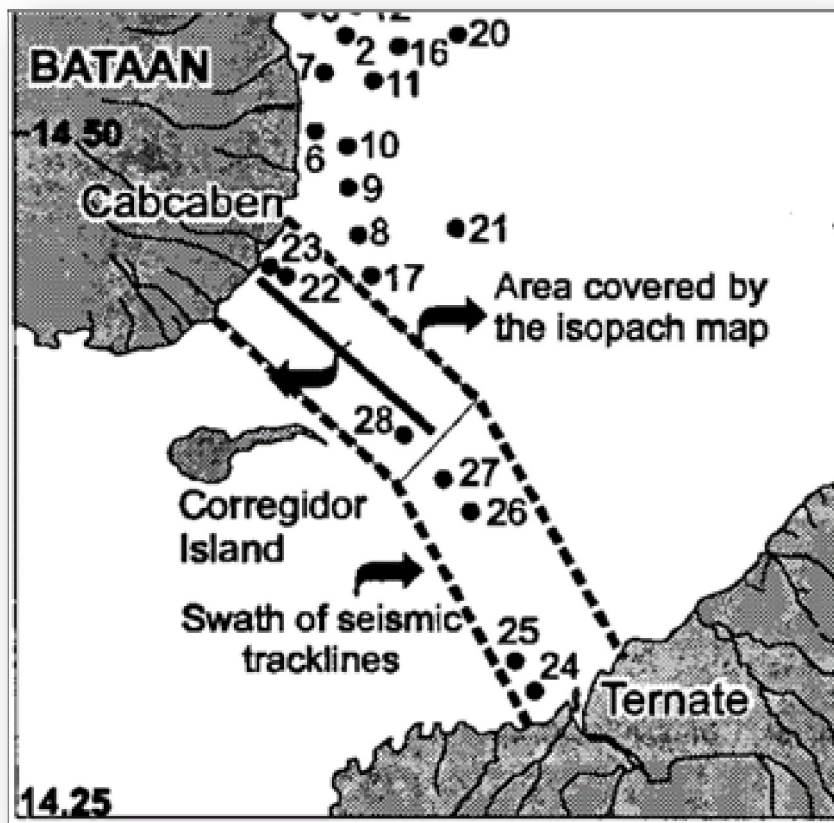
Figure 2.8 Interpreted cross-section logs from borehole data. Vertical scale in meters (m) from surface.



Data Source: Bore hole data from LWUA

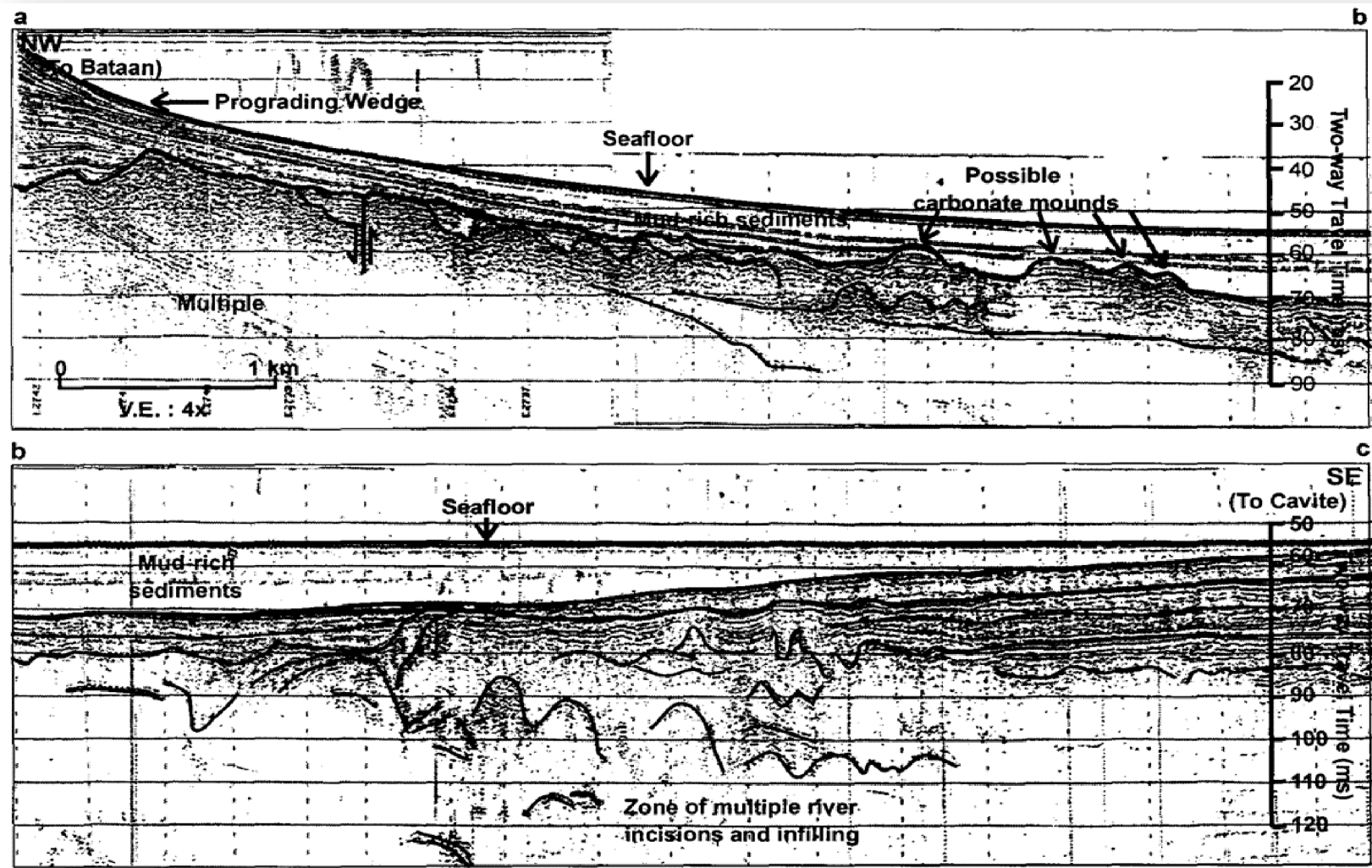
Figure 2.8 cont. Interpreted cross-section logs from borehole data. Vertical scale in meters (m) from surface.

Available borehole data made it possible for a more extensive study of the underlying geology. Figure 2.8a and 2.8b shows the interpreted cross-sections logs from borehole data. The location, depths and extent of confining units can be derived from the logs. Confining layers mainly composed of fine (clay- to silt-sized), form discontinuous layers at different depths. The characteristics of the sediments in the seaward side of the study area are determined using isopach maps, both of muddy sediments (Figure 2.11a) and sand (Figure 2.11b).



Modified from: [Siringan and Ringor, 1998](#).

Figure 2.9 Index map showing the swath of seismic track lines of and the area covered by the isopach maps. Numbers indicate the sampling sites used by the authors.



Source: Siringan and Ringor, 1998.

Figure 2.10 Seismic reflection profiles across the bay mouth.

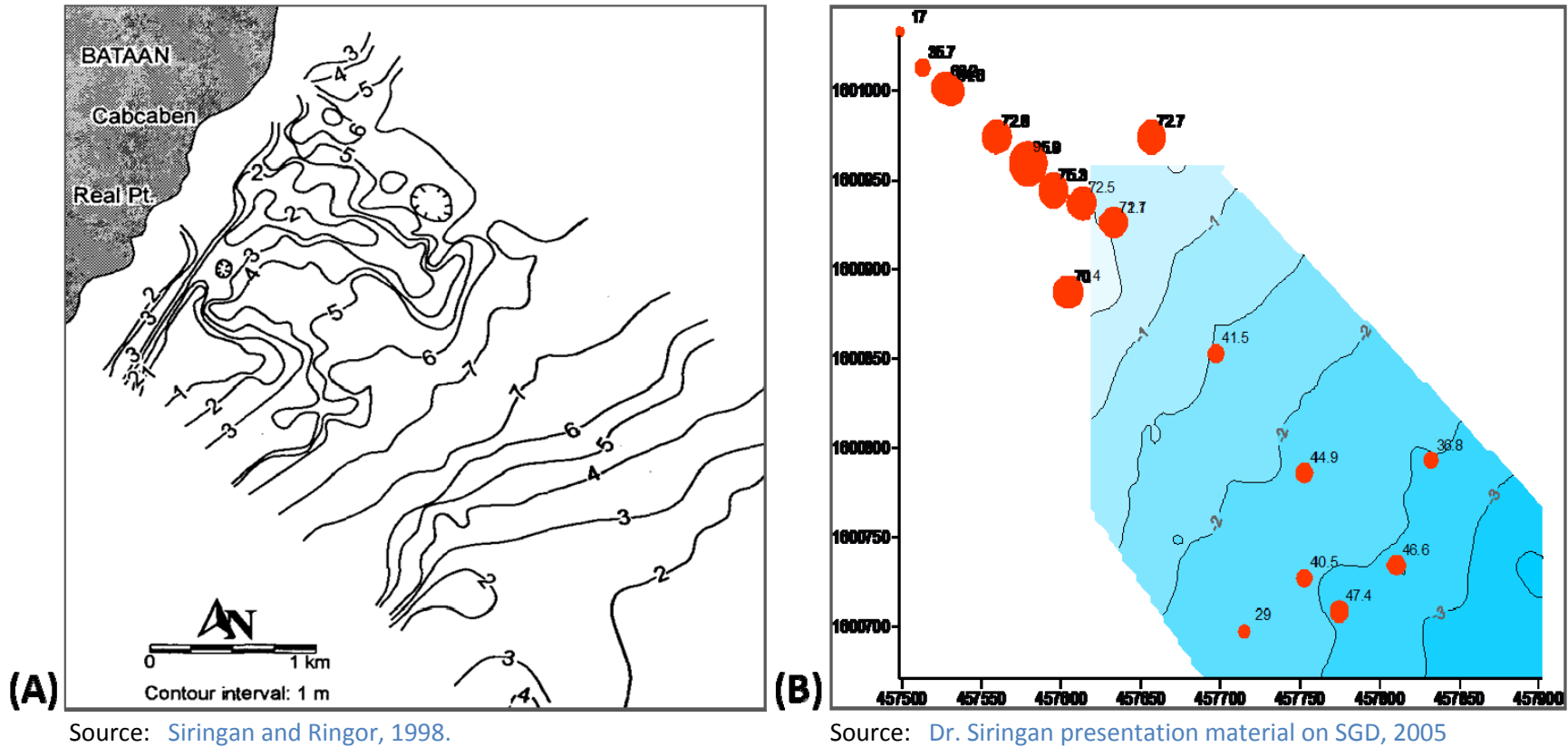


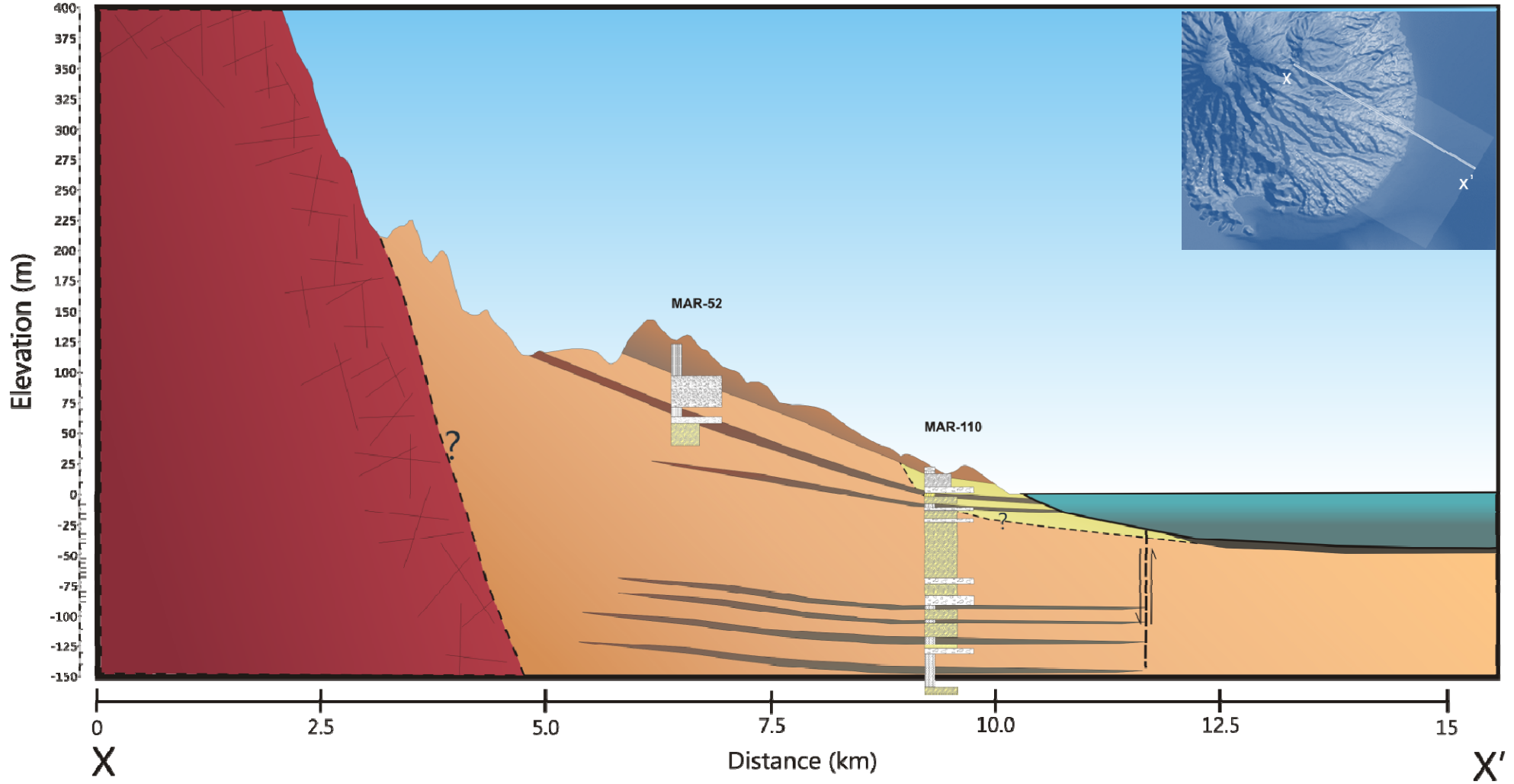
Figure 2.11 (A) Isopach map of muddy sediments (B) Variations in sand composition (%) of the bay sediments in the study area.

Combining the knowledge of the topography, geology, cross-section logs, seismic profiles and isopach maps – conceptual geology profiles for the study area with 4 main lithologic units for the hydrogeology are created. The representative hydrogeologic profile for the study area is shown in [Figure 2.12](#), other profiles made for the model area are found in **Appendix III**. These profiles are done at different strategic locations based on the available data. These lithologic interpretations were used to create a 3D (hydro) geology model ([Figure 2.13](#)), containing the information of the different hydrogeologic units.

Detailed descriptions of these groups are summarized in [Table 2.1](#). This grouping is the basis for assigning the different hydraulic parameters in the model.

Table 2.1 Geologic description of each hydrogeologic group

Group	Description	
Qv	Fractured lava flows and intercalated pyroclastic	
Qvp	Volcaniclastics – Breccia and agglomerate intercalated with tuff	
Qal	Quaternary Alluvium	
Interpreted confining (clay) units	Type 1	Top soil and sea floor mud
	Type 2	Buried soil profiles, ash layers (clayey sand or clayey silt)
	Type 3	Buried soil profiles, tuffaceous clay



Lithologic Units

- Qv Fractured andesite lava flows and intercalated pyroclastic
- Qvp Volcaniclastics - Breccia and agglomerate intercalate with Tuff
- Qal Alluvium, beach deposits, alternating layers of sand, sil and mud

Supplementary

- Interpreted clay layers - possibly buried soil profiles, fine volcanic ash, or deep sea mud

Figure 2.12 Representative hydrogeologic profile for the study area. Also shown are the cross section logs used for the interpretation. Index map on the upper right side shows the location of the profile.

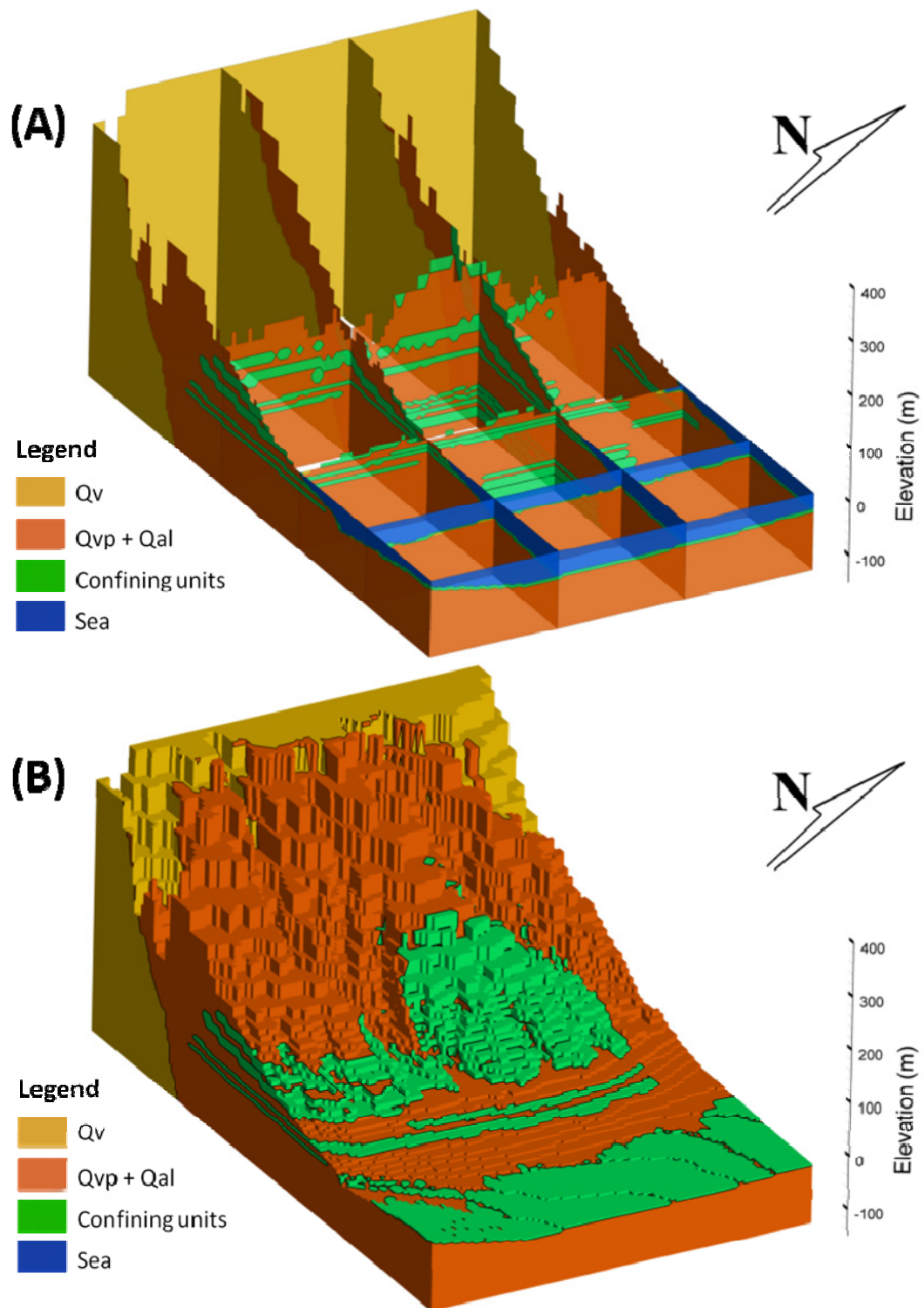


Figure 2.13 Created 3D (hydro) Geology Model of the study area. **(A)** Combined cross sections **(B)** Block model – sea is blanked for a better view of the underlying confining units.

There are two types of aquifer in the study area (confined and unconfined). Both aquifer units are mainly composed of Quaternary sand- to gravel-sized volcanoclastic sediments derived from the nearby inactive volcanoes (Group Qvp and Qal). The confining layers are mainly composed of fine (clay- to silt-sized) ash and soil which form discontinuous layers at different depths (clays in [Figure 2.13A and B](#)). The extent of the confining units offshore is set at 1km from the shoreline, inferred from the presence of a fault in the seismic profile ([Figure 2.10](#)). Based on interpreted cross-section logs ([Figure 2.8A and B](#)), the materials of the unconfined aquifers in the study area the same as those found in the confined aquifers.

2.6 Numerical Model

2.6.1 Governing Equations

In modeling the submarine groundwater discharge, it is necessary to use a density-dependent groundwater flow model to incorporate the effects of spatial variations in fluid density on groundwater flow patterns and fluxes especially on the freshwater – saltwater boundary.

The governing equations for the groundwater flow are as follows:

The mathematical **expression for groundwater flow** in a porous media as described by [Bear \(1972\)](#) is given by:

$$S_s \frac{\partial h}{\partial t} = - \left[\frac{\partial q_x}{\partial x} + \frac{\partial q_y}{\partial y} + \frac{\partial q_z}{\partial z} \right] - W$$

where S_s is the specific storage (L^{-1}), h the hydraulic head (L), q the Darcy specific discharge ($L T^{-1}$) and W is a source or sink term (T^{-1}), examples of sources of sources and sinks are natural recharge, artificial recharge and abstraction. The **Darcy specific discharge** in the x, y and z-direction is given as:

$$q_x = -\frac{\kappa_x}{\mu} \frac{\partial p}{\partial x} \quad , \quad q_y = -\frac{\kappa_y}{\mu} \frac{\partial p}{\partial y} \quad , \quad q_z = -\frac{\kappa_z}{\mu} \left(\frac{\partial p}{\partial z} + \rho g \right)$$

where, $\kappa_x, \kappa_y, \kappa_z$ are the intrinsic permeabilities (L^2) of the porous media in x, y and z-directions, μ is the viscosity of the groundwater ($M L^{-1} T^{-1}$), p is the pressure ($M L^{-1} T^{-2}$), g is the gravity constant ($L T^{-2}$), ρ is the density of the groundwater ($M L^{-3}$). The **hydraulic head** is defined as:

$$h = \frac{p}{\rho g} + z$$

where, h is the the hydraulic head (L), z is the elevation head (L). If ρ is constant the **hydraulic conductivities** in the x, y and z-direction are defined as:

$$K_x = \frac{\kappa_x \rho g}{\mu} \quad , \quad K_y = \frac{\kappa_y \rho g}{\mu} \quad , \quad K_z = \frac{\kappa_z \rho g}{\mu}$$

when the term ρg is constant then the combination turn out to be the equation for **specific discharge** given by:

$$q_x = K_x \frac{\partial h}{\partial x} \quad , \quad q_y = K_y \frac{\partial h}{\partial y} \quad , \quad q_z = K_z \frac{\partial h}{\partial z}$$

To relate density to concentration (Cl or TDS), salinity, temperature and pressure, there are several conversion formulas used. The relation describes the **density as a function of chloride concentration** (Sorey, 1978; Holzbecher, 1998):

$$\rho(C) = \rho_f \left(1 + \alpha \frac{C}{C_s} \right)$$

Where, $\rho(C)$ is the density of the groundwater ($M L^{-3}$), ρ_f is the reference density which is usually the density of fresh groundwater at mean subsoil temperature ($M L^{-3}$), α is the **relative density difference** (-) given by:

$$\alpha = \frac{\rho_s - \rho_f}{\rho_f}$$

C is the chloride concentration or the so-called chlorinity ($\frac{mg Cl^-}{l}$) and C_s is the reference chloride concentration ($\frac{mg Cl^-}{l}$). Often seawater is used as a reference.

The following values for the different parameters are used in the calculation:

$$\rho_f = 1000 \text{ kg/m}^3; \quad \rho_s = 1025 \text{ kg/m}^3; \quad \text{thus } \alpha = 0.025;$$

$$C_s = 19300 \text{ mg Cl}^-/l; \quad \text{in TDS} = 34500 \text{ mg/l}.$$

The freshwater head, which takes into account the density differences, is defined as:

$$h_f = \frac{p}{\rho_f g} + z$$

Where, h_f is the freshwater head (L) and ρ_f is the reference density ($M L^{-3}$). To take into account groundwater density differences in the Darcy specific discharge the vertical specific discharge equation becomes:

$$q_z = -\frac{\kappa_z \rho_f g}{\mu} \left(\frac{\partial h_f}{\partial z} + \frac{\rho - \rho_f}{\rho_f} \right)$$

If the density differences are very small, then the viscosity difference may also be neglected and the vertical specific discharge may be re-written as:

$$q_z = -K_z \left(\frac{\partial h_f}{\partial z} + \frac{\rho - \rho_f}{\rho_f} \right)$$

Hydraulic head and density differences drive groundwater flow and affect the transport of solutes. As a result of porous medium heterogeneity and differences in concentration, there is hydrodynamic dispersion and diffusion. Dispersion and diffusion in the porous media is described in the ***solute advection-dispersion equation*** below:

$$R \frac{\partial C}{\partial t} = D_x \frac{\partial^2 C}{\partial x^2} + D_y \frac{\partial^2 C}{\partial y^2} + D_z \frac{\partial^2 C}{\partial z^2} - \frac{\partial v_x C}{\partial x} - \frac{\partial v_y C}{\partial y} - \frac{\partial v_z C}{\partial z} - \lambda C + \psi$$

where R is the retardation factor (-) for equilibrium sorption. This represents the interaction between the solute and soil, which is significant to solutes that are travelling with a lower averaged velocity than the groundwater. D_x , D_y and D_z is the hydrodynamic dispersion in the xyz -direction ($L^2 T$). This phenomenon describes the dispersion of the solute in the porous medium since different flow paths cause the solute to travel in all directions due to tortuosity. λ is the decay factor (L^{-1}). Decay is the process that describes the decay of solutes due to

microbiological activity. Ψ ($L^3 T^{-1}$) is the term for other sources and sinks. This could mean removal of solutes by abstraction and infiltration of salt water. For salts as chlorine there is no decay so the ***advection-dispersion equation for salt transport*** is then given by:

$$\frac{\partial C}{\partial t} = D_x \frac{\partial^2 C}{\partial x^2} + D_y \frac{\partial^2 C}{\partial y^2} + D_z \frac{\partial^2 C}{\partial z^2} - \frac{\partial v_x C}{\partial x} - \frac{\partial v_y C}{\partial y} - \frac{\partial v_z C}{\partial z} + \Psi$$

2.6.2 PMWIN and MOCDENS3D

As a modeling environment the Graphical User Interface PMWIN has been used. This modeling software is a shell around MODFLOW (McDonald and Harbaugh, 1988) and uses this code for groundwater flow in a porous medium.

The hydrogeological model for SGD in this study is created using MOCDENS3D (Oude Essink, 1998; Oude Essink, 2001). MOCDENS3D is a three-dimensional finite-difference, density-dependent solute transport model originally developed for salt-water intrusion related problems. This model has proven its value in several models created for the different areas in the Netherlands (e.g. Oude Essink, 2001a, Oude Essink 2001b, Oude Essink, 2002). Its main characteristics are: 1) it is block-centered 2) it uses the numerical solution technique of MODFLOW (McDonald and Harbaugh, 1988) and MOC3D (Konikow *et al.*, 1996), and has been adapted for density differences; 3) Advective and hydrodynamic dispersive solute transport processes through porous media are modeled by a particle tracking technique (Peaceman, 1977) in combination with the finite difference method (Konikow *et al.*, 1996), respectively.

MOCDENS3D uses the equations enumerated in the governing equations section to model the density driven groundwater flow.

The whole model structure resembles the MODFLOW structure which allows packages to be added as required by the problem (e.g., drain package, general head boundary package etc.) Most of the MODFLOW packages are manually created by programs done in Dev-Pascal using input maps created with GIS software such as ARCMAP and Global Mapper. The detailed procedure and created codes for each of the packages can be found in **Appendix II**.

2.7 Model Set-up

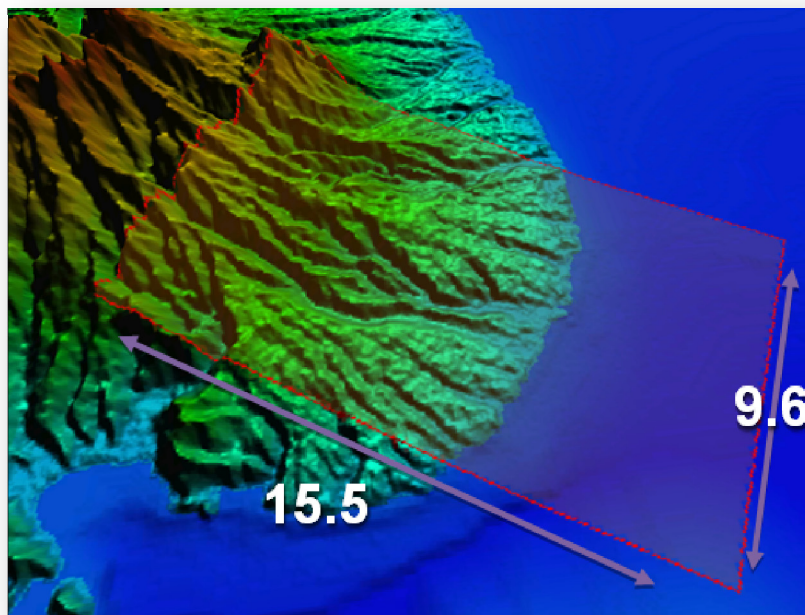
The model area has been selected for practical reasons. In 2005, [Taniguchi *et al.* \(2008\)](#) made SGD measurements using seepage meter and radon in Bataan, Philippines, which makes a possible comparison for the simulation results. Due to other limitations, such as running time of the model, a cell resolution of 100m x 100m is selected (model with more than 200 columns and 200 rows is impractical) and the extent of the model area is also limited. The model area is shown in red box in [Figure 2.14](#) and the model specifications used in [Table 2.2](#).

The surface level geometry of the model has been determined by an Aster GDEM from [ERSDAC \(2009\)](#) with a resolution of 30x30m. The top of the model is set at 400m above msl and the bottom at -150m. 48 layers are created to ensure the detail in vertical direction. The layer thicknesses varies from 50m (top 4 model layers), 25m (next 4 model layers), 10m (next 10

model layers), 4m (next 25 model layers), grid refinement is applied in this region immediately beneath the sea level (0 m elevation) where SGD is occurring, then lastly 10m (last 5 layers).

Table 2.2 Model Specifications

Type	Dimensions
Length	15.5 km
Width	9.6 km
Rows	96
Columns	155
Cell Resolution	100 x 100 m
Layers	48



Data Source: DEM from [ERSDAC, 2009](#)

Figure 2.14 3D view of the model area showing the model extent in km.

2.7.1 Hydrogeologic Parameters

Table 2.3 shows the hydrogeologic parameters used in the simulation models. Pumping tests in the partially confined aquifers (Qvp and Qal units) give relatively low hydraulic conductivity values, within the range of 2.2 to 5.1 m day⁻¹ (average of 4 m day⁻¹) and transmissivity values commonly from 270 to 730 m² day⁻¹. The low hydraulic conductivities can be explained by the very poor sorting of the sediments due to the presence of subordinate amounts of clay (Figure 2.8a and 2.8b). Due to scarce information in majority of the areas, the K_h values for the other units are assumed using known K_h values of similar lithologies from literature. A single value of hydraulic conductivity was assigned to each hydrogeologic unit. It is also assumed that the setting of this model is anisotropic with the vertical conductivity 10 times smaller than the horizontal value. A uniform longitudinal dispersivity of 1 m and transverse dispersivity of 0.1 m was assigned for all units.

2.7.2 Boundary Conditions

Source and sink fluxes have been applied on the top of the model such as recharge, rivers and extraction wells. These fluxes are specified as flow boundary conditions with monthly variations (fluctuations are also implicit). All source fluxes that recharge the groundwater system have specified TDS-concentration input. Infiltrating precipitation (effective recharge) is assumed to be 0 mg l⁻¹ TDS. The infiltrating rivers and dams either have 50 or 20 mg l⁻¹ TDS depending on its catchment area and type.

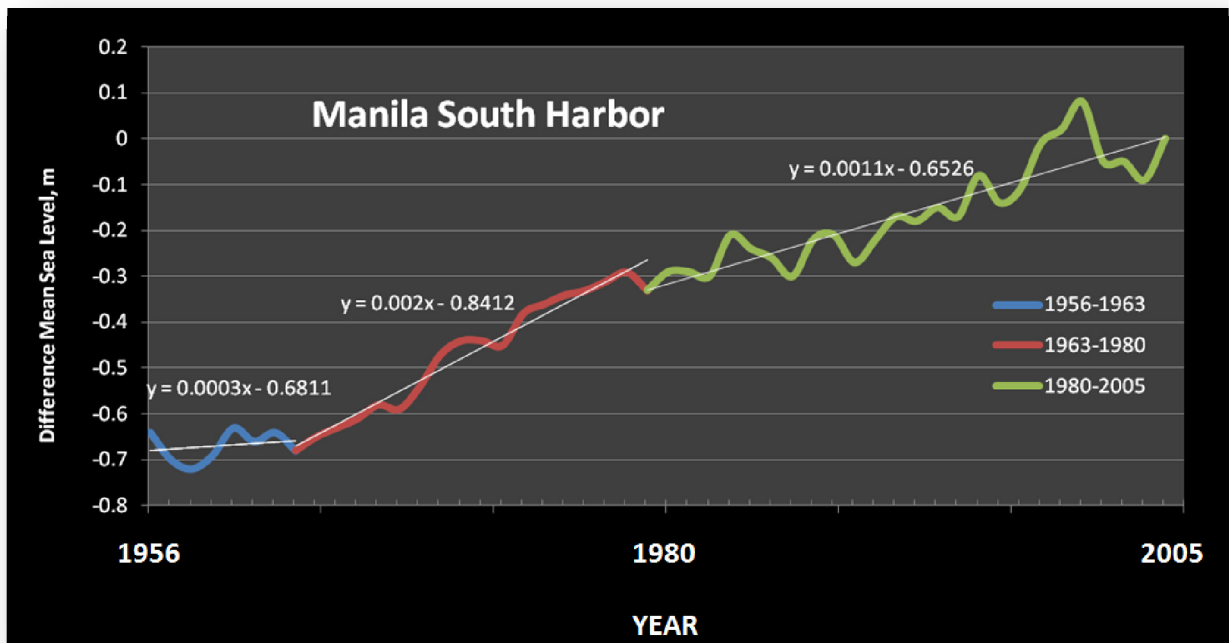
Table 2.3 Hydrologic parameters used in the simulation of the reference case

Horizontal Hydraulic Conductivity, K_h (m d ⁻¹)	Value
Qv unit	1
Qvp unit	4
Qal unit	4
Confining Unit Type 1	0.1
Confining Unit Type 2	0.01
Confining Unit Type 3	0.001
Sea	20
Anisotropic ratio – K_h/K_v – all units (-)	10
Porosity (-)	
Permeable units	0.25
Confining units	0.1
Sea	1
Specific Storage – all units (m ⁻¹)	2.0×10^{-5}
Longitudinal dispersivity – all units (m)	1
Transverse dispersivity – all units (m)	0.1

It is assumed that there is no groundwater flow and solute transport through the bottom of the model. The cells at the bottom are inactive. In reality, the Qvp unit may have extended deeper, however for the purpose of simulating the SGD fluxes which only occurs in the near surface until the near shore sea surface, the bottom of the model at 150m below msl can be considered appropriate. In addition, deepest portion of the Manila bay included in the model area only reaches 50 m below msl which is relatively shallow.

The north and south sides of the model are defined as a no groundwater flow/no solute transport boundary. The overall groundwater flow direction is parallel to these lateral sides hence no flow is assumed over these boundaries.

Hydrostatic pressure condition is assumed at the western end (mountain boundary) and eastern end (deep sea boundary) of the model. At the mountain boundary a mass boundary condition is defined, the concentration increases from 0 to 400 mg l⁻¹ TDS along the 48 layers. From 1956 to 2005, there is an observed sea level rise of 0.65 m in Manila Bay. The sea level rise is not constant (Figure 2.15). This sea level rise is also incorporated in the model as a general head boundary (top sea boundary) varying with time. The concentration of the seawater is set to constant 35000 mg l⁻¹ TDS. This is due to the assumption that the seawater is always being replenished. Tidal fluctuations are not taken into account; also the simulation time is in months anyway.



Data Source: MSL data from [NAMRIA](#) obtained from [Geological Oceans Laboratory, MSI](#).

Figure 2.15 Mean sea level difference (m). 0 is equivalent to present day msl.

2.7.3 Modeling Approach

Several simulations were completed to derive estimates of SGD fluxes. Sensitivity simulation runs were completed and compared to the reference case to assess how physical parameters affect the SGD fluxes. Due to the input parameter complexity of each model scenario, the discussion will include the initial boundary conditions used if different from the base case. This way, it will be easy to spot the differences and significance of each parameter.

Both steady state and transient simulation were carried out depending on the requirement of the case. The time variation in model input is on a monthly basis. This means that per month, different input values for precipitation, evaporation, groundwater uses etc. are specified. It is assumed that this is detailed enough to include the time-dependent processes that are significant in the model area.

Each scenario is done in 3 consecutive runs, first 150 years, then 100 years and 50 year period, equivalent to 1800, 1200 and 600 time steps, where the output of last time step of the first run is applied to next and so on. A detailed explanation of this process will be done in the next section. 1 time step is equivalent to 1 month (30.25 days), the chosen time variation for the model.

2.8 Model Scenarios

2.8.1 Base Case

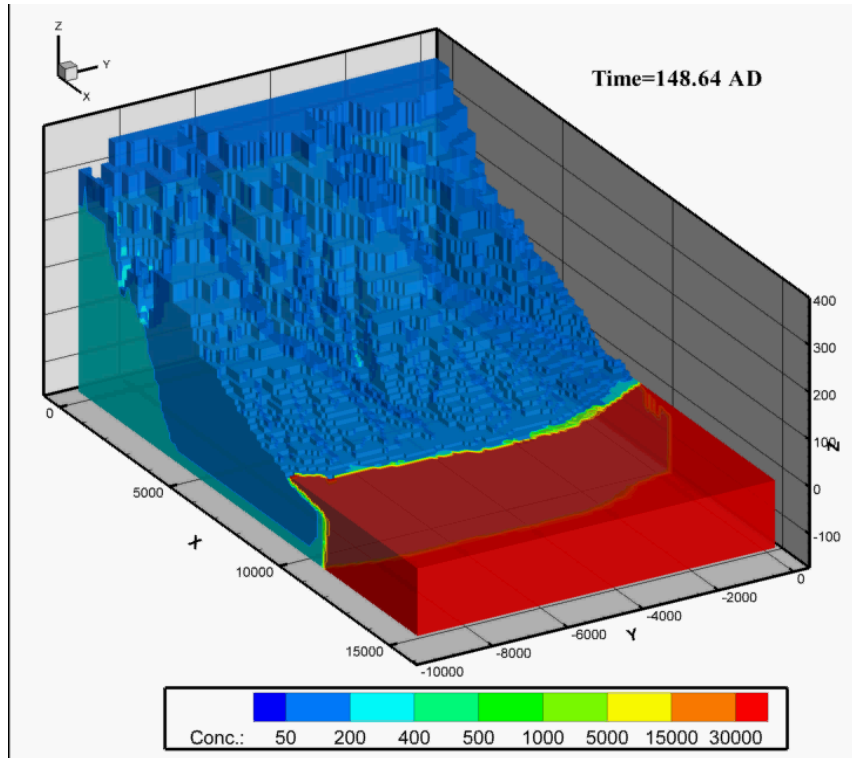
2.8.1.1 Initial Conditions

The base case scenario uses the parameter values and boundary conditions listed above (Sections 2.5.2 and 2.5.3). The initial freshwater heads are modeled using the results of a steady state simulation while the pre-initial concentration (TDS) is implemented based on expert judgment of the very limited TDS data from shallow observation wells. There is no information on the salt-freshwater interface, which is very important for the model. So using the very limited knowledge of the concentration, the interface is assumed to be vertical from top (starting on the coastline) to bottom.

These set-up is then used to do the model “spin-up” run (**S1-R1**) of 150 years equivalent to 1800 time steps in steady state to see how the saltwater or freshwater wedge would develop with the given the model system, the sea level is assumed to be at 0.6 m lower than the msl and no extraction well is applied.

Figure 2.16 shows the development of the water wedge through time. The characteristics of the model area lead to the development of a freshwater wedge which extends approximately 1 to 2 km from the coastline at the end of **S1-R1** (150 years).

(A) Block Model



(B) Profile Slices

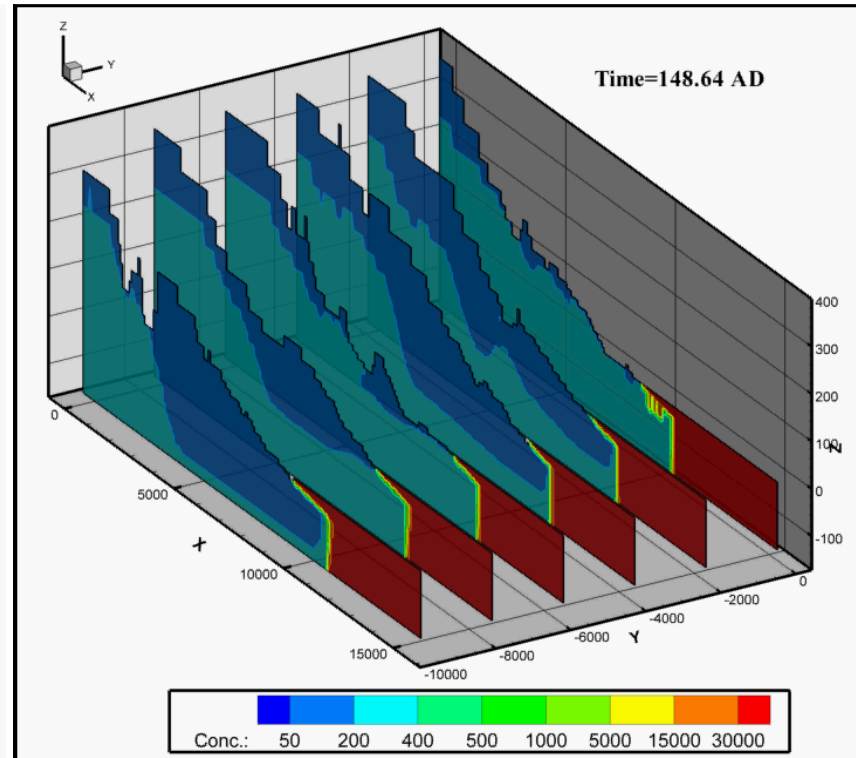


Figure 2.16 (Animation) Time series development of the freshwater wedge in the spin-up run (S1-R1). (A) shows the block model time series concentration development and (B) the representative profile sections for a detailed observation. Time is in years. Applied translucency = 30%.

Important note: This animation can ONLY be viewed using Adobe Reader 9, for earlier versions of Adobe Reader please refer to Appendix IV for the development of the freshwater wedge.

Output concentration plots in the observation wells (Figure 2.17) show that the concentration values stabilize after approximately 100 years (1200 time steps) although in some locations within a few years.

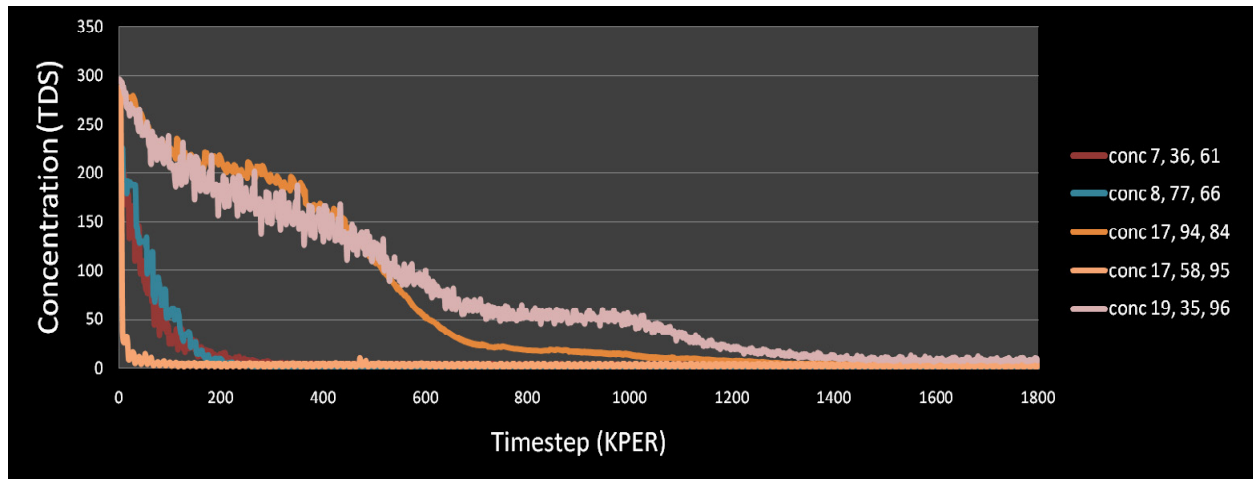


Figure 2.17 Change in TDS concentration in some observation wells. Conc (i, j, k) is the concentration at observation well location layer, row, column respectively.

With the freshwater head distribution and the TDS-distributions from the steady-state simulation the model is run in transient simulation (**S1-R2**) to get better TDS-distributions, which are used as initial conditions to run the model in a scenario mode (**S1-R3**) where the model SGD fluxes will be extracted. **S1-R2** represents the period 1856 to 1956 (100 years).

The mean sea level is still set at 0.6 m below the present msl and extraction wells are applied but the extraction rates are halved in the assumption that there is less demand for groundwater in the earlier times because the population in the area is also less. Figure 2.18a and 2.18b shows the initial concentration to run the base case scenario.

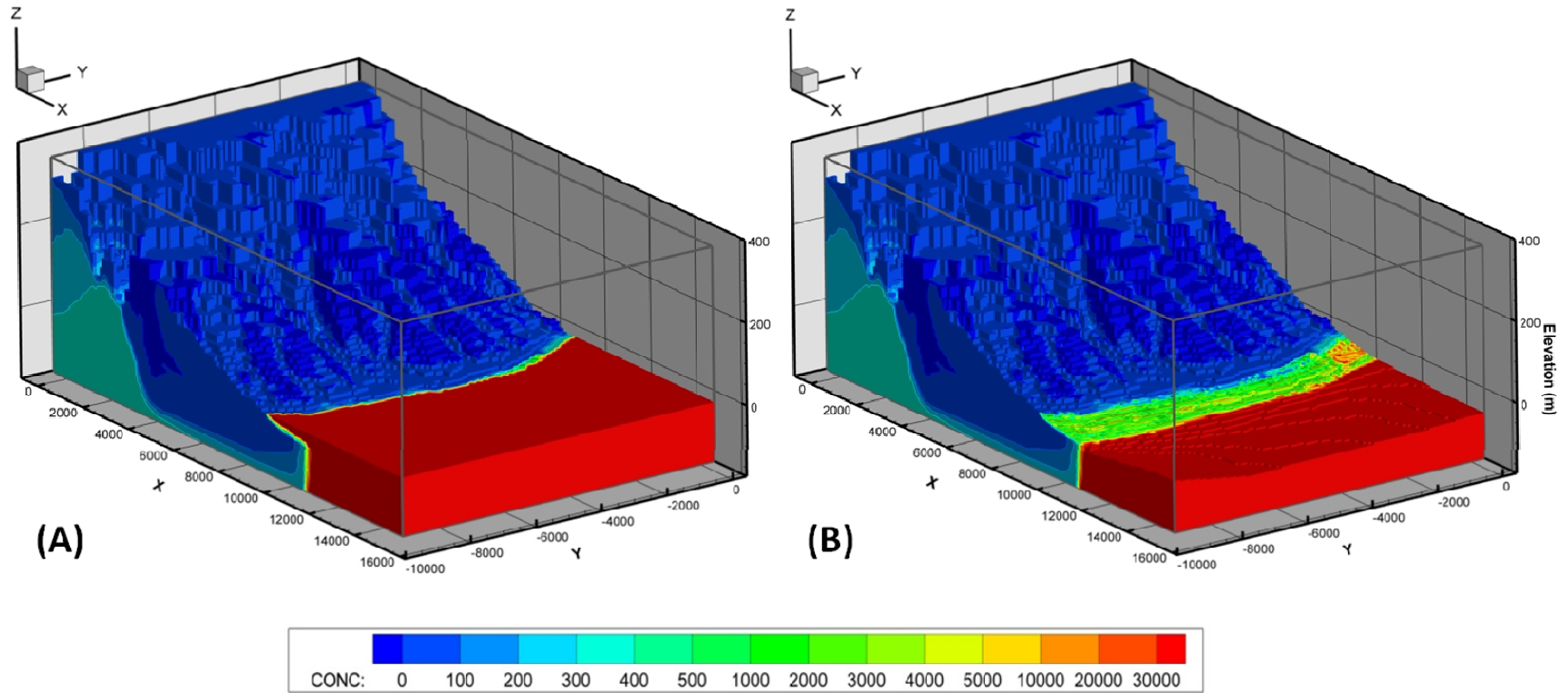


Figure 2.18 (A) Initial concentration distribution of Total Dissolved Solids (TDS) (B) The sea is blanked for a better view of the concentrations.

Table 2.4 shows the summary of the steps for each part of the simulation carried out for the reference case – Scenario 1. Also included are the summary of the different assumptions, period length (simulation time) and the type of simulation carried out.

Table 2.4 Summary of inputs for each section/part of the reference case scenario (Scenario 1)

Scenario 1 (base case)	Description	Period	Simulation type
Part 1 S1 – R1	model spin-up run monthly variation no wells top sea (0.6m below msl)	150 years (to reach equilibrium)	Steady state
Part 2 S1 – R2	pre-initial values run with extraction wells ($Q_{well}/2$) top sea (0.6m below msl)	100 years (1856 – 1956)	Transient
Part 3 S1 – R3	model SGD fluxes are extracted with full extraction wells top sea changing based on actual sea level curve	50 years (1956 – 2005)	Transient

2.8.1.2 Results and Discussions

Figure 2.19 shows the monthly variation, snapshot in year 2005 of total SGD flux in the reference case. The SGD flux peaks correspond to the rainfall peaks in the system however the applied specific storage of 0.00002 seems to dampen the response. The trend of the SGD fluxes highly resembles the pattern of the calculated effective recharge showing the immense influence of rainfall to the calculated SGD flux.

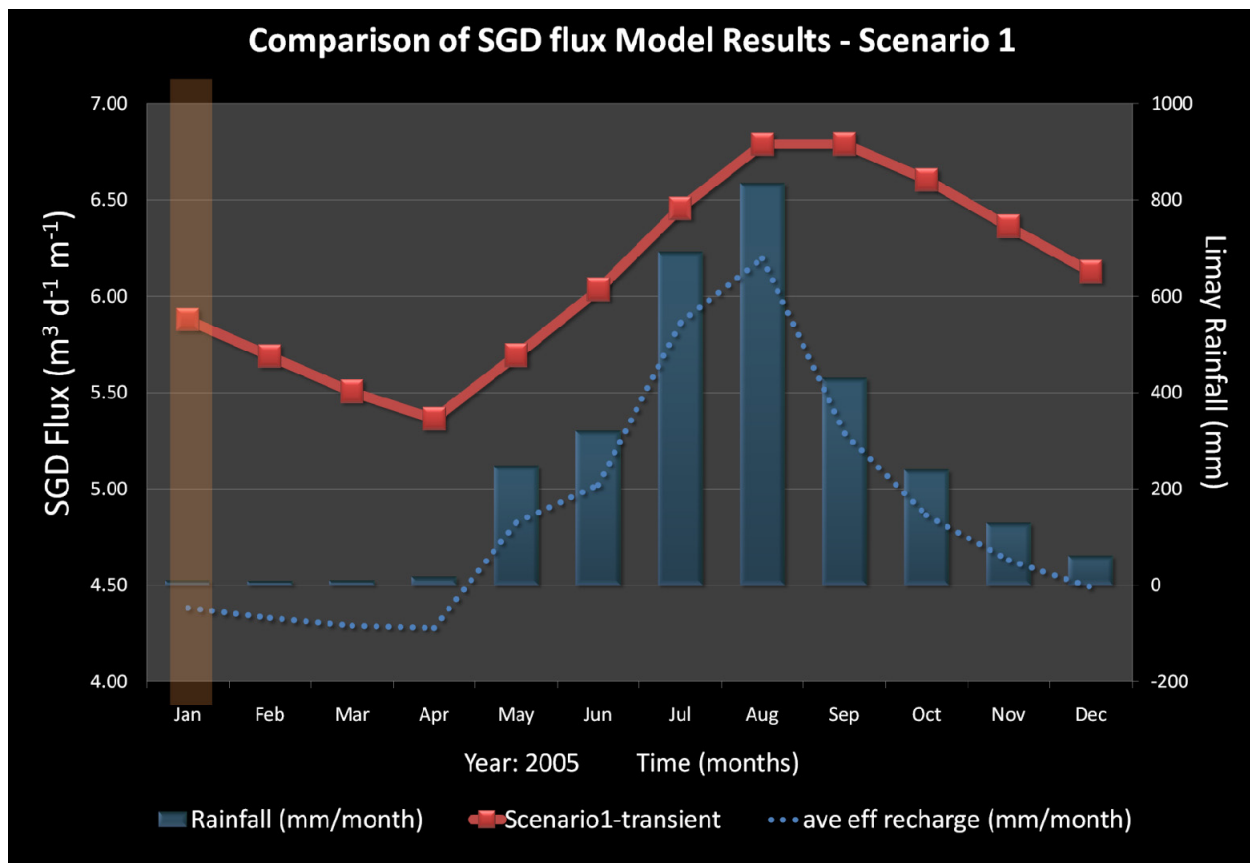


Figure 2.19 Scenario 1 model results – monthly total integrated SGD shoreline flux (in 2005) compared with rainfall and calculated effective recharge. Shaded region corresponds to the time Taniguchi *et al.* (2008) did the SGD measurements and used as comparison for the subsequent model results analysis.

The model result total integrated shoreline flux averaged over 12 months (2005) is $6.1 \text{ m}^3 \text{ m}^{-1} \text{ day}^{-1}$ (Figure 2.20). This value is lower (~50%) but in the same order as the SGD flux measured by Taniguchi *et al.* (2008), estimated to be about $12.4 \text{ m}^3 \text{ m}^{-1} \text{ day}^{-1}$.

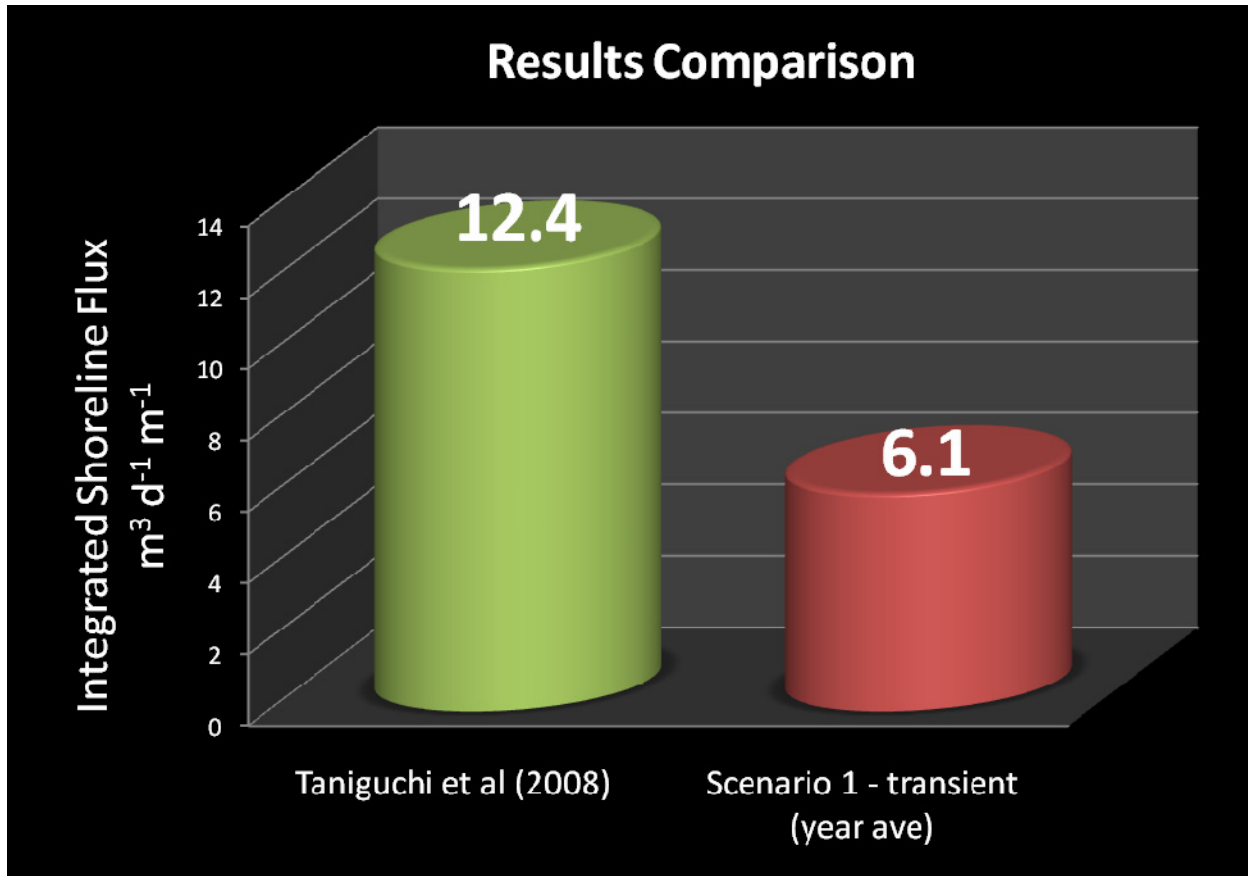


Figure 2.20 Scenario 1 model results - total integrated shoreline flux year 2005 average compared with Taniguchi *et al.* (2008) measured SGD flux.

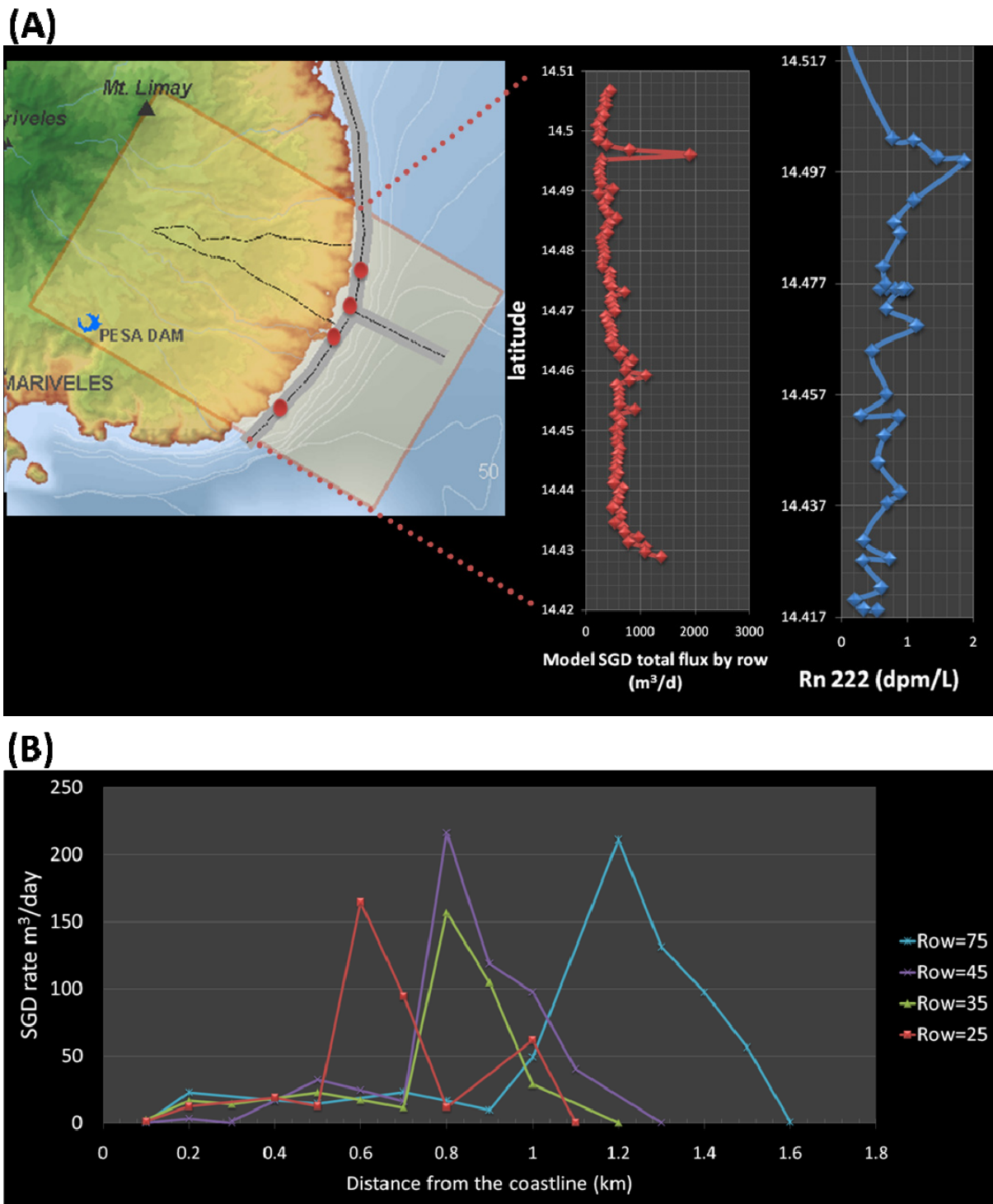


Figure 2.21 (A) Latitudinal variation of model SGD fluxes compared with radon measurements (B) Plot of model SGD fluxes vs. distance from the coastline. Location of these transects are the red dots in Figure 2.21A. (Model results both extracted from Jan-2005)

The latitudinal variability of the model SGD fluxes are shown in [Figure 2.21a](#). These model results are taken from the period Jan-2005 to be compared with the SGD measurements done by [Taniguchi *et al.* \(2008\)](#). We can see in the trend that some shoreline segments have higher SGD fluxes compared to others. Higher SGD fluxes are found north of the model area and a more regular trend towards the south. This variation is a relatively good fit to the trend of the radon survey results in the area.

[Figure 2.21b](#) shows the model SGD flux change with distance from the coastline. SGD flux peaks coincide with the relative position of the confining units intersecting the sea surface. Multiple peaks can be explained by the several confining units in the system located at different depths. This will be explained further in the geological effects on SGD flux in the sensitivity analysis section.

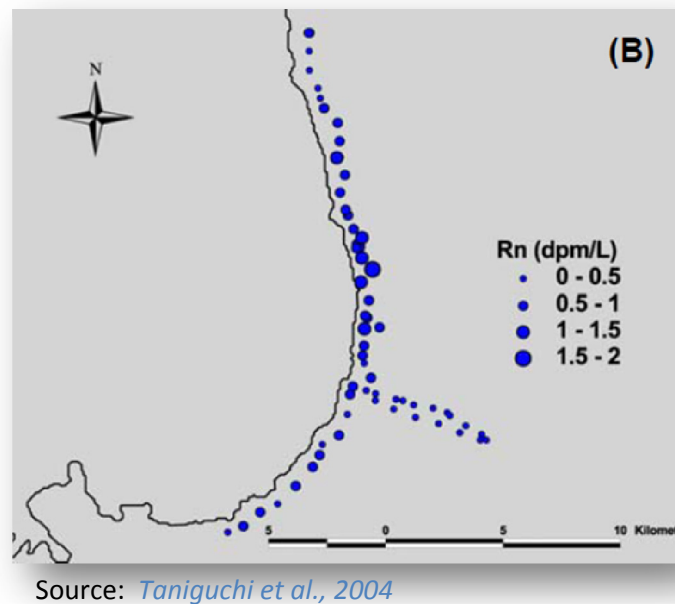


Figure 2.22 Distribution of Rn-222 (dpm L^{-1}) in surface waters along the coast of the Bataan Peninsula and along a shore normal transit out into Manila Bay.

The measured SGD flux for Manila Bay by [Taniguchi *et al.* \(2008\)](#) is approx 50% higher than the reference case model result (**Scenario 1**). The difference in the measured SGD and standard model result (**Scenario 1**) could be explained by the following:

- 1) ***Difference in the extent of the study area.*** [Taniguchi *et al.* \(2008\)](#) did their seepage meter measurement within 500m offshore and 500m length of shoreline and the radon survey measurements extend approx 10 km further north of the model area. Whereas the model area in this 3D model covers the area up to 5km offshore and 11.66 km of shoreline. [Figure 2.22](#) show higher Rn-222 (dpm L^{-1}) in surface waters north of the study area, which is not covered by the model. Since high radon readings correspond to high SGD fluxes, this could be one of the reasons for the underestimation in the model SGD flux.
- 2) ***Underestimation of hydraulic conductivity values.*** There are very limited pumping well tests in the study area and thus high uncertainty in the hydraulic parameter estimation. Higher assigned hydraulic conductivities will result to higher SGD fluxes.

2.8.2 Sensitivity Analysis

The main objective of this research is to identify the major factors which influence the magnitude of SGD flux, and this can be attained by a detailed sensitivity analysis. In lieu to this, several sensitivity case scenarios are developed. [Table 2.5](#) gives information on what parameter is being investigated for each sensitivity case, and the assumptions that come with it. Details of each scenario case and how it is translated as model input for the simulation runs are discussed in [Section 2.8.2.1](#).

Table 2.5 Various scenarios created for the sensitivity analysis.

Scenarios	Goal	Variations	
Scenario 2	Determine the effects of changes in geology to the overall SGD flux	Scenario 2-1	No confining units present, a homogenous sand aquifer is assumed for the whole coastal aquifer system.
		Scenario 2-2	Confining units are present as scattered patches in the whole system.
Scenario 3	Determine effects of groundwater extraction to the overall SGD flux	No extraction wells	
Scenario 4	Determine the contribution of rivers to changes in SGD flux	Scenario 4-1	No rivers applied in the model
		Scenario 4-2	River water contribution in the system is increased
Scenario 5	Determine the effects of variations in assumed boundary conditions	Scenario 5-1	Constant freshwater head boundary is lowered, happens when the water table is deep in the system
		Scenario 5-2	Water contribution from the mountain head boundaries is increased

2.8.2.1 Translation of sensitivity scenarios to model input

Some of the model inputs are modified to fit the requirements of each scenario:

- In **Scenario 2**, a new 3D geology is created for each scenario variation. **Scenario 2-1** the confining units are all removed. A homogenous sand aquifer is assumed for the coastal aquifer. For **Scenario 2-2**, the 3D geology created for the base case is modified by manually creating breaks in between the continuous confining units. This way the confining units will be like “patches” in the system, similar to a fault/fracture bounded area or a region with only localized clay units. These modifications are implemented in the bcf and the mocmain packages. The initial freshwater head and concentration distribution is created using the same method in **Scenario 1**, and created exclusively for each case.
- In **Scenario 3**, the well package is not applied to the system. The initial freshwater head and concentration distribution is created using the same method in **Scenario 1** but not including the well package in the runs.
- In **Scenario 4-1**, the rivers are not implemented. In this set-up it is assumed that the area does not have rivers even from the beginning. The initial freshwater head and concentration distribution is created using the same method in **Scenario 1** but not implementing the river package. In **Scenario 4-2** conductance of the rivers is increased from 100 to 1000 in the river package. This way we assume that the river bed is more

conductive and thus contributes more water to the system. Note that the river conductance value in the reference case is an assumed value as well since there are no data indicating the river bed properties in the study area.

- **Scenario 5-1** implements the effects when the freshwater heads in a similar system is lower. This is done by modifying the mountain head boundary in the general head boundary package to a lower value. From the variation at 400 m above msl in the reference case; it is changed to 200 above msl in this scenario. In **Scenario 5-2** the conductance of the mountain freshwater heads is increased from 100 to 1000 in the general head boundary package.

Table 2.6 shows the summary of the different modifications made on the model inputs of different sensitivity cases at each part.

Table 2.6 Summary of inputs for each part in the sensitivity analysis scenarios.

Scenario	Description	Part 1 spin up (150 years)	Part 2 pre-initial (1856 – 1956)	Part 3 3D model (1956 – 2005)
Scenario 2-1	Effect of geology - no confining units	unique packages - bcf & mocmain No wells	initial conc and heads from part 1 Qwell/2	initial conc and heads from part 2 Qwell full
Scenario 2-2	Effect of geology - patchy confining units	unique packages - bcf & mocmain No wells	initial conc and heads from part 1 Qwell/2	initial conc and heads from part 2 Qwell full
Scenario 3	Effect of extraction wells	same as Scenario1	initial conc and heads from part 1 no wells	initial conc and heads from part 2 no wells
Scenario 4-1	Effect of rivers - no rivers	No rivers	initial conc and heads from part 1 Qwell/2 No rivers	initial conc and heads from part 2 Qwell full No rivers
Scenario 4-2	Effect of rivers - increased river conductance	River conductance = 1000	initial conc and heads from part 1 Qwell/2 River conductance = 1000	initial conc and heads from part 2 Qwell full River conductance = 1000
Scenario 5-1	Effect of ghb - mountain boundary heads lower	same as Scenario1	same as Scenario1	initial conc and heads from part 2 mountain boundary heads lower
Scenario 5-1	Effect of ghb - increase in mountain boundary conductance	same as Scenario1	same as Scenario1	initial conc and heads from part 2 mountain boundary conductance = 1000

2.8.2.2 Results and Discussions

Figure 2.23 shows the results of the sensitivity analysis. Here we can see that changes in geology have the most effect on the SGD flux, other parameters have very minimal effect. A detailed discussion of how each parameter affects the simulated SGD flux results can be found in the following sections.

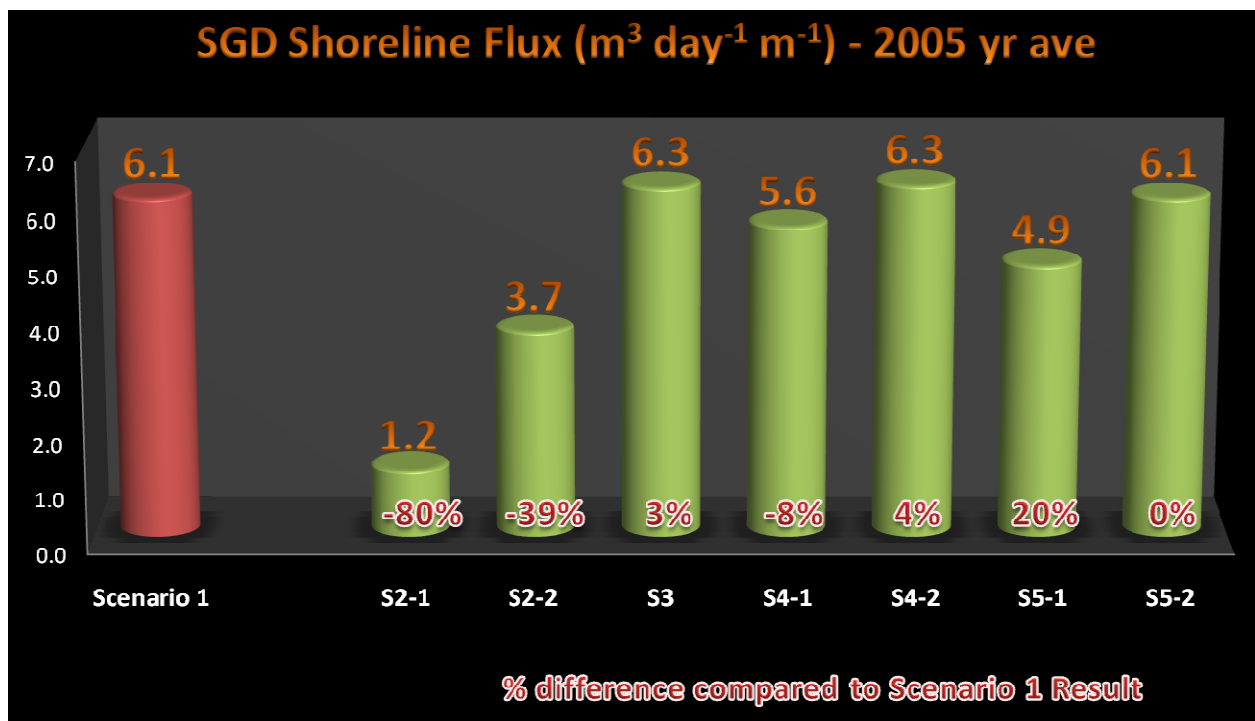


Figure 2.23 Graph of the resulting 2005 year average total SGD shoreline flux from the different scenarios. Also shown in red is the percentage difference of each sensitivity run result to the reference case. All values are converted to m³/day per m shoreline width for comparison purposes.

Effect of geology

Modeled SGD fluxes with **Scenario 2-1** are on average 80% lower than with **Scenario 1**, while **Scenario 2-2** is 39% lower. Figure 2.24 shows the modeled extent offshore of SGD as

influenced by the geology. With **Scenario 1**, the freshening of coastal sediments pore water reaches up to 2 km offshore whereas in **Scenario 2-1** it only extends to <1 km. Similar to **Scenario 1**, **Scenario 2-2** shows a freshening up to 2 km offshore also, but the freshening is relatively irregular. There are zones with low and high concentrations, unlike the one from **Scenario 1** which is fairly regular.

The differences in the SGD fluxes model result is highly influenced by the presence and geometry of the confining units. The screenshot of the concentration plots at $Y=-3500$ in [Figure 2.25 Scenario 1](#), shows how the relatively continuous confining units at different depths affect the groundwater flow. This creates “submarine tunnels” for groundwater at different depths which are conduits for SGD out to the shore (these are called “submarine springs”). Here we can also see how groundwater can be directly discharged 2km offshore through the submarine tunnels created by the confining units.

[Figure 2.25 Scenario 2-1](#) (homogenous sand system) demonstrate how the denser saline water pushes the freshwater landward, especially on the deeper parts, restricting the extent of the freshwater wedge and also thus SGD. Arrows which indicate the direction of water flow show the presence of SGD but it is only restricted to shallow, near shore seepage and mixing where the influence of the heavy seawater is less. [Figure 2.25 Scenario 2-2](#) illustrate how the discontinuous/scattered confining units affect the groundwater flow and also in turn SGD. The “breaks” in the confining units disrupts the regularity in the direction of groundwater flow. This allows the dense saline water to have influence in some sections of the system creating a localized system similar to **Scenario 2-1** which lessens the SGD flux.

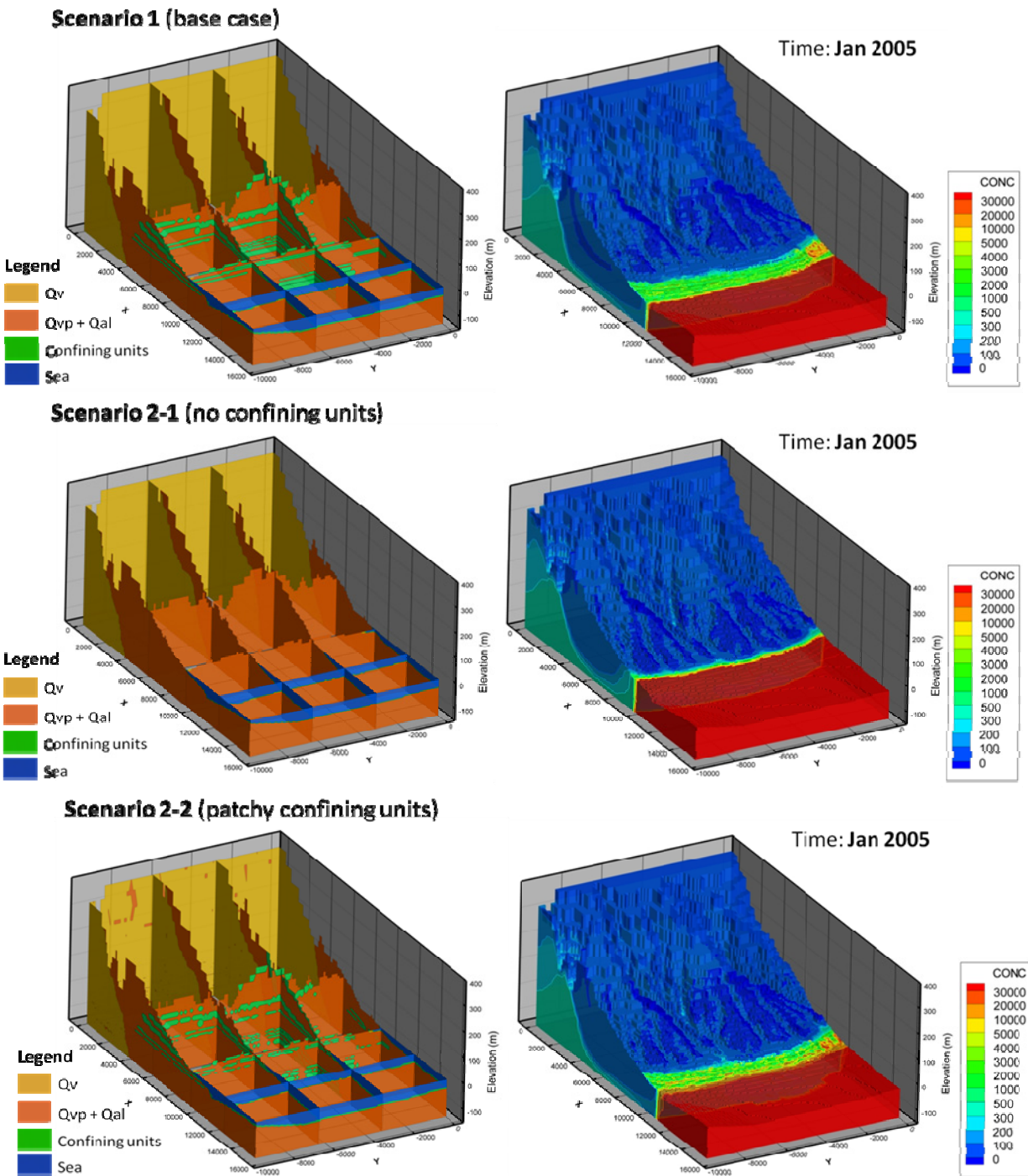
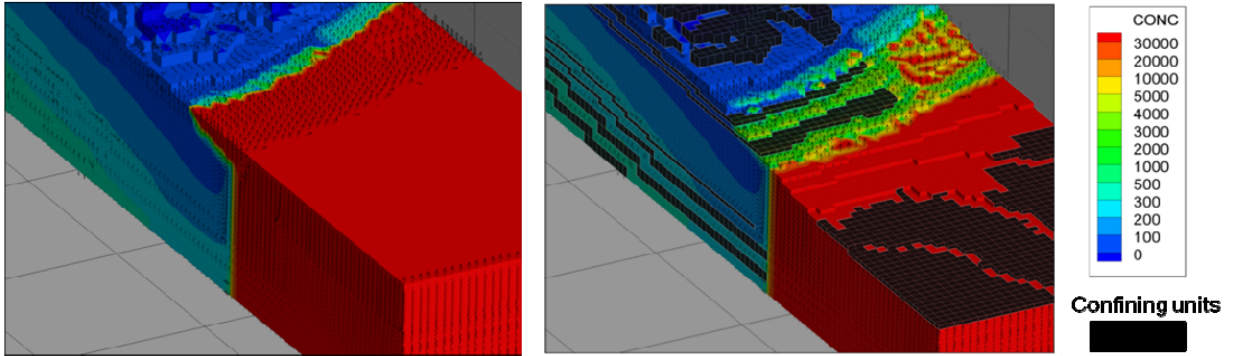
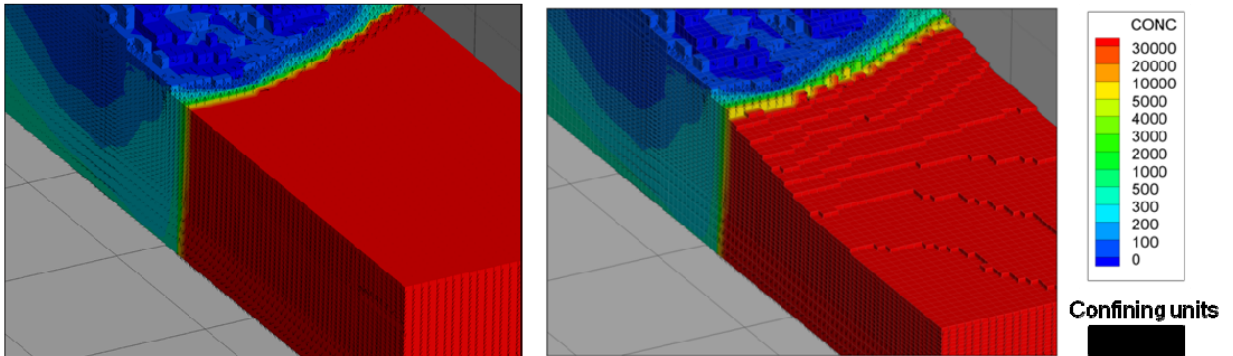


Figure 2.24 Comparison of the different 3D Geology created for the different scenarios and their subsequent influence on the developed freshwater wedge. All 3D concentration plots are extracted from Jan 2005 result. Translucency of 30% is applied to see the form of the wedge.

Scenario1



Scenario2-1



Scenario2-2

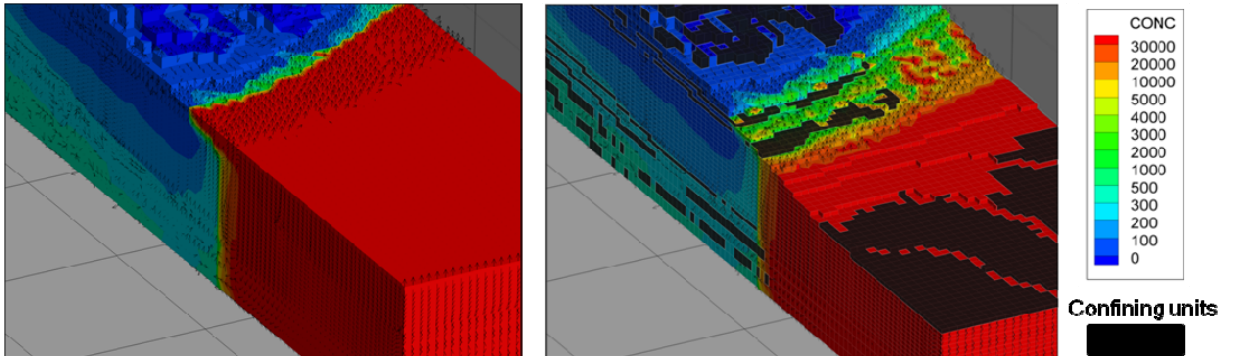


Figure 2.25 On the left hand side, zoomed concentration screenshots at $Y=-3500$ at the freshwater-saltwater interface of the different geology scenarios. This location is directly in front of Lucanin River Catchment. On the right side is the same screenshots with the confining units overlain, and sea blanked for better view of concentrations. Arrows indicate direction of water flow

This underlines the importance of identifying the presence and morphology of confining units which are greatly affecting the SGD flux values and therefore its potential impact on the regional environment.

Topographic (elevation) effects

Scenario 5-1 model SGD flux result is 20% lower than the base case. This scenario simulates a system with lower freshwater heads, from **Scenario 1** where the head variations are at approximately 400m above msl and changed to 200m above msl. Alternately we can interpret this system as a set-up where the elevation is lower or mountains with lower relief. So a decrease in 200 m in elevation would significantly change the SGD flux, since there will be less volume of water in the system and also take note that one of the major drivers of SGD is the hydraulic gradient which is dependent on head differences. Lower elevation in turn gives lower head differences.

Also another way of interpreting this would be the influence of assigning the right value for the freshwater heads. If in case a lower value is selected, it highly influences the output discharge so, good model calibration for the freshwater heads is absolutely necessary.

Effect of rivers

Rivers have a relatively minor importance to the calculation of SGD fluxes. Having no rivers contributing water in the system decreases the SGD flux result by 8%. On the other hand, increasing the contribution of rivers in the model by changing the river conductance from 100 to 1000 increases the SGD flux by 4%.

Effect of extraction wells

Removing the extraction wells in the system increases the SGD flux by 3% which is a very small change considering the enormous amount of water being extracted from the system. This only proves that there is sufficient amount of recharge in this area.

Others effects

In this model, various assumptions are made due to lack of sufficient data. One of these is the conductance values for the general head boundary conditions. In this model we chose 100 as conductance value for the mountain head boundaries. Changing this value to a higher conductance 1000 does not give any change to the resulting SGD flux result. Also another scenario made but not included in the [Figure 2.23](#) is running the model but not including the deep sea boundary, which also resulted to the same value for SGD flux. This gives more confidence to the model, since even changing the assumed parameter, similar values are being obtained.

2.9 Conclusions

Based on the hydrogeological modeling of submarine groundwater discharge on the SE flank of Mt. Mariveles, Bataan the main findings are as follows:

- 1) Model results are consistent with the rates of SGD measured by [Taniguchi *et al.* \(2008\)](#), using seepage meters and geochemical tracers. Radon survey and model result both indicate higher SGD fluxes on the northern section of the model area and a more regular trend towards the south.
- 2) The model result is approximately 50% lower than the measured SGD fluxes. This could be explained by:
 - a) The difference in the extent and size of the study area. SGD fluxes vary in latitudinal extent (shoreline) and also with distance from the coastline.
 - b) Misinterpretation in the extent and morphology of the confining units. The 3D geology is created based on very loose data in the area and thus a lot of incorporated personal interpretations.
 - c) An underestimation of the hydraulic parameters from very limited well data. It's highly probable that the hydraulic conductivities used in the model are very low compared to reality.
- 3) Simulations results show that significant SGD from terrestrial origin discharges to Manila Bay from the southeastern flank of Mt. Mariveles as a consequence of the steep topography, geology and high rainfall conditions. There's also a marine

- component (sea-water recirculation) in the SGD flux result but its contribution is difficult to quantify.
- 4) Sensitivity analysis results allow the quantification of the major influence of geology especially the presence of confining units, topography and rainfall on SGD fluxes. Ideally, data from field campaigns should be coupled to hydrogeological modeling in order to establish key control factors of SGD rates and to ultimately allow coupling water fluxes to nutrient fluxes.
 - 5) This study enables the first 3D approach and representation of SGD systems, resulting in a more realistic model, and therefore in a better understanding of the underlying mechanisms.
 - 6) Even with minimal amount of field data, resources and time, significant results can still be obtained from models.

References

- Almero R (1989). Engineering Geology Aspects of Characterization Study for a Radioactive Waste Disposal Site in PNPP-1, Morong, Bataan Province. Univ. Philippines Unpubl. M.Sc. Thesis, 209p.
- Earth Remote Sensing Data Analysis Center (ERSDAC) (2009). AsterGDEM 30x30m resolution for Bataan tiles ASTGTM_N14E121, ASTGTM_N15E120, and ASTGTM_N16E119.
- Ferguson BK (1996). Estimation of Direct Runoff in the Thornthwaite Water Balance, *The Professional Geographer*; 48(3): 263-271.
- Food and Agriculture Organization (FAO) (1998). Crop evapotranspiration - Guidelines for computing crop water requirements - FAO Irrigation and drainage paper. Rome
- Holzbecher E (1998). *Modeling Density-Driven Flow in Porous Media: Principles, Numerics, Software*, Springer Publications, Heidelberg / New York, 286 pp.
- Konikow LF, DJ Goode and GZ Hornberger (1996). A three-dimensional method-of-characteristics solute-transport model (MOC3D). USGS Water-Resources Investigations Report; 96-4267, 87 pp.
- Maleterre P (1989). Histoire sedimentaire, magmatique, tectonique et metallogenique d'un arc cenozoic deforme en regime de transpression: La Cordillere Centrale de Luzon, a l'extremite de la faille Philippine, sur les transects de Baguio et de Cervantes-Bontoc, Contexte structural et geodynamique des mineralisations epithermales auriferes. Ph.D. Dissertation, L'universite de Bretagne Occidentale; 304 pp.
- McDonald MG and AW Harbaugh (1998). A modular three-dimensional finite-difference ground-water flow model, U.S.G.S. *Techniques of Water-Resources Investigations*, Book 6, Chapter A1, pp 586
- Oude Essink GHP (1998). MOC3D adapted to simulate 3D density-dependent groundwater flow. Modflow'98 Conference, Golden, Colorado.
- Oude Essink GHP (2001a). Salt water intrusion in a three-dimensional groundwater system in The Netherlands: a numerical study. *Transport in Porous Media* 43: 137-158.
- Oude Essink GHP (2001b). Saltwater intrusion in 3D large-scale aquifers: a Dutch case. *Physics and chemistry of the Earth* submitted.
- Oude Essink GHP (2002). Density dependent groundwater at the island of Texel, The Netherlands. *Water Resources Research* submitted.
- Peaceman DW (1977). Fundamentals of numerical reservoir simulation, in: *Developments in Petroleum Science* 6, Elsevier Scientific Publishing Company, Amsterdam

- Rimando RE and PLK Knuepfer (2006). Neotectonics of the Marikina Valley fault system (MVFS) and tectonic framework of structures in northern and central Luzon, Philippines. *Tectonophysics*; 415: 17-38.
- Siringan FP and CL Ringor (1998). Changes in bathymetry and their implications to sediment dispersal and sedimentation rates in Manila Bay. *Science Diliman*; 10(2): 12-26.
- Sorey ML (1978). Numerical modelling of liquid geothermal systems. U.S. Geological Survey Prof. Pap. 16044-D
- Soria JA (2009). Paleoenvironmental and paleo-sea level reconstructions, and natural compaction in the delta complex bordering north of Manila Bay. Univ. Philippines. Unpubl. M.Sc. Thesis
- Taniguchi M, WC Burnett, H Dulaiova, F Siringan, J Foronda, G Wattayakorn, S Rungsupa, EA Kontar and T Ishitobi (2008). Groundwater Discharge as an Important Land-Sea Pathway into Manila Bay, Philippines. *Journal of Coastal Research*, 24 (1), 15-24
- Taniguchi M, WC Burnett, H Dulaiova, F Siringan, J Foronda, G Wattayakorn, S Rungsupa, EA Kontar and T Ishitobi (2004). Groundwater Discharge as an Important Land-Sea Pathway in Southeast Asia. Final Report for APN Project 2004-16NSY pp. 2-17
- United States Defense Mapping Agency (USDMA) Hydrographic Topographic Center (1982). Bathymetric Map of Manila Bay and Approaches, Sheet 91280, 1:125,000, US Defense Mapping Agency, Washington, D.C.
- United States Geological Survey (USGS) (2004). Shuttle Radar Topography Mission, 3 Arc Second scene n014e120, n014e121, n015e120, and n015e121. Unfilled Unfinished. Global Land Cover Facility, University of Maryland, College Park, Maryland, February 2000.

Chapter 3

Simulation of Climate and Anthropogenic Effects on SGD



Image: PESA Dam , Mariveles – Bataan (Source: Google Earth)

3.1 Abstract

Submarine groundwater discharge (SGD) is an important component of the coastal hydrologic cycle, affecting mixing and biogeochemistry in the near shore environment. Climate change and anthropogenic factors affect SGD by influencing the hydrologic factors which control it. El Niño–Southern Oscillation (ENSO) alters rates of precipitation evapotranspiration, and soil moisture patterns; sea level rise influences the freshwater heads, and groundwater concentrations; excessive pumping of ground water lowers the level of the water table and removes water from storage in the aquifer; and land-use modifications, changes the amount of groundwater recharge by changing the infiltration rates. To determine how these factors affect the magnitude of SGD, several scenarios were developed. These simulations are a continuation of those presented in **Chapter 2**, thus the same physical and hydrological parameters, and boundary conditions as in the reference case (**Scenario 1**) are implemented in the model, otherwise indicated to be different. Model results are in the same order of magnitude as the measured fluxes. ENSO affects SGD fluxes in two different ways. During El Niño, the SGD fluxes are significantly reduced at an average of 7% change. La Niña does not change or influence the SGD flux greatly. High amounts of rain poured during La Nina are just flushed out of the system through the drains. Sea level rise have a minor effect on the SGD fluxes, lowering of SGD fluxes by 2-3% depending on the height of sea level rise. Excessive groundwater extraction and land-use changes can greatly influence the magnitude of SGD flux especially when combined with sea level rise resulting to 8-10% change in the SGD fluxes by yr 2055.

3.2 Introduction

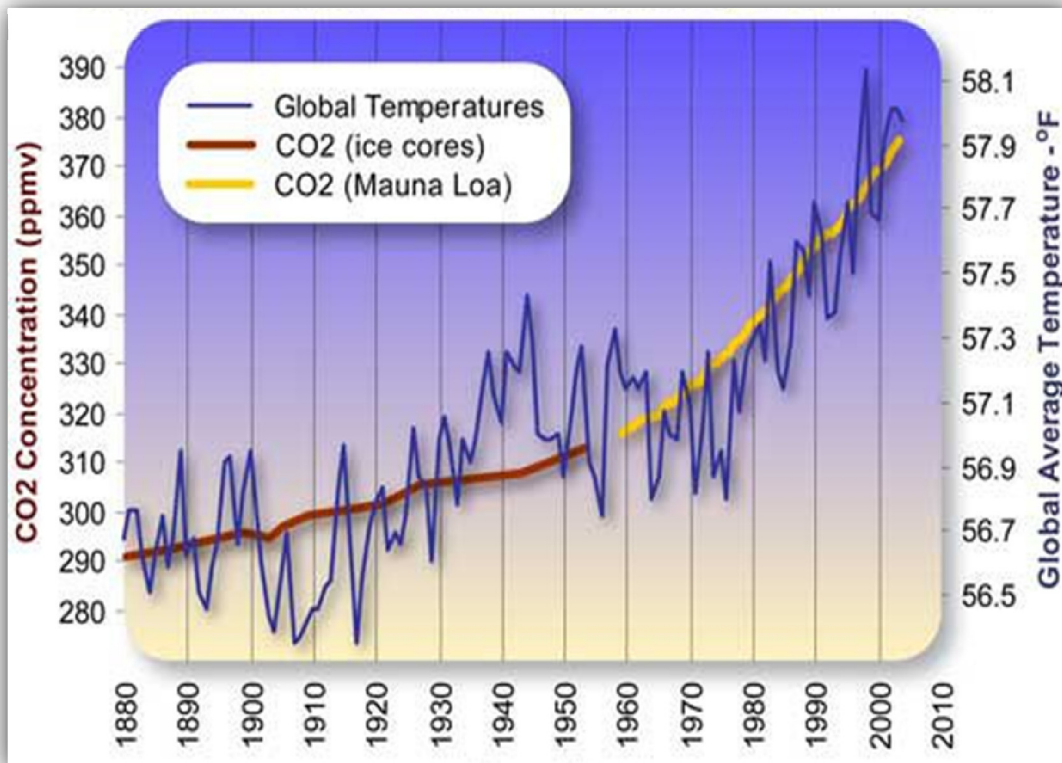
Submarine groundwater discharge (SGD) is now considered an important component of the coastal hydrologic cycle, affecting mixing and biogeochemistry in the near shore environment. Coastal areas have been increasingly vulnerable to human alteration and climatic changes; however the relationship of these factors to SGD is still poorly understood. In lieu to this, this study focused on the conceptual understanding and indirect quantification using hydrogeological modeling of SGD and how it is affected by climatic and human-induced changes. This chapter presents the results of the simulations made to incorporate changing climate conditions (El Niño–Southern Oscillation - ENSO), sea level rise and anthropogenic induced effects to the magnitude of SGD flux. These scenarios are an addition to the 3D model scenarios presented in **Chapter 2**. This is to evaluate the potential influence of climate and humans to the quantity and quality of SGD fluxes.

3.2.1 Background

3.2.1.1 Climate Change Factors

Atmospheric concentrations of carbon dioxide and other greenhouse gases have continually increased since the industrial revolution resulting to extra warming of the earth's surface ([Figure 3.1](#)). The continuation of this phenomenon may significantly alter global and local climate characteristics, including temperature and precipitation ([Reay and Pidwirny, 2006](#)).

Two of the consequences of this global warming are changing weather patterns (ENSO) and sea level rise.



Source: [WHRC \(2010\)](#); Data from: [NOAA's National Climate Data Center \(NCDC\)](#) and [Oak Ridge National Laboratory](#)

Figure 3.1 Global average temperature and CO₂ concentration since 1880.

3.2.1.1.1 *El Niño/La Niña Southern Oscillation (ENSO) Phenomenon*

ENSO Occurrence

El Niño refers to disruption of the ocean-atmosphere system, it is described by a warm phase of a naturally occurring sea surface temperature oscillation in the tropical Pacific Ocean, and **southern oscillation** refers to a seesaw shift in surface air pressure at Darwin, Australia and

the South Pacific Island of Tahiti (NOAA, 2010). *La Niña* on the other hand is the unusually cool temperatures in the equatorial Pacific.

ENSO phenomenon significantly alters global and local climate characteristics, including temperature and precipitation. Some areas may receive extra precipitation while some parts may experience significant reductions, or major alterations in the timing of wet and dry seasons.

In the local climate of the Philippines, an El Niño event is manifested by a drier-than-normal weather conditions that can last for one or more seasons, causing dry spells or even drought in many parts of the country (Jose, 2002). This is caused by (1) suppressed tropical cyclone activity in the western equatorial Pacific (2) weak monsoon activity characterized by the delayed onset of the rains, monsoon "breaks", and an early termination of the monsoon season (Jose, 2002). A La Niña event is the complete reverse of El Niño. It is characterized by an early to near-normal onset of the rainy season, a longer rainy season, above-normal rainfall and near-to-above normal tropical cyclone activity in the Philippine Area of Responsibility (PAR) during the northeast monsoon season (Jose, 2002).

ENSO Impacts

El Niño impacts in the Philippines inevitably leads to tremendous pressure on the water-resources sector. During El Niño, the annual water inflows in major reservoirs are significantly decreased, which results to water shortages and problems with irrigation of farmlands (Jose, 2002). Environmental impacts include soil degradation, changes in water quality due to salt-

water intrusion, and a high risk of forest fires. Social impacts include the disruption of normal human activities, migration to urban communities, and human and health problems brought about by scarcity of water.

La Niña, on the other hand, doesn't lead to distinct responses in multi-purpose dam operations. The impacts of La Niña and neutral conditions on the reservoirs are similar, thus providing more than enough irrigation and domestic water to the populace. During La Niña, thousands of hectares of prime agricultural lands were destroyed by floodwaters.

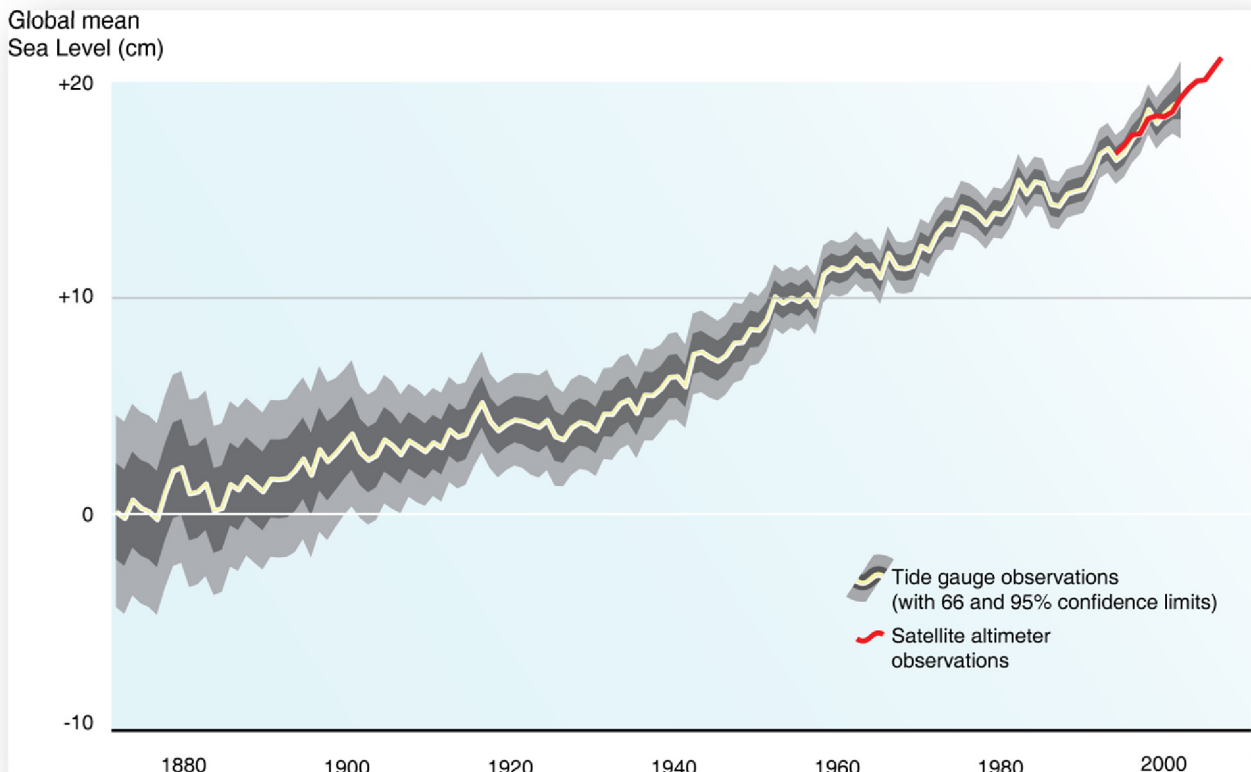
3.2.1.1.2 Sea Level Rise (SLR)

A 1 meter rise in sea levels would displace around 100 million people in Asia, mostly Bangladesh, eastern China and Vietnam; 14 million in Europe and eight million each in Africa and South America (UNEP, 2009).

Cause of SLR

Global warming affects the atmospheric pressure and cause inverse variation in the sea level. With a one millibar decrease in atmospheric pressure, the sea level rises by 10 millimeters (Sherif, 1999). A series of depressions in atmospheric pressure can cause a considerable rise in water levels in shallow ocean basins (Theon, 1993).

Sea water level may also rise for two other reasons. First, warmer oceans would expand; and secondly, melting ice sheets and glaciers would add to the total volume of water in the oceans (Theon, 1993).



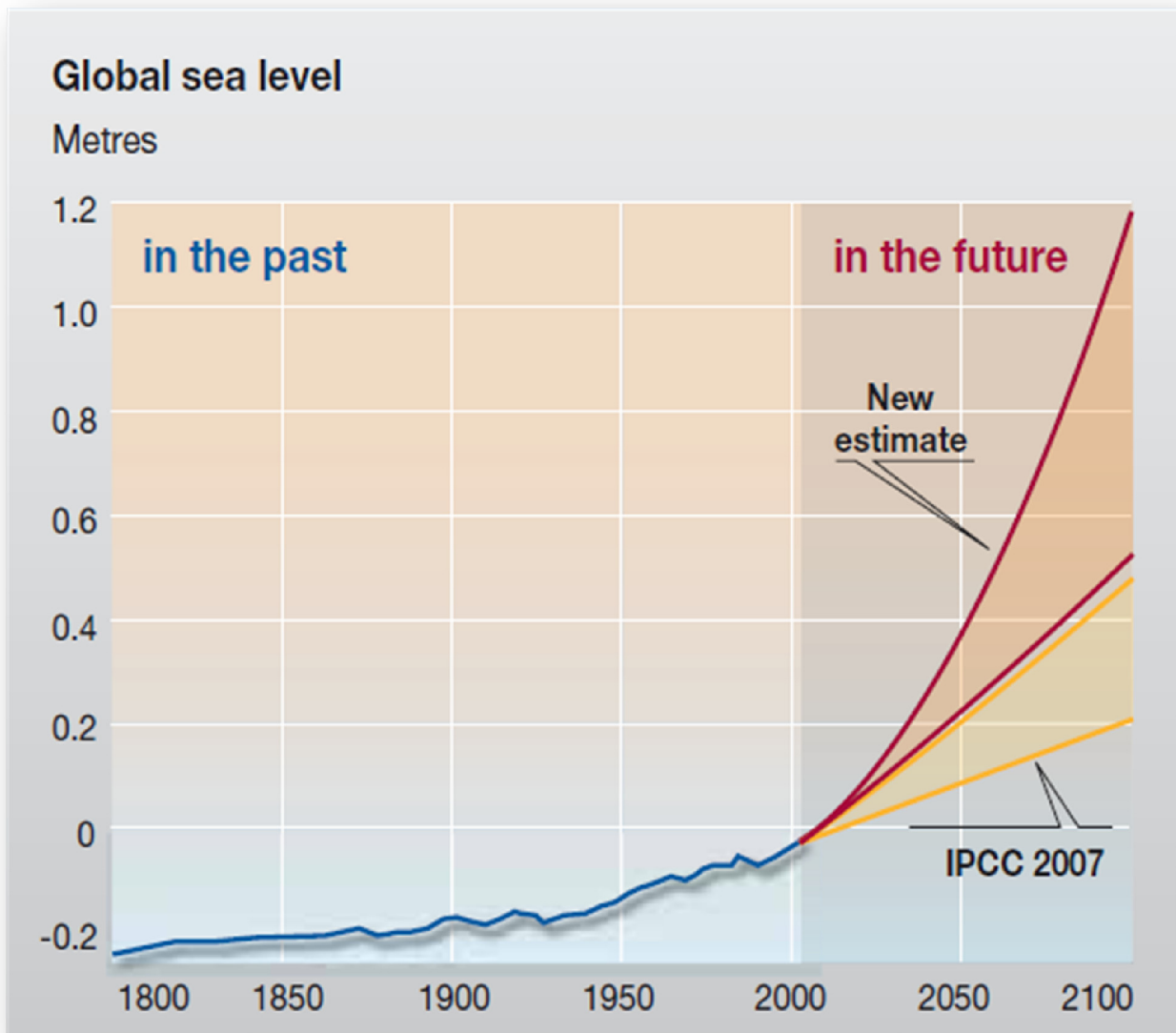
Source: UNEP/GRID-Arendal, 2007 after Church and White, 2006

Figure 3.2 Trends in sea level rise from 1880 to present derived from tide gauge observations and satellite.

SLR Measurements

Since the mid-19th century, sea level has been rising, likely primarily as a result of human-induced climate change. The data obtained from tidal gauges indicate that the sea level has risen by 10 ± 20 cm over the past century (roughly 1.5 to 2.0 mm/year), with an average rise of 1.7 mm/year during the 20th century and with the rate at the end of the century greater than over the early part of the century (Figure 3.2). This is consistent with the geological data and the few long records of sea level from coastal tide gauges (Church and White, 2006). High

precision satellite altimeters measurements (done between 65°N and 65°S) indicate a global average rise in sea level from 1993 – 2006 to be 3.1 ± 0.4 mm/year, which is significantly higher than the average rate for the 20th century (Church and White, 2006).



Source: UNEP/GRID-Arendal, 2009 after Cazenave and Llovel, 2009

Figure 3.3 Global sea level rise projections. Yellow zone and lines represent the minimum and maximum estimate of sea level rise by the IPCC (2007), the red zone and line represents the higher sea level rise projections from other more recent studies, which argue that projections done by IPCC (2007) are an underestimate.

SLR Projections

Projections suggest that the rate of sea level rise is likely to increase during the 21st century, although there is considerable controversy about the likely size of the increase.

The most robust projections of 21st century sea-level rise are the Assessments of the Intergovernmental Panel on Climate Change (IPCC) of 2001 and 2007. IPCC estimates that the global average sea level will rise by 0.18 - 0.59m with a central value of 0.48m by 2100 relative to 1980 - 1999 under a range of scenarios. The central value gives an average rate of 2.2 – 4.4 times the rate over the 20th century.

New estimates argue that the IPCC's projections of sea level rise are too conservative. Recent studies suggest that the most likely sea level rise by 2100 is 0.8 - 2.0 meters due to the increased loss of ice from the Greenland Ice Sheet ([Pfeffer *et al.*, 2008](#) and [Cazenave and Llovel, 2009](#)). The Greenland ice sheet is currently losing more than 100 cubic km a year-faster than can be explained by natural melting ([UNEP, 2009](#)).

Another study looked at the observed relationship of global temperature since 1900 and changes in sea level rise ([Rahmstorf, 2007](#)). Rahmstorf showed a direct relationship between the two: 0.1 - 0.3 meters of sea level rise occurs per °C increase in global temperature. Using this relationship, Rahmstorf predicted 0.5 - 1.4 m of sea level rise by 2100 using the IPCC predicted global temperature rise of 1.4° to 5.8°C.

[Grinsted *et al.* \(2009\)](#) used the same approach but extended the relationship to 200 AD using proxy records. They predicted that the global sea level will be rising 11 mm/year by 2050

which is four times faster than the 20th century rise. They forecasted that sea level will rise 0.9 - 1.3 meters, using the IPCC's A1B "business as usual" scenario.

Impacts of SLR

Over 600 million people live in coastal areas that are less than 10 meters above sea level, and two-thirds of the world's cities that have populations over five million are located in these at-risk areas ([McGranahan *et al.*, 2007](#)). With sea level projected to rise at an accelerated rate for at least several centuries, very large numbers of people are in vulnerable locations.

The Philippines, with its long coastline of 18000 km, the impact of sea level rise can be very significant. Physical effects of sea level rise include inundation (submergence) of low-lying wetland and dry land areas, erosion, salt-water intrusion into estuaries and aquifers, higher water tables, and increased risk of flooding and storm damages. In turn, these physical changes may lead to substantial socioeconomic losses such as loss of coastal structures, both natural and artificial; dislocation of the population; and changes of livelihood. The same physical changes may bring about certain ecological consequences such as redistribution of wetlands, destruction of coral reefs, and reduction in biological diversity, wildlife extinction, and changes in biophysical and biochemical properties of the coastal zones. This may necessitate a range of possible responses such as construction of seawalls and dikes, upgrading of coastal infrastructure to accommodate higher water levels, relocation of coastal populations, and mangrove regeneration.

3.2.1.2 Anthropogenic Factors

Although we can also argue that the present climate change is actually human-induced as well, there are also other changes brought about directly by humans that change the dynamics of the groundwater system, these are excessive groundwater extraction and land-use changes.

Pumping ground water from a well both lowers the level of the water table and removes water from storage in the aquifer, causing a decrease in the amount of ground-water discharge equal to the amount of pumping. In settings where ground water discharges to streams, the lowering of water-table levels by pumping can result in reduced stream flows. In a freshwater-lens system, pumping also shrinks the freshwater lens, resulting in upward movement of the transition zone. These effects are greatest near the source of water withdrawal.

If too much ground water is pumped, the freshwater lens may shrink enough that brackish water from the transition zone is drawn into the well, a process known as saltwater intrusion. When this occurs, the wells may be needed to shut down and this may reduce the availability of drinking water. In some other cases, over-pumping causes the ground level subsidence. Land subsidence resulting from excessive extraction of groundwater is particularly acute in East Asian countries. In the Manila Bay area in Philippines, the land surface is lowering by several centimeters to more than a decimeter per year, which is the major cause of flooding (Rodolfo and Siringan, 2006).

With growing density population especially on coastal areas, land-use changes are unavoidable. Changes in land-use influence recharge and run-off. Construction of roads, cities, houses, commercial and industrial sites, accompanied by forest degradation all alter the original land cover and in turn change the infiltration and run-off rates of the groundwater system.

3.3 Model Set-Up

The simulations presented here are a continuation of those presented in **Chapter 2**, thus the same physical and hydrological parameters, and boundary conditions as in the reference case (**Scenario 1**) are implemented in the model.

Scenario 6 (ENSO) is run using the same initial concentration and head as from the reference case (**Scenario 1**), thus from output of **S1-R2**. This is to be able to compare the output SGD fluxes during El Niño and La Niña years to the results of the reference case.

Scenario 7 to **Scenario 9** are run using the output concentration and heads of the last time step from the **Scenario 1 – Part 3** (reference case) equivalent to Dec 2005, since **Scenario 7** to **Scenario 9** are all predictive futuristic scenarios.

All models in this chapter are run using transient simulation.

Table 3.1 Various scenarios used for the simulation of climate and anthropogenic effects on SGD.

Scenarios	Goal	Variations/Details	
Scenario 6	Determine the effects of El Niño/La Niña Southern Oscillation (ENSO) Phenomenon on SGD	Modify the recharge package	
Scenario 7	Determine effects of Sea Level Rise (SLR) on SGD	Scenario 7-0	No sea-level rise, mean sea level at 0 meters
		Scenario 7-1	Using IPCC (2007) min (lower boundary) sea level rise value
		Scenario 7-2	Using IPCC (2007) max (upper boundary) sea level rise value
		Scenario 7-3	Using projected sea level rise value for the Philippines (Perez <i>et al.</i> , 1996)
Scenario 8	Determine the effect of Human-induced changes on SGD	Scenario 8-1	Doubled groundwater extraction rates, no sea level rise
		Scenario 8-2	Land-use modification – Deforestation, no sea level rise
		Scenario 8-3	Land-use modification – Reforestation, no sea level rise
Scenario 9	Determine the effects of combined sea level rise and human-induced changes on SGD	Scenario 9-1	IPCC max SLR and doubled groundwater extraction rates
		Scenario 9-2	IPCC max SLR and deforestation
		Scenario 9-3	IPCC max SLR and reforestation

3.4 Model Scenarios

To determine how climate change and humans affect SGD, several scenarios were developed. [Table 3.1](#) gives information on what parameter is being investigated for each case, and the assumptions that come with it. Details of each scenario and how it is translated as model input for the simulation runs is discussed in [Section 3.4.1](#).

3.4.1 Translation of scenarios to model input

Scenario 6 – ENSO Phenomenon

- To incorporate ENSO phenomenon in the model, a daily rainfall input is necessary. This is due to the assumption that ENSO influences the amount of rainfall. During El Niño, rainfall should be lower than normal and during La Niña it should be higher.
- In [Chapter 2](#), the reference case ([Scenario 1](#)) uses the mean monthly rainfall (Limay) as input for the recharge package due to absence of daily rainfall data in the area. Daily rainfall data is only available in locations located on the other side of the bay: In rain gauge stations Science Garden and Port Area (see [Figure 3.4](#)).
- From [Figure 3.5](#) we can see that the mean monthly rainfall at Limay (model area location) is higher compared to the rest of the stations. Using this knowledge, a modified Limay rainfall curve which incorporates the “*signal*” of daily changing rainfall is created. The daily rainfall value (mm) divided by the mean monthly rainfall (mm) from Port Area and Science Gauge Station gives the “*signal*” of the changing rainfall. This

combined with the mean monthly rainfall data for Limay will be the modified rainfall used in the ENSO effect simulation. Illustration of this procedure is shown in Figure 3.6.

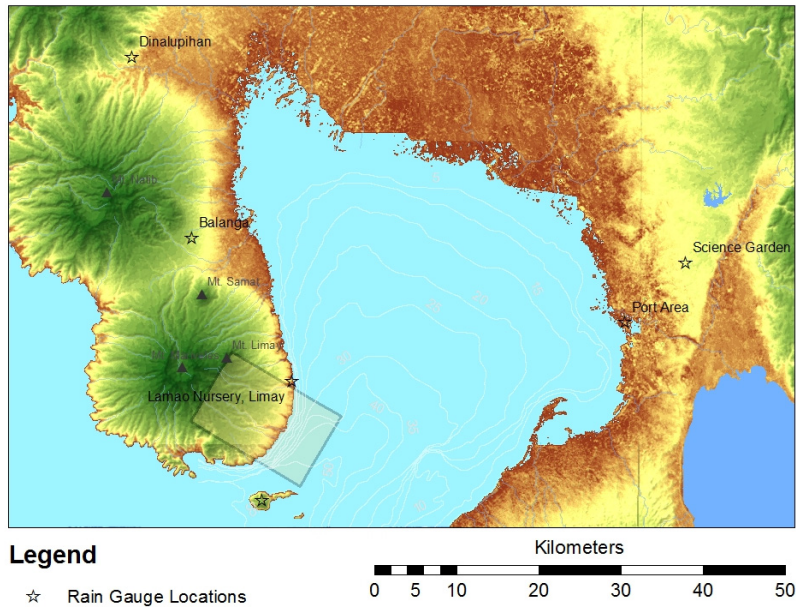
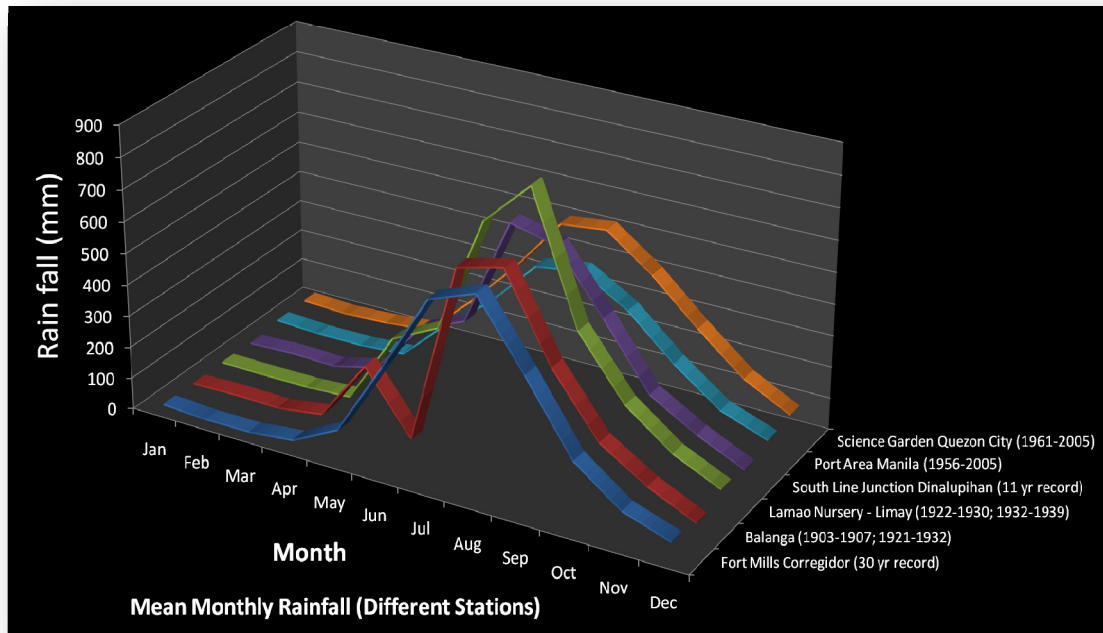


Figure 3.4 Locations of available rain gauges in Manila Bay.



Data Source: Rainfall data from PAGASA obtained from Geological Oceans Laboratory, MSI and MGB

Figure 3.5 Mean monthly rainfall values at different rain gauge sites.

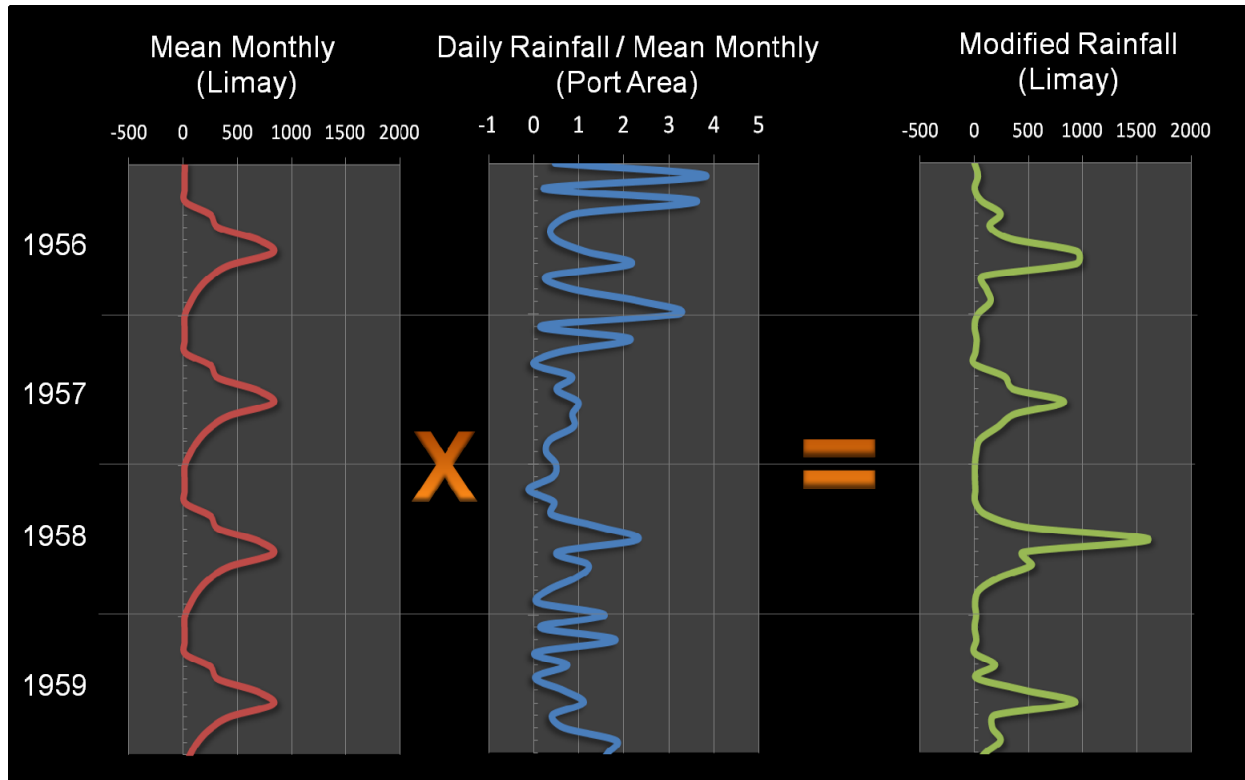


Figure 3.6 Procedure to create daily rainfall input for ENSO case. Available mean monthly rainfall data from the study area (Limay rainfall) is combined with the ratio of daily rainfall/mean monthly rainfall from Port Area to obtain a rainfall data for Limay which includes the daily rainfall “signal”.

Scenario 7 – Sea Level Rise (Projections 2055)

- In **Scenario 7-0**, no sea level rise is assumed for the next 50 years. In **Scenario 7-1**, the lower limit sea level rise of 0.15m in 50 years is applied based on the IPCC predictions. In **Scenario 7-2**, the upper limit of 0.5m in 50 years sea level rise. Using the results of the study of [Perez et al. \(1996\)](#) in Manila Bay, sea level rise of 0.475m in 50 years is implemented in **Scenario 7-3**. The sea level rise values are applied as linear increase in mean sea level. This is done by modifying the top sea level values in the general head

boundary package. The back-water effect of sea level rise in the area is negligible and not taken into account.

Scenario 8 – Anthropogenic induced changes (Projections 2055)

- To just look at the influence anthropogenic-induced changes alone, no sea level rise is implemented in this group. In **Scenario 8-1**, the well extraction rates are doubled, assuming an increased demand for water in the next 50 years. In **Scenario 8-2**, the forest area is assumed to be completely deforested; this in turn changes the ET and run-off values in the recharge package. In **Scenario 8-3**, assuming considerable efforts by the policy makers in the area will be made, a reforestation of the barren areas are executed; changes in ET and run-off values in the recharge package.

Scenario 9 – Combination sea level rise and human induced changes (Projections 2055)

- The max value (0.50m/50yr) of sea level rise is implemented in this group. In **Scenario 9-1**, the well extraction rates are doubled, assuming an increased demand for water in the next 50 years. In **Scenario 9-2**, the forest area is assumed to be completely deforested; this in turn changes the ET and run-off values in the recharge package. In **Scenario 9-3**, assuming considerable efforts by the policy makers in the area will be made, a reforestation of the barren areas are executed; changes in ET and run-off values in the recharge package.

3.4.2 Results and Discussions

3.4.2.1 Effects of ENSO Phenomenon on SGD

El Niño Periods

Using the Oceanic Niño Index (ONI) values from NOAA (Figure 3.7), the periods with extreme/strong El Niño is determined (Figure 3.8A) (i.e. warm episodes correspond to ONI 0.5-1, moderate El Niño ONI 1-1.5, and strong El Niño ONI >1.5). These periods are extracted from the Scenario 6 model results and compared with the results of the reference case (Figure 3.8B).

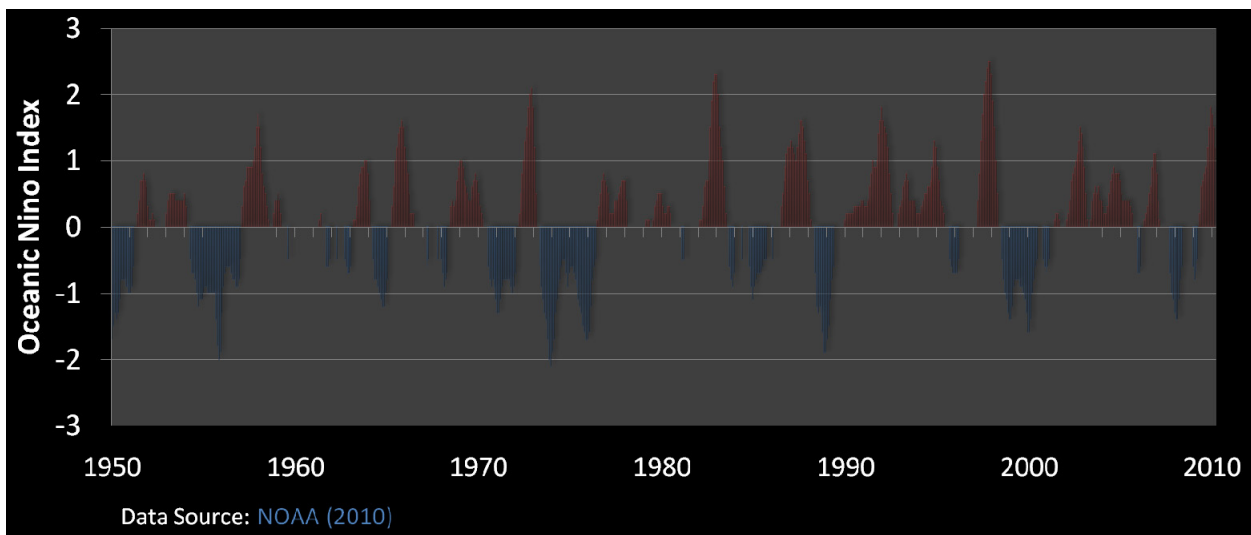


Figure 3.7 Monthly values of the Oceanic Niño Index from 1950 through present.

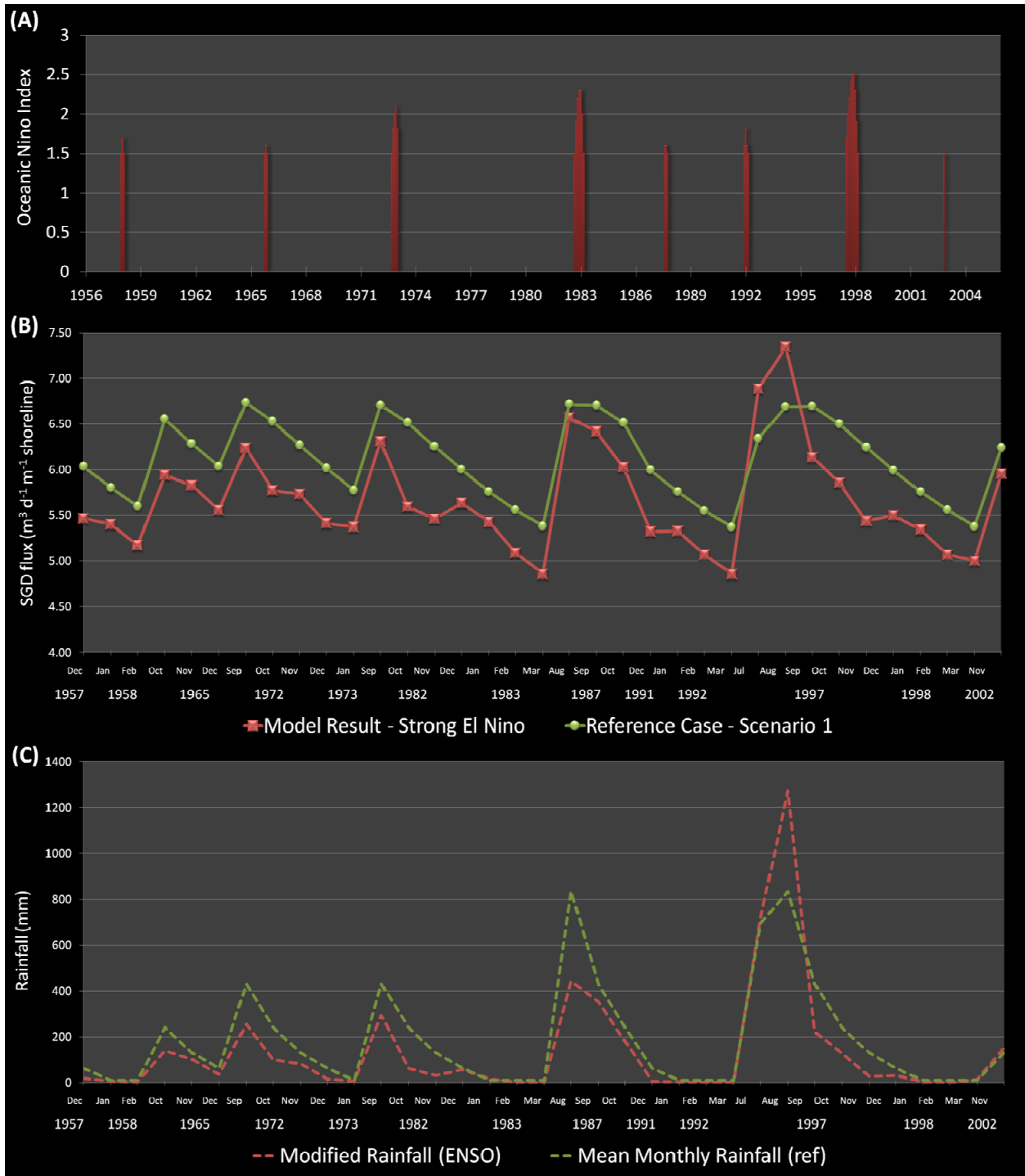


Figure 3.8 (A) Strong El Niño periods (B) Comparison of Scenario 1 and Scenario 6 model SGD flux results (C) Corresponding scenario rainfall input values used for each stress period.

Figure 3.8B shows that the model El Niño period SGD fluxes are lower compared to the reference case results. The difference in values is between the ranges of 2-14% with an average of 7%. These values satisfy the expected results, since the assumption is that SGD is largely influenced by the amount of rainfall. Lower rainfall during El Niño conditions would also result to lower SGD fluxes. There is an anomaly however in the results extracted from Aug-Sep 1997, where the El Niño period SGD fluxes results are higher than the reference case by approximately 9-10%. This anomaly can be explained in Figure 3.8C. Here the input rainfall values used for each case is plotted, the period between Aug-Sep 1997 have higher ENSO rainfall values than the reference case. Note that, the reference case uses the mean monthly rainfall, so the same monthly values for rainfall are recurring each year which is actually not always the case. It's highly probable that the actual rainfall values during this period are higher than the one used for the reference case.

La Niña Periods

Similar to the El Niño periods, using the Oceanic Index (ONI) values from NOAA (Figure 3.7), the periods with extreme/strong La Niña is determined (Figure 3.9A) (i.e. cold episodes correspond to ONI -0.5 to -1, moderate La Niña ONI -1 - -1.5, and strong La Niña ONI <-1.5). These periods are extracted from the Scenario 6 model results and compared with the results of the reference case (Figure 3.9B).

Figure 3.9B shows that the model La Niña period SGD fluxes are generally having comparable values to the reference case results.

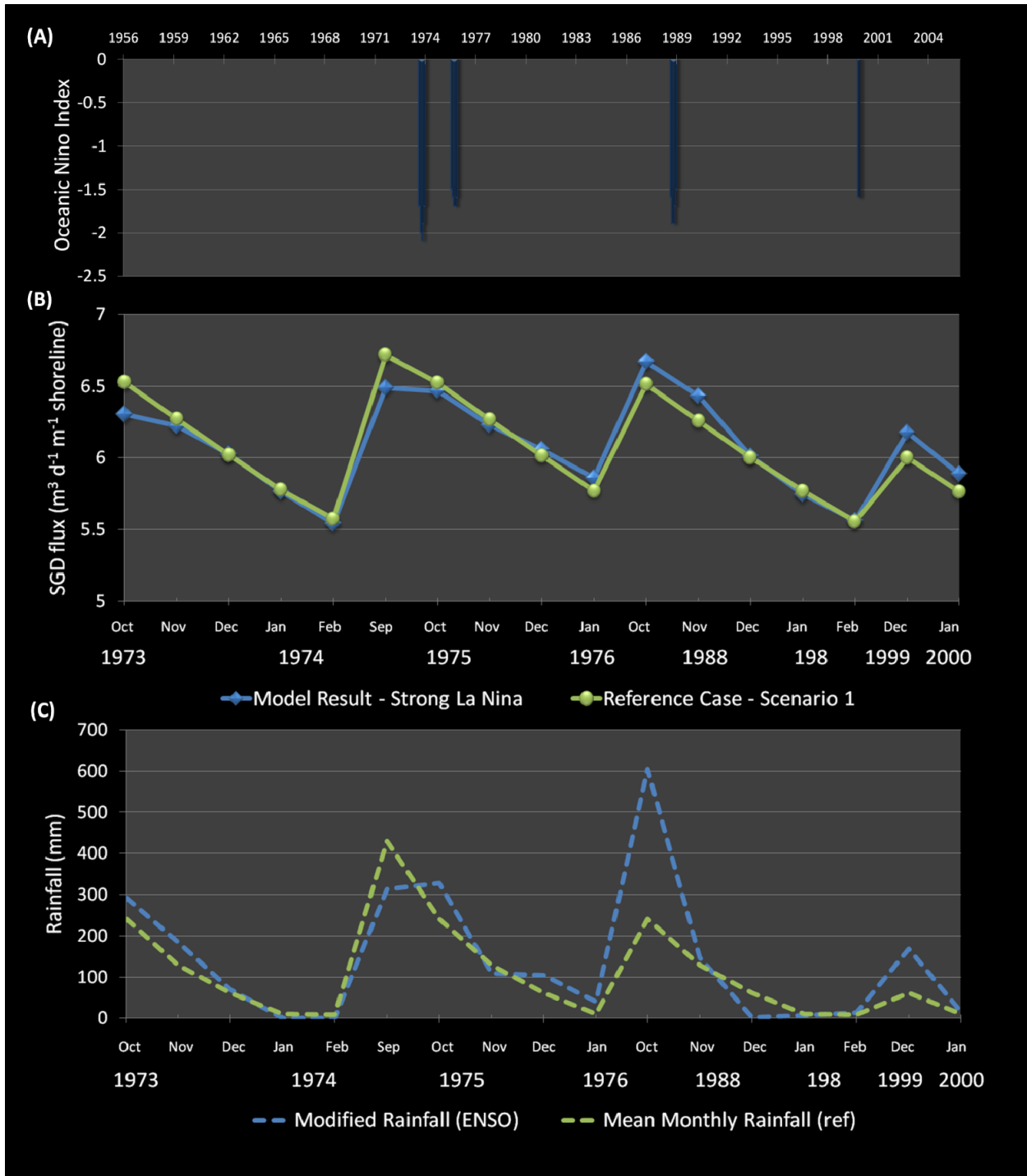


Figure 3.9 (A) Strong La Niña periods (B) Comparison of Scenario 1 and Scenario 6 model SGD flux results (C) Corresponding scenario rainfall input values used for each stress period.

The difference in values between Scenario 1 and Scenario 6 is between the ranges of 0 to -3% with an average of 0%. Indicative of almost equal SGD fluxes during “normal” conditions and La Niña. Several “anomalous” values, with inverse relationship -- “normal” conditions have higher SGD fluxes than La Niña – extracted from periods 1973 and by approximately 1-3%. This anomaly can be partly explained by Figure 3.9C but not completely because for the period Oct-Dec 1973, ENSO rainfall values are higher than the reference rainfall but the SGD flux results from La Niña are still lower or almost equal.

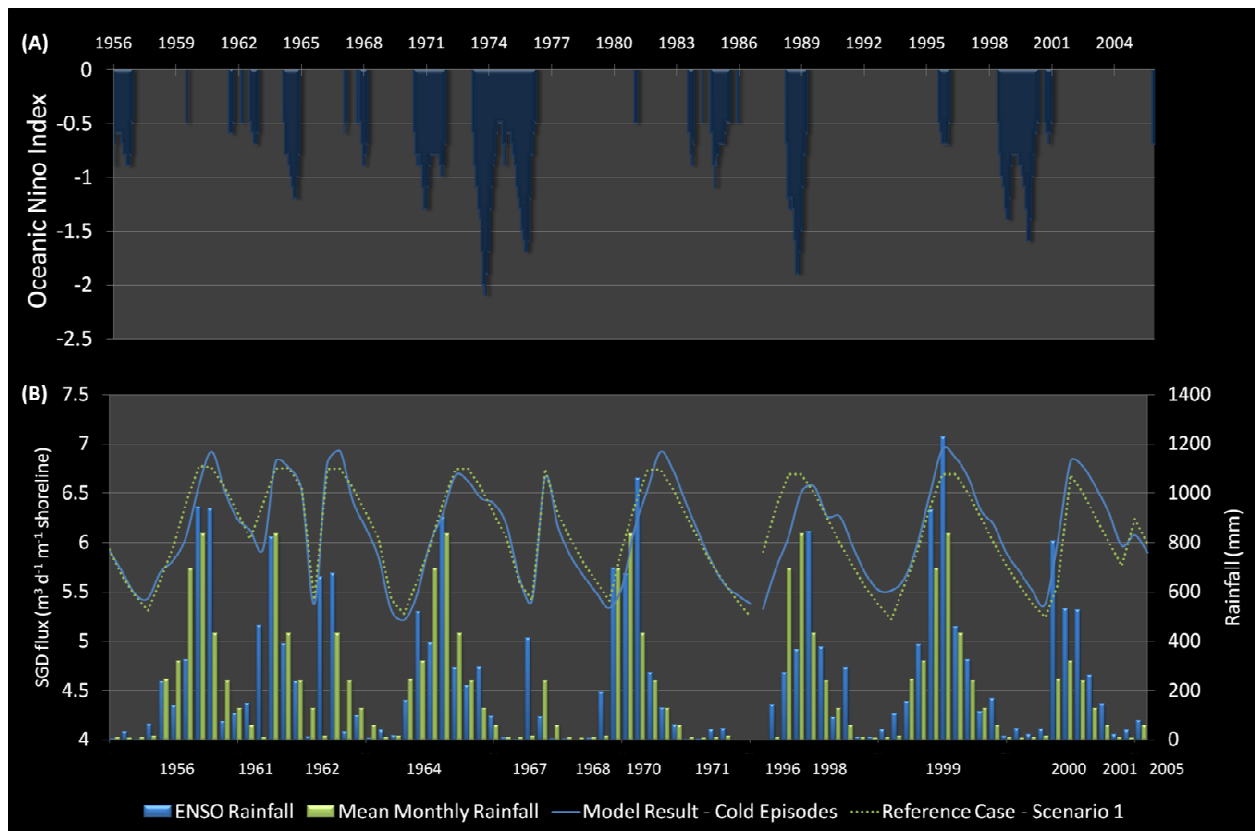


Figure 3.10 (A) Weak and strong La Niña periods (cold episodes) (B) Comparison of Scenario 1 and Scenario 6 model SGD flux results and the corresponding scenario rainfall input values used for each stress period.

Figure 3.10A shows the of model SGD flux results of Scenario 1 and Scenario 6 for the cold episodes from beginning of the simulation year 1956-1971 and the later part of the simulation year 1996-2005. Here we can clearly see that the SGD fluxes during “normal” conditions and La Niña are almost following the same trend and only have a $\pm 3\%$ deviation. This relationship can be possibly explained by how the model is set-up. Drains are implemented in the model at certain fixed elevation points. So any excess water from the system will just be flushed out through the drains. Possibly the reason why during the period Oct-Dec 1973, even when the ENSO rainfall values are higher than the reference rainfall, the SGD flux results from La Niña are almost equal.

3.4.2.2 Sea Level Rise effects on SGD

Figure 3.11 shows the model SGD flux results of the different sea level rise scenarios. Generally we can see that sea level rise have minimal effect on changing the SGD fluxes. Assuming no sea level rise will occur for the next 50 years from 2006 in Scenario 7-0; by 2055 the SGD flux will only decrease by 2%. Similar values are obtained by implementing the lower limit value for sea level rise equal to 0.15m in 50yr. IPCC max sea level rise of 0.5m/50year implemented for Scenario 7-2 and Philippines sea level rise of 0.475m/50yr implemented for Scenario 7-3 would lower the SGD flux by approximately 3% -- from 6.2 to 5.9 $\text{m}^3\text{day}^{-1}$ m width of shoreline. Higher estimates of sea level rise however would influence more the SGD fluxes, as seen with the trend from min to max sea level rise scenarios.

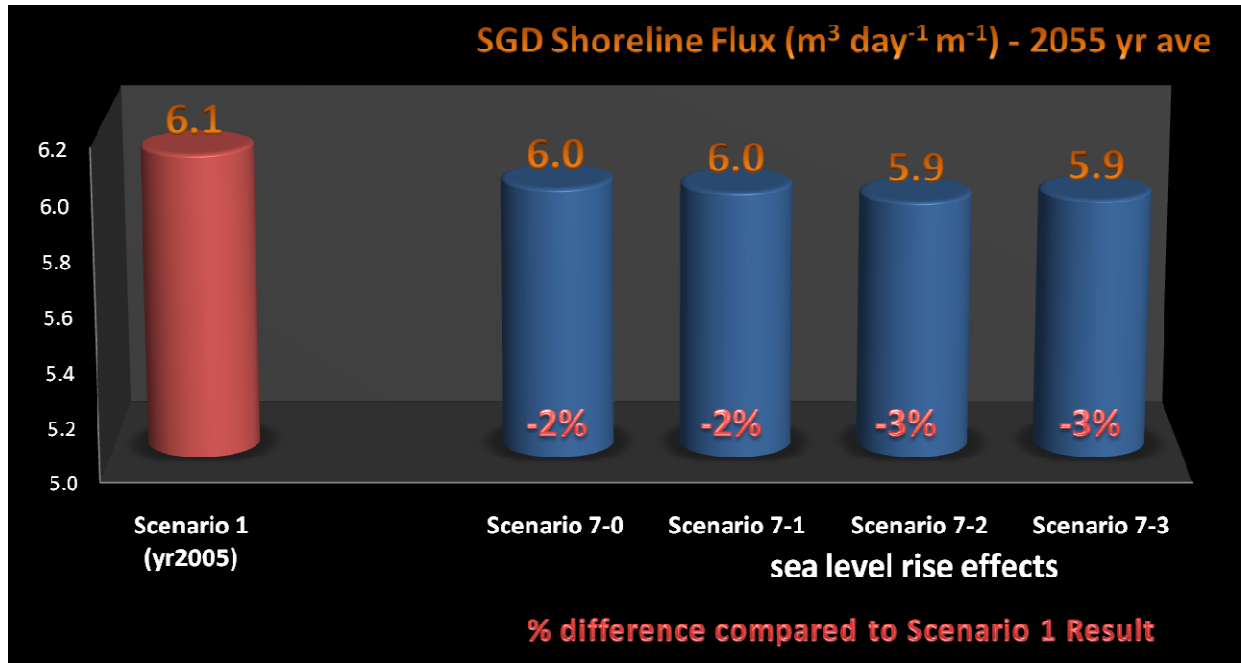


Figure 3.11 Graph of the resulting 2055 year average total SGD shoreline flux from the different sea level rise scenarios. Also shown in red is the percentage difference of each scenario result to the reference case. All values are converted to m^3/day per m shoreline width.

3.4.2.3 Anthropogenic-induced effects

The results of the simulations run using the different anthropogenic induced scenarios are shown in [Figure 3.12](#). Assuming continuous pumping and doubled groundwater well extraction, with no accompanied sea level rise, the SGD flux by 2055 will be decreased by 8% as shown by the results in Scenario 8-1. If the whole forest area will be completely deforested (**Scenario 8-2**), while the rest of the other area continuous to have the same type of land-use, the SGD flux will increase by 1%. This is because of the significant change in evapotranspiration and run-off which directly affects the amount of recharge ([Figure 3.13](#)). On the contrary, reforestation of barren areas will actually decrease the SGD fluxes by 9%.

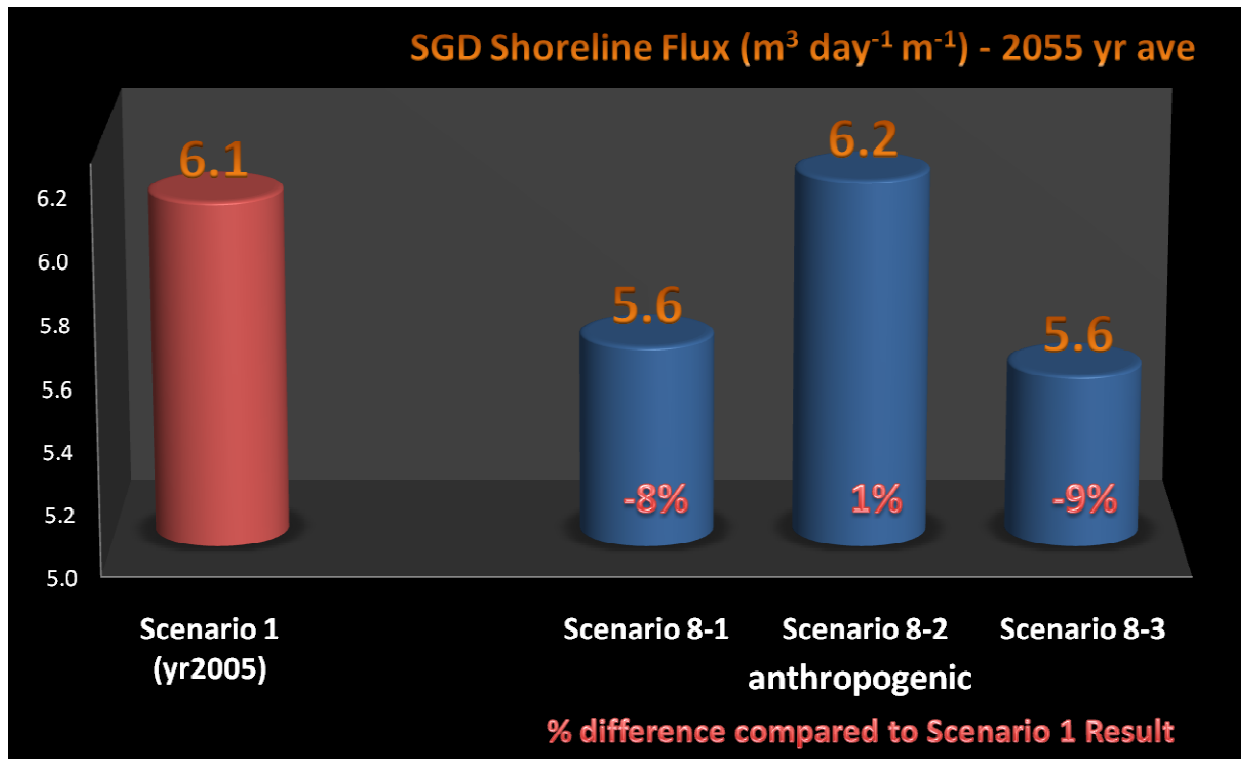


Figure 3.12 Graph of the resulting 2055 year average total SGD shoreline flux from the different ant anthropogenic induced scenarios. Also shown in red is the percentage difference of each scenario result to the reference case and in blue to Scenario 7-0 (no sea level rise scenario). All values are converted to m^3/day per m shoreline width.

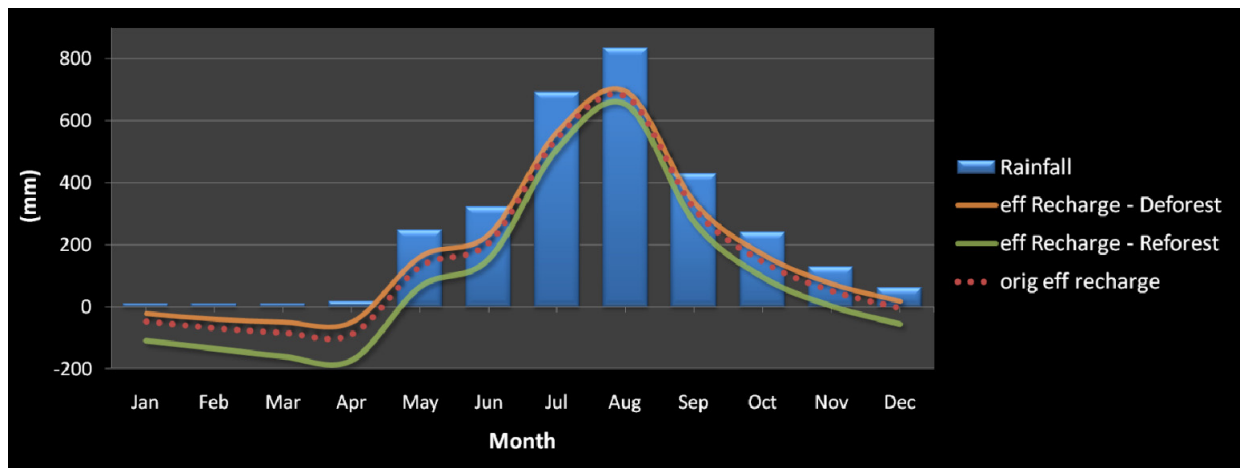


Figure 3.13 Comparison of calculated average monthly effective recharge with changing land-use conditions.

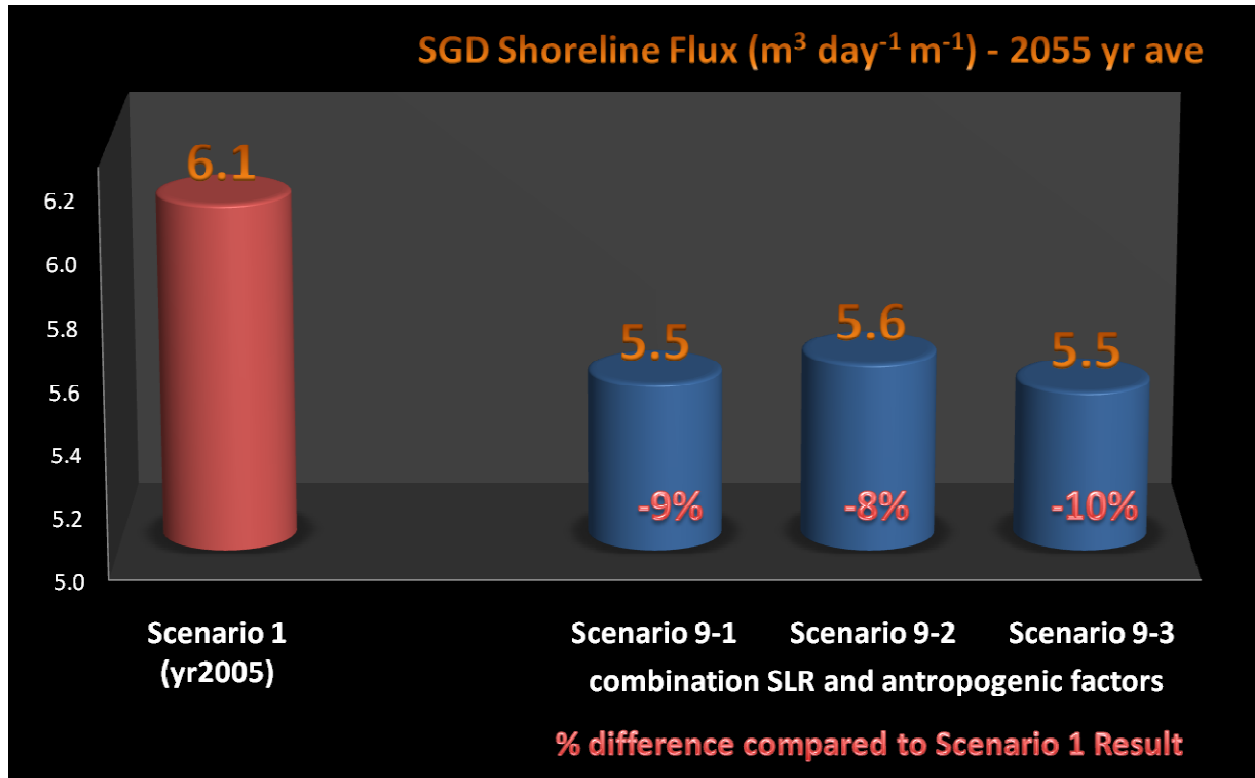


Figure 3.14 Graph of the resulting 2055 year average total SGD shoreline flux from the different ant combined anthropogenic induced and max sea level rise scenarios. Also shown in red is the percentage difference of each scenario result to the reference case. All values are converted to m^3/day per m shoreline width.

3.4.2.4 Combined Effects

The results of the simulations run using the combination of IPCC max value for sea level rise and the different anthropogenic induced scenarios are shown in [Figure 3.14](#). In Scenario 9-1, assuming continuous pumping and doubled groundwater well extraction, with accompanied sea level rise, the SGD flux by 2055 will be decreased by 9% as shown by the results in Scenario 9-1. This value is 1% lower compared to the result simulated with no sea level rise. Deforestation combined with sea level rise implemented in Scenario 9-2 results to a decrease in

SGD flux by 8% in 2055. This result is very different from the deforestation case with no sea level rise. Scenario 8-2 resulted to an SGD flux value of $6.2 \text{ m}^3\text{day}^{-1} \text{ m}^{-1}$, which is higher than the 2005 yr average reference case result. Scenario 9-3 resulted to a decrease of 10% in the SGD flux.

3.5 Conclusions

Based on the simulation of climate and anthropogenic effects on SGD at the SE flank of Mt. Mariveles, Bataan the main findings are as follows:

- 1) ENSO affects SGD fluxes in two different ways. During El Niño, the SGD fluxes are significantly reduced at an average of 7% change. This is due to the ENSO influence on the rates of precipitation and groundwater recharge. La Niña does not change or influence the SGD flux greatly. High amounts of rain poured during La Nina are just flushed out of the system through drains.
- 2) Sea level rise have a minor effect on the SGD fluxes. This results to lowering of SGD fluxes by 2-3% depending on the height of sea level rise. Only conservative IPCC sea level rise values are applied in the model, but there are other larger estimates which are not implemented which could probably result to large changes in SGD flux
- 3) Excessive groundwater extraction and land-use changes can greatly influence the magnitude of SGD flux especially when combined with sea level rise resulting to 8-10 % change in SGD fluxes by yr 2055.

References

- Church JA and NJ White (2006). A 20th century acceleration in global sea-level rise. *Geophysical Research Letters*; 33: L01602
- Global Sea-level Rise (2009). In UNEP/GRID-Arendal Maps and Graphics Library. Retrieved 04:23, August 31, 2010 from <http://maps.grida.no/go/graphic/global-sea-level-rise>.
- Grinsted A, JC Moore and S Jevrejeva (2009). Reconstructing sea level from paleo and projected temperatures 200 to 2100 AD. *Climate Dynamics*; DOI 10.1007/s00382-008-0507-2, 06 January 2009.
- IPCC (Intergovernmental Panel on Climate Change) (2007): *Climate Change 2007: The Physical Science Basis. Contribution of Working Group I to the Fourth Assessment Report of the Intergovernmental Panel on Climate Change* [Solomon, S., D. Qin, M. Manning, Z. Chen, M. Marquis, K.B. Averyt, M. Tignor, and H.L. Miller (eds.)]. Cambridge University Press, Cambridge, UK, and New York, 996 pp.
- Jose AM (2002). Updates on Monitoring the Sea Surface Temperature Anomaly in the Warm Pool Area and Climate Variability in the Philippines for 2000 to 2001. Philippine Atmospheric, Geophysical and Astronomical Services Administration (PAGASA), Quezon City, Philippines.
- McGranahan G, D Balk and B Anderson (2007). The rising tide: assessing the risks of climate change and human settlements in low elevation coastal zones. *Environment and Urbanization*; 19: 17-37.
- Pfeffer WT, JT Harper and S O'Neel (2008). Kinematic Constraints on Glacier Contributions to 21st-Century Sea-Level Rise. *Science*; 321(5894): 1340-1343.
- Rahmstorf, S (2007). Sea-Level Rise: A Semi-Empirical Approach to Projecting Future. *Science*; 315: 368–370.
- Rodolfo KS and FP Siringan (2006). Ignoring groundwater overuse, the main cause of regional subsidence and worsening flood at the head of Manila Bay, Philippines. *Disasters. Special Issue on Climate Change and Disasters*; 30(1): 118-139.
- Trends in sea level, 1870-2006. (2007). In UNEP/GRID-Arendal Maps and Graphics Library. Retrieved 04:24, August 31, 2010 from <http://maps.grida.no/go/graphic/trends-in-sea-level-1870-2006>.
- United Nations Environment Programme (UNEP) Year Book (2009). *New Science and Developments in our Changing Environment*.

Acknowledgements

This research was accomplished with the financial support from the System Earth Modeling Scholarship of Utrecht University through **Dr. Majid Hassanizadeh** and the SGD project of the Marine Science Institute, University of the Philippines through **Dr. Fernando Siringan**.

I am very thankful to my supervisors **Dr. Gualbert Oude Essink** and **Dr. Hans Dürr**, who believed in my abilities and whose encouragement, guidance and support from the initial to the final stage of this research made me attain my goals and perform to my highest potential.

During my fieldwork in the Philippines, **Peter Zamora** and **Maria Isabel Senal** of the Marine Science Institute enthusiastically helped me during the 3-day fieldwork in Bataan, under the scorching heat of the sun, to both of you thank you very much. Many thanks also to **Lea Soria**, **Dr. Joseph Foronda**, the staff from LWUA, MGB and NWRB for giving me some of the important data for my research.

My deepest gratitude to **Dr. Fernando Siringan** who, when I told about my plans of doing my research in the Philippines, supported and encouraged me and tried to find the funds as soon as possible to support my fieldwork expenses there, also for being a very important influence on the early stages of my career as a scientist and researcher.

I would also like to thank my colleagues from Deltares (Netherlands) – **Martha, Esther, Sonia** and **Jos**, and from Universiteit Gent (Belgium) – **Dr. Luc Lebbe, Caroline** and **Alexander**, where I did my internship; I enjoyed working with all of you and thank you for the very interesting discussions.

To my classmates thank you for making my MSc years very interesting and fun. To my university friends especially to **Haydon, Amir, Tom, Goulven** and **Vasso**, thanks for the meaningful conversations.

To my **mentors** and **teachers**, thank you so much for sharing your knowledge and also for some of you who have become a very important influence and motivation for my chosen path.

Most importantly, I thank my very good friends and family. I am very grateful to have them by my side especially on those moments that I am near to losing my sanity. To my extended family in France who treated me as their own, to my best friends **Jomar, Carla** and **Astrid**, to my parents **Ferdie** and **Judy** who have been missing me constantly, and my only sister **Shelby** who came to Europe just so we can be together, I cannot thank you enough for all the love and affection you've given me.

To **Brice**, the only love of my life, thank you for being my inspiration.

Appendix

Appendix I

Abbreviations

CIESIN	Center for International Earth Science Information Network
CIAT	Centro Internacional de Agricultura Tropical
DENR	Department of Environment and Natural Resources.
DEM	Digital Elevation Model
DIN	Dissolved Inorganic Nitrogen
ERSDAC	Earth Remote Sensing Data Analysis Center
ENSO	El Niño–Southern Oscillation
FAO	Food and Agriculture Organization
GRCO	General Resources Co., Ltd.
GIST	Geographic Information Support Team
GDEM	Global Digital Elevation Map
HAB	Harmful Algal Blooms
IPCC	Intergovernmental Panel on Climate Change
LWUA	Local Water Utilities Administration
MSI	Marine Science Institute
MARIWAD	Mariveles Water District
MGB	Mines and Geosciences Bureau
NAMRIA	National Mapping and Resource Information Authority
NOAA	National Oceanic and Atmospheric Administration
NRCS	Natural Resources Conservation Service
ONI	Oceanic Niño Index
PAR	Philippine Area of Responsibility
PAGASA	Philippine Atmospheric, Geophysical and Astronomical Services Admin
PNRI	Philippine Nuclear Research Institute
SLR	Sea Level Rise
SGD	Submarine Groundwater Discharge
TDS	Total Dissolved Solids
UNEP	United Nations Environment Programme
USDMA	United States Defense Mapping Agency
WHOI	Woods Hole Oceanographic Institution
WHRC	Woods Hole Research Center

Appendix II

Preparation of MOCDENS3D (MODFLOW and MOC3D) Packages

MODFLOW

2.1	Basic Package	BAS.DAT
2.2	Block-Centered Flow Package	BCF.DAT
2.3	Drain Package	DRN.DAT
2.4	General-Head Boundary Package	GHB.DAT
2.5	Output Control	OC.DAT
2.6	Preconditioned Conjugate Gradient 2 Package (PCG2)	PCG2.DAT
2.7	River Package	RIV.DAT
2.8	Recharge Package	RCH.DAT
2.9	Well Package	WEL.DAT

MOC3D

2.10	Main MOC3D Package	MOCMAIN.DAT
2.11	Source Concentration in Recharge	MOCCRCH.DAT
2.12	Observation Well File	MOCOBS.DAT

Appendix 2.1

BAS Package

The **BAS Package** contains the basic information of the model area, i.e. the number of layers, top and bottom elevation, number and duration of each stress periods. Also it contains the *ibounds* which determines which cells will be active or inactive – active cells will be included in the calculation. This also contains the initial head levels.

To prepare the **bas.dat** file, first the information on the elevation has to be converted into an ascii format file such as the one seen below. Here the AsterGDEM and the bathymetric data of the study area are combined in ArcMap and exported as an ASCII raster file.

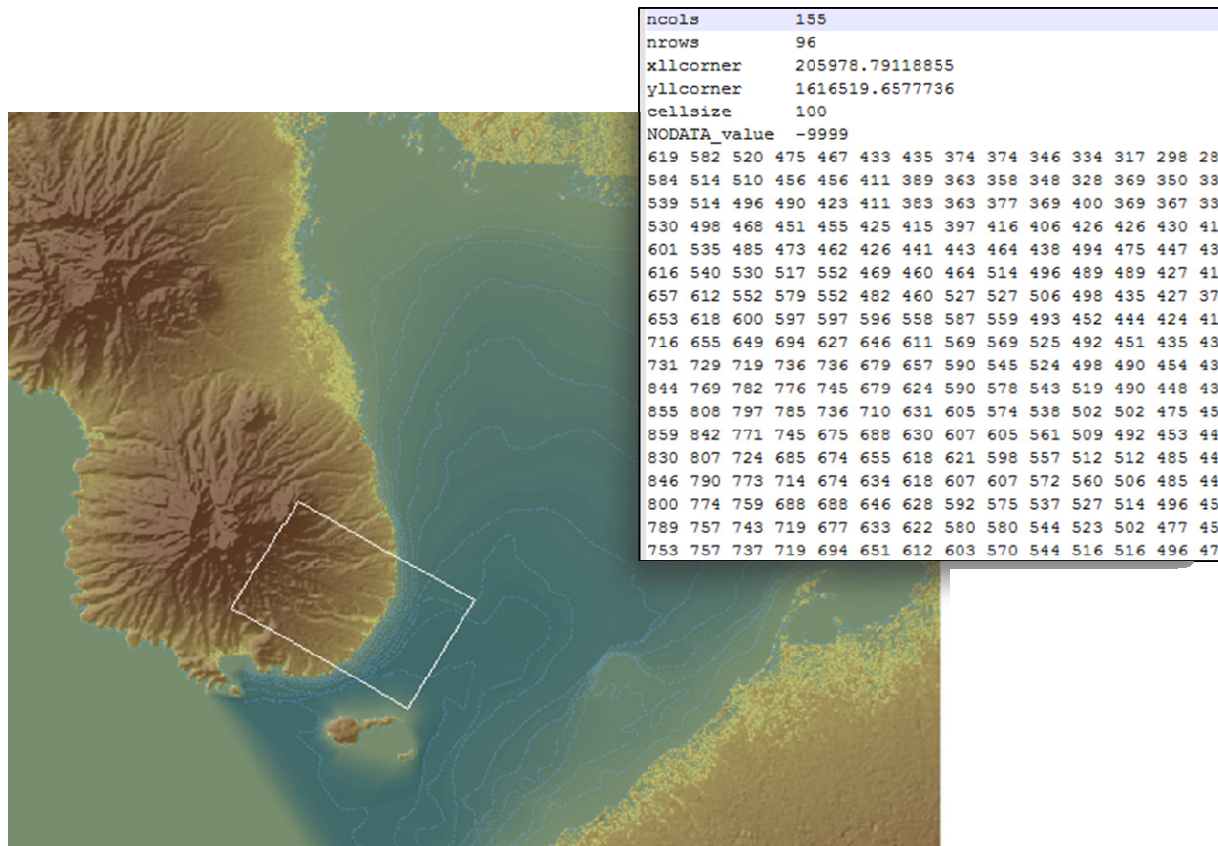


Figure above shows the AsterGDEM combined with the bathymetric data. The model area is represented by the white rectangular box. On the upper right side, the generated ASCII raster file generated in ArcMap.

Using the generated elevation ASCII file from ArcMap, a program (see below) is created to write the ibound3Dmatrix file. This 3Dmatrix file will be implemented in PMWIN and converted to the .ibd file (also called ibound package). The output .ibd package along with other information mentioned earlier is again implemented in PMWIN for the BAS package.

```

48 procedure readasc;
49 //var fname: string;
50 begin
51   filename:=ahnfile;assign(dat1,filename);reset(dat1);
52   writeln('read ahn: ',ahnfile);
53   readln(dat1,ncol,nrow);
54   for irow:=1 to nrow do
55     begin
56       for icol:=1 to ncol do
57         begin
58           read(dat1,ahn[icol,irow]);
59           if ahn[icol,irow]<=0 then ahn[icol,irow]:=-9999;
60         end;
61       end;
62     close(dat1);
63   end;
64
65 procedure inputfile;
66 begin
67   filename:='mk_ibound.inp';assign(geol,filename);reset(geol);
68   writeln('read inputfile: ',filename);
69   readln(geol,ncol,nrow);
70   readln(geol,ahnfile);
71   readasc;
72   readln(geol,top);
73   readln(geol,nz);
74   nlay:=0;
75   for i:=1 to nz do
76     begin
77       readln(geol,zl[i],zd[i]);
78       nlay:=nlay+zl[i];
79     end;
80   close(geol);
81 end;
82

```

Here the elevation ascii file is read

```

83 procedure writebound3dmatrix;
84 begin
85   filename:='ibound_3dmatrix.asc';assign(asc1,filename);rewrite(asc1);
86   writeln('write matrix file: ',filename);
87   for layer:=1 to nlay do
88     begin
89       writeln(asc1,'          1          1('',ncol:2,'I2)          -1 6. DATA IBOUND Array for Layer ',layer:1);
90       for irow:=1 to nrow do
91         begin
92           for icol:=1 to ncol do
93             begin
94               if (icol/ncol-trunc(icol/ncol)<>0) then write(asc1,' ',ibound[icol,irow,layer]:1) else writeln(asc1,' ',ibound[icol,irow,layer]:1);
95             end;
96           end;
97         end;
98       close(asc1);
99     end;
100

```

This procedure creates the ibound3dmatrix

Below are screenshots of the different essential sections of the created **bas.dat** file used for the reference case **Scenario 1** in this study. Numbers on the leftmost side indicate the line number. Note that this **bas.dat** file can also be directly made by using a computer code if preferred.

```
bas.dat
1 Lucania Catchment, Philippines
2
3      48      96      155      1800      4
4 FREE
5      0      1
6      1      1(2019)      -1 6. DATA IBOUND Array for Layer 1
7 1 1 1 1 1 1 1 0 0 0 0 0 0 0 0 0 0 0 0 0 0 0 0 0 0 0 0 0 0 0 0
8 0 0 0 0 0 0 0 0 0 0 0 0 0 0 0 0 0 0 0 0 0 0 0 0 0 0 0 0 0 0 0
9 0 0 0 0 0 0 0 0 0 0 0 0 0 0 0 0 0 0 0 0 0 0 0 0 0 0 0 0 0 0 0
10 0 0 0 0 0 0 0 0 0 0 0 0 0 0 0 0 0 0 0 0 0 0 0 0 0 0 0 0 0 0 0
11 0 0 0 0 0 0 0 0 0 0 0 0 0 0 0 0 0 0 0 0 0 0 0 0 0 0 0 0 0 0 0
12 0 0 0 0 0 0 0 0 0 0 0 0 0 0 0 0 0 0 0 0 0 0 0 0 0 0 0 0 0 0 0
13 0 0 0 0 0 0 0 0 0 0 0 0 0 0 0 0 0 0 0 0 0 0 0 0 0 0 0 0 0 0 0
14 0 0 0 0 0 0 0 0 0 0 0 0 0 0 0 0 0 0 0 0 0 0 0 0 0 0 0 0 0 0 0
15 1 1 1 1 1 1 1 1 0 0 0 0 0 0 0 0 0 0 0 0 0 0 0 0 0 0 0 0 0 0
```

Information on the number of layers, rows, columns, time step are given on top followed by the ibound information per layer

```
36910 1 1 1 1 1 1 1 1 1 1 1 1 1 1 1 1 1 1 1 1 1 1 1 1 1 1 1 1 1 1 1
36911 1 1 1 1 1 1 1 1 1 1 1 1 1 1 1 1 1 1 1 1 1 1 1 1 1 1 1 1 1 1 1
36912 1 1 1 1 1 1 1 1 1 1 1 1 1 1 1 1 1 1 1 1 1 1 1 1 1 1 1 1 1 1 1
36913 1 1 1 1 1 1 1 1 1 1 1 1 1 1 1 1 1 1 1 1 1 1 1 1 1 1 1 1 1 1 1
36914 1 1 1 1 1 1 1 1 1 1 1 1 1 1 1 1 1 1 1 1 1 1 1 1 1 1 1 1 1 1 1
36915 1 1 1 1 1 1 1 1 1 1 1 1 1 1 1 1 1 1 1 1 1 1 1 1 1 1 1 1 1 1 1
36916 1 1 1 1 1 1 1 1 1 1 1 1 1 1 1 1 1 1 1 1 1 1 1 1 1 1 1 1 1 1 1
36917 1 1 1 1 1 1 1 1 1 1 1 1 1 1 1 1 1 1 1 1 1 1 1 1 1 1 1 1 1 1 1
36918 -999.99
36919 1 1(20G14.0) -1 8. DATA Starting Heads in Layer 1
36920 0 0 0 0 0 0 0 0 0 0 0 0 0 0 0 0 0 0 0 0 0 0 0 0 0 0 0 0 0
36921 0 0 0 0 0 0 0 0 0 0 0 0 0 0 0 0 0 0 0 0 0 0 0 0 0 0 0 0 0
36922 0 0 0 0 0 0 0 0 0 0 0 0 0 0 0 0 0 0 0 0 0 0 0 0 0 0 0 0 0
36923 0 0 0 0 0 0 0 0 0 0 0 0 0 0 0 0 0 0 0 0 0 0 0 0 0 0 0 0 0
36924 0 0 0 0 0 0 0 0 0 0 0 0 0 0 0 0 0 0 0 0 0 0 0 0 0 0 0 0 0
36925 0 0 0 0 0 0 0 0 0 0 0 0 0 0 0 0 0 0 0 0 0 0 0 0 0 0 0 0 0
36926 0 0 0 0 0 0 0 0 0 0 0 0 0 0 0 0 0 0 0 0 0 0 0 0 0 0 0 0 0
36927 0 0 0 0 0 0 0 0 0 0 0 0 0 0 0 0 0 0 0 0 0 0 0 0 0 0 0 0 0
36928 0 0 0 0 0 0 0 0 0 0 0 0 0 0 0 0 0 0 0 0 0 0 0 0 0 0 0 0 0
36929 0 0 0 0 0 0 0 0 0 0 0 0 0 0 0 0 0 0 0 0 0 0 0 0 0 0 0 0 0
36930 0 0 0 0 0 0 0 0 0 0 0 0 0 0 0 0 0 0 0 0 0 0 0 0 0 0 0 0 0
36931 0 0 0 0 0 0 0 0 0 0 0 0 0 0 0 0 0 0 0 0 0 0 0 0 0 0 0 0 0
36932 0 0 0 0 0 0 0 0 0 0 0 0 0 0 0 0 0 0 0 0 0 0 0 0 0 0 0 0 0
36933 0 0 0 0 0 0 0 0 0 0 0 0 0 0 0 0 0 0 0 0 0 0 0 0 0 0 0 0 0
36934 0 0 0 0 0 0 0 0 0 0 0 0 0 0 0 0 0 0 0 0 0 0 0 0 0 0 0 0 0
36935 0 0 0 0 0 0 0 0 0 0 0 0 0 0 0 0 0 0 0 0 0 0 0 0 0 0 0 0 0
36936 0 0 0 0 0 0 0 0 0 0 0 0 0 0 0 0 0 0 0 0 0 0 0 0 0 0 0 0 0
```

initial head level information per layer

```
73827 0 0 0 0 0 0 0 0 0 0 0 0 0 0 0 0 0 0 0 0 0 0 0 0 0 0 0 0
73828 0 0 0 0 0 0 0 0 0 0 0 0 0 0 0 0 0 0 0 0 0 0 0 0 0 0 0 0
73829 0 0 0 0 0 0 0 0 0 0 0 0 0 0 0 0 0 0 0 0 0 0 0 0 0 0 0 0
73830 0 0 0 0 0 0 0 0 0 0 0 0 0 0 0 0 0 0 0 0 0 0 0 0 0 0 0 0
73831 1.157E-05 1 1
73832 30.5 1 1
73833 30.5 1 1
73834 30.5 1 1
73835 30.5 1 1
73836 30.5 1 1
73837 30.5 1 1
```

information of the duration of each stress period

```
73883 30.5 1 1
73884 30.5 1 1
73885 30.5 1 1
73886 30.5 1 1
73887 30.5 1 1
73888 30.5 1 1
73889 30.5 1 1
73890 30.5 1 1
```

Appendix 2.2

BCF Package

The **BCF package** computes the conductance between each of the grid cells and sets up the finite difference equations for the cell to cell flow. It also computes the terms that determine the rate of movement of water to and from storage.

Thus the **bcf package** would contain/require the following data array:

1) Layer Type

Data arrays are required for a particular layer and are dependent on the layer type. The layer arrays required for each layer type are shown in the following table.

Layer Type	Required Arrays
Confined (LAYCON=0)	Transmissivity Leakance Primary Storage Coefficient (storativity)
Unconfined (LAYCON=1)	Bottom Elevation Hydraulic Conductivity Leakance Primary Storage Coefficient (specific yield)
Confined/Unconfined (LAYCON=2)	Top Elevation Transmissivity Leakance Primary Storage Coefficient (storativity) Secondary Storage Coefficient (specific yield)
Confined/Unconfined (LAYCON=3)	Top Elevation Bottom Elevation Hydraulic Conductivity Leakance Primary Storage Coefficient (storativity) Secondary Storage Coefficient (specific yield)

For this model, a confined layer type (LAYCON=0) is selected for all layers.

2) Leakance – is a function of the layer thickness and the vertical hydraulic conductivity.

Vertical hydraulic conductivity (.lea file)

3) Transmissivity is equal to the horizontal hydraulic conductivity multiplied by the layer thickness.

Horizontal hydraulic conductivity (.con file)

4) Primary storage coefficient

In this case, a calculated value of specific storage is applied

A 3D Geology Model is created for the study area (see **Section 2.5** for details) using existing topography, geological, sedimentological, seismic, and borehole data. Based on the 3D geology model, hydraulic parameter values are assigned. The 3D Geology Model makes it easier to implement the series of array values required in PMWIN. Each of these array values can be created by programming (Pascal, FORTRAN, or any programming code you wish to use) or manually input the values in PMWIN.

Hydraulic parameter values assigned for the model are enumerated in **Section 2.7.1 – Hydrogeologic Parameters**. The series of arrays required for the BCF package is manually inputted in PMWIN.

These hydraulic parameters are based on pump tests measurements and literature data available in the area.

Pumping tests results for the confined aquifers within the study area. Data from below from [LWUA](#).

Well Name	Trans- missivity (m ² /s)	Trans- missivity (m ² /day)	Storativity	Aquifer thickness (m)	Hydraulic Conductivity (m/day)
PNOC#4/DRU-14	0.0069	596.16		162	3.68
PNOC#3 / DRU-13	0.00587	507.168		142	3.57
PNOC#1 / DRU-11	0.00572	494.208		Partially penetrating well	
DRU-2	0.00187	161.568		Partially penetrating well	
DRU-24	0.00433	374.112	0.00433	150	2.49
DRU-18	0.00546	471.744	0.00019-.00028	150	3.14
DRU-17	0.0067	578.88	0.00546	150	3.86
DRU-25	0.0114	984.96	0.00027-0.00035	150	6.57
DRU-26	0.0036	311.04	0.00226	150	2.07
Average		497.76			3.63

Appendix 2.3

Drain Package

The **Drain Package** is used to simulate head-dependent flux boundaries. If the head in the cell falls below a certain threshold, the flux from the drain to the model cell drops to zero.

Using the same generated elevation ASCII file (as in **Appendix 2.1**) as input, a program (see below) is created to create the **DRN.DAT** file.

```

134 procedure makeiboundary;
135 begin
136   //...   Ibound
137   for icol:=1 to ncol do
138     begin
139       for irow:=1 to nrow do
140         begin
141           for layer:=0 to nlay do
142             begin
143               ibound[icol,irow,layer]:=1;
144               if layer=0 then ibound[icol,irow,layer]:=0;
145             end;
146           end;
147         end;
148       for icol:=1 to ncol do
149         begin
150           for irow:=1 to nrow do
151             begin
152               for layer:=1 to nlay do
153                 begin
154                   conc[icol,irow,layer]:=-1;
155                   if (zm[layer]>ahn[icol,irow]) then
156                     begin
157                       // in air ibound is 0
158                       ibound[icol,irow,layer]:=0;
159                       // in sea ibound is 2
160                       if (ahn[icol,irow]=-9999) and (layer>layeraboveMSL) then ibound[icol,irow,layer]:=2;
161                       writeln('zm[' ,irow:1, ']=' ,zm[irow]:10:1, ' ahn=' ,ahn[icol,irow]:10:1, ' ibound=' ,ibound[icol,irow,layer]:10);
162                     end;
163                   end;
164                 end;
165             end;
166           end;
167         end;
168       end;
169     end;
170   end;

```

*Here the **ibound** (active and inactive) cells are assigned; using this information the drain cells are determined*

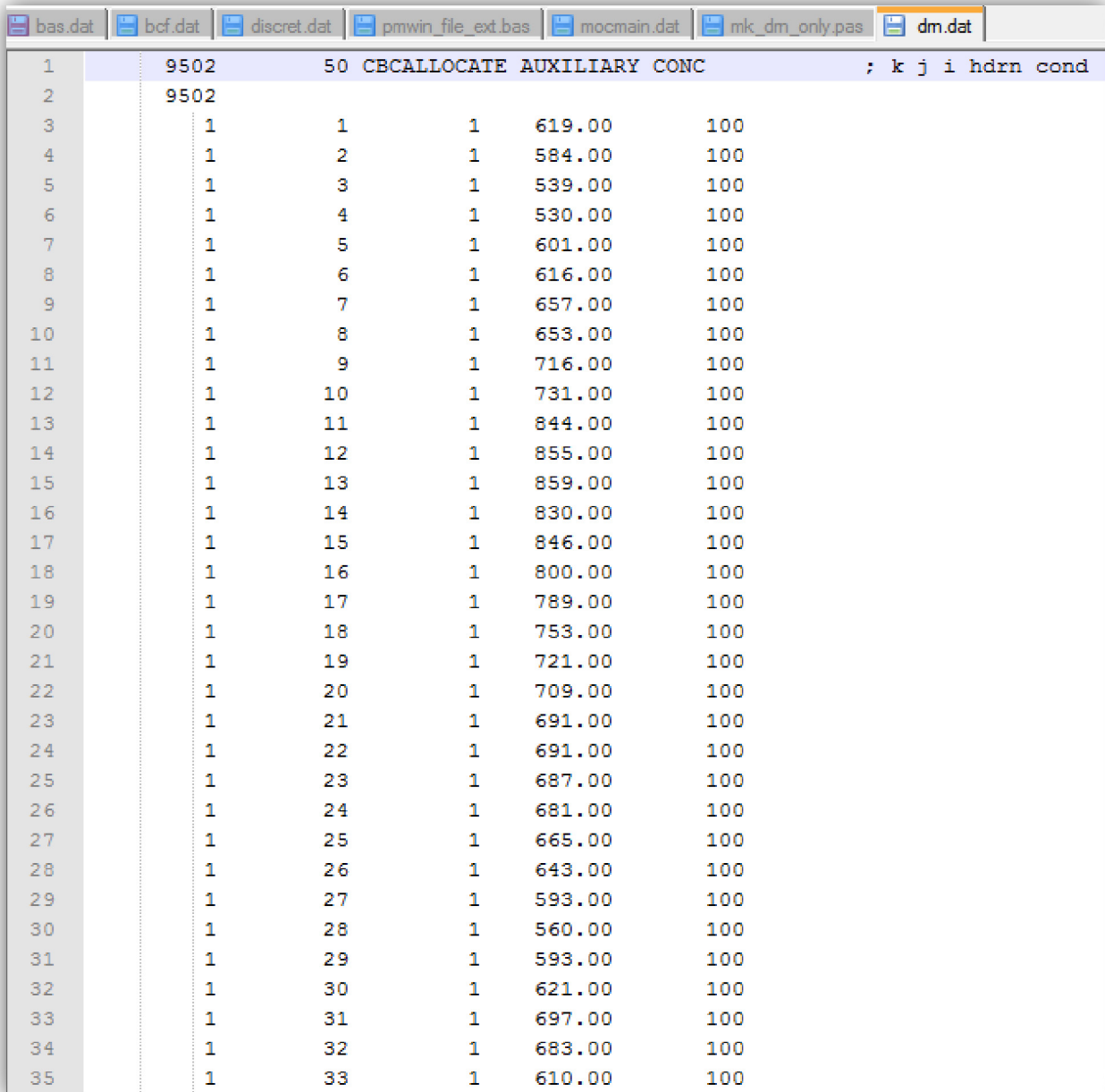
```

199 procedure readwritedrain;
200 begin
201   filename:='drn.dat';assign(drn1,filename);rewrite(drn1);
202   writeln('write drain file: ',filename);
203   writeln(drn1,' ',drnarray:5,'          50 CBCALLOCATE AUXILIARY CONC          ; k j i hdrn cond');
204   writeln(drn1,' ',drnarray:5);
205   for icol:=1 to ncol do
206     begin
207       for irow:=1 to nrow do
208         begin
209           layer:=1;
210           while ibound[icol,irow,layer]=0 do
211             begin
212               layer:=layer+1;
213             end;
214           dum1:=ahn[icol,irow];dum2:=drncond;
215           if ahn[icol,irow]<=-9999 then writeln(drn1,layer:10,irow:10,icol:10,ahn[icol,irow]:10:2,dum2:10:0);
216           // if ibound[icol,irow,layer]< then writeln(drn1,layer:10,irow:10,icol:10,ahn[icol,irow]:10:2,dum2:10:0,' ; k j i hdrn cond');
217         end;
218       end;
219       for n:=1 to stressperiods do writeln(drn1,'-1');
220     end;
221   close(drn1);
222 end;

```

Appendix II

Below is the screenshot of the created **drn.dat** file used for the reference case Scenario 1 in this study. Numbers on the top left = 9502 correspond to the total number of drain cells



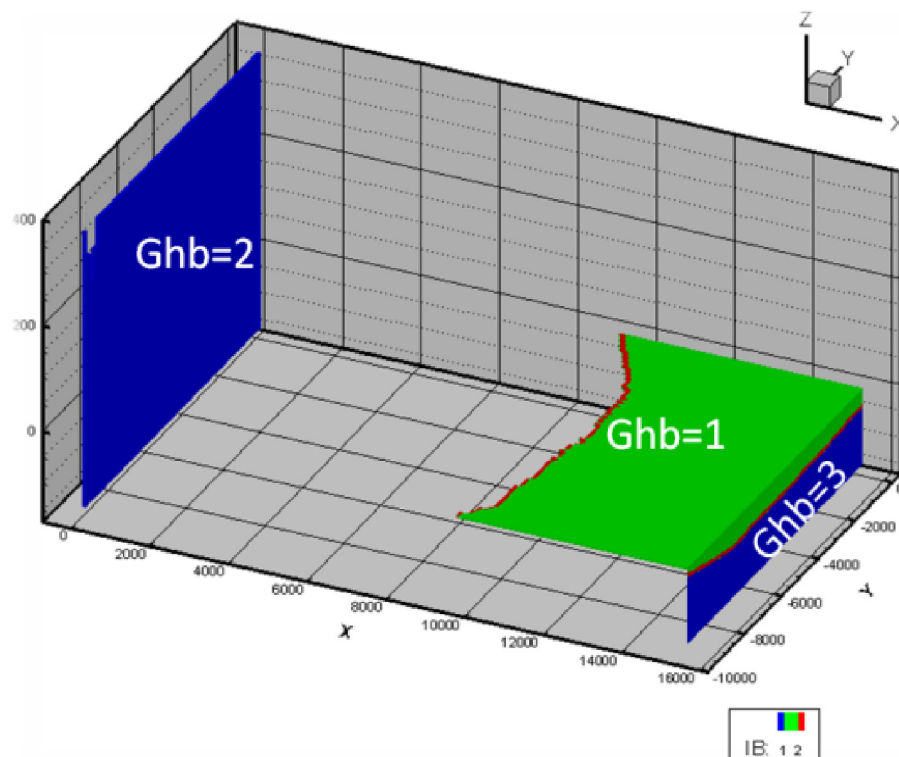
	9502	50	CBCALLOCATE	AUXILIARY	CONC					
1	9502									; k j i hdnr cond
2	9502									
3	1	1	1	619.00	100					
4	1	2	1	584.00	100					
5	1	3	1	539.00	100					
6	1	4	1	530.00	100					
7	1	5	1	601.00	100					
8	1	6	1	616.00	100					
9	1	7	1	657.00	100					
10	1	8	1	653.00	100					
11	1	9	1	716.00	100					
12	1	10	1	731.00	100					
13	1	11	1	844.00	100					
14	1	12	1	855.00	100					
15	1	13	1	859.00	100					
16	1	14	1	830.00	100					
17	1	15	1	846.00	100					
18	1	16	1	800.00	100					
19	1	17	1	789.00	100					
20	1	18	1	753.00	100					
21	1	19	1	721.00	100					
22	1	20	1	709.00	100					
23	1	21	1	691.00	100					
24	1	22	1	691.00	100					
25	1	23	1	687.00	100					
26	1	24	1	681.00	100					
27	1	25	1	665.00	100					
28	1	26	1	643.00	100					
29	1	27	1	593.00	100					
30	1	28	1	560.00	100					
31	1	29	1	593.00	100					
32	1	30	1	621.00	100					
33	1	31	1	697.00	100					
34	1	32	1	683.00	100					
35	1	33	1	610.00	100					

Appendix 2.4

General Head Boundary Package

The **GHB Package** simulates the head-dependent flux boundaries; here the flux is always proportional to the difference in head.

Boundary Conditions:



- 1) Assumed no flow at N and S edge of model area
- 2) Assumed hydrostatic pressure on the western edge – Mountain boundary
 GHB = 2
 Here the assumption is that the head in the mountains vary monthly (see code), a no flow boundary cannot be assumed for this edge because the drainage divide is situated farther west of the model domain.

Using the same generated elevation ASCII file (as in **Appendix 2.1**) as input, a program (see below) is created to implement the mountain boundary *ghb*.

```

260   if (icol=1) and (ibound[icol,irow,layer]<>0) then
261   begin
262     ghb[icol,irow,layer]:=2;
263     if (ibound[icol,irow,layer-1]=0) then
264     begin
265       case month of
266         1 : dum:=400-18;    //jan
267         2 : dum:=400-20;    //feb
268         3 : dum:=400-19;    //mar
269         4 : dum:=400-17;    //apr
270         5 : dum:=400-15.5;  //may
271         6 : dum:=400-13.5;  //jun
272         7 : dum:=400-11;    //jul
273         8 : dum:=400-9;     //aug
274         9 : dum:=400-10;    //sep
275        10 : dum:=400-13;   //oct
276        11 : dum:=400-15;   //nov
277        12 : dum:=400-16;   //dec
278       end;
279       fwh[icol,irow,layer]:=dum;
280       writeln(ghb2,layer:10,irow:10,icol:10,fwh[icol,irow,layer]:10:4,ghbcond:10,conc[icol,irow,layer]:10:1,' ; k j i
281     end
282     else
283     begin
284       deltacorrection:=alpha*(conc[icol,irow,layer-1]/2+conc[icol,irow,layer]/2)/c0*(ztmp[layer-1]+ztmp[layer])/2;
285       fwh[icol,irow,layer]:=fwh[icol,irow,layer-1]+deltacorrection;
286       writeln(ghb2,layer:10,irow:10,icol:10,fwh[icol,irow,layer]:10:4,ghbcond:10,conc[icol,irow,layer]:10:1,' ; k j i
287     end;
288   end;

```

- 3) Assumed hydrostatic pressure on the eastern edge – Deep sea boundary
 GHB = 3. A program (see below) is created to implement the deep sea boundary *ghb*

```

304   if (icol=ncol) and (layer>layerMSL) and (ibound[icol,irow,layer]=2) then
305   begin
306     ghb[icol,irow,layer]:=3;
307     deltacorrection:=alpha*(conc[icol,irow,layer-1]/2+conc[icol,irow,layer]/2)/c0*(ztmp[layer-1]+ztmp[layer])/2;
308     fwh[icol,irow,layer]:=fwh[icol,irow,layer-1]+deltacorrection;
309     writeln(ghb2,layer:10,irow:10,icol:10,fwh[icol,irow,layer]:10:4,ghbcondsea:10,conc[icol,irow,layer]:10:1,' ;
310   end;

```

- 4) Top sea boundary with applied sea level rise.
 GHB = 1. A program (see below) is created to implement the top sea boundary *ghb*

```

289   if (ibound[icol,irow,layer]=2) and (ibound[icol,irow,layer-1]=0) then
290   begin
291     ghb[icol,irow,layer]:=1;
292     //for (time:=1) to stressperiods do then
293     begin
294       case time of
295         1..84 : dum:=(0.0003*time)-0.6811;    //
296         85..288 : dum:=(0.002*time)-0.8412;    //
297         289..600 : dum:=(0.0011*time)-0.6526;    //
298       end;
299       deltacorrection:=alpha*conc[icol,irow,layer]/c0*(ztmp[layer])/2;
300       fwh[icol,irow,layer]:=msl+(slr*(-1))+deltacorrection;
301       writeln(ghb2,layer:10,irow:10,icol:10,fwh[icol,irow,layer]:10:4,ghbcondsea:10,conc[icol,irow,layer]:10:1,'
302     end;
303   end;

```

Below is a screenshot of the different essential sections of the created **ghb.dat** file used for the reference case **Scenario 1**. Numbers on the leftmost side indicate the line number.

```

1 12787 50 CBCALLOCATE AUXILIARY CONC
2 12787 stress period=1 year= 1 month= 1
3 1 1 1 382.0000 100 56.0 ; k j i h cond conc mountain boundary
4 2 1 1 382.0030 100 112.5 ; k j i h cond conc mountain boundary
5 3 1 1 382.0076 100 145.6 ; k j i h cond conc mountain boundary
6 4 1 1 382.0132 100 169.1 ; k j i h cond conc mountain boundary
7 5 1 1 382.0180 100 187.2 ; k j i h cond conc mountain boundary
8 6 1 1 382.0215 100 202.1 ; k j i h cond conc mountain boundary
9 7 1 1 382.0252 100 214.7 ; k j i h cond conc mountain boundary
10 8 1 1 382.0291 100 225.6 ; k j i h cond conc mountain boundary
11 9 1 1 382.0320 100 235.2 ; k j i h cond conc mountain boundary
12 10 1 1 382.0337 100 243.8 ; k j i h cond conc mountain boundary
13 11 1 1 382.0355 100 251.5 ; k j i h cond conc mountain boundary
14 12 1 1 382.0373 100 258.6 ; k j i h cond conc mountain boundary
15 13 1 1 382.0392 100 265.2 ; k j i h cond conc mountain boundary
    
```

Location (k, l, j), head, conductance and concentration values for the mountain head boundary

```

9866 19 79 154 -0.5500 1000 35000.0 ; k j i h cond conc top sea boundary
9867 19 80 154 -0.5500 1000 35000.0 ; k j i h cond conc top sea boundary
9868 19 81 154 -0.5500 1000 35000.0 ; k j i h cond conc top sea boundary
9869 19 82 154 -0.5500 1000 35000.0 ; k j i h cond conc top sea boundary
9870 19 83 154 -0.5500 1000 35000.0 ; k j i h cond conc top sea boundary
9871 19 84 154 -0.5500 1000 35000.0 ; k j i h cond conc top sea boundary
9872 19 85 154 -0.5500 1000 35000.0 ; k j i h cond conc top sea boundary
9873 19 86 154 -0.5500 1000 35000.0 ; k j i h cond conc top sea boundary
9874 19 87 154 -0.5500 1000 35000.0 ; k j i h cond conc top sea boundary
9875 19 88 154 -0.5500 1000 35000.0 ; k j i h cond conc top sea boundary
9876 19 89 154 -0.5500 1000 35000.0 ; k j i h cond conc top sea boundary
9877 19 90 154 -0.5500 1000 35000.0 ; k j i h cond conc top sea boundary
9878 19 91 154 -0.5500 1000 35000.0 ; k j i h cond conc top sea boundary
9879 19 92 154 -0.5500 1000 35000.0 ; k j i h cond conc top sea boundary
9880 19 93 154 -0.5500 1000 35000.0 ; k j i h cond conc top sea boundary
9881 19 94 154 -0.5500 1000 35000.0 ; k j i h cond conc top sea boundary
9882 19 95 154 -0.5500 1000 35000.0 ; k j i h cond conc top sea boundary
9883 19 96 154 -0.5500 1000 35000.0 ; k j i h cond conc top sea boundary
9884 19 1 155 -0.5500 1000 35000.0 ; k j i h cond conc top sea boundary
9885 20 1 155 -0.4500 1000 35000.0 ; k j i h cond conc deep sea boundary
9886 21 1 155 -0.3500 1000 35000.0 ; k j i h cond conc deep sea boundary
9887 22 1 155 -0.2500 1000 35000.0 ; k j i h cond conc deep sea boundary
9888 23 1 155 -0.1500 1000 35000.0 ; k j i h cond conc deep sea boundary
9889 24 1 155 -0.0500 1000 35000.0 ; k j i h cond conc deep sea boundary
9890 25 1 155 0.0500 1000 35000.0 ; k j i h cond conc deep sea boundary
    
```

*Location (k, l, j), head, conductance and concentration values for the top sea and deep sea head boundary
Implemented ghb for the dam present in the model area*

```

12760 45 96 155 2.2750 1000 35000.0 ; k j i h cond conc deep sea boundary
12761 46 96 155 2.8250 1000 35000.0 ; k j i h cond conc deep sea boundary
12762 47 96 155 2.7750 1000 35000.0 ; k j i h cond conc deep sea boundary
12763 48 96 155 3.0250 1000 35000.0 ; k j i h cond conc deep sea boundary
12764 6 93 20 156.0000 50 20 ; k j i h cond conc pesa_dam
12765 8 94 20 156.0000 50 20 ; k j i h cond conc pesa_dam
12766 6 88 21 156.0000 50 20 ; k j i h cond conc pesa_dam
12767 7 94 21 156.0000 50 20 ; k j i h cond conc pesa_dam
12768 7 89 22 156.0000 50 20 ; k j i h cond conc pesa_dam
12769 5 93 22 156.0000 50 20 ; k j i h cond conc pesa_dam
12770 6 94 22 156.0000 50 20 ; k j i h cond conc pesa_dam
12771 7 95 22 156.0000 50 20 ; k j i h cond conc pesa_dam
12772 7 88 23 156.0000 50 20 ; k j i h cond conc pesa_dam
12773 7 89 23 156.0000 50 20 ; k j i h cond conc pesa_dam
12774 6 93 23 156.0000 50 20 ; k j i h cond conc pesa_dam
12775 6 94 23 156.0000 50 20 ; k j i h cond conc pesa_dam
12776 5 86 24 156.0000 50 20 ; k j i h cond conc pesa_dam
12777 7 87 24 156.0000 50 20 ; k j i h cond conc pesa_dam
12778 7 88 24 156.0000 50 20 ; k j i h cond conc pesa_dam
12779 7 89 24 156.0000 50 20 ; k j i h cond conc pesa_dam
12780 7 90 24 156.0000 50 20 ; k j i h cond conc pesa_dam
12781 6 91 24 156.0000 50 20 ; k j i h cond conc pesa_dam
12782 6 92 24 156.0000 50 20 ; k j i h cond conc pesa_dam
12783 6 93 24 156.0000 50 20 ; k j i h cond conc pesa_dam
12784 7 89 25 156.0000 50 20 ; k j i h cond conc pesa_dam
12785 7 90 25 156.0000 50 20 ; k j i h cond conc pesa_dam
12786 7 91 25 156.0000 50 20 ; k j i h cond conc pesa_dam
12787 7 92 25 156.0000 50 20 ; k j i h cond conc pesa_dam
12788 6 89 26 156.0000 50 20 ; k j i h cond conc pesa_dam
12789 7 90 26 156.0000 50 20 ; k j i h cond conc pesa_dam
12790 12787 stress period=2 year= 1 month= 2
    
```


Appendix 2.5

Output Control

The **Output Control Option** (oc.dat) is used to specify which head, drawdown, or budget data should be printed or saved.

The oc.dat file for the model is created using the code below. All outputs are deactivated to limit computer space.

```

241 procedure writeocdat;
242 begin
243   filename:='oc.dat';assign(ascl,filename);rewrite(ascl);
244   writeln('write oc.dat file: ',filename);
245   // number of loops of same data
246   writeln(ascl,'      0      0      51      52');
247   // number of months (600 months)
248   for time:=1 to nnt do
249   begin
250     writeln(ascl,'      0      0      0      0      0 PERIOD:',time:1, '      TIME STEP: 1      Output deactivated');
251     writeln(ascl,'      0      0      0      0      0');
252   end;
253 end;
254

```

Below is a screenshot of the created **oc.dat** file.

Line	Head	Drawdown	Budget	Output Status	
1	0	0	51	52	
2	0	0	0	0	PERIOD:1 TIME STEP: 1 Output deactivated
3	0	0	0	0	
4	0	0	0	0	PERIOD:2 TIME STEP: 1 Output deactivated
5	0	0	0	0	
6	0	0	0	0	PERIOD:3 TIME STEP: 1 Output deactivated
7	0	0	0	0	
8	0	0	0	0	PERIOD:4 TIME STEP: 1 Output deactivated
9	0	0	0	0	
10	0	0	0	0	PERIOD:5 TIME STEP: 1 Output deactivated
11	0	0	0	0	
12	0	0	0	0	PERIOD:6 TIME STEP: 1 Output deactivated
13	0	0	0	0	
14	0	0	0	0	PERIOD:7 TIME STEP: 1 Output deactivated
15	0	0	0	0	
16	0	0	0	0	PERIOD:8 TIME STEP: 1 Output deactivated
17	0	0	0	0	
18	0	0	0	0	PERIOD:9 TIME STEP: 1 Output deactivated
19	0	0	0	0	
20	0	0	0	0	PERIOD:10 TIME STEP: 1 Output deactivated
21	0	0	0	0	
22	0	0	0	0	PERIOD:11 TIME STEP: 1 Output deactivated
23	0	0	0	0	
24	0	0	0	0	PERIOD:12 TIME STEP: 1 Output deactivated
25	0	0	0	0	
26	0	0	0	0	PERIOD:13 TIME STEP: 1 Output deactivated
27	0	0	0	0	
28	0	0	0	0	PERIOD:14 TIME STEP: 1 Output deactivated
29	0	0	0	0	
30	0	0	0	0	PERIOD:15 TIME STEP: 1 Output deactivated
31	0	0	0	0	
32	0	0	0	0	PERIOD:16 TIME STEP: 1 Output deactivated
33	0	0	0	0	
34	0	0	0	0	PERIOD:17 TIME STEP: 1 Output deactivated
35	0	0	0	0	

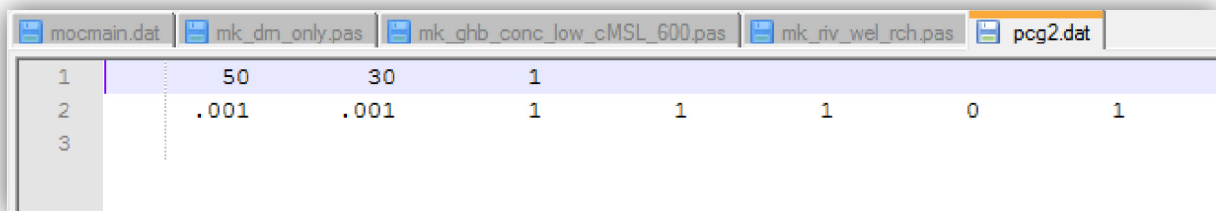
normal text file 236533 chars 243733 bytes 3601 lines Ln:1 Col:1 Sel:0 (0 bytes) in 0 ranges Dos/Windows ANSI

Appendix 2.6

Preconditioned Conjugate Gradient 2 Package (PCG2)

The **Preconditioned Conjugate-Gradient package** (pcg2.dat) is used to solve the finite difference equations in each step of a MODFLOW stress period.

The applied pcg2.dat in the simulations is shown below.



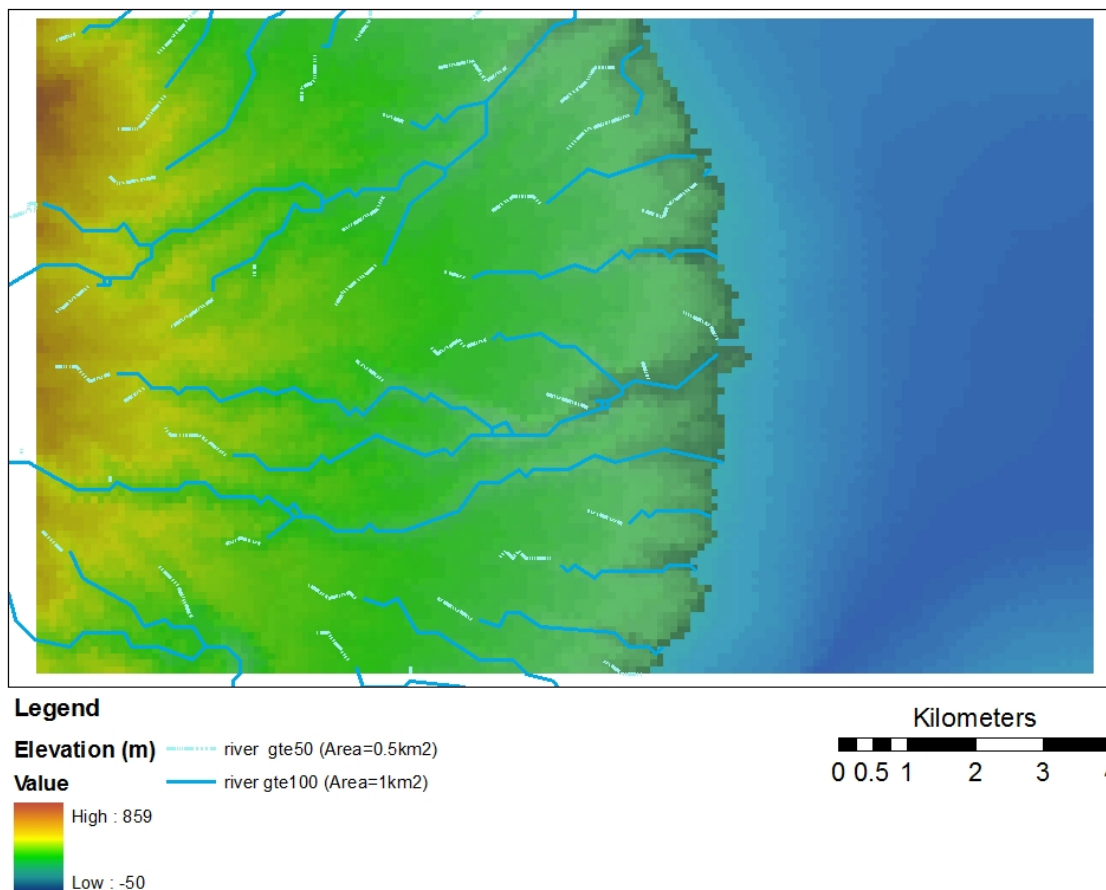
The screenshot shows a software window with several tabs. The active tab is 'pcg2.dat'. The content of the file is displayed in a table with three rows and eight columns.

	1	2	3	4	5	6	7	8
1	50	30	1					
2	.001	.001	1	1	1	0	1	
3								

Appendix 2.7

River Package

The **River Package** is used to simulate head-dependent flux boundaries. In the River package, if the head in the cell falls below a certain threshold, the flux from the river to the model cell is set to a specified lower bound.



2 types of rivers are applied in the model. RIV1, are the main rivers with an equivalent catchment area of 1 sq. km RIV2, are the smaller rivers with an equivalent catchment of 0.5 sq. km. These are calculated using ArcMap and converted to an ascii raster file format to be implemented in the program formed to create the River Package file. The code for the river package program is shown in the next page.

```

453 procedure readriv;
454 //var fname: string;
455 begin
456   filename:='luc_riv_gte100.txt';assign(riv1,filename);reset(riv1);
457   writeln('read main river: ',filename);
458   readln(riv1,ncol,nrow);
459   for irow:=1 to nrow do
460     begin
461       for icol:=1 to ncol do
462         begin
463           read(riv1,riveribound[icol,irow]);
464         end;
465       end;
466     close(riv1);
467   end;
468
469 procedure readriv2;
470 begin
471   filename:='luc_riv_gte50.txt';assign(riv2,filename);reset(riv2);
472   writeln('read secondary river: ',filename);
473   readln(riv2,ncol,nrow);
474   for irow:=1 to nrow do
475     begin
476       for icol:=1 to ncol do
477         begin
478           read(riv2,riveribound2[icol,irow]);
479         end;
480       end;
481     close(riv2);
482   end;

```

Here the river maps are read, using this information the cells which will be occupied by the rivers are determined

```

484 procedure writerriver;
485 begin
486   filename:='riv.dat';assign(riv1,filename);rewrite(riv1);writeln('write river file: ',filename);
487   writeln(riv1,' ',rivarray:5,'          50 CBGALLOCATE AUXILIARY CONC          ; k j i stageriv cond hbottom conc');
488   writeln(riv1,' ',rivarray:5);
489   for icol:=1 to ncol do
490     begin
491       for irow:=1 to nrow do
492         begin
493           layer:=1;
494           while ibound[icol,irow,layer]=0 do
495             begin
496               layer:=layer+1;
497             end;
498           dum1:=ahn[icol,irow];dum2:=rivcond;dum3:=rivconcl;dum4:=rivconcl;
499           if riveribound[icol,irow]=1 then
500             writeln(riv1,layer:10,irow:10,icol:10,ahn[icol,irow]+heightriver:10:2,dum2:10:0,ahn[icol,irow]:10:2,dum3:10:0,' no=1');
501           if riveribound2[icol,irow]=1 then
502             writeln(riv1,layer:10,irow:10,icol:10,ahn[icol,irow]+heightriver2:10:2,dum2:10:0,ahn[icol,irow]:10:2,dum4:10:0,' no=2');
503         end;
504       end;
505     for n:=1 to stressperiods-1 do writeln(riv1,'-1');
506     close(riv1);
507   end;

```

The riv.dat file is created

Below is a screenshot of the created **riv.dat** file, for the reference case.

Line	Value 1	Value 2	Value 3	Value 4	Value 5	Value 6	Value 7	Value 8
1	943	50	CBCALLOCATE AUXILIARY CONC			; k j i stageriv cond hbottom conc		
2	943							
3	1	27	1	595.50	100	593.00	50	no=1
4	1	36	1	491.50	100	489.00	50	no=1
5	1	66	1	401.50	100	399.00	50	no=1
6	1	75	1	514.50	100	514.00	20	no=2
7	3	91	1	291.50	100	289.00	50	no=1
8	1	28	2	543.50	100	541.00	50	no=1
9	1	36	2	485.50	100	483.00	50	no=1
10	1	67	2	395.50	100	393.00	50	no=1
11	1	76	2	445.50	100	445.00	20	no=2
12	3	91	2	283.50	100	281.00	50	no=1
13	1	3	3	496.50	100	496.00	20	no=2
14	1	28	3	544.50	100	542.00	50	no=1
15	1	36	3	457.50	100	455.00	50	no=1
16	1	43	3	547.50	100	547.00	20	no=2
17	1	51	3	570.50	100	570.00	20	no=2
18	1	68	3	378.50	100	376.00	50	no=1
19	1	77	3	426.50	100	426.00	20	no=2
20	4	92	3	275.50	100	273.00	50	no=1
21	1	2	4	456.50	100	456.00	20	no=2
22	1	28	4	552.50	100	550.00	50	no=1
23	1	36	4	480.50	100	478.00	50	no=1
24	1	42	4	497.50	100	497.00	20	no=2
25	1	51	4	568.50	100	568.00	20	no=2
26	1	68	4	393.50	100	391.00	50	no=1
27	1	78	4	401.50	100	401.00	20	no=2
28	4	92	4	274.50	100	272.00	50	no=1
29	1	2	5	456.50	100	456.00	20	no=2
30	1	29	5	510.50	100	508.00	50	no=1
31	1	36	5	451.50	100	449.00	50	no=1
32	1	41	5	492.50	100	492.00	20	no=2
33	1	51	5	544.50	100	544.00	20	no=2
34	1	68	5	393.50	100	391.00	50	no=1
35	1	78	5	396.50	100	394.00	50	no=1

Normal text file 77255 chars 82743 bytes 2745 lines Ln:1 Col:1

Appendix 2.8

Recharge Package

The **Recharge package** is used to simulate a specified flux distributed over the top of the model and specified in units of length/time. Within MODFLOW, these rates are multiplied by the horizontal area of the cells to which they are applied to calculate the volumetric flux rates.

The preparation of this package uses the ideas of the water balance models developed in the 1940s by [Thorntwaite \(1948\)](#) and revised by [Thorntwaite and Mather \(1955\)](#). The soil water balance can be represented by the equation:

$$R = P - aET - Ro + \Delta S$$

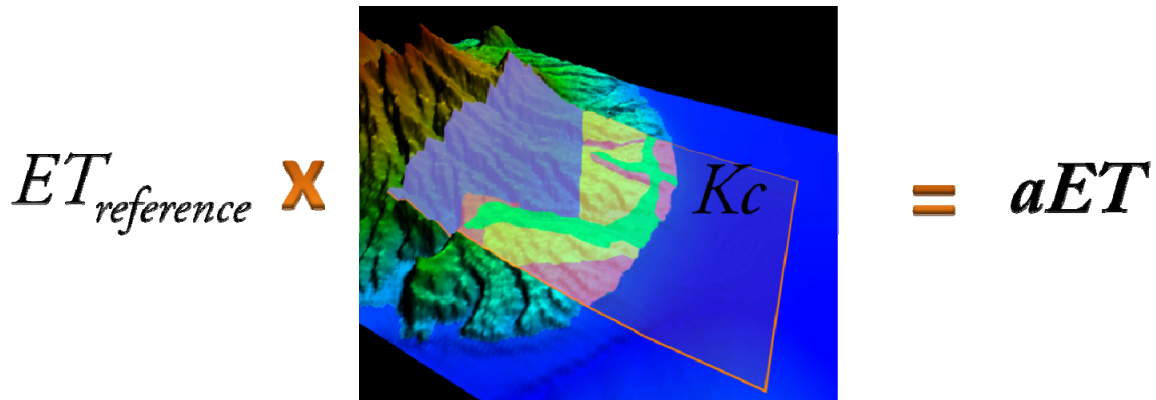
Where:

- R is the effective recharge
- P is precipitation
- aET is the actual evapotranspiration
- Ro is the run-off
- ΔS is the change in soil water storage

The precipitation data used in the model is the available mean monthly rainfall data from Limay, Bataan.

mm/month	
Month	Rainfall
Jan	9.9
Feb	8.6
Mar	9.4
Apr	17.5
May	247.6
Jun	320.8
Jul	692.4
Aug	834.6
Sep	430
Oct	240.2
Nov	129.5
Dec	60.7

The actual evapotranspiration (aET) in the study area is estimated using the FAO Penman-Monteith Method (FAO, 1998), where the reference evapotranspiration (ET_{ref}) is multiplied by a crop factor (K_c) which represents the type of vegetation in the area. K_c is approximated using the information from the land-use map obtained from the Mariveles Municipal Planning and Development Office. The figure below explains this process:



mm/month
ref ET
109.8
131.15
152.5
170.8
152.5
134.2
128.1
118.95
118.95
118.95
109.8
106.75

Kc (crop factor)			
LU1	LU2	LU3	LU4
1.104086	0.567985	0.2	0.2
1.10617	0.814213	0.2	0.2
1.12171	0.893891	0.2	0.2
1.12604	0.920276	0.2	0.2
1.12604	0.920276	0.2	0.2
1.12604	0.920276	0.2	0.2
1.12604	0.920276	0.2	0.2
1.12604	0.920276	0.2	0.2
1.12604	0.920276	0.2	0.2
1.12425	0.909018	0.2	0.2
1.12157	0.893083	0.2	0.2
1.09549	0.767137	0.2	0.2

The actual evapotranspiration is calculated from the monthly reference evapotranspiration for the area multiplied by the crop factor which is depending on the type of land-use. LU1 is forest, LU2 is agricultural, LU3 is industrial and LU4 is build-up (Data from FAO).

The direct run-off is estimated using the *Thornthwaite water balance approach* (Ferguson, 1996). Given by the equation:

$$Q_r = 0 \quad \text{if} \quad \frac{-0.095 + 0.208 P}{S^{0.66}} < 0$$

$$Q_r = \frac{-0.095 + 0.208 P}{S^{0.66}} \quad \text{if} \quad \frac{-0.095 + 0.208 P}{S^{0.66}} \geq 0$$

Where: Qr is the average monthly direct runoff
 S is related to the soil and cover characteristics of the soil

S is represented through its relationship to the value of the runoff curve number (CN) given by:

$$S = \frac{100}{CN} - 10 \quad (\text{inches})$$

CN is the curve number, estimated based on land-use and soil group
 P is the average monthly precipitation.

CN is affected by the soil properties; it influences the relationship between rainfall and runoff by affecting the rate of infiltration. NRCS divides soils into four hydrologic soil groups based on infiltration rates (Groups A-D).

Group A. Group A soils have a low runoff potential due to high infiltration rates even when saturated (0.30 in/hr to 0.45 in/hr or 7.6 mm/hr to 11.4 mm/hr). These soils primarily consist of deep sands, deep loess, and aggregated silts.

Group B. Group B soils have a moderately low runoff potential due to moderate infiltration rates when saturated (0.15 in/hr to 0.30 in/hr or 3.8 mm/hr to 7.6 mm/hr). These soils primarily consist of moderately deep to deep, moderately well to well drained soils with moderately fine to moderately coarse textures (shallow loess, sandy loam).

Group C. Group C soils have a moderately high runoff potential due to slow infiltration rates (0.05 in/hr to 0.5 in/hr or 1.3 mm/hr to 3.8 mm/hr if saturated). These soils primarily consist of soils in which a layer near the surface impedes the downward movement of water or soils with moderately fine to fine texture such as clay loams, shallow sandy loams, soils low in organic content, and soils usually high in clay.

Group D. Group D soils have a high runoff potential due to very slow infiltration rates (less than 0.05 in./hr or 1.3 mm/hr if saturated). These soils primarily consist of clays with high swelling potential, soils with permanently high water tables, soils with a claypan or clay layer at or near the surface, shallow soils over nearly impervious parent material such as soils that swell significantly when wet or heavy plastic clays or certain saline soils.

For the study area, the soil group type is B.

The table below shows the different CN number assigned for different land-use types and soil groups based on the TR-55 publication:

Land Use Description on Input Screen	Description and Curve Numbers from TR-55					
	Cover Description		Curve Number for Hydrologic Soil Group			
	Cover Type and Hydrologic Condition	% Impervious Areas	A	B	C	D
Agricultural	Row Crops - Straight Rows + Crop Residue Cover-Good Condition ⁽¹⁾		64	75	82	85
Commercial	Urban Districts: Commercial and Business	85	89	92	94	95
Forest	Woods ⁽²⁾ - Good Condition		30	55	70	77
Grass/Pasture	Pasture, Grassland, or Range ⁽³⁾ - Good Condition		39	61	74	80
High Density Residential	Residential districts by average lot size: 1/8 acre or less	65	77	85	90	92
Industrial	Urban district: Industrial	72	81	88	91	93
Low Density Residential	Residential districts by average lot size: 1/2 acre lot	25	54	70	80	85
Open Spaces	Open Space (lawns, parks, golf courses, cemeteries, etc.) ⁽⁴⁾ Fair Condition (grass cover 50% to 70%)		49	69	79	84
Parking and Paved Spaces	Impervious areas: Paved parking lots, roofs, driveways, etc. (excluding right-of-way)	100	98	98	98	98
Residential 1/8 acre	Residential districts by average lot size: 1/8 acre or less	65	77	85	90	92
Residential 1/4 acre	Residential districts by average lot size: 1/4 acre	38	61	75	83	87
Residential 1/3 acre	Residential districts by average lot size: 1/3 acre	30	57	72	81	86
Residential 1/2 acre	Residential districts by average lot size: 1/2 acre	25	54	70	80	85
Residential 1 acre	Residential districts by average lot size: 1 acre	20	51	68	79	84
Residential 2 acres	Residential districts by average lot size: 2 acre	12	46	65	77	82
Water/ Wetlands		0	0	0	0	0

Notes

⁽¹⁾ Hydraulic condition is based on combination factors that affect infiltration and runoff, including (a) density and canopy of vegetative areas, (b) amount of year-round cover, (c) amount of grass or close-seeded legumes, (d) percent of residue on the land surface (good >=20%), and (e) degree of surface roughness.

⁽²⁾ Good: Woods are protected from grazing, and litter and brush adequately cover the soil.

⁽³⁾ Good: >75% ground cover and lightly or only occasionally grazed.

⁽⁴⁾ CN's shown are equivalent to those of pasture. Composite CN's may be computed for other combinations of open space cover type.

Based from the CN table, the CN value assigned for each specific land-use type is as follows:

Land-use type	Description	Characteristics	Assigned CN from TR-55
1	Forest	Fair (grazing but not burned)	60
2	Agricultural	With conservation treatment - contouring	71
3	Industrial	72 % impermeable	88
4	Residential	38 % impermeable	75

Using the above information, a program is created to calculate the effective recharge.

```

378 begin
379   filename:='rch.dat';assign(asc1,filename);rewrite(asc1);
380   writeln('write recharge file: ',filename);
381   // number of loops of same data
382   writeln(asc1,'      3      50      1');
383   for again:=1 to 1 do
384     begin
385       // number of months (600 months)
386       for time:=1 to nmt do
387         begin
388           writeln(asc1,'      ',time:3,'      0');
389           year:=1+trunc((time-1)/12);
390           month:=12+time-(year)*12;
391           writeln('stress period=',time:1,' year=',year:2,' month=',month:2);
392           writeln(asc1,'      18      1(','ncol:1,'G10.0)      -1 Recharge, stress period=',time:1,' year=',year:2,' month=',month:2);
393           for irow:=1 to nrow do
394             begin
395               for icol:=1 to ncol do
396                 begin
397                   for i:=1 to databaserow do
398                     case landusetype[icol,irow] of
399                       0 : dum:=0;
400                       1 : dum:=monthdata[time]-((ETlandusetype11[time]))-(runoff11[time]);
401                       2 : dum:=monthdata[time]-((ETlandusetype22[time]))-(runoff22[time]);
402                       3 : dum:=monthdata[time]-((ETlandusetype33[time]))-(runoff33[time]);
403                       4 : dum:=monthdata[time]-((ETlandusetype33[time]))-(runoff44[time]);
404                     end;
405                     rech[icol,irow]:=dum*0.001/30.5; //dum is in mm/month convert to m3/day
406                     //writeln(asc1,'      ',rech[icol,irow]:9:5);
407                     if (icol/ncol-trunc(icol/ncol)<>0) then
408                       write(asc1,'      ',rech[icol,irow]:9:5) else writeln(asc1,'      ',rech[icol,irow]:9:5);
409                   end;
410                 end;
411             end;
412           end;

```


This created initial wel.dat file has very high extraction rate on a single top cell, but in reality the well takes water from cells even below the top cell, depending on the depth of the well. Thus this initial wel.dat file is applied to PMWIN and manually edited to distribute the discharge value Q with depth, resulting to the wel.dat file below:

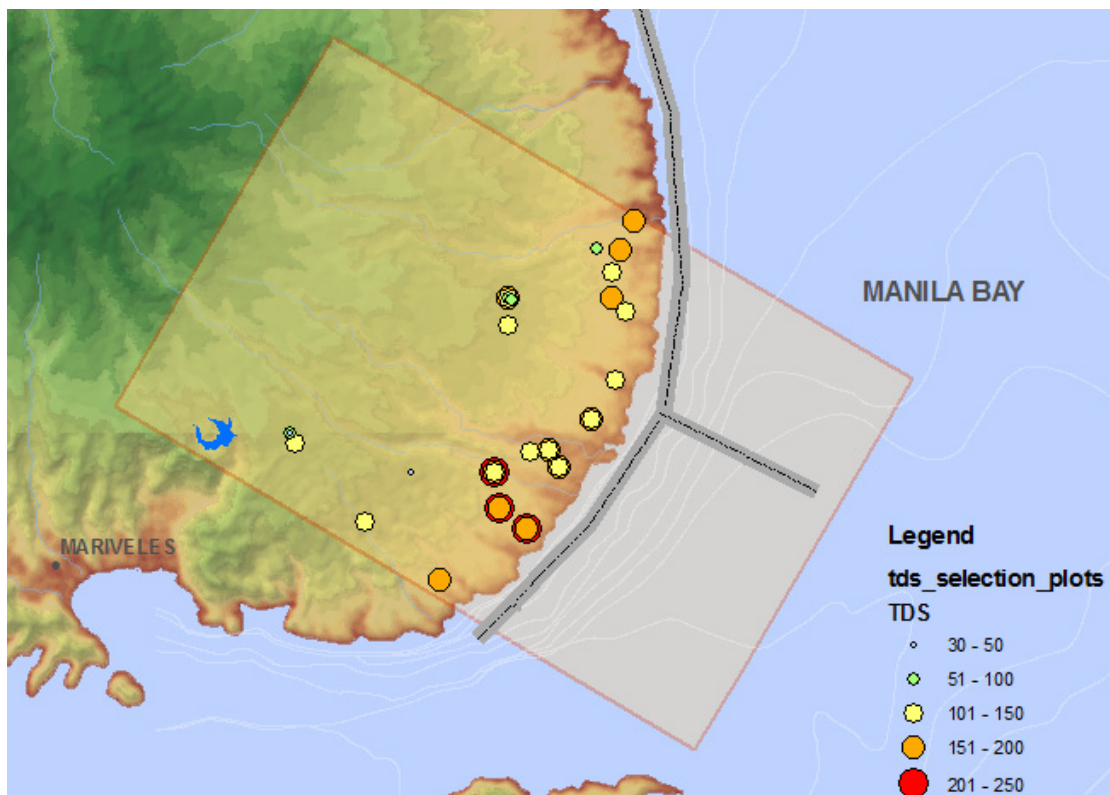
Cell No.	Discharge Rate	Concentration
1	3905	50 CBCALLOCATE AUXILIARY CONC
2	3905	
3	4	77 37 -.864
4	4	81 37 -1.58
5	4	81 38 -1.58
6	4	81 39 -1.58
7	4	82 37 -1.58
8	4	82 38 -1.58
9	4	82 39 -1.58
10	4	82 42 -.864
11	4	83 37 -1.58
12	4	83 38 -1.58
13	4	83 39 -8
14	4	83 40 -.864
15	4	84 34 -.864
16	4	86 39 -5
17	4	86 40 -.864
18	4	87 40 -.864
19	5	81 37 -1.58
20	5	81 38 -1.58
21	5	81 39 -1.58
22	5	82 37 -1.58
23	5	82 38 -1.58
24	5	82 39 -1.58
25	5	83 37 -1.58
26	5	83 38 -1.58
27	5	83 39 -10
28	5	83 45 -.2592
29	5	87 43 -.864
30	6	32 60 -.864
31	6	33 57 -1.2
32	6	33 58 -1.2
33	6	33 59 -1.2
34	6	34 57 -1.2
35	6	34 58 -1.2
36	6	34 59 -1.2
37	6	35 57 -1.2
38	6	35 58 -4.32
39	6	35 59 -1.2

- 3905 is the number of cells with extraction value Q

Appendix 2.10

Main MOC3D Package

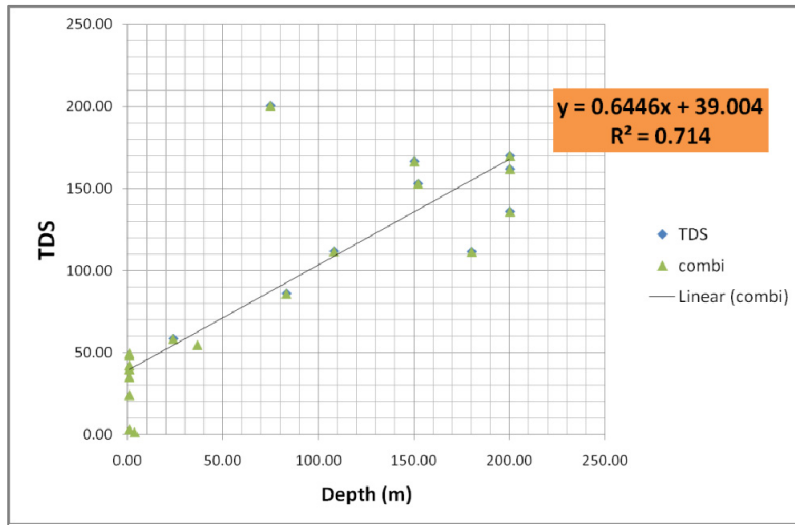
The **Main MOC3D Package** contains the information of the initial concentration and porosity values of the mocmain.dat file.



The mocmain.dat file is created in a series of steps, and changed or modified as the simulation goes from Part1 to Part 3 in the reference case, the details of this is already explained in **Section 2.8.1**.

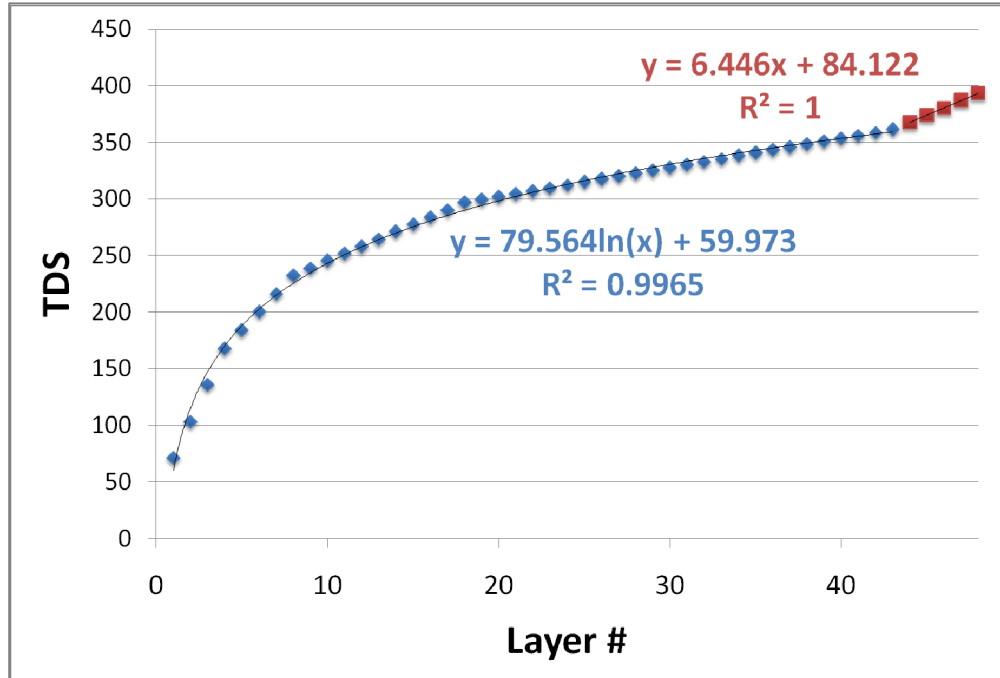
Preparation of mocmain.dat for Part 1 reference case:

The available TDS concentration values from the wells in the area are shown above. The graph below shows the relationship of TDS concentration vs. depth (m).



A linear relationship between the TDS (conc) vs. depth (m) from surface is observed from the well data in the area. This information is then used to calculate the concentration at different depths starting from the elevation of the top layer to the bottom.

The resulting relationship between the layer number and the elevation for the mountain boundary (see **Appendix 2.4** for description) is:



This relationship is then applied create a concentration distribution for the model called the concmatrix.

See the program below shows the creation of the concmatrix:

```

92  procedure writeconcascmatrix;
93  begin
94  filename:='conc_3Dmatrix.asc';assign(asc1,filename);rewrite(asc1);
95  writeln('write matrix file: ',filename);
96  for icol:=1 to ncol do
97  begin
98  for irow:=1 to nrow do
99  begin
100  for layer:=1 to nlay do
101  begin
102  case layer of
103  1..43: conc[icol,irow,layer]:=79.564*(ln(layer))+59.973;
104  44..48: conc[icol,irow,layer]:=6.446*(layer)+84.112;
105  end;
106  if ibound[icol,irow,layer]=2 then conc[icol,irow,layer]:=35000;
107  if (ibound[icol,irow,layer]=2) and (ibound[icol-1,irow,layer]=1) then
108  begin
109  icol0:=icol;
110  layer0:=layer;
111  x:=0;
112  y:=0;
113  for icolwedge:=icol0-1 downto 1 do
114  begin
115  for layerwedge:=layer0 to 48 do
116  begin
117  y:=(ztmp[layerwedge]+(layerwedge-layer0)*ztmp[layerwedge]);
118  x:=(xcell+(icol0-icolwedge)*xcell);
119  //if y<=-sqrt(-2.729*x) then conc[icolwedge,irow,layerwedge]:=35000;
120  if y<=-(-2.729*x) then conc[icolwedge,irow,layerwedge]:=35000;
121  end;
122  end;
123  end;
124  end;
125  end;
126  end;

```

Pascal source file 14537 chars 15357 bytes 411 lines Ln:1 Col:1 Sel:0

A vertical interface is assumed between the saltwater (TDS=35000) and the freshwater, since there is no information available regarding the interface.

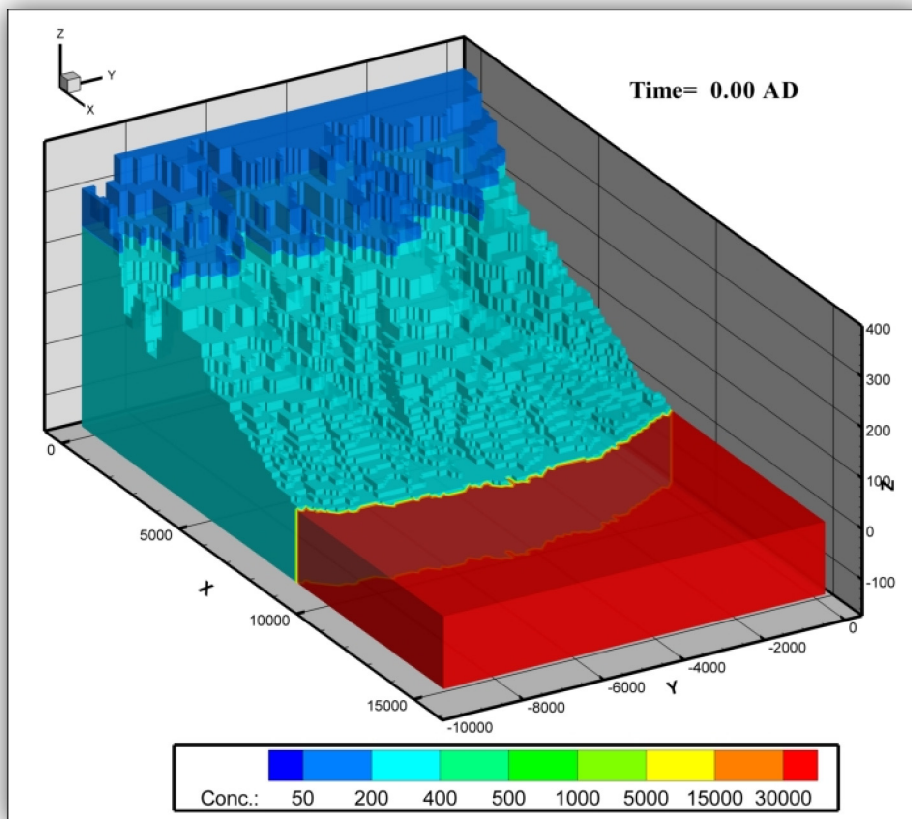
```

127  for layer:=1 to nlay do
128  begin
129  writeln(asc1,'      1      1(',ncol:2,'I6)      -1 6. DATA CONC Array for Layer ',layer:1);
130  for irow:=1 to nrow do
131  begin
132  for icol:=1 to ncol do
133  begin
134  if (icol/ncol-trunc(icol/ncol)<>0) then write(asc1,' ',conc[icol,irow,layer]:5:0) else writeln(asc1,' ',conc[icol,irow,layer]:5:0);
135  //if (irow/nrow-trunc(irow/nrow)<>0) then write(asc1,' ',conc[icol,irow,layer]:5:0) else writeln(asc1,' ',conc[icol,irow,layer]:5:0);
136  end;
137  end;
138  end;
139  close(asc1);
140  end;
141

```

Here a concentration value is assigned for the different cells.

The output concmatrix file applied in the model is shown below:



TDS concentration values (in ppm or mg/L) of different water types based on [US EPA](#) and the [Water Quality Association](#)

<i>Ideal drinking water</i>	0-50
<i>Mountain springs</i>	50-170
<i>Ave. tap water</i>	170-320
<i>Mineral springs</i>	300-500
<i>Fresh water</i>	<1,000
<i>Brackish:</i>	1,000-5,000
<i>Highly Brackish:</i>	5,000-15,000
<i>Saline:</i>	15,000-30,000
<i>Sea Water:</i>	30,000-40,000

The concmatrix is applied in PMWIN to create the mocmain.dat file.

The created mocmain.dat file for Part 1 – **Scenario 1** (ref case) contains the following information:

```

1 Lucanin Catchment, Philippines
2
3      1      48      1      96      1      155
4      0      0      .0000864
5      9000000 8
6      10 .02 1
7      0 2 0 2 0 2 0
8      -1
9      102      1(5G14.0)      -1 10. DATA Initial concentration in Layer 1
10     56      56      56      56      56      56
11     56      56      56      56      56      56
12     56      56      56      56      56      56
13     56      56      56      56      56      56
14     56      56      56      56      56      56

```

Initial concentration values

```

285835     0.1      0.1      0.1
285836     102      1(5G14.0)      -1 17. Data: Retardation factor
285837     1      1      1      1      1
285838     1      1      1      1      1
285839     1      1      1      1      1
285840     1      1      1      1      1
285841     1      1      1      1      1
285842     1      1      1      1      1
285843     1      1      1      1      1
285844     1      1      1      1      1
285845     1      1      1      1      1
285846     1      1      1
285847     102      1(5G14.0)      -1 18a. Data: Cell thickness in Layer 1
285848     50      50      50      50      50
285849     50      50      50      50      50
285850     50      50      50      50      50
285851     50      50      50      50      50
285852     50      50      50      50      50
285853     50      50      50      50      50

```

Cell thickness value

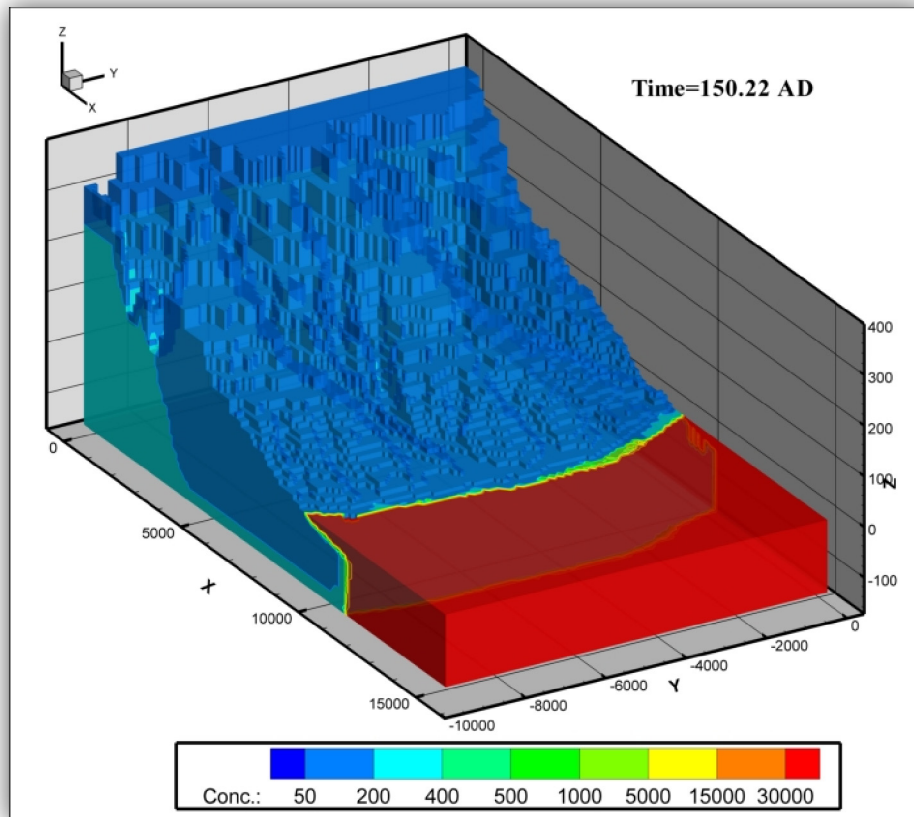
```

288822     50      50      50      50      50
288823     50      50      50      50      50
288824     102      1(5G14.0)      -1 18b. Data: Cell porosity of layer 1
288825     .25      .25      .25      .25      .25
288826     .25      .25      1      1      1
288827     1      1      1      1      1
288828     1      1      1      1      1
288829     1      1      1      1      1
288830     1      1      1      1      1
288831     1      1      1      1      1
288832     1      1      1      1      1
288833     1      1      1      1      1

```

Cell porosity values

After 150 years run time the conc distribution is as follows:



This concentration distribution is then used as an initial concentration distribution for the next run – Part 2.

The rest of the steps which follows are explained in detail in **Section 2.8.1**.

Appendix 2.11

Source Concentration in Recharge

The **Source Concentration in Recharge Package** (moccrch.dat) as the name suggests is the concentration of the water coming in the system in the **Recharge Package**.

In this model, a default value of 0 TDS is used.

The applied moccrch.dat in the simulations is shown below.

1	1					
2	103	1 (5G14.0)		-1	18b. Data: Cell conc in recharge	
3		0	0	0	0	0
4		0	0	0	0	0
5		0	0	0	0	0
6		0	0	0	0	0
7		0	0	0	0	0
8		0	0	0	0	0
9		0	0	0	0	0
10		0	0	0	0	0
11		0	0	0	0	0
12		0	0	0	0	0
13		0	0	0	0	0
14		0	0	0	0	0
15		0	0	0	0	0
16		0	0	0	0	0
17		0	0	0	0	0
18		0	0	0	0	0
19		0	0	0	0	0
20		0	0	0	0	0
21		0	0	0	0	0
22		0	0	0	0	0
23		0	0	0	0	0
24		0	0	0	0	0
25		0	0	0	0	0
26		0	0	0	0	0
27		0	0	0	0	0
28		0	0	0	0	0
29		0	0	0	0	0
30		0	0	0	0	0
31		0	0	0	0	0
32		0	0	0	0	0
33		0	0	0	0	0
34		0	0	0	0	0
35		0	0	0	0	0

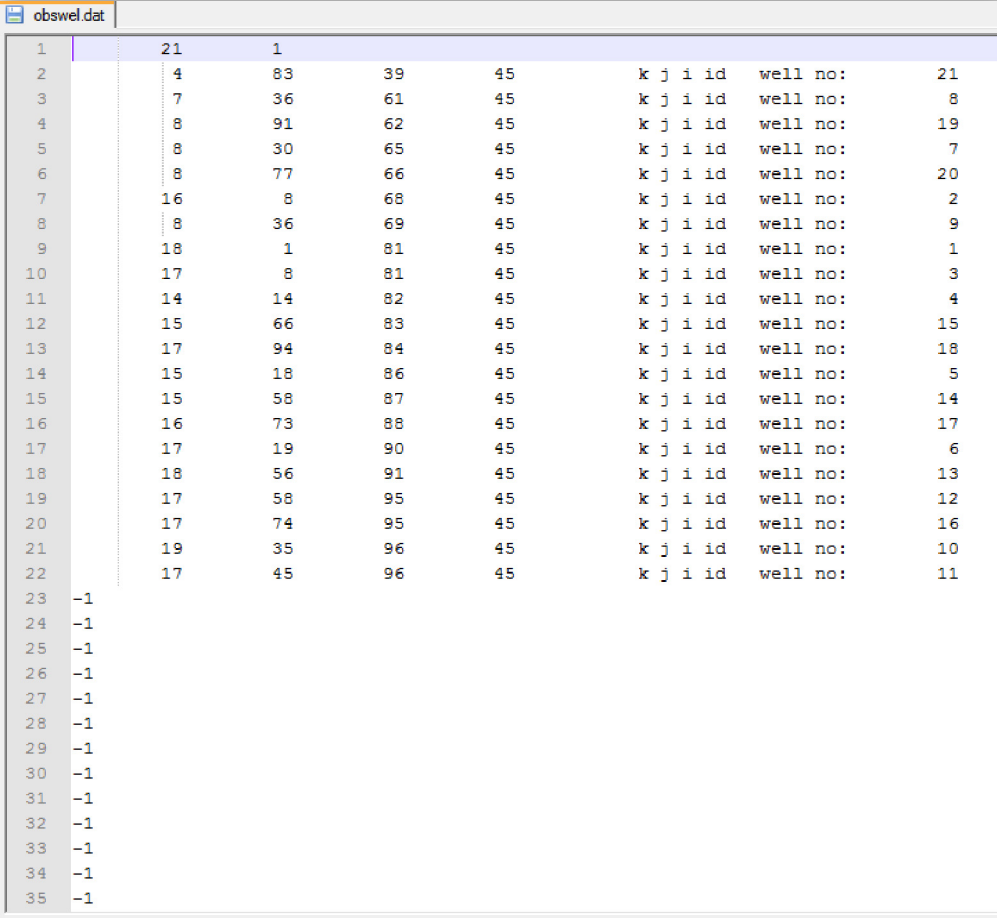
Normal text file 10007190 chars 10296584 bytes 144698 lines

Appendix 2.12

Observation Well File

The **observation well file** (obswel.dat) contains the information of the well locations with known concentration and/or water levels used for the calibration and also for data analysis.

The obswel.dat file used in the simulation is as follows:

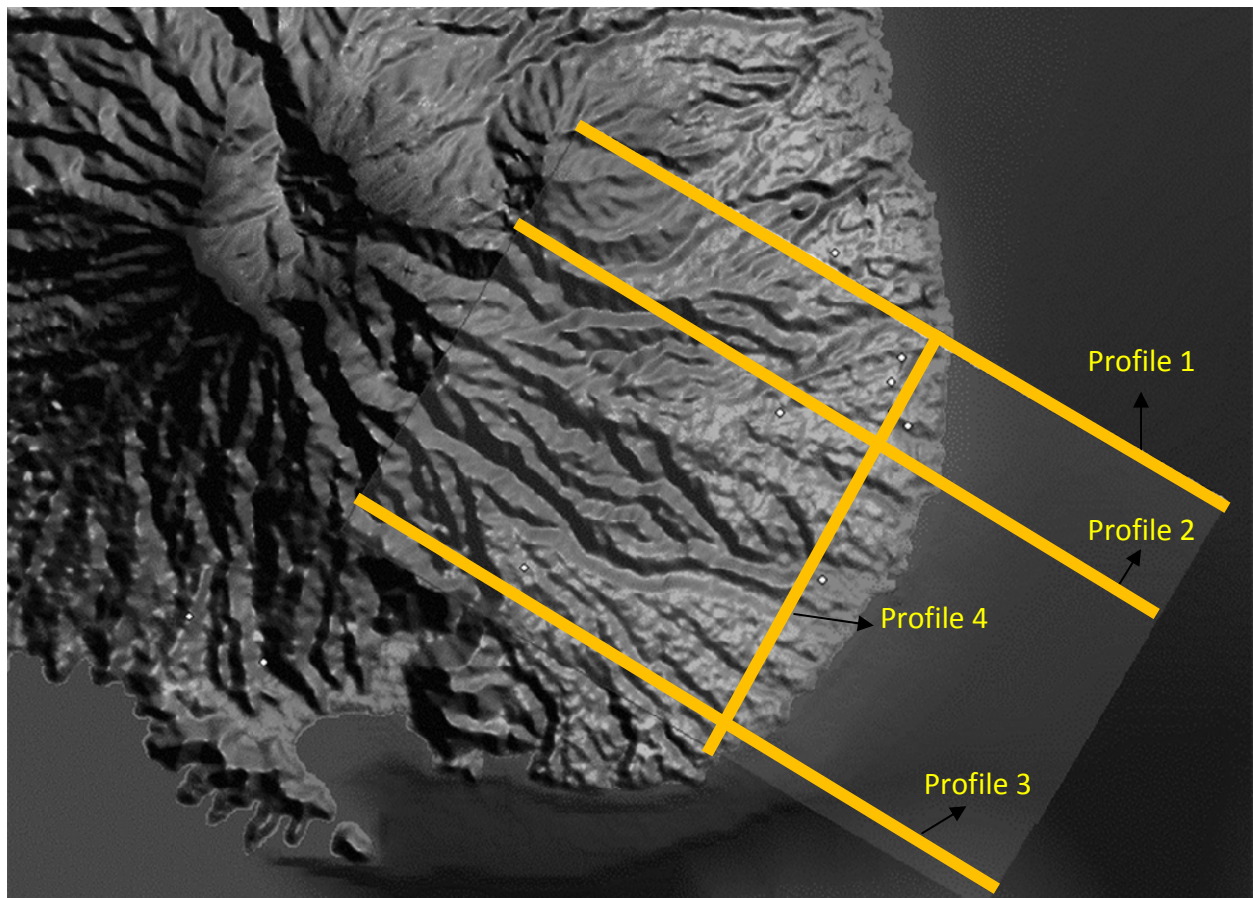


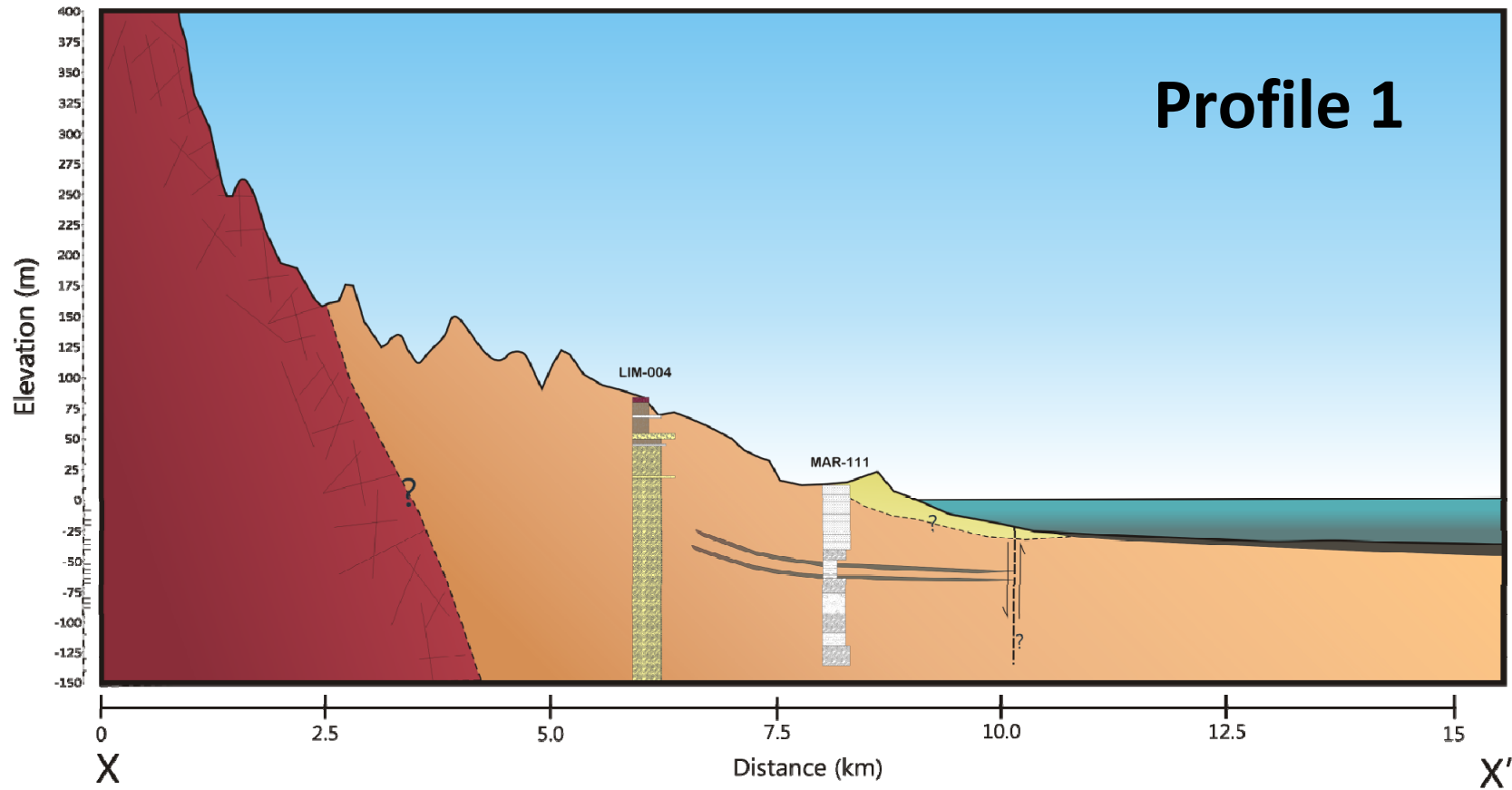
```
obswel.dat
1      21      1
2      4      83      39      45      k j i id well no: 21
3      7      36      61      45      k j i id well no: 8
4      8      91      62      45      k j i id well no: 19
5      8      30      65      45      k j i id well no: 7
6      8      77      66      45      k j i id well no: 20
7      16     8      68      45      k j i id well no: 2
8      8      36      69      45      k j i id well no: 9
9      18     1      81      45      k j i id well no: 1
10     17     8      81      45      k j i id well no: 3
11     14     14     82      45      k j i id well no: 4
12     15     66     83      45      k j i id well no: 15
13     17     94     84      45      k j i id well no: 18
14     15     18     86      45      k j i id well no: 5
15     15     58     87      45      k j i id well no: 14
16     16     73     88      45      k j i id well no: 17
17     17     19     90      45      k j i id well no: 6
18     18     56     91      45      k j i id well no: 13
19     17     58     95      45      k j i id well no: 12
20     17     74     95      45      k j i id well no: 16
21     19     35     96      45      k j i id well no: 10
22     17     45     96      45      k j i id well no: 11
23    -1
24    -1
25    -1
26    -1
27    -1
28    -1
29    -1
30    -1
31    -1
32    -1
33    -1
34    -1
35    -1
```

Normal text file 5299 chars 8943 bytes 1823 lines

Appendix III

Created Hydrogeologic Profiles





Lithologic Units

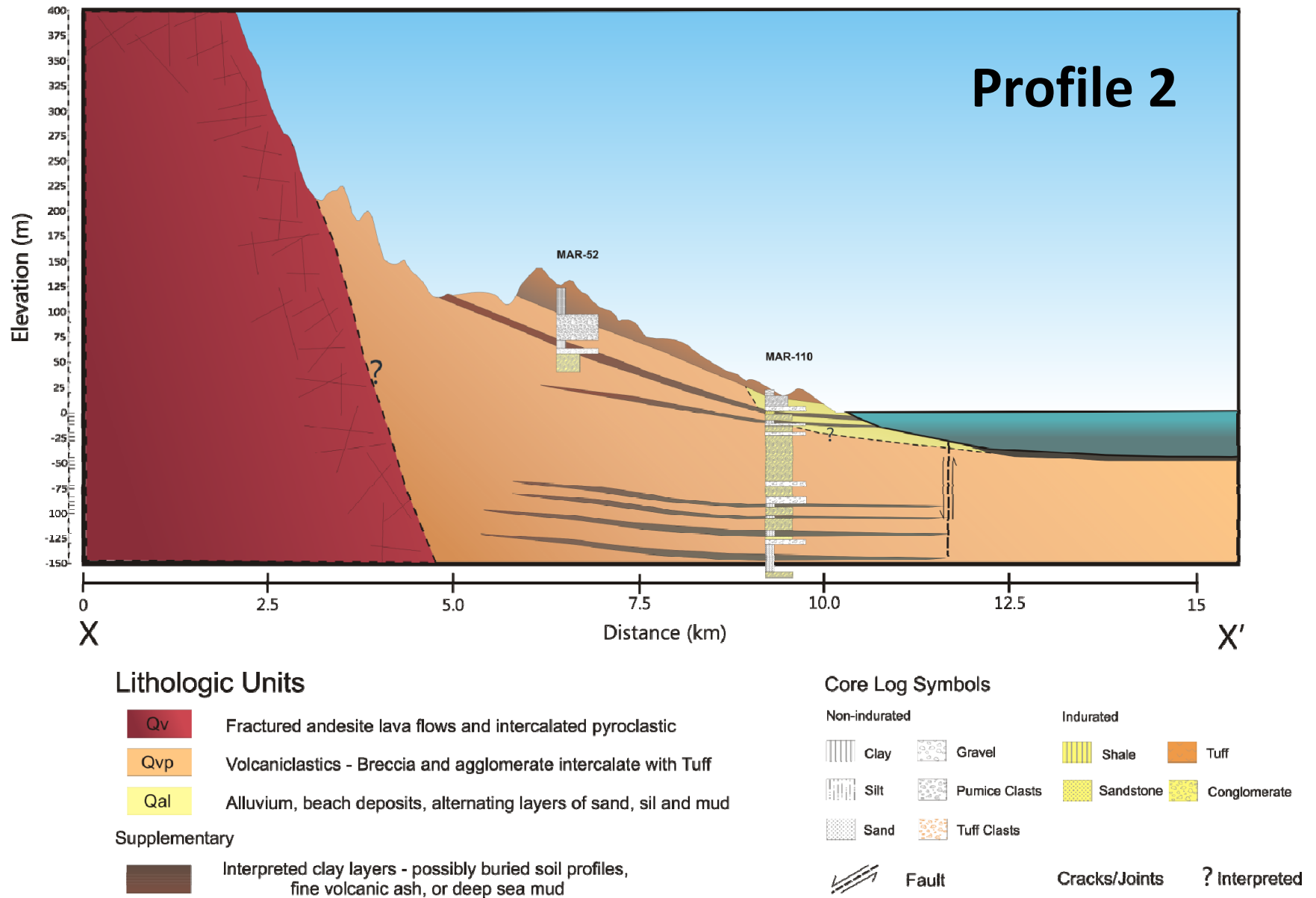
- Qv** Fractured andesite lava flows and intercalated pyroclastic
- Qvp** Volcaniclastics - Breccia and agglomerate intercalate with Tuff
- Qal** Alluvium, beach deposits, alternating layers of sand, sil and mud

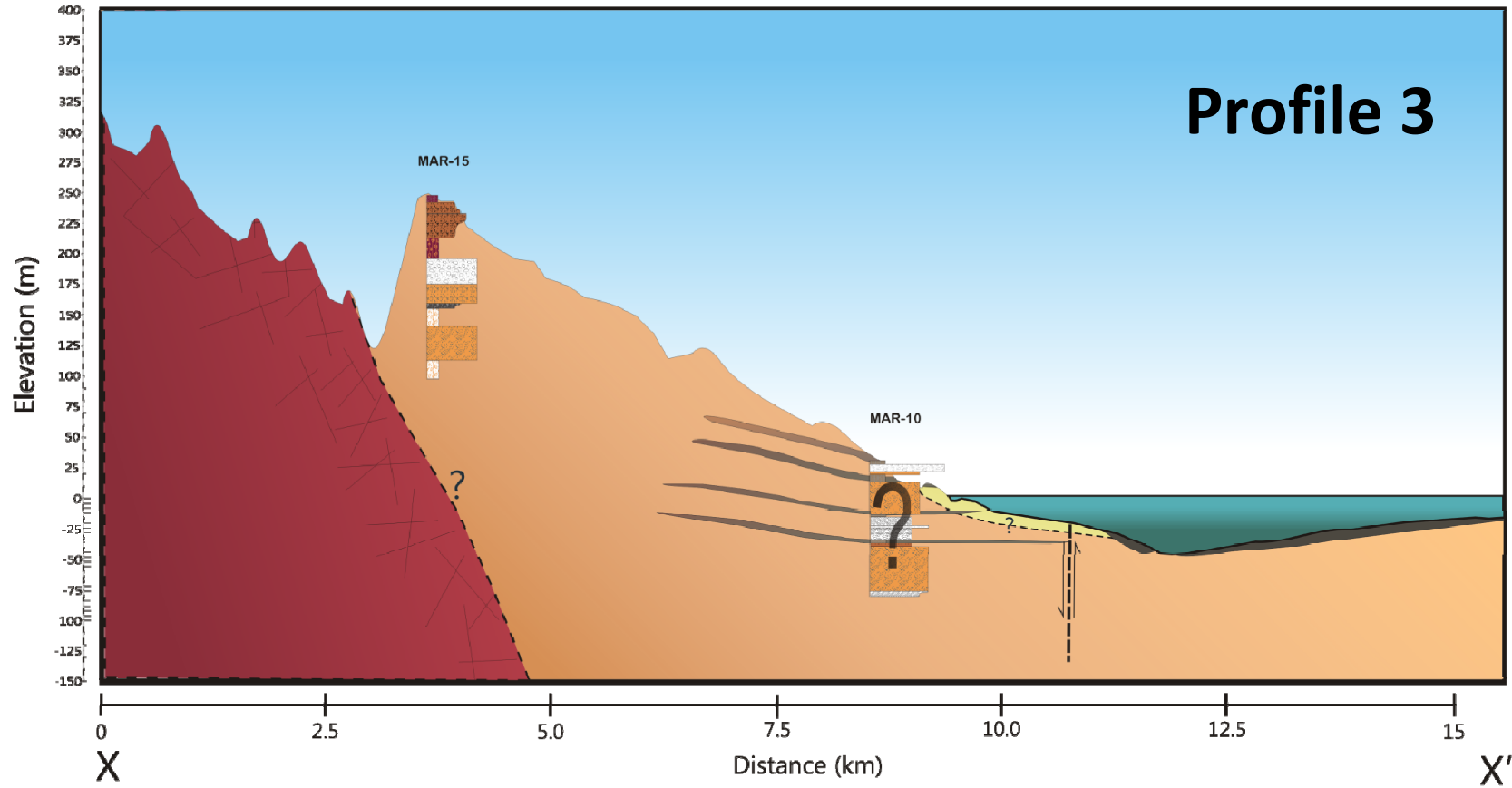
Supplementary

- Interpreted clay layers - possibly buried soil profiles, fine volcanic ash, or deep sea mud

Core Log Symbols

- | Non-indurated | | Indurated | |
|---------------|---------------|-----------|---------------|
| Clay | Gravel | Shale | Tuff |
| Silt | Pumice Clasts | Sandstone | Conglomerate |
| Sand | Tuff Clasts | | |
| | Fault | | Cracks/Joints |
| | | | ? Interpreted |





Lithologic Units

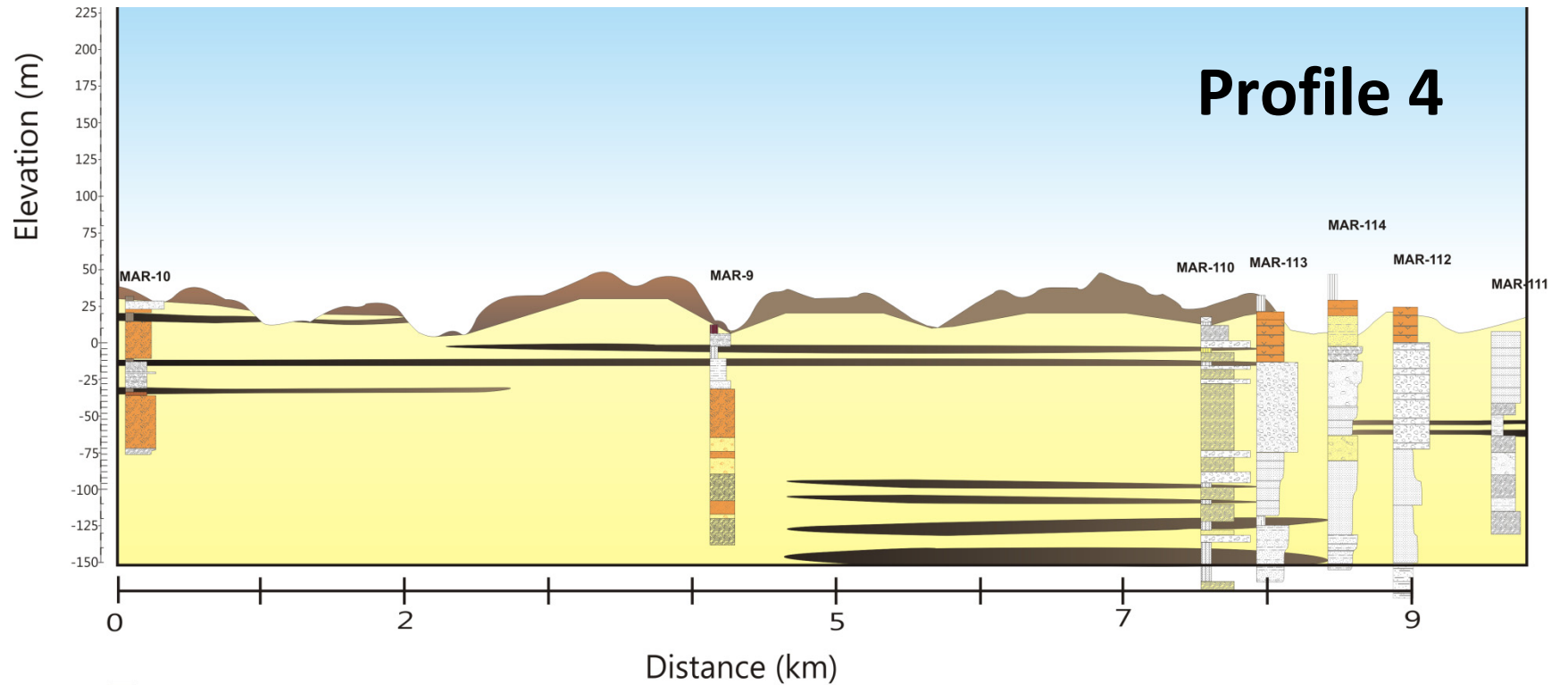
- Qv** Fractured andesite lava flows and intercalated pyroclastic
- Qvp** Volcaniclastics - Breccia and agglomerate intercalate with Tuff
- Qal** Alluvium, beach deposits, alternating layers of sand, sil and mud

Supplementary

- Interpreted clay layers - possibly buried soil profiles, fine volcanic ash, or deep sea mud

Core Log Symbols

- | | | | |
|---|---|--|---|
| Non-indurated | | Indurated | |
| Clay | Gravel | Shale | Tuff |
| Silt | Pumice Clasts | Sandstone | Conglomerate |
| Sand | Tuff Clasts | | |
| Fault | | Cracks/Joints ? Interpreted | |



Z

Lithologic Units

- Qv Fractured andesite lava flows and intercalated pyroclastic
- Qvp Volcaniclastics - Breccia and agglomerate intercalate with Tuff
- Qal Alluvium, beach deposits, alternating layers of sand, sil and mud

Supplementary

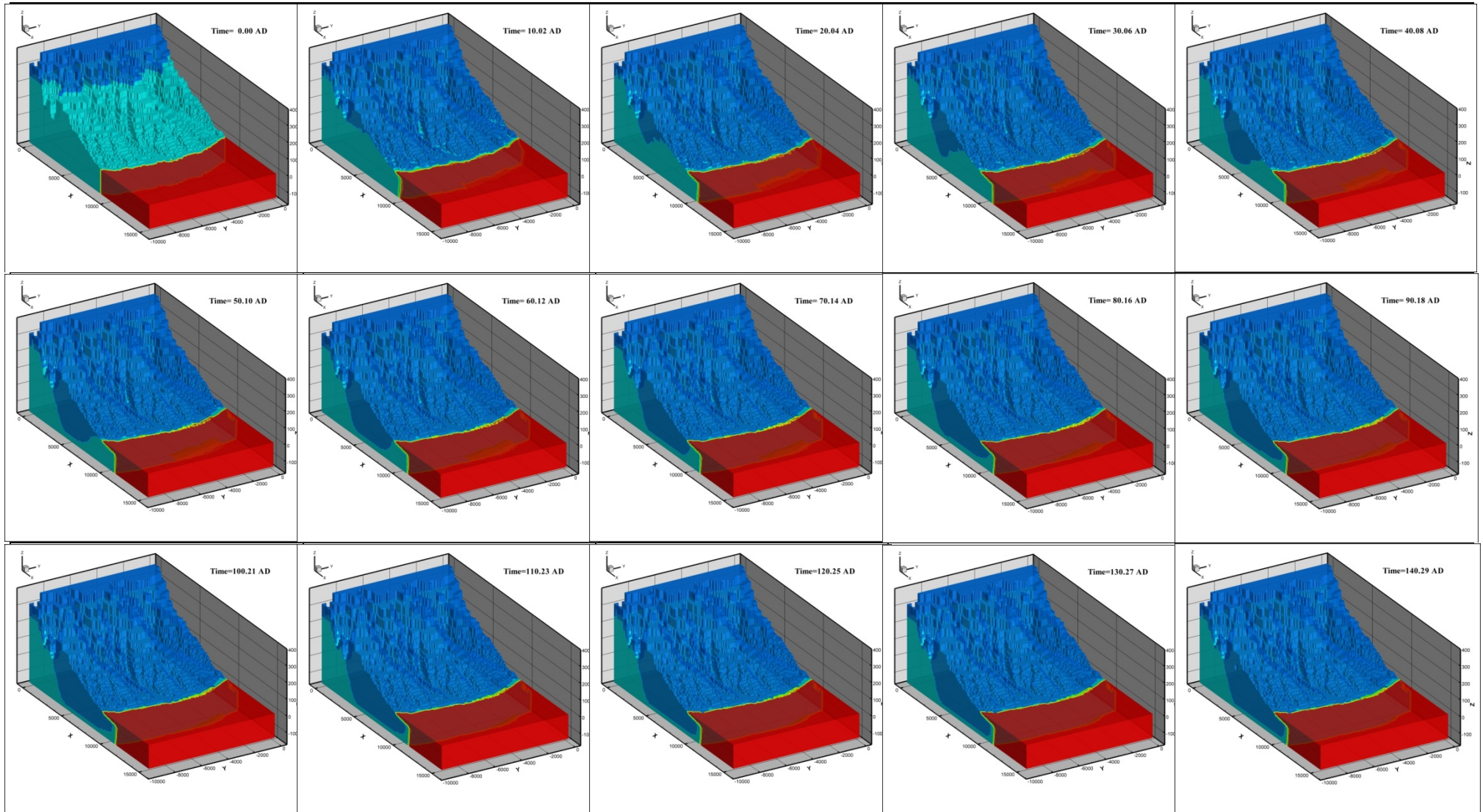
- Interpreted clay layers - possibly buried soil profiles, fine volcanic ash, or deep sea mud

Core Log Symbols

- | Non-indurated | | Indurated | |
|---------------|---------------|-----------|--------------|
| Clay | Gravel | Shale | Tuff |
| Silt | Pumice Clasts | Sandstone | Conglomerate |
| Sand | Tuff Clasts | | |
| Fault | Cracks/Joints | | |

Z'

Appendix IV (Block view) Time series development of the freshwater wedge (S1-R1)



Appendix IV cont. (Block view) Time series development of the freshwater wedge (S1-R1)

